Office of Naval Research
Contract N00014-67-A-0298-0012 NR-017-303
ARPA Contract SD-86

THE CONSTRUCTION AND ANALYSIS OF A RATIO REFLECTOMETER

By
Paul T. McElroy

May 1968

Technical Report No. HP-20
Technical Report No. ARPA-33

Division of Engineering and Applied Physics
Harvard University • Cambridge, Massachusetts

Office of Naval Research

Contract N00014-67-A-0298-0012

NR - 017 - 508

THE CONSTRUCTION AND ANALYSIS OF A RATIO REFLECTOMETER

By

Paul T. McElroy

May 1968

Technical Report No. HP-20

Technical Report No. ARPA-33

The research reported in this document was made possible through support extended the Division of Engineering and Applied Physics, Harvard University, by the Office of Naval Research, under Contract N00014-67-A-0298-0012 and by the Advanced Research Projects Agency under Contract ARPA SD-88.

Division of Engineering and Applied Physics

Harvard University Cambridge, Massachusetts

PREFACE

This technical report, entitled "The Construction and Analysis of a Ratio Reflectometer", is the first of two related reports based on the author's work at Harvard. The second, HP-21 (also known as ARPA-34), is entitled "The Application of the Ratio Reflectometer to Energy Band Studies in Germanium and Gray Tin". The report has been divided into these two parts both because of length and because individual readers will usually have greater interest in one than in the other. Cross references between the two parts have been minimized but not entirely eliminated.

TABLE OF CONTENTS

LIST OF FIGURES

FIGURE PAGE

LIST OF TABLES

ABSTRACT

In our work we have conducted four related investigations: (1) the design and construction of a ratio reflectometer for optical measurements; (2) the description and analysis of a polarization dependent false structure in the reflectivity, which arises in the system monochromator; (3) the application of the ratio reflectometer to the accurate measurement of reflectivity structure in germanium and gray tin, which are then interpreted in terms of energy band models; and (4) the development of an improved method for theoretically computing ϵ_2 through the study of the dependence of the diamond double group selection rules on light polarization direction, and a suggested modification to the double group labels at L, with particular reference to gray tin.

In this technical report we discuss (1) and (2) while (3) and (4) are considered in Technical Report HP-21 (ARPA-34), entitled "The Application of the Ratio Reflectometer to Energy Band Studies in Germanium and Gray Tin".

(1) We have designed and built an optical-electronic system for reflectivity studies which has the following characteristics. Amplitude changes as small as .05% can be detected, permitting the experimenter to measure fine structure and the effects of perturbations. The readout of reflectivity data is direct and rapid, and the sample volume is very large, enabling one to modify the sample crystal environment with a variety of stimuli.

Our discussion of the ratio reflectometer contains a full description of the design problems and the final form of the optical, mechanical, and electronic components. We deal with the various sources of noise and their reduction, the factors affecting linearity and its optimization, and scattered light and electronic drift as sources of false reflectivity structure. Normal operating conditions are described and a guide for locating system malfunctions is included.

(2) False reflectivity structure of small magnitude, arising from the polarizing characteristics of our monochromator grating, was exactly correlated with peaks in the I_0 curve occurring under the same polarization conditions. Our analysis shows the effect is not unique to our system; it may account for fine structure occasionally noted in the work of other investigators.

We have studied the false structure in detail, dividing our effort into two parts. First, we examine the evidence supporting the hypothesis that <u>some</u> of the structure in $I_0(\lambda)$ arises from changes in the angle of incidence of light on the grating, rather than wavelength changes. Second, we assume that <u>all</u> the $I_0(\lambda)$ variation is due to angle of incidence variation in order to determine the importance of this in creating false structure. We derive an expression for the reflectivity which indeed shows false structure correlated with the I_0 structure. In carrying out this analysis, we make use of two geometrical factors: the light incident on the grating

is not perfectly collimated; and our optical system obscures varying amounts of light from the incident light and reflected light optical paths.

The false structure has been eliminated from our system by using light polarized parallel to the monochromator slit and by ensuring that the incident and reflected light paths do not obscure differing amounts of light.

CHAPTER I

INTRODUCTION

A. THE UTILITY OF REFLECTIVITY MEASUREMENTS IN BAND STRUCTURE DETERMINATION

Optical measurements are very useful in determining the allowed energies of electrons in solids. Our understanding of semiconductor energy bands rests in large measure on such studies.

1. Short Discussion of Band Theory

Electrons in atoms have discrete energies which are very narrowly defined. When these atoms are brought together to form a solid, the overlap of electronic wave functions results in a broadening of the energies into energy bands.

The understanding of these bands has been advanced by the one-electron model. In this model, the wave function describing all the electrons in a solid is assumed to be the product of single electron wave functions. These one-electron wave functions take on different forms: they are localized on individual atomic sites in the case of electrons with high ionization energies, while higher energy electrons in the valence and conduction bands are more appropriately described by wave functions of the Bloch form which extend over the entire crystal volume.

Both types of electron states can be studied using optical techniques, provided one extends his studies into the vacuum UV and X-ray regions. However, in our work, interest will be centered on the near

UV, the visible, and the near IR, where Bloch functions provide the appropriate description of the electron. Bloch functions have the form.

$$b_n(\vec{k},\vec{r}) = e^{i\vec{k}\cdot\vec{r}}\, u_n(\vec{k},\vec{r}) \qquad (1.1)$$

where $\vec{k}$ is the crystal momentum of the electron and n is an index labeling the various energy bands.

Within the Bloch electron framework, the crystal momentum, $\vec{k}$, serves to label the various electron states, and electron band energy, $E(\vec{k})$, is a function of $\vec{k}$. Because the energies $E(\vec{k})$ repeat throughout $\vec{k}$ space, $E(\vec{k})$ need not be specified for all $\vec{k}$ values, but only for those lying within the first Brillouin zone (a volume in the $\vec{k}$ space) appropriate to the crystal being studied. The first Brillouin zone for the diamond crystal lattice is shown in Fig. 4-1. This is the zone for germanium and gray tin, the specific materials we shall study. The letters in the figure label various directions or points in $\vec{k}$ space which have high symmetry.

A major goal of solid state studies is to determine the shape of the energy bands within the Brillouin zone since many properties of interest can be predicted from a knowledge of the zone.

The band shape is not known a priori. Optical measurements comprise one of many techniques for determining band detail. This information is restricted to small regions of the Brillouin zone. So that we may know the character of the bands throughout the entire zone, we resort to theoretical one-electron calculations such as the k·p, pseudopotential, or "first principles" techniques. Crystal symmetries allow

us to apply group theory as an aid in the calculations. These same symmetries suggest preferred crystal orientations to the experimenter so that his data will most simply give information on the particular region of $\vec{k}$ space of interest.

Once the band structure information is complete, we can make a quantum mechanical calculation of a macroscopic quantity, such as the dielectric constant. This calculation provides a partial check on the internal consistency of much of the process described above. We can compare the calculated value of ϵ with its measured value. ϵ may either have been measured directly or computed phenomenologically by applying the Kramers-Kronig theory to optical data.

Thus, optical measurements provide both fundamental data to determine band structure and a means for checking the correctness of theoretical models by using additional sources of data. The work of Brust [1-01], in which ϵ_2 is calculated from bands derived from pseudopotential theory and compared with experiment, is an exciting example of this process at work. The rough agreement in structure is encouraging, but the differences in magnitudes and positions show that further work is necessary.

The labors of theorist and experimentalist are complementary. The experimentalist often needs the insight provided by a band theory calculation to identify the Brillouin zone location of the effect he is studying; the theorist needs experimentally determined band separations and curvatures at certain discrete points in order to perform his calculations. Although generally fruitful, the exchange

occasionally shows signs of inbreeding, resulting is misidentifications which may take some time to root out. The process of reidentification and recalculation continues even in silicon and germanium, some of the best understood semiconductors.† Until this process is refined, we cannot hope to attain a perfect match of theory and experiment in the type of comparison Brust performed.

2. Optical Measurements

Perhaps the simplest optical measurement is absorption, which is actually measured by noting the transmitted light. Measurement of the absorption edge of a semiconductor is one of the most direct ways to determine its minimum band gap. With care, one can determine other important band separations lying near the gap, but as one studies the light absorption of higher energies, a limitation is soon reached: too little light is transmitted to permit detection of changes due to further gaps. One possible solution is the use of thin films, provided great care is taken in growing and preparing them so that they replicate bulk material properties as much as possible [1-04, pp. xiii, 5-7].

Philipp and Taft [1-05], amongst others, pointed out the real utility of reflection measurements in determining band properties at energies inaccessible by absorption techniques. There is an intimate relation between absorption and reflection; knowing the values of one for all wavelengths, one can then determine the values of the other.

---

†The papers by Herman [1-02] and Kane [1-03] are two recent examples.

This relationship between absorption and reflection is expressed analytically in the Kramers-Kronig relations which connect n and k, or ϵ_1 and ϵ_2, or reflection amplitude and phase. Thus, by measuring reflection amplitude, one can compute reflection phase from the relations. These in turn give us n and k from which T, the quantity of light transmitted through the sample, can be computed. This close relationship between reflection and transmission encourages us in reflection studies for, knowing k or ϵ_2, we can determine more energy gaps.

However, we must recognize certain experimental limitations: an accurate determination of n and k presupposes an accurate knowledge of the absolute value of R for all wavelengths. R must be estimated at unmeasured wavelengths and this estimate will affect n and k values at measured wavelengths.

B. EXPERIMENTAL PROBLEMS

Once one has admitted the usefulness of reflectivity measurements, the problem arises of designing equipment to measure magnitudes accurately and to determine fine structure.

1. Standard Method

The usual method employed in reflection and absorption measurements is to arrange a simple optical system in which monochromatic light illuminates a sample, is reflected (or transmitted), collected at a detector and amplified for display on a recorder. The spectral range of interest is swept twice: once with the sample in the light

beam and again without the sample. The two resultant traces, when divided, give the percent of light reflected.

There are two major disadvantages to this technique. Drift in the components, particularly the light source, occurs between the two sweeps. This limits resolution of amplitude changes to 1% of reflection amplitude. The standard employed is that amplitude change / drift = signal / noise = 1.

A second disadvantage is the delay that arises from the laborious process of reading intensities, dividing them, and then plotting the results before the experiment can be evaluated. This objection is not just a matter of convenience. Often one experiment suggests another, and if results are not known immediately, it may be difficult or impossible to return to the original conditions. Changes of conditions during the time of the experiment may be difficult to detect, and the need for further measurements requiring greater amplitude or wavelength resolution will be less obvious.

C. FURTHER MOTIVATION PROVIDED BY PHYSICAL PROBLEMS

The objections just cited are concrete enough, but one should ask if they are of significance in the types of experiments one considers performing. A number of examples can be adduced to support the construction of an improved experimental system: specifically, the ratio reflectometer to be discussed later.

(1) In the first measurement of the reflectivity of germanium at normal incidence [1-05], a bump was noted at 2.15 eV, eventually ascribed to transitions occurring at a point along the 111 direction in $\vec{k}$ space. Determination of the splitting of this peak awaited the work of Tauc and Antončík [1-06]. The dip between the two peaks was small, about 1% at a reflectivity of 55%. Very careful point by point measurements were necessary to resolve them. A ratio system could and does display them directly. In general, such spin-orbit splittings are small and are crucial in identifying reflectivity structure in terms of the Brillouin zone energy bands.

(2) One can modify reflectivity structure by applying various stimuli to a sample. Uniaxial stress can cause splittings and wavelength shifts [1-07]. Electric fields will cause wavelength shifts and change structure [1-08], while magnetic fields will add an undulant ripple to the basic structure [1-09]. Often these changes are small, either because of limitations in the size of the stimulus one can apply, or because one wishes to study the effect as a function of the magnitude of the stimulus. Often a small value of a parameter, such as electric field, will produce a different effect from a large value [1-10].

One applies these stimuli because they give additional information, such as an effective mass, deformation potential, or symmetry information, not derivable from reflectivity alone. An experimental system with good resolution in amplitude and wavelength is necessary to measure these effects.

(3) Another class of experiments is concerned with the absorption caused by deep-lying impurities in semiconductors. Their energy levels lie closer to the center of the fundamental gap than do those of the hydrogenic impurities. It has generally proved impossible to get concentrations of these impurities large enough to note their direct effect on the absorption of light. One exception is sulfur-doped silicon, but even here concentrations are low: 10^{15} - 10^{16} impurities/cm^3 [1-11]. The presence of impurities is usually detected in photoconductivity measurements. The direct absorption measurement is more satisfactory, since one need not contend with the conduction mechanism which complicates interpretation. Electron spin resonance experiments are complementary, but do not replace the information gained in an absorption experiment.

Because deep-lying impurity concentrations are low and their wave functions highly localized, one must have high amplitude sensitivity to detect their presence over background absorption. Commercial double-beam units are not well adapted to this problem. The Cary 14 spectrophotometer† cannot detect changes smaller than .1% near 100% transmission. The ratio reflectometer, when modified for absorption, should be better by an order of magnitude.‡

Thus, three classes of measurement motivate the construction of a ratio reflectometer: the fine structure of reflectivity, fine structure induced in reflection spectra by applied stimuli, and the

---

†Applied Physics Corp., Monrovia, California.

‡This estimate is based on sensitivity in reflection measurements. No absorption measurements were made.

small absorption in certain materials such as that caused by deep-lying impurities in semiconductors.

D. THE RATIO REFLECTOMETER

A ratio reflectometer is an admirable solution to the two problems of amplitude sensitivity and slow data readout. Indeed, it was the experimental limitations which they implied that provided the initial motivation to construct this instrument.

Conceptually, a ratio reflectometer is very similar to the double-beam units sold commercially for absorption measurements. Light from a monochromator is divided into two beams. One beam illuminates the sample and the other provides a reference channel without sample. Detection and electronics are contrived to present ultimately the light intensity reflected from the sample divided by that from the reference channel. A recorder displays R, the reflectivity.

1. Sensitivity

By switching the light quickly from one channel to the other, drift and noise of frequency which is low compared to the switching frequency do not affect the reflectivity ratio. Amplitude sensitivity is improved. Under optimum conditions (Sec. II-D-5) signal changes as small as .05% can be detected. Again, the criterion is that signal change/noise = 1. Various experimental complications, detailed in the next chapter, prevent realization of this sensitivity under some conditions.

When even greater sensitivity is required, a multichannel analyser can be coupled to the ratio reflectometer, thereby improving signal amplitude sensitivity by a factor equal to the square root of the number of scans through the spectrum. Use of the multichannel analyser proved desirable in magnetic field studies.

7. Rapid Readout

The ratio reflectometer displays directly and immediately the reflectivity on a chart recorder. If care is taken in alignment, this readout is within ±5% of the absolute reflectivity.†

Scale expansion capabilities provide selection of nearly any arbitrary upper and lower percentage limits for the recorder presentation. Thus, an initial run can be made looking at a sample spectrum in gross detail and then immediately followed by a finer examination of regions of special interest. This does not merely save time, although that is important in that it enables one to make corroboratory measurements, but more important, one can make different measurements before experimental conditions change. Time dependent phenomena are strikingly displayed. Some relate to phenomena in the samples themselves. Others are a result of degradation in certain experimental components. Both are worth knowing about; the first suggests new effects, the latter prevents waste effort on false effects.

---

† Bennett and Koehler [1-12] give a description of an instrument where absolute errors are reduced to .1%. If one wishes an absolute calibration for our system, an instrument conceptually similar to theirs should be constructed and sample reflectivity then checked at a few discrete wavelengths.

3. Sample Geometry

A third consideration in designing and constructing a ratio reflectometer is the flexibility it provides in ensuring that the sample volume be sufficiently large. By sample geometry, we mean not just the sample and its mounts, but also the ancillary equipment necessary for temperature control and application of stimuli, including magnetic field. Commercial units are limited in this respect, since volumes are small and not easily modified.

In conclusion, a ratio reflectometer is justified in terms of its improved performance in sensitivity, rapid readout, and adequate sample volume.

E. $\Delta R/R$ EFFECTS

Close to the time of completion of the ratio reflectometer, new techniques were advanced, capable of measuring far smaller changes in reflectivity. These are called $\Delta R/R$ measurements and utilize phase sensitive detection of the effects upon sample reflectivity of an AC stimulus such as an electric field [1-13, 1-14] or uniaxial stress [1-15]. Alternatively, one can modulate the wavelength of light incident on the sample and again use phase sensitive detector systems to measure the results [1-16]. Changes as small as 1 in 10^6 have been detected [1-17].

ΔR is the modification to reflectivity caused by the given AC stimulus. Thus, when we modulate wavelength, $\Delta R = (dR/d\lambda)\Delta\lambda$, where

$\Delta\lambda$ is the rms excursion of the wavelength. Similarly, with electric field the ΔR is related to dR/dE. The way in which the experiments are typically performed results in normalizing ΔR with R.

By measuring slope, such as $dR/d\lambda$ or dR/dE, the $\Delta R/R$ measurement may isolate structure much more readily than a measurement of R. Further, the detection only of that quantity related to the slope, ΔR, and not the far larger R, results in greatly enhanced sensitivity. More explicitly, we are not detecting R and then differentiating it; rather, we measure the quantity ΔR directly.

If one is interested in structure from an unperturbed sample, the best technique is that of varying the light wavelength by use of an oscillating slit assembly. The variation of any other type of stimulus, such as electric field or stress, raises the question of how the stimulus modifies the effect being studied. Change certainly occurs with electric field measurements and the effect of the field must become an intimate part of any evaluation of the experimental data. Fortunately, present theory for electric field measurements gives direct interpretations of the optical structure in terms of the energy bands [1-18, 1-19]. Incidentally, the electric field of the light probing the sample is too small to be of concern except in the case of laser sources.

In short, $\Delta R/R$ techniques provide a sensitive probe of band structure, differing from R measurements in their capabilities. The AC modulation can be used to study the unperturbed sample or the effect on it of various stimuli such as electric field, magnetic field, or stress.

F. ΔR/R INSTRUMENTATION

The ratio system proved readily adaptable to ΔR/R measurements in which electric field is the stimulus. The only major addition was feedback circuitry to permit automatic normalization of the data. One measures ΔI_R = change of the intensity of the reflected light. This is proportional to the level of reflected light = I_R. In general, $\Delta I_R/I_R = \Delta R/R$, so if I_R = constant, ΔI_R is proportional to ΔR/R. Feedback keeps I_R = constant.

The ΔR/R instrumentation offers the same advantages cited in the ratio reflectometer design itself: higher sensitivity, faster viewing of results, and large sample volume. The smallest signal change detectable in these experiments depends on total light intensity which in turn is determined by source intensity and slit width. The latter can be varied somewhat at will provided necessary resolution is not lost.

We applied the electric field by using the sample as one electrode of an electrolytic cell, a technique originally developed by Williams [1-20] and applied with great success by Cardona [1-21].

G. COMPARISON OF R AND ΔR/R METHODS

In our own work, we have made both R and electric field ΔR/R measurements. The primary focus has been upon reflectivity. But we have attempted to see how that technique might supply information either lacking or confused in ΔR/R studies.

$\Delta R/R$ techniques are generally superior:

(1) $\Delta R/R$ structure which is many times the noise level often has no reflectivity counterpart which is discernible above the noise.

(2) $\Delta R/R$ line widths are narrower. For instance, the "Q" of the germanium Λ transitions is roughly 50 in Seraphin's electric field $\Delta R/R$ study [1-14] and 3 in reflection. (Compare Figs. 4-21 and 4-6.)

(3) The $\Delta R/R$ peaks suffer less broadening with temperature increase.

(4) $\Delta R/R$ peaks induced by electric field are generally quite close in energy to the corresponding transition in the Brillouin zone, while reflectivity peaks may be .1 to .2 eV away.†

(5) We have noted the effect of an H field on the Λ transition in germanium in the presence of an electric field where no effect was noted in a straight reflectivity measurement.

Nonetheless, reflectivity serves a number of useful purposes:

(1) The analysis of $\Delta R/R$ data requires a knowledge of n and k. These are derivable from reflectivity provided one makes a reasonable attempt to measure the absolute level of R and not just relative changes in its magnitude. Our own wide spectral range studies of gray tin can be used in a Kramers-Kronig analysis to give the first n and k values for that material.

---

†The peaks in $\Delta R/R$ occur at the same energies as those in $\Delta\epsilon_1$ and $\Delta\epsilon_2$ (Eq. 5.16), both of which theoretically peak when the joint density of states factor is a maximum. On the other hand, R is a function not only of ϵ_2 but of ϵ_1. The dispersive contribution results in a shift in R from the peak in ϵ_2.

(2) We have noted structure in R which is missing in $\Delta R/R$ studies, e.g., one of the $L_{3'} \rightarrow L_3$ transitions in gray tin.

(3) R structure is not subject to the satellite effects occurring in $\Delta R/R$ measurements under electric field. These satellites are additional structural features associated with one transition. Consequently, R structure, when seen, may be more easily interpreted. In our own work, this has proved relevant in the analysis of structure in germanium near 3.2 eV and in α-Sn near 3.3 eV.

(4) Optical transition selection rules change under the application of an electric field. For example, some forbidden transitions become allowed. $\Delta R/R$ structure in the α-Sn spectrum has been tentatively assigned to an electric field permitted transition [1-22]. By noting small structure at the same energy in reflectivity, we have disproved the original identification.

BLANK PAGE

CHAPTER II

RATIO REFLECTOMETER INSTRUMENTATION

In the design and construction of the ratio reflectometer there were three major areas of concern.

(1) Optics: implementation of beam splitting so as to permit ratio measurements with a minimum of reflectivity error.

(2) Electronics: maximization of linearity and sensitivity in the processing of the signal and minimization of noise.

(3) Sample geometry: sample arrangement to permit measurements at low temperature and under magnetic fields or applied stress.

The reduction of noise, electronic and vibrational, was a major problem in all three areas. Once this was solved, the system worked with linearities of about 1% and maximum sensitivities of .05%.

The discussion of the ratio reflectometer is divided into three parts:

(1) Design features of the final state with discussion of relevant problems.

(2) Capabilities and limitations.

(3) Alignment and use.

A. OPTICAL DESIGN FEATURES OF THE RATIO REFLECTOMETER IN ITS FINAL STATE AND RELEVANT PROBLEMS

1. Basic Concepts in Design

Care in optical design was central to the attainment of improved sensitivity, rapid readout and adequate sample volume. The prime optical feature was the use of a double-beam system, whereby monochromatic light is switched alternately between the sample and reference paths. The beam splitter itself was of major importance. Equally important was the quality of optical components, such as mirrors, where reflectivity structure might induce errors in $R(\lambda)$, the reflectivity of the sample. The System Block Diagram (Fig. 2-1) shows a generalized layout of the double-beam system. The special features are more evident in the details seen in Fig. 2-2.

Light from a source (xenon arc or tungsten) is focussed on the entrance slit of a grating monochromator (JACO 82-000). Dispersed light is chopped (1080 Hz) and filtered upon leaving the monochromator. After passing through the first mirror system, it is divided into two beams by the beam splitter at 13 Hz. After the sample beam is reflected, both beams are spatially recombined though temporally separated. The second mirror system permits focussing on a choice of detectors, usually photomultiplier tubes. The remaining processing is electronic.

Aluminum mirrors have structure which modifies in time due to oxidation [2-01]. Therefore, the light intensity at the monochromator

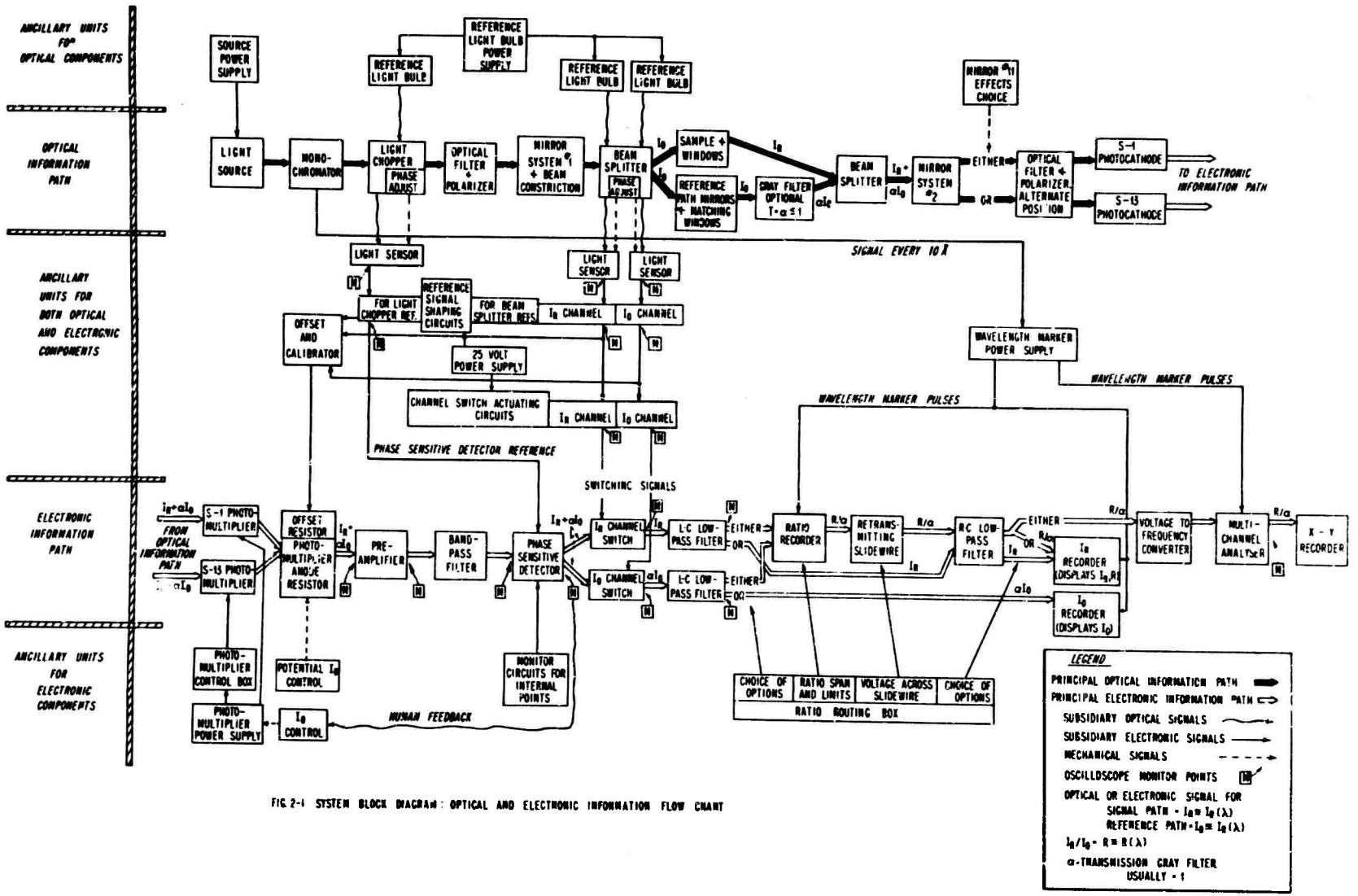

FIG. 2-1 SYSTEM BLOCK DIAGRAM: OPTICAL AND ELECTRONIC INFORMATION FLOW CHART

exit slit ($= I_0^{m.s.}(\lambda)$) is reduced at each reflection by the factor $R_x(\lambda)$, which is the reflectivity of the xth aluminum mirror. These aluminum reflection factors may vary from one mirror to another or over a given mirror surface. If light from the two beams should fall on different mirrors, or on different portions of the same mirror, false structure in the reflectivity measurement could result.

This would certainly occur if the sample and reference beams underwent an unequal number of aluminum mirror reflections. Figure 2-2 shows the optical layout in detail. When the beams are separated, each undergoes the same number of reflections from mirrors whose surfaces were simultaneously deposited; when recombined, the two beams' images are superposed. By affecting each beam in the same way and to the same degree, the effects of mirror reflections are cancelled out.

A similar philosophy is applied to the detector (and also the electronics). A single detector is employed and the images of the two beams are defocussed and superposed to minimize the effects of variation in detector sensitivity. Analytically we could say, if:

$I_0^{m.s.}(\lambda)$ = light intensity at the monochromator exit slit, (2.1)

$I_R(\lambda)$ = detected light level reflected from the sample, (2.2)

$I_0(\lambda)$ = detected light level in the reference beam, (2.3)

$R(\lambda)$ = percent of light reflected from the sample, (2.4)

$R_x(\lambda)$ = percent of light reflected from mirror # x, (2.5)

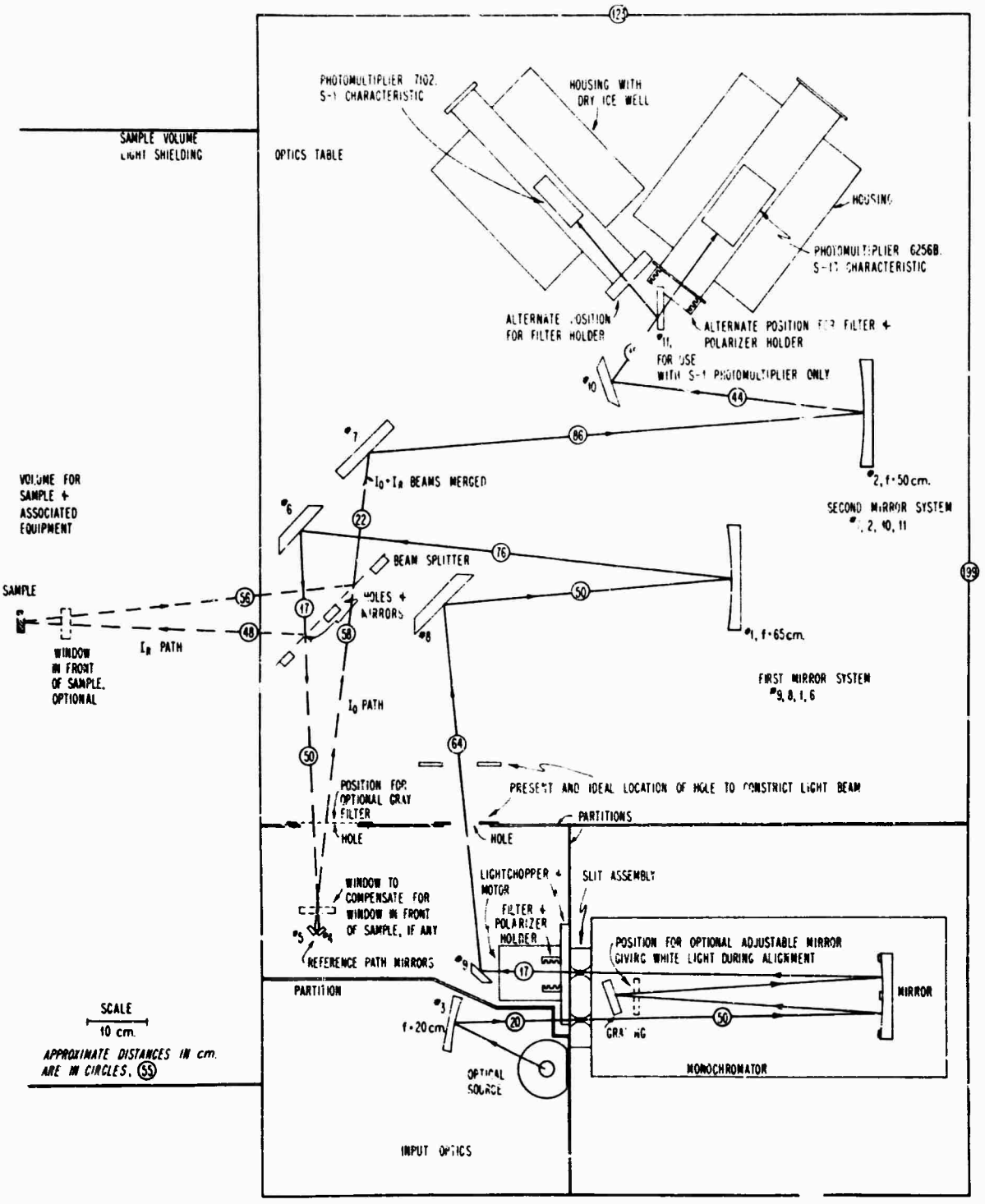

FIG 2-2 OPTICAL LAYOUT

$D(\lambda)$ = a function proportional to the response of the detector to light, (2.6)

then

$$\frac{I_R(\lambda)}{I_0(\lambda)} = \frac{I_0^{m.s.}(\lambda)R_9R_8R_1R_6R_{B.S.}R(\lambda)R_{B.S.}R_7R_2R_{10}R_{11}D(\lambda)}{I_0^{m.s.}(\lambda)R_9R_8R_1R_6R_5 \qquad R_4 \quad R_7R_2R_{10}R_{11}D(\lambda)} = R(\lambda) \qquad (2.7)$$

provided $R_5 = R_4 = R_{B.S.} \equiv R_{\text{Beam Splitter}}$[†], and provided images are superposed on individual mirrors.

The wavelength range is determined by the source, monochromator grating, and detector. At the time of writing this range was 2300-11,000Å although it could be extended into the infrared.

A double-beam system, employing a beam splitter in conjunction with a specially chosen optical layout, ensures proper performance of the ratio reflectometer with a minimum of distortion. Individual components can be considered within this framework.

2. Sources

The criteria for sources are simple. First, they must exhibit short term stability to eliminate noise. Slow drifts pose no problem because of the dual beam nature of the system. Second, they must maximize the intensity of light entering the monochromator. This requires that the source have as high a brightness temperature as possible and that its area be large enough to fill the entrance slit of the monochromator. Shot effects in the detector are a significant

---

[†] In the instrument described in ref. [1-12], high accuracy in absolute R values (.1%) is attained by interchanging mirrors equivalent to our mirrors #4, 5, and the beam splitter, and then averaging the R values measured under the different conditions.

source of noise. Since S/N is proportional to $\sqrt{\text{Intensity}}$ in the case of shot noise, high source intensity ensures that this noise is not the limiting factor in over-all system performance. Third, source intensity should vary slowly with wavelength. Emission spikes resulting in sudden large amplitude changes may bring the electronic system into regions of nonlinearity.

a. Tungsten Sources. The best tungsten sources are the iodine quartz lamps which can operate as much as 400°C hotter than the usual tungsten ribbon filament. The iodine vapor serves as a catalyst to scour the inside of the quartz envelope free of vaporized tungsten. The filament lasts longer and there is no coating of tungsten on the envelope to cut down intensity. The light output is remarkably stable in time, and long term drift does not exceed 1%/hour, 3% over its lifetime. Intensity is higher than in the usual filament lamps, as shown in Table 2-1, and varies smoothly with wavelength over the useful range of 2800Å-2.7μ (the quartz cutoff). The question of range is discussed more fully under filters.

The disadvantages of these tungsten sources are their short life at maximum temperatures and their coil-like shape, which results in uneven illumination of the slit and hence of the sample. Also, it is important that the lamps be run at no less than 90% of rated wattage. If they are too cool, the iodine catalyst is ineffective and they become noisy.

TABLE 2-1 LIGHT SOURCE CHARACTERISTICS

Source Type	Identifying Number	Color Temperature	Relative Brightness at 5300Å	Lifetime	Size of Hot Element (HxW)
Ribbon filament tungsten	GE 9A/T8½/L	2950-3000°K	0.08	200 Hrs.	.68" × .04"
Iodine quartz tungsten	GE 6.6A/T4/CL	3050-3100°K	0.17	500 Hrs.	.4" × .12"
Iodine quartz tungsten	SYL DXM	3400°K	0.44	10 Hrs.	.325" × .08"
Xenon arc	Osram 450 watt	9000°K	2.0	2000 Hrs.	.105" × .020"
Xenon arc	Osram 150 watt	9000°K	1.2	1200 Hrs.	.088" × .035"

b. Xenon Sources. Xenon sources have extraordinarily high brightness temperatures and considerable intensity in the UV range, a region inadequately covered by the tungsten source (Table 2-1 and Fig. 2-5a). Disadvantages limit their usefulness, however. Short term stability is worse than in the tungsten source; at best, there are noise spikes and steps of about ½%. As the source ages, or if it is initially poor, these may increase to 20%. To minimize this effect, the current level must be carefully chosen to ensure that the source is neither too hot nor too cool. As a consequence, noise due to source instability is often the limiting factor in system performance. The bright spot is only 1/3 of maximum slit height, resulting in only partial filling of the slit. Motion of this spot can add to noise. Emission spikes mar much of the range. Useful

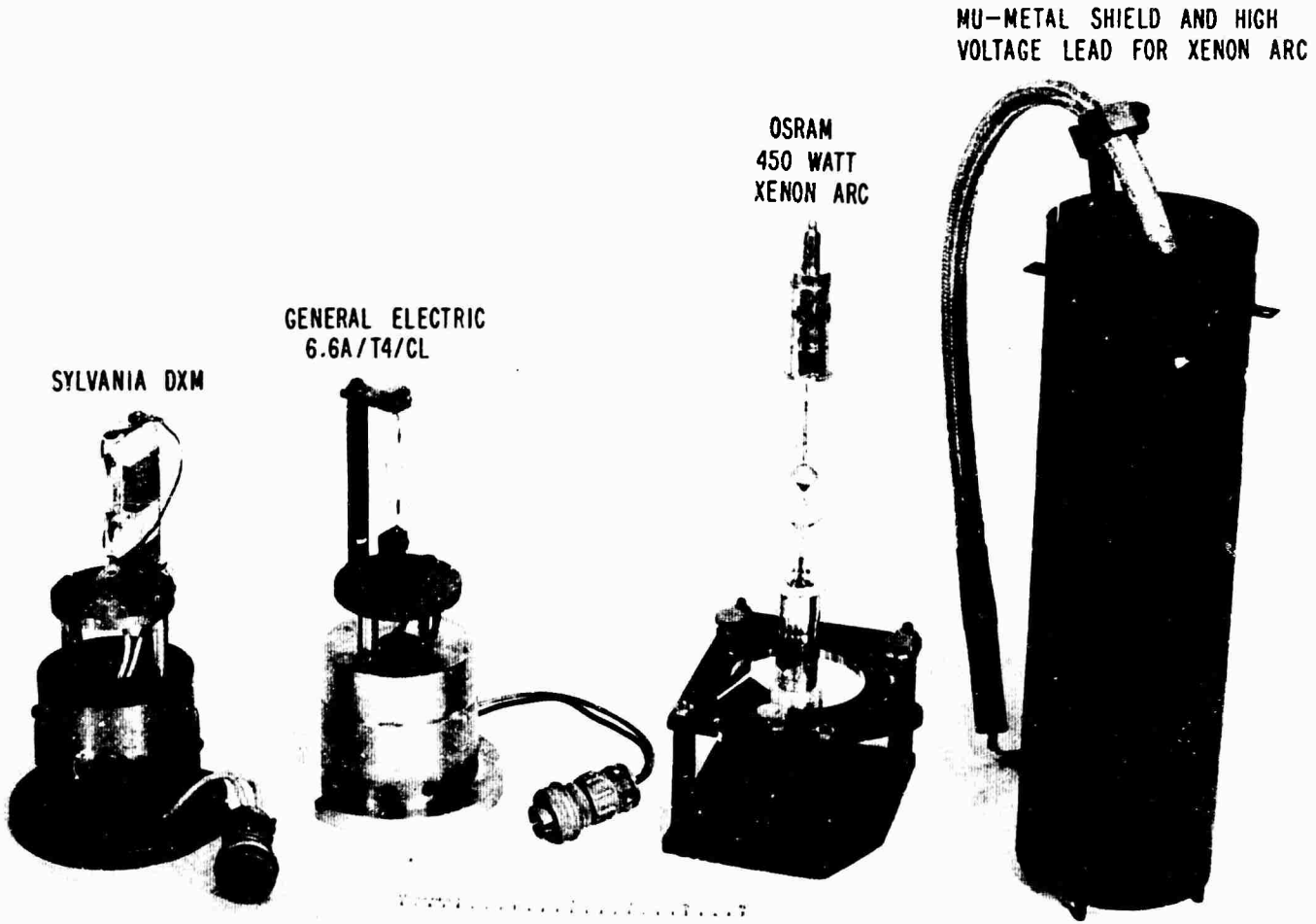

FIG. 2-3 OPTICAL SOURCES MOUNTED IN THEIR HOUSINGS

wavelength ranges are 2300-4500Å, 5000-7500Å, 7620-8010Å. Ozone production can at times pose a health hazard.

Since the gas discharge plasma moves as the ambient magnetic field changes, one must shield the source with a mu-metal housing during magnetic field measurements. Fringing fields from the electromagnet as low as 5 gauss cause the arc to distort so much that it is extinguished. Lower fields will deflect it, causing a change in slit illumination. This in turn can result in a modification of reflectivity structure if the sample's reflectivity varies over its surface.

c. Other Sources. Other possible light sources include the deuterium arc source. In choosing between the deuterium and xenon arcs, the important criterion is the relative noise each imparts to the total system. The shot noise of the dimmer deuterium arc is more serious than the xenon arc's greater instability, so that the xenon arc is the preferred choice.‡ The Sylvania Metal Arc source was tested and found unsatisfactory because of its low intensity compared to the xenon and tungsten sources. For the infrared, one would use a globar.

d. Sources Utilized in the System. An Osram 450 watt xenon arc source† is used for the UV and part of the visible spectrum (2300-4500Å) and occasionally for the full visible range (out to 7500Å). When maximum intensity is needed in the visible and near infrared, the Sylvania DXM is the best choice, while the General Electric

---

†MacBeth Sales Corp., Newburgh, New York

‡The exception to this occurs at wavelengths less than about 2500Å where the smaller scattered light level of the deuterium source makes it definitely preferable.

6.6A/T4/CL is better for long runs where lesser intensity is tolerable.

There are adjustable mounts for each of these sources, and they are imaged on the entrance slit of the monochromator with a concave, aluminum-coated mirror. This was chosen in preference to a quartz lens so that the ultraviolet range could be extended as far as possible. Figure 2-3 is a photograph of these three sources.

e. Input Optics. The object distance and image distance of the source optics are adjusted to maximize the amount of light collected by the monochromator and to minimize the changes in intensity due to source motion arising from vibration or thermal effects. A complete theoretical study of this problem takes into account the source dimensions, slit dimensions, and f number of the monochromator, as well as mirror diameter and focal length. The conclusions depend on the relative size of the source and slit. If the source is larger, as in the tungsten sources, then magnification should be 1, and the f number of the input optics and monochromator† should match so that the monochromator acceptance angle is filled with light.

If the source is smaller than the slit, as in the xenon source, then theory predicts that more light will be collected if there is sufficient magnification to fill the slit with light. Again, f numbers should match. In practice, when the magnification is large enough to fill the slit, the source is so close to the mirror that it blocks part of its own image and aberrations further reduce the amount of light collected. Since there is no gain from increasing the magnification, in actual use it has been left at about 1 for all sources.

---

†Monochromator f number is f/9.

The considerations above determine mirror magnification and f number. The mirror focal length is determined by the finite size of the sources and their housings. Figure 2-2 shows that the input optics are slightly off-axis. For a given size of source, the shorter the focal length, the more off-axis will be the input optics if the source is not to block its own reflected image. But the more off-axis the optics, the more light is lost by aberrations. Thus, the focal length of mirror 3 has been chosen long enough to permit the input optics to be only slightly off-axis when magnification is about 1.

f. Source Power Supplies. To prevent intermodulation effects, discussed later (Sec. II-B-21), sources should be fed from direct current power supplies. If the ripple in the power supply results in a source output ripple of no more than 1% (peak to peak) of the DC level, then this noise will be nearly an order of magnitude less than that created by unavoidable fluctuations in the electronics.† Both tungsten sources are powered by a Sorensen DCR 40-10‡ supply, and the xenon arc by an Ionics PSXE-450.†† Both supplies fulfill the ripple criterion.

g. Wavelength Calibration Sources. Two calibration sources are useful: a low pressure mercury lamp and the Philips' Hg-Zn-Cd lamp Type 94136. Most of the wavelength range is covered by the

---

† This fluctuation is found in the phase sensitive detector DC level discussed in Sec. II-B-6-a.

‡ Sorensen, South Norwalk, Connecticut

†† Ionics, Inc., Watertown, Massachusetts

mercury lamp. A few gaps, particularly in the UV range of 2000-2300Å, are nicely supplemented by the Zn and Cd lines in the Philips' lamp.†

The wavelengths of the calibration lines are those listed in the article by Zwerdling and Theriault [2-02].

3. Monochromator

a. Capabilities. The light is dispersed by a Jarrell Ash 82-020 ½ meter grating monochromator of Ebert design. Entrance and exit slits are adjustable in synchronization from 5 to 3000μ with a maximum resolution of .2Å in first order in the visible. Slit height can be set from 20 to zero mm. A kinematic mount permits swift grating interchange: the system is supplied with one 30,000 lines/inch grating blazed at 7500Å and another with 7500 lines/inch blazed at 1.1μ. The resultant wavelength range is from 2300Å to greater than 1.1μ. A wavelength counter, coupled directly to the grating drive, gives wavelength readings within 2Å of the true wavelength for the 7500Å grating. For the other grating, this figure is multiplied by the inverse ratio of dispersion; e.g., $2 \times \frac{30,000}{7500} = 8$Å. Once the system is calibrated for the 7500Å grating, the grating removed and then replaced in its kinematic mount, one can be assured that the output wavelength will be within 2Å of its calibrated value over the grating wavelength range without further calibration. These features are summarized in Table 2-2.

Wavelength can be adjusted by hand,or swept by motor drive at a rate linear with time. Rates are 2, 5, 10, 20, 50, 125, 250, 500Å/min.

---

† Philips, Eindhoven, Netherlands

TABLE 2-2 MONOCHROMATOR CHARACTERISTICS

Grating Number	Blaze λ	Lines/ Inch	Dispersion At Exit Slit	Wavelength Range	Maximum Resolution	Counter Accuracy Over Full Range	Reset-ability Over Full Range
35-00-58-38 #423BB	7500Å	30,000	16Å/mm. in first order	1750[1]-9250Å	.2Å [2]	2Å [3]	2Å [3]
35-00-58-69 #489H9	1.1μ	7,500	64Å/mm. in first order	7600Å-1.32μ[4]	.8Å [2]	8Å [3]	8Å [3]

[1] Scattered light and low source intensity limit the lower wavelength to around 2300Å.

[2] The maximum resolution can be improved by a factor of 2 over limited wavelength ranges if care is taken in adjustment.

[3] Counter accuracy and resetability can be improved with careful adjustment.

[4] Measurements have been made up to 1.32μ, although intensity diminishes quickly above 1.1μ. With infrared detectors, other than the S-1 photomultiplier, this upper limit could be extended.

A signal suitable to actuate a wavelength marker is created every 10Å. Error in the firing of this signal does not exceed .25Å.

b. Problems and Changes. Those capabilities enumerated above did not always exist and represent considerable improvement in the original monochromator.

The original grating interchange procedure was laborious, requiring up to a day for change, adjustment and calibration. This delay adversely affected the rapid readout feature of the system. Certain

measurements, requiring full wavelength range, were not very feasible. A company installed modification, employing a kinematic mount in the monochromator and a mating kinematic holder for each grating, facilitates interchange. With this new arrangement, grating interchange time is reduced to two minutes, a time compatible with general system philosophy. One precaution should be noted. The grating holder is held in the mount by a spring. If this spring is improperly positioned or weak, the grating will shake in response to beam splitter and light chopper vibrations. Any imbalance in the light chopper blade will aggravate the problem.

Adequate intensity is indispensable for attaining amplitude sensitivity. A combination of bright source and widely variable slits is necessary. When white light is employed, intensity at the monochromator output is proportional to slit width squared. The monochromator is now fitted with an improved slit assembly which gives 30 times the maximum slit width of the former unit, or 900 times as much light. In general, one would use the maximum slit width consistent with necessary resolution.

A wavelength marker pulse is essential to accurate reading of experimental data. The original monochromator came without this feature.

Too much scattered light is a deficiency of the JACO monochromator. Over most of the wavelength range, the ratio of light intensity at a given wavelength to scattered light intensity is satisfactory (between 100 and 5000). But below 2600Å the ratio

falls off steeply. Excess scattered light distorts the measured reflectivity and imposes a practical lower wavelength limit of 2200-2300Å. There is a more complete discussion in Sec. II-A-5, where partial solutions to this problem are discussed.

Slit height adjustment serves two functions. When a small source only partially fills the entrance slit, blocking off the remainder reduces scattered light. Secondly, some samples are shorter than the slit. Reducing the slit height ensures that only the sample reflects light, which in turn reduces reflectivity errors; it also diminishes noise due to light beam motion.

c. Polarization Dependent Structure Created by the Grating. The grating and slits in a monochromator partially polarize the light. The intensity of light polarized parallel to the slits varies smoothly with wavelength, while that polarized perpendicular to the slits shows a large amount of additional structure. When the perpendicular polarization is used in reflectivity measurements, the reflectivity exhibits false structure which correlates closely with the I_0 structure.

Elimination of this structure requires certain precautions. Only light polarized parallel to the slits should be used. Measurements with unpolarized or perpendicularly polarized light should be avoided. Because of the variation with wavelength in the spatial distribution of the light, the beam should be constricted prior to arriving at the beam splitter by an iris (shown in Fig. 2-2) so that

no light is lost at the beam splitter in either the I_O or I_R channels. Care should be taken in the rest of the system to ensure that the light beam does not extend beyond the mirrors or sample. At the photomultiplier the images of both channels must be exactly superposed and must not extend beyond the photocathode. Finally, no measurements should be performed with optically active samples or system components unless total compensation can be assured.

This problem is discussed in considerable detail in Chapter III, where some physical insight is gained. For those interested only in an enumeration of conclusions and related experimental procedures, Secs. III-B, III-F-4 and III-H are particularly relevant.

d. Calibration. Calibration is easy because the wavelength drive is nearly linear and deviates only slightly from counter readings.

The important features of the monochromator are: its adjustable intensity; good resolution; swift, accurate grating interchange; and easy wavelength readout.

4. Light Chopper

A light chopper, placed close to the monochromator exit slit, alternately obscures and passes the light at 1080 Hz. The need for it is twofold, arising from the electronic detection method.

(1) Certain detectors with good signal-to-noise characteristics exhibit 1/f noise. While photomultiplier noise has a flat frequency characteristic [2-03], various semiconductor detectors used in the

infrared, such as PbS, InAs, and impurity-doped germanium, display 1/f noise. Causes are found in photoconductive dark current [2-04], generation and recombination of charge carriers [2-04], and crystal surfaces and contacts [2-05]. By operating at a high enough frequency, 1/f noise becomes negligible compared to that from other sources such as shot noise. Any frequency over 400 Hz is satisfactory.

(2) It is preferable to use AC amplification methods since they eliminate the drift problems found in DC methods.

The light chopper is shown in Figs. 2-4a and 2-4b. Each of its components serves an important function.

a. Frequency and Blade. The chopping frequency is adjustable by changing the number of holes in the blade. The motor rotates at 30 Hz. A lower limit on frequency is set by 1/f noise considerations, and the attempt to reduce intermodulation effects between this frequency and that of the beam splitter (see Sec. II-B-21), which suggests raising the frequency. An upper limit is imposed by two factors.

(1) As frequency is raised, the width of each hole decreases until it soon becomes comparable with the size of the beam. (Remember that slit width varies from 5μ to 3000μ = 3 mm.) When they are comparable, the average light intensity is reduced and the fundamental of the chop frequency becomes smaller. This adversely affects signal/noise. Average chopper hole width for a 1080 Hz chopper is .22" and ½" for a 450 Hz blade.

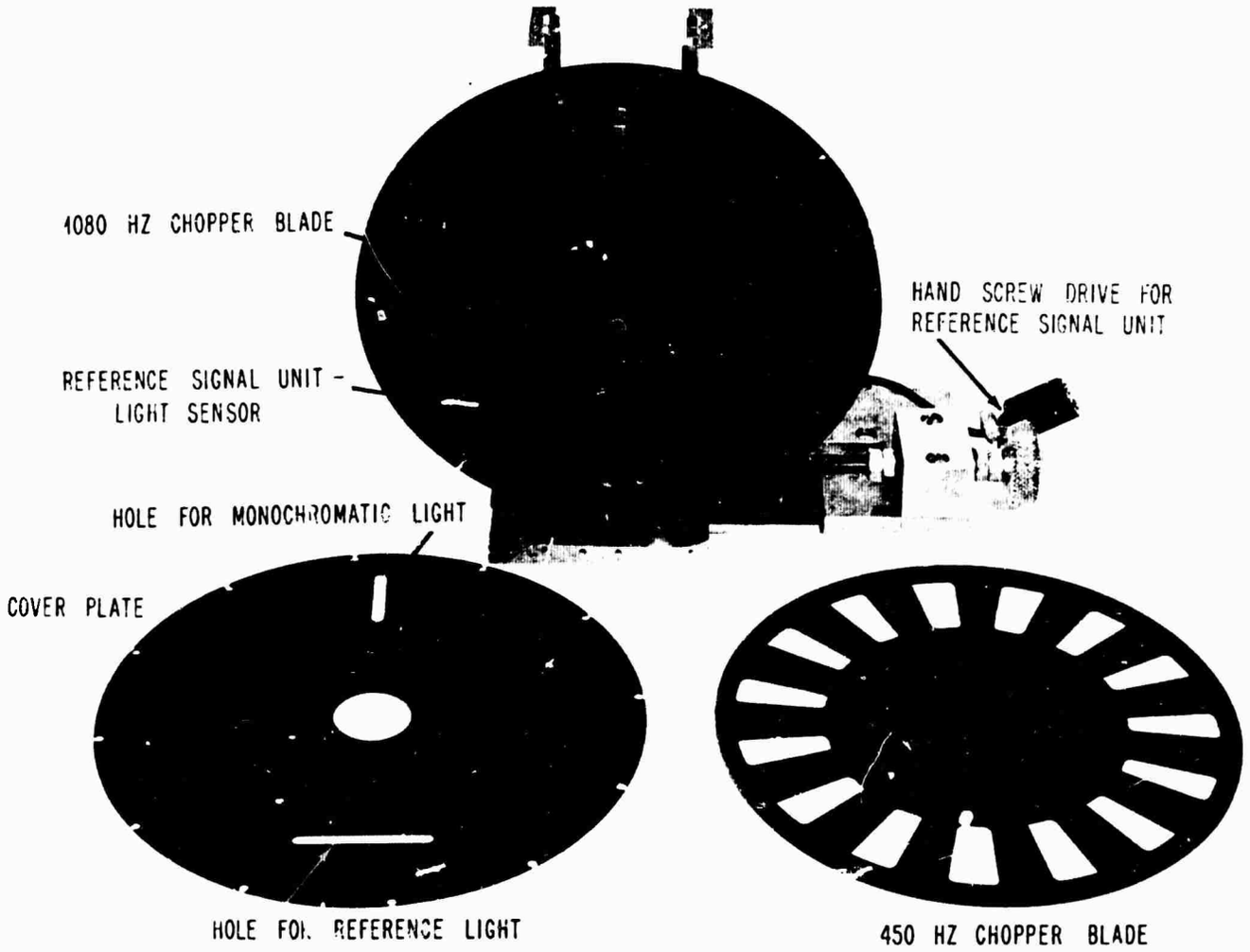

FIG. 2-4a LIGHT CHOPPER, FRONT VIEW

(3) Machining tolerances become an increasing fraction of the hole width as frequency increases. However, the resultant modulation of the chopping frequency is not serious because it occurs at the rotation rate of the blade, 30 Hz, and is filtered out.

There are chopper blades for 400, 450, and 1080 Hz.

b. Blade Position. The light leaving the monochromator diverges from the exit slit. To ensure that the beam size is as small as possible in relation to the chopper holes, the chopper unit is placed in contact with the exit slit. This placement is based on the same consideration, light intensity, cited above in determining the upper limit on chopper frequency.

c. Reference Signal Unit. The AC component of the light is eventually processed by a phase sensitive detector. These detectors require a reference signal phase-locked to the experimental signal. As the monochromatic light for the experiment passes through a hole in the upper portion of the chopper, light from a small bulb† passes through another hole, 180° away, and is detected with a light sensor.‡ The reference light is processed in electronic units described later. Thus, experimental and reference signals are phase-locked. Their relative phase can be controlled and optimized by moving the light-sensor assembly relative to the lower hole by means of a hand screw drive. In practice, this method of adjustment proves to have adequate sensitivity. It is reliable and not subject to the shifts due to component aging which might occur in electronic equivalents.

---

†Dialco #39, Dialight Corp., Brooklyn, New York

‡Type LS 222, Texas Instruments, Dallas, Texas

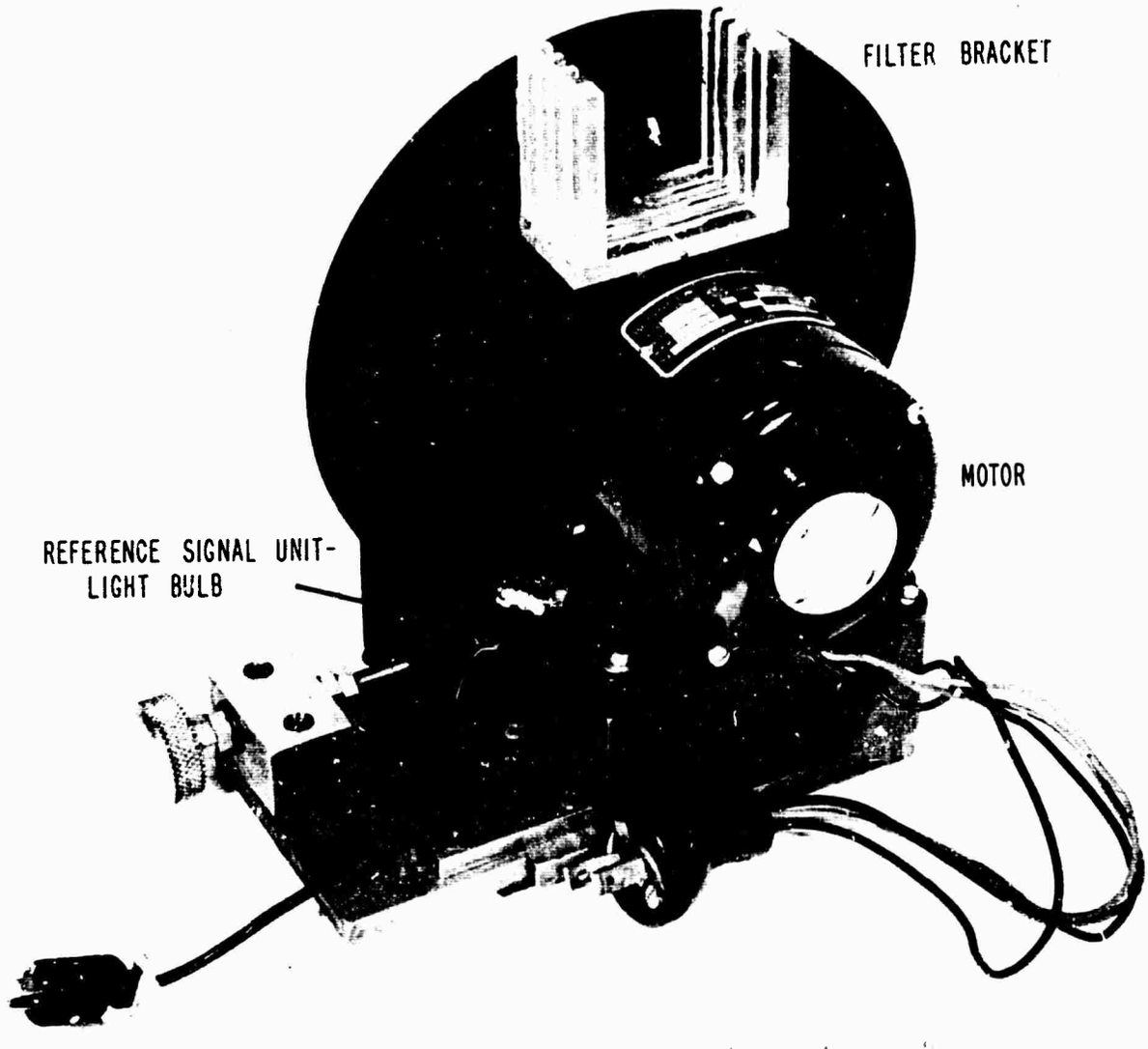

FIG. 2-4b LIGHT CHOPPER, REAR V'EW

The small bulb is powered by a DC supply to ensure that there are no intermodulation effects between 120 Hz (AC heating frequency) and the chop frequency.

d. Motor. The blade is mounted directly on the shaft of a 1/75th hp, 1800 rpm synchronous motor. It is important that the motor be synchronous and of adequate power so that the blade will rotate at a constant velocity with no slippage or oscillation.

At first consideration, one might think that irregular speed would make no difference because of the phase-lock of reference and experimental signal. This is not so. Over the time of transition from one speed to another, the light on and off periods may be unevenly weighted relative to one another. The result is noise. To understand this better consider a Fourier approach. During the period of changing speed, the AC signal must be analyzed using, not just the instantaneous frequency, but others as well. Some of the information is in these other frequencies, but we detect only at the instantaneous value. This lost information results in noise.

e. Construction. The motor is mounted on a cast-iron block, which is more effective than other materials in damping out vibrations. The entire unit sits on a $\frac{1}{2}$" sheet of polyurethane foam to isolate it from the table. The blade and its housing are black anodized to minimize light from the reference bulb mixing with the monochromatic light.

5. Optical Filters

Attached to the chopper is a bracket capable of firmly holding up to three optical filters of varying thicknesses. Filters are necessary to ensure the spectral purity of light leaving the monochromator. Although only the first order diffractions of the monochromator gratings are used, there are wavelength ranges in which significant second order light leaves the monochromator as well. The wavelength at which second order light becomes a problem depends on which combination of source, grating, and detector is used. Second order light is easily eliminated by an appropriate choice of filter.

Scattered light is more difficult to deal with. It is light of all frequencies and it leaves the monochromator with the monochromatic light. Filters help reduce it by ensuring that only that scattered light within their pass band is permitted to enter the rest of the system.

a. Criteria. Scattered light and second order light distort optical spectra. Since scattered light contains a range of frequencies, it would appear that the scattered light is unlikely to add new structure in optical measurements but only to change the amplitudes of the first order structure. Actually, it can add structure as well. In addition, second order is monochromatic light and can add new structure to a spectrum. Since the elimination of scattered light and second order light is never total, some criterion is necessary to assess the distortion created by

them. Measurement of scattered light provides that criterion.

By adjusting wavelength beyond the transmission range of a filter or the output of a lamp, any residual signal which is measured will be due to scattered light or second order. If this signal is constant with λ, the cause is scattered light ($\equiv I_0(\text{scatt})$), not second order. This constancy indeed occurs beyond the low wavelength limits of the filters. Figures 2-5a, b, c, and d plot the ratio $I_0(\lambda)/I_0(\text{scatt}) \equiv a(\lambda)^{-1}$ versus wavelength for various combinations of source, grating, detector and filter. $I_0(\lambda)$ is defined in Eq. 2.3. It is the reference channel light intensity and includes the effects of source, grating, filter, polarizer, mirrors, and detectors. Slit width has little effect on the plots.

(1) Structure Magnitude. These plots provide a means for determining the correctness of structure magnitude. Consider the following analysis of scattered light:

Let

$R_m(\lambda) \equiv$ reflectivity measured at wavelength λ. (2.8)

$R_t(\lambda) \equiv$ true reflectivity at λ. (2.9)

$I_R(\lambda) \equiv R_t(\lambda)I_0(\lambda)$ = true reflected intensity at detector. (2.10)

$R(\text{scatt}) \equiv$ sample reflectivity of the scattered light occurring in a given experiment. It is an average of all wavelengths in the band pass of the optical filter, weighted by their relative intensities. It is easily determined experimentally by measuring (2.11)

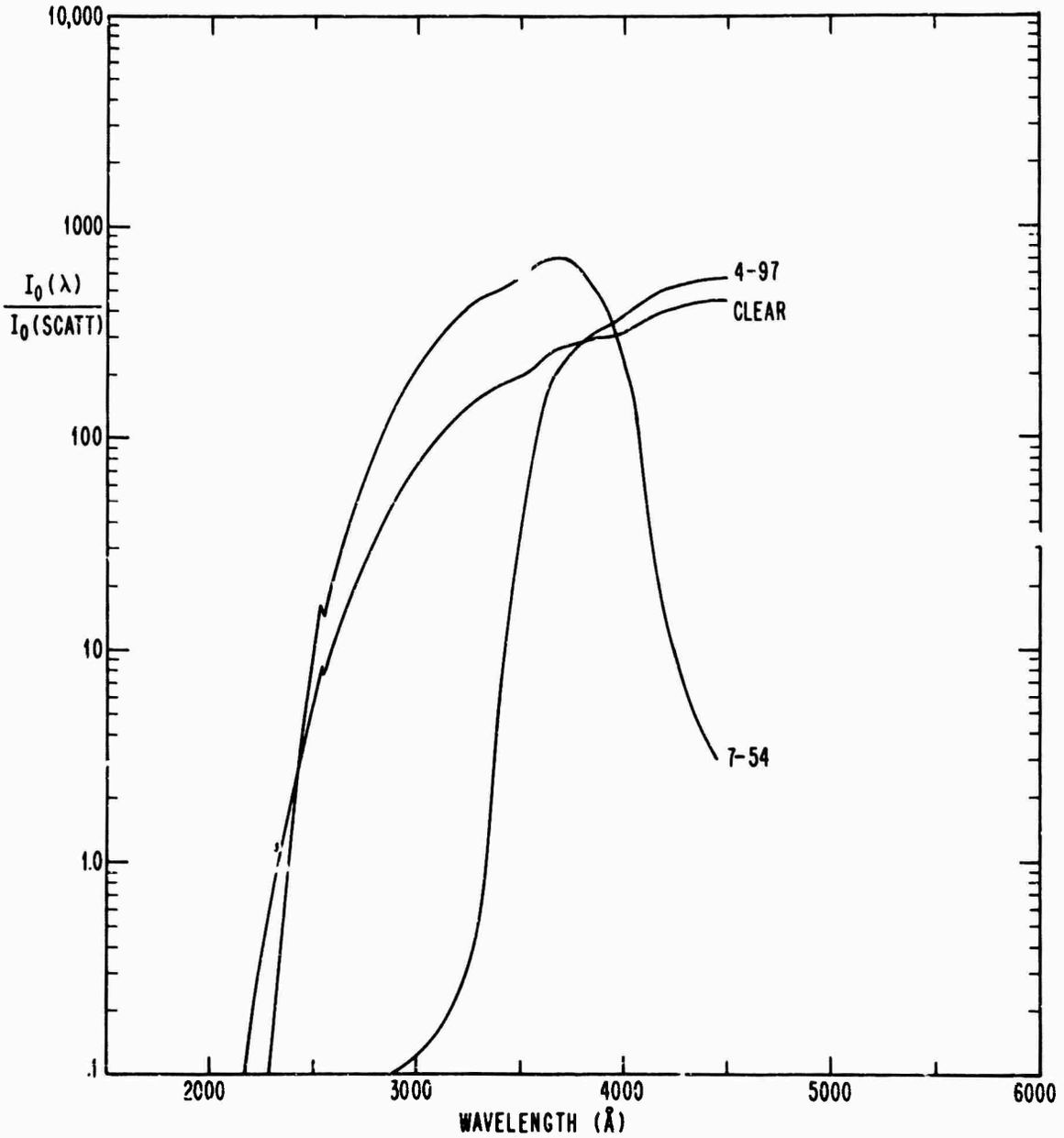

FIG. 2-5a LIGHT INTENSITY AT WAVELENGTH λ NORMALIZED BY THE SCATTERED LIGHT VS. WAVELENGTH. CONDITIONS: XENON ARC, 7500Å BLAZE GRATING, S-13 PHOTOMULTIPLIER, VARIOUS FILTERS. Filters listed by Corning number.

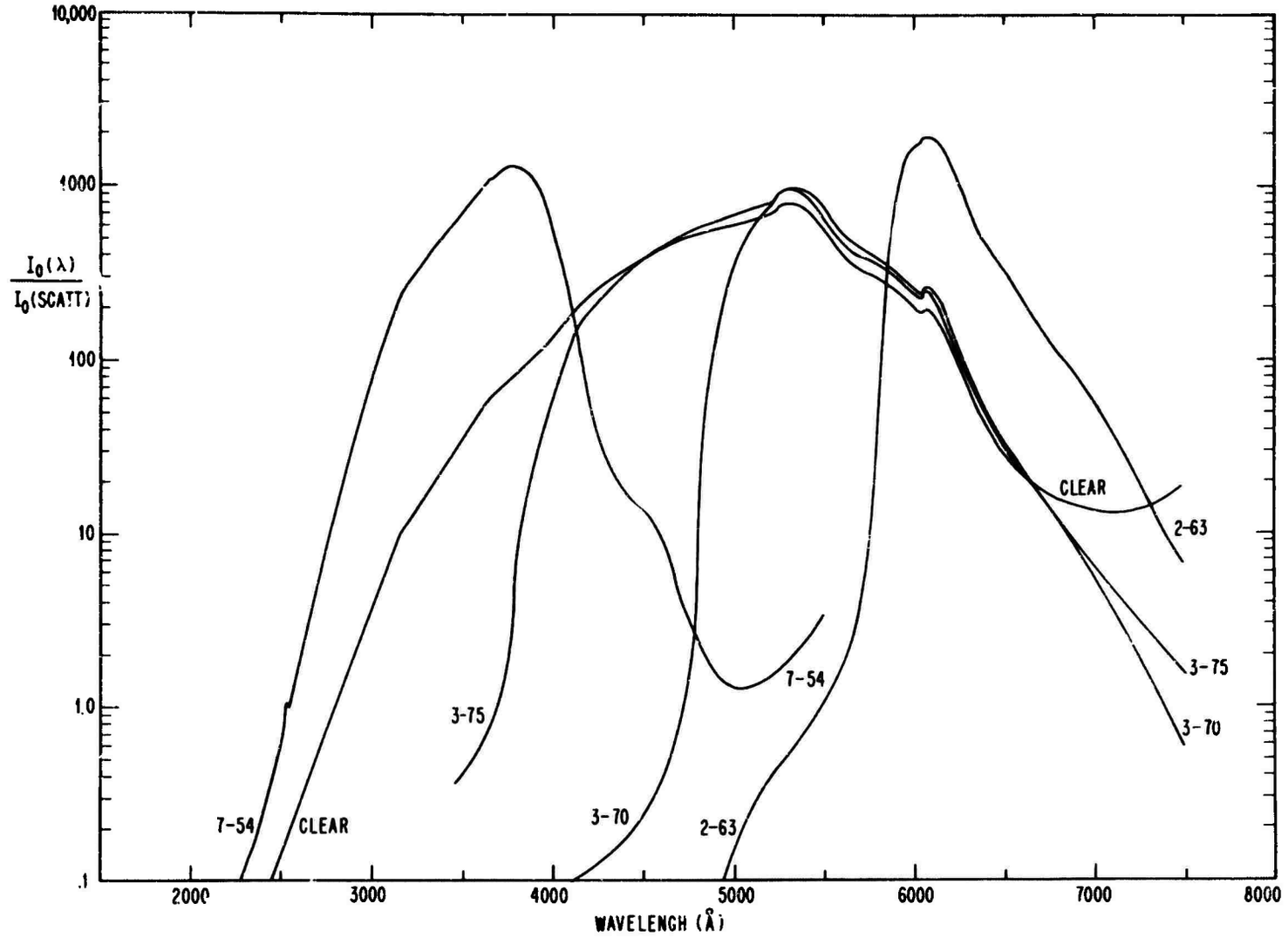

FIG. 2-5b LIGHT INTENSITY AT WAVELENGTH λ NORMALIZED BY THE SCATTERED LIGHT VS. WAVELENGTH. CONDITIONS: IODINE QUARTZ SOURCE, 7500Å BLAZE GRATING, S-13 PHOTOMULTIPLIER, VARIOUS FILTERS. Filters listed by Corning number.

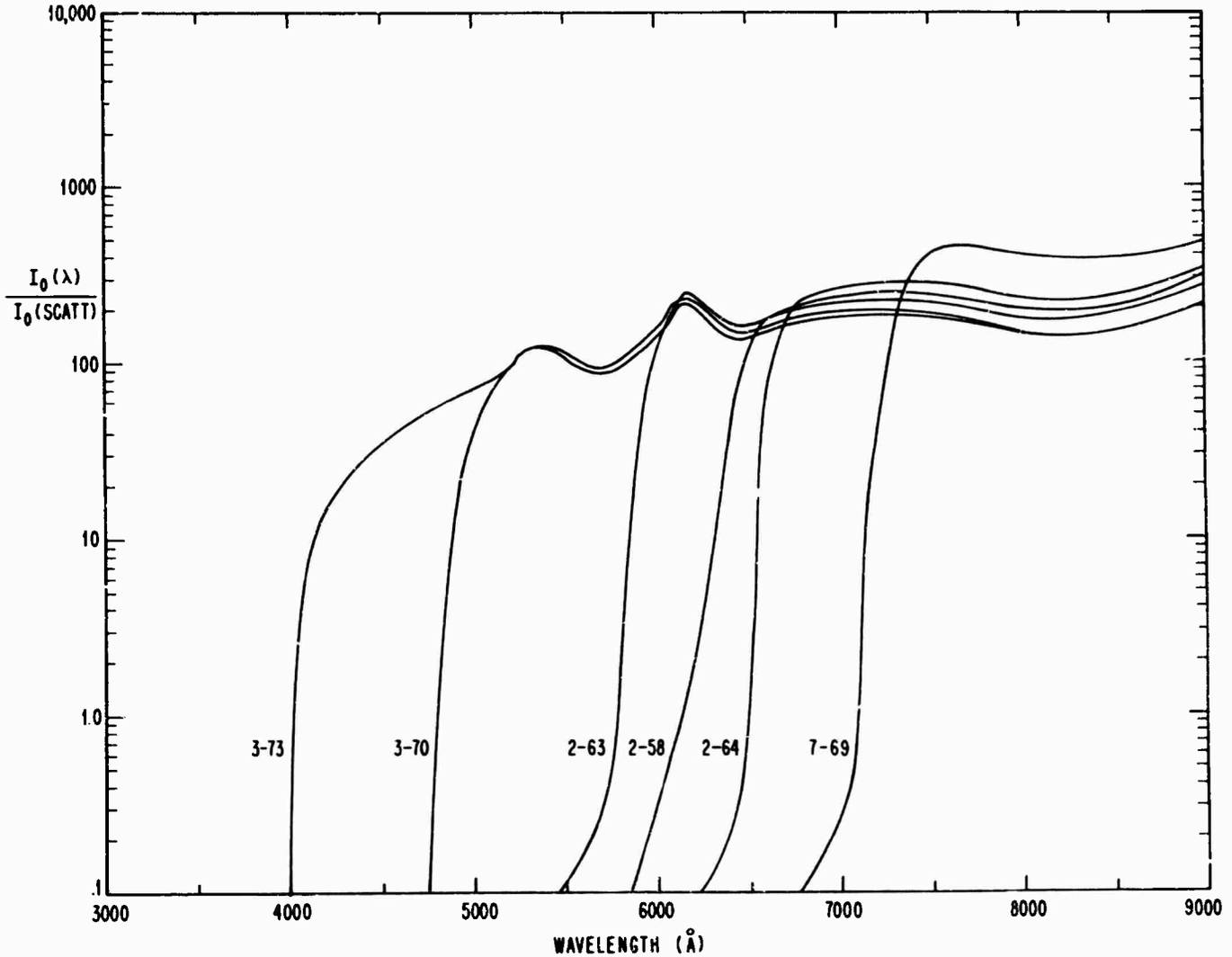

FIG 2-5c LIGHT INTENSITY AT WAVELENGTH λ NORMALIZED BY THE SCATTERED LIGHT VS. WAVELENGTH.
CONDITIONS: IODINE QUARTZ SOURCE, 7500Å BLAZE GRATING, S-1 PHOTOMULTIPLIER, VARIOUS FILTERS.
Filters listed by Corning number.

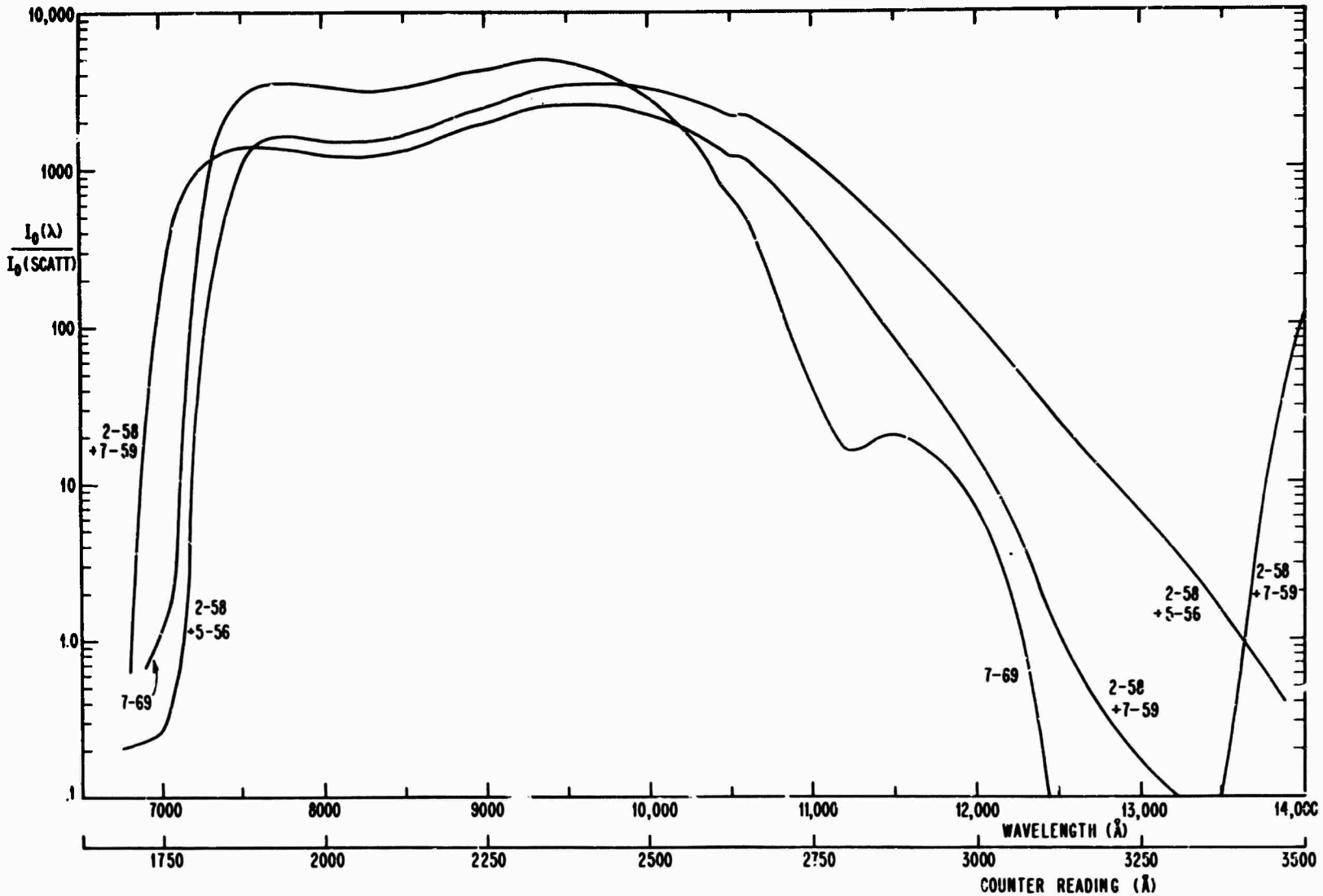

FIG. 2-5d LIGHT INTENSITY AT WAVELENGTH λ NORMALIZED BY THE SCATTERED LIGHT VS. WAVELENGTH. CONDITIONS: IODINE QUARTZ LAMP, 1.1μ BLAZE GRATING, S-1 PHOTOMULTIPLIER, VARIOUS FILTERS. Filters listed by Corning number.

R in the λ region where only scattered light occurs. This is typically found at wavelength settings below the optical filter cutoff.

$$I_R(\text{scatt}) \equiv R(\text{scatt})I_0(\text{scatt}) \tag{2.12}$$

By summing monochromatic and scattered light intensities we get the measured reflectivity.

$$R_m(\lambda) \equiv \frac{I_R^m(\lambda)}{I_0^m(\lambda)} = \frac{I_R(\lambda) + I_R(\text{scatt})}{I_0(\lambda) + I_0(\text{scatt})} = \frac{R_t(\lambda)I_0(\lambda)+R(\text{scatt})I_0(\text{scatt})}{I_0(\lambda) + I_0(\text{scatt})} \tag{2.13}$$

Employing simple algebraic manipulation, we get

$$R_m(\lambda) - \frac{R(\text{scatt})a(\lambda)}{1+a(\lambda)} = \frac{R_t(\lambda)}{1 + a(\lambda)} \tag{2.14}$$

$$R_t(\lambda) = R_m(\lambda)(1+ a(\lambda)) - R(\text{scatt})a(\lambda) \tag{2.15}$$

$$[R_t(\lambda) - R_m(\lambda)] = [R_m(\lambda) - R(\text{scatt})]a(\lambda) \tag{2.16}$$

Noting that $R_m(\lambda) < 1$, $R(\text{scatt}) < 1$,

then

$$|R_m(\lambda) - R(\text{scatt})| \leq 1$$

Hence,

$$|R_t(\lambda) - R_m(\lambda)| \leq a(\lambda) = \frac{I_0(\text{scatt})}{I_0(\lambda)} \tag{2.17}$$

An approximate criterion for the effect of scattered light is given by Eq. 2.17. The error in R_t is less than $a(\lambda)$. Equation 2.15 is an exact expression of the effect, and in theory permits one to correct $R_m(\lambda)$ for the effects of scattered light. R(scatt) is measurable and $a(\lambda)$ is given by Figs. 2-5a through d. Usually this correction is of interest only for small effects where errors in $a(\lambda)$

and R(scatt) would prevent an accurate reconstruction of $R_t(\lambda)$. The R(scatt) measurement is noisy due to low light intensities. For a graphic solution, see the note in Sec. II-B-6-a.

(2) False Structure Created by Scattered Light. The scattered light can not only modify magnitudes, but also create false structure under certain circumstances. This structure will match structure in the I_0 curve as is demonstrated by Figs. 2-6a through e, which could be thought of as showing the low UV end of a spectrum or the behavior at the low wavelength cutoff of a filter.

Suppose that the true sample reflectivity, $R_t(\lambda)$, is shown in Fig. 2-6a and that $I_0(\lambda)$ has the form shown in Fig. 2-6b, where we have temporarily eliminated scattered light. A sinusoidal variation in I_0 has been postulated to show clearly the effects of I_0 structure.

$$I_0(\lambda) = \frac{x}{\pi}\left(1 + \frac{1}{5}\sin x\right) \qquad \text{for } x > 0$$

where $x = \dfrac{(\lambda - \lambda_o)}{(\lambda_c - \lambda_o)/3}\pi$ and

$$I_0(\lambda) = 0 \quad \text{for } x \leq 0.$$

Note that $(\lambda_c - \lambda_o)/3$ determines the horizontal wavelength scale.

When there is no scattered light, $I_R(\lambda)$ will have the form shown in Fig. 2-6b since

$$I_R(\lambda) = R_t(\lambda)I_0(\lambda) \qquad \text{(from Eq. 2.10)}.$$

In Fig. 2-6c, scattered light, $I_0(\text{scatt})$, is introduced and the measured intensities, $I_0^m(\lambda)$ and $I_R^m(\lambda)$, are shown.

$$I_0^m(\lambda) = I_0(\lambda) + I_0(\text{scatt}),$$

$$I_R^m(\lambda) = I_R(\lambda) + R(\text{scatt})I_0(\text{scatt}) \quad \text{from Eq. 2.13.}$$

We somewhat arbitrarily let R(scatt) = 30%.

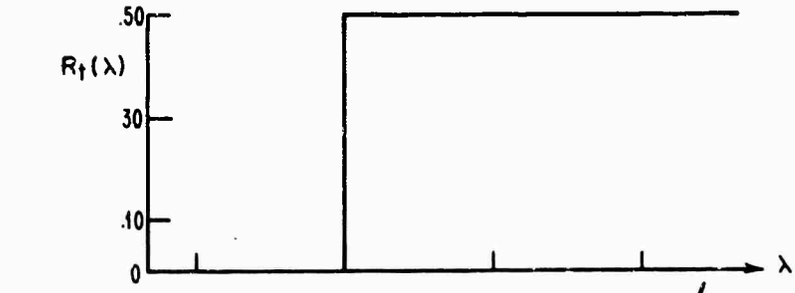

a. POSTULATED TRUE SAMPLE REFLECTIVITY VS. WAVELENGTH

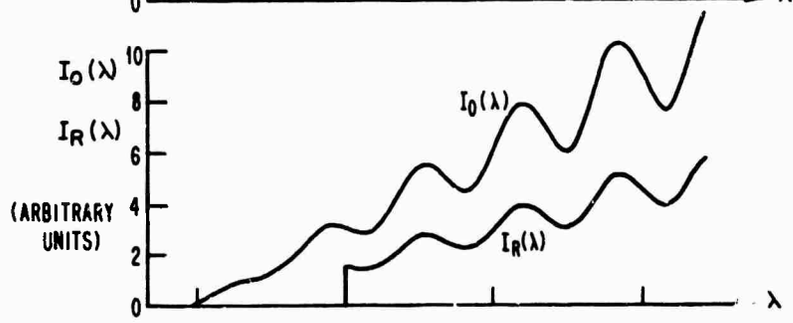

b. POSTULATED SHAPES OF $I_0(\lambda)$ AND $I_R(\lambda)$ VS. WAVELENGTH

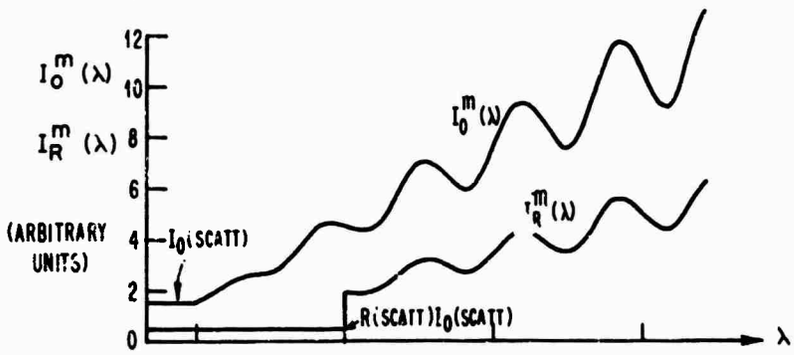

c. CHANGE IN $I_0(\lambda)$ AND $I_R(\lambda)$ DUE TO SCATTERED LIGHT

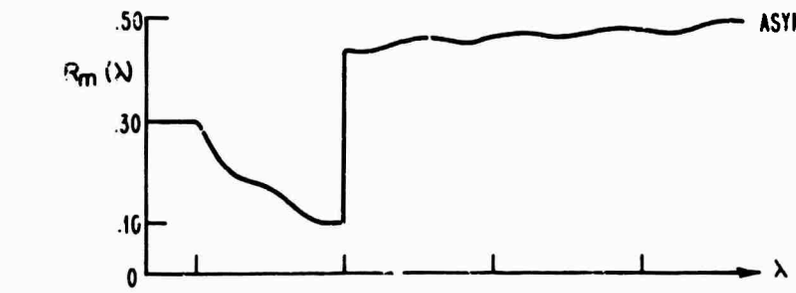

ASYMPTOTIC TO 0.5

d. MEASURED REFLECTIVITY SHOWING FALSE STRUCTURE

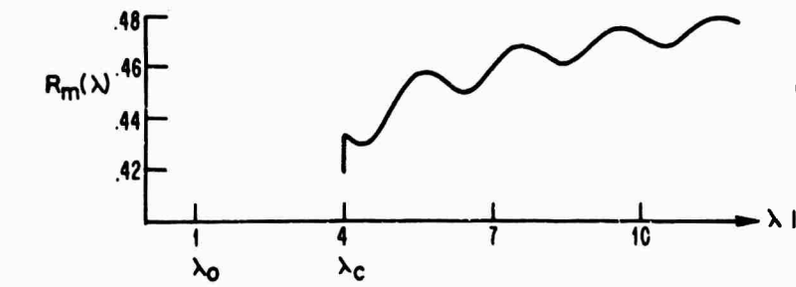

e. EXPANSION OF d. TO SHOW STRUCTURE DECREASING WITH WAVELENGTH

FIG. 2-6 FALSE REFLECTIVITY STRUCTURE CREATED BY SCATTERED LIGHT

Finally, in Figs. 2-6d and e, we see the measured reflectivity, $R_m(\lambda)$, which should be compared with $R_t(\lambda)$. Particular features of interest are the false peak at λ_o (the wavelength where light intensity becomes zero) and the sinusoidal bumps correlated with I_0 structure. Note that these bumps decrease in magnitude as $I_0(\lambda)$ increases with increasing λ.

There are concrete examples of both false features. (a) As wavelength approaches a filter cutoff frequency, a false rise or drop often occurs. (b) At 2535Å in the xenon arc spectrum, there is a small sharp peak which is regularly found in reflectivity spectra.

Equations 2.15 and 2.17 of the prior subsection have application here as well for determining the reality of structure.

(3) False Structure Created by Second Order Light. A similar analysis provides the criterion for determining the effect of second order light in creating false structure. This light is at wavelength $\lambda/2$.

$$R_m(\lambda) = \frac{I_R(\lambda) + I_R(\lambda/2)}{I_0(\lambda) + I_0(\lambda/2)} = \frac{R_t(\lambda)I_0(\lambda) + R(\lambda/2)I_0(\lambda/2)}{I_0(\lambda) + I_0(\lambda/2)} \tag{2.18}$$

$$b(\lambda) \equiv \frac{I_0(\lambda/2)}{I_0(\lambda)} = \frac{a(\lambda)}{a(\lambda/2)} \tag{2.19}$$

$$[R_t(\lambda) - R_m(\lambda)] = [R_m(\lambda) - R(\lambda/2)]b(\lambda) \tag{2.20}$$

$$|R_t(\lambda) - R_m(\lambda)| \leq b(\lambda) \tag{2.21}$$

Equation 2.21 indicates that second order light causes a deviation of reflectivity from its true value by an amount less than $b(\lambda)$. In applying this criterion, let us suppose that there is no

reflectivity structure at λ and a peak in $R_m(\lambda)$ is due to an effect at $\lambda/2$. Then $R_m(\lambda) - R(\lambda)$ is the measured increase in R in the vicinity of the peak. If this difference is $< b(\lambda)$ it could be due to second order light. However, if it is $> b(\lambda)$, the peak must arise from first order light. In practice, we need not use the more general equations to correct $R_m(\lambda)$ as we did in the case of scattered light. It is far better to use adequate optical filtering to reduce $b(\lambda)$ to an acceptable level.

$b(\lambda)$ is not quite the function we wish. The plots (Figs. 2-5a through d) give us $a(\lambda)^{-1}$ for a given λ, and hence for a given angular position of the grating. We should like $a(\lambda/2)$ for the same grating angle, but we must settle for $a(\lambda/2)$ at the angle corresponding to $\lambda/2$. However, the two $a(\lambda/2)$ values should be of the same order of magnitude and $b(\lambda)$ has nearly the correct value.

b. Actual Filters--Range of Use. Corning Glass filters are suitable over almost the entire present range of the system, 2400Å--1.1μ. Figures 2-5a through d suggest their individual regions of validity.

Below 2400Å there are no band-pass filters. As an alternative, one could use interference filters such as the Bausch and Lomb Type III Fabry Perot First-Order Ultraviolet Filters, extending down to a center wavelength of 2000Å.

c. Lens Effect of Filters. The plane parallel filters shift the light beam and its focus whenever the component beams are not normally incident. This shift is particularly noticeable when some

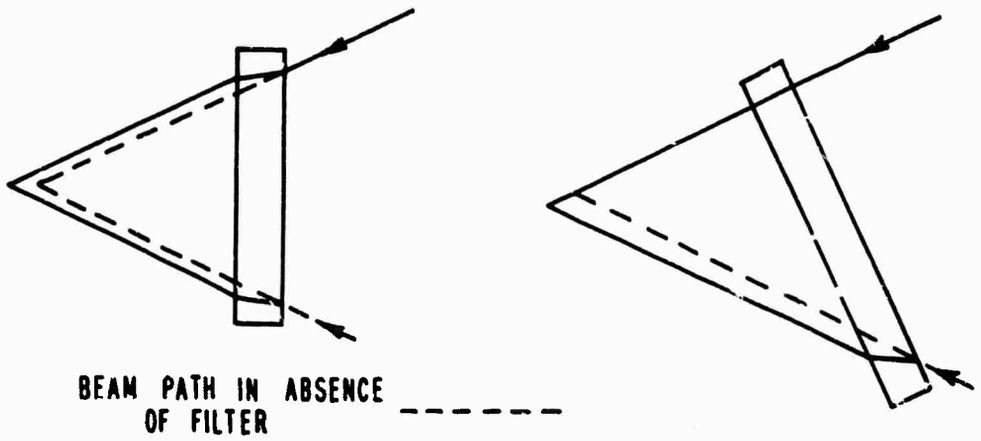

FIG. 2-7 LIGHT BEAM DEFLECTION BY PLANE PARALLEL FILTERS

light is blocked by the beam splitter. Different blockage occurs for the I_O and I_R paths, and when this blockage is changed by inserting a filter, the measured reflectivity changes as well.

By shifting the slit image focus onto different portions of a sample with varying reflectivity, the filter can cause further changes in R_m.

The effect is small, typically .5% at R_m = 40%, and can be reduced in two ways. Both are employed in practice.

(1) When the light beam is constricted before reaching the beam splitter (Sec. II-A-3-c), light is no longer lost at the splitter and one of the two causes of error is removed.

(2) If the filters are placed at the photomultiplier instead of at the monochromator exit slit, the only effect they can have is to shift slightly the I_0 and I_R images on the photocathode. Provided these two images are well superposed, this shift will cause minimal changes in R_m (.1% or less).

Any residual change in R_m will vary from filter to filter as a function of its thickness, which determines the lens effect. In the common wavelength range of the two filters, reflectivity values measured using them can be matched by a small scaling factor. For this matching to be correct, however, it should be done only in those wavelength ranges where neither filter absorbs strongly. When the absorption is strong, there will be errors in reflectivity due to the decrease of $I_0(\lambda)/I_0(\text{scatt})$.

d. Gray Filters. Gray filters† provide a rough means of checking system linearity. They are screens with varying sizes and spacing of conical shaped holes and are reported as nearly wavelength independent [2-06].

Their real usefulness lies in reducing the size of the reference channel signal when the reflected signal is relatively weak. The need for the two channel signals to be of roughly the same size arises from noise considerations in the electronics. The gray filters are mounted on a bracket in the I_0 channel.

---

†Electroplate conical hole screens, Perforated Products, Inc., Brookline, Massachusetts

6. First and Second Mirror Systems

The first mirror system takes the light from the monochromator exit slit up to the beam splitter. It includes plane mirrors #9, 8, 6, and concave mirror #1 (Fig. 2-2). The second takes light from the beam splitter to the detectors and includes plane mirrors #7, 10, 11, and concave mirror #2. Mirror #11 is used only when light is to be deflected to the alternate detector.

The mirrors are coated on their front surfaces with aluminum by evaporation, thus assuring adequate reflection over the entire range (2000Å-1.1μ). There is no SiO_2 coating so they must be handled with care. The plane mirrors are flat to ¼ wave and the concave mirrors deviate from a spherical curve by no more than 1/10 wavelength.

Figures 2-8 and 2-9a, b show a plane and a concave mirror in their mounts. Each has a large number of degrees of freedom. The plane mount can be attached to the table surface as desired by using the clamps shown. Mirror height and rotation about vertical and horizontal axes are then adjustable. Once the concave mirror's table position is selected (by means of the clamps), it can be moved back and forth along its axis of rotation, thereby changing focus. The four screws permit angular adjustment about vertical and horizontal axes.

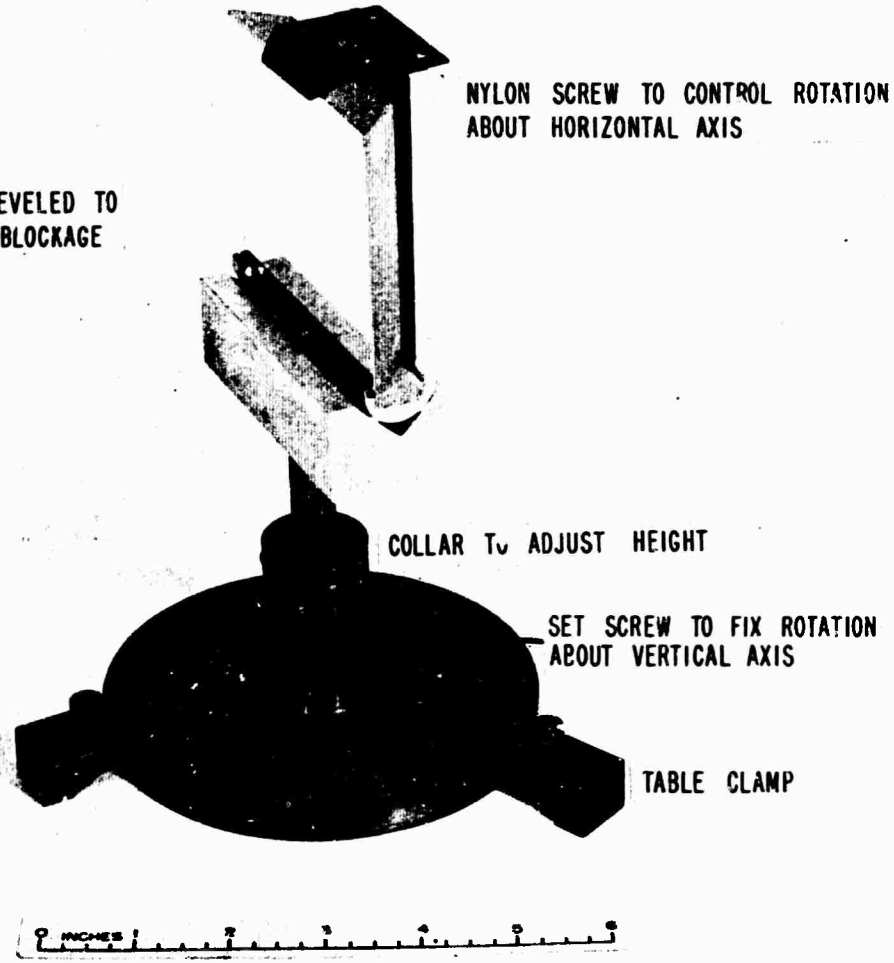

FIG. 2-8 PLANE MIRROR IN ITS MOUNT

Reflection from the plane mirrors is at close to 45° incidence. Like reflection from a dielectric, reflection from a metallic surface introduces polarization (Fig. 3-6). Consequently, care must be taken in any experiment where the plane of polarization of the I_O channel light rotate by an amount different from that of the I_R channel light. This point is discussed in more detail in Sec. III-H. Ideally, reflection from the concave mirrors would be on-axis. Incident light as little as 10° off-axis results in an intolerable amount of image distortion at focus due to aberrations, primarily coma. Light incidence is kept as close to on-axis as possible consistent with ensuring that no light is lost elsewhere by blockage. Note that the glass behind mirror #10 (as in others) is shaped so that it will interfere as little as possible with the light paths.

Concave mirror #1 is used with a magnification of 1 so that the image size on the sample is that of the slit. The object-image distances of concave mirror #2 are adjusted to reduce the image size at the detector.

7. Beam Splitter

The beam splitter is the optical heart of the dual beam system. At 13 times a second it directs light first into the reference path and then into the sample path. Light reflected from reference path mirrors and the sample return to the beam splitter and are then

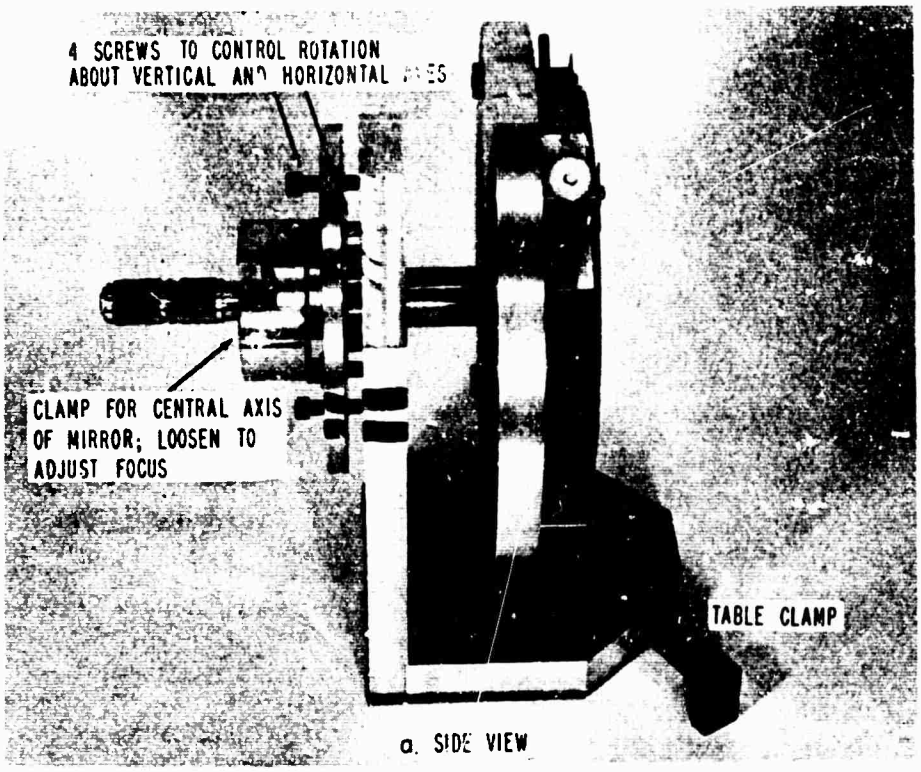

a. SIDE VIEW

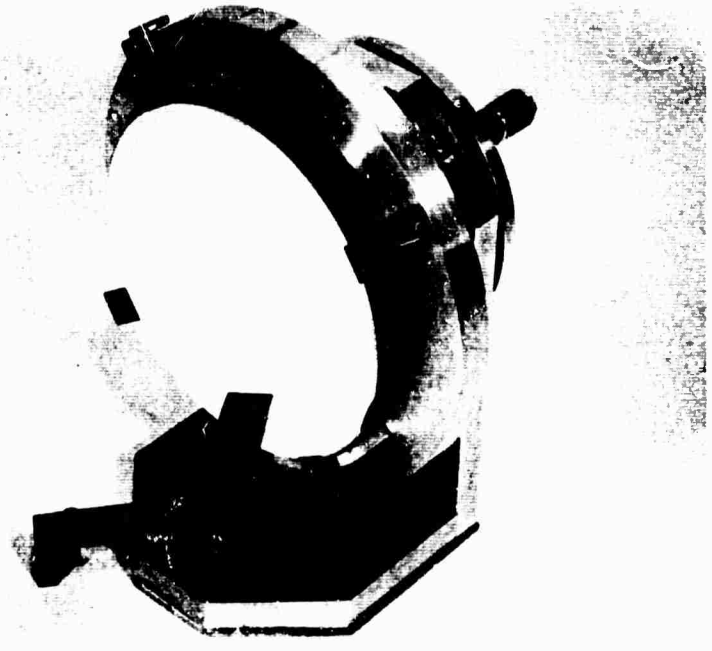

b. FRONT VIEW

FIG. 2-9 CONCAVE MIRROR IN ITS MOUNT

merged into the same spatial path to pass through the second mirror system to the detector. The operation of the splitter ensures that the reference and sample signals are separated in time.

a. Basic Design. The beam splitter is shown in Figs. 2-10a through d. Light from mirror #6 passes through the right-hand triangular hole in the shield and is incident at 45° either on a mirror or a hole. If a mirror, the light passes to the sample, is reflected to the second mirror on the splitter and then to mirror #7. If a hole, it passes to the two reference path mirrors, and back through the second hole to mirror #7. Note that we have two mirror reflections in each channel plus the reflection from the sample in the sample channel; the effects of mirror reflections compensate.

The mirror-hole unit is mounted in a thin section ball bearing, which in turn is mounted in a housing. It is rotated at 6½ Hz by a brass wheel with rubber ring, similar to a phonograph drive. Its angular position is sensed by two light bulb-detector assemblies like that found in the light chopper. They, too, are adjustable in phase relative to the experimental signals from the reference and sample channels. The sensor signals permit separating the information in the two experimental channels after electronic processing.

Each of the beam splitter components is worth considering in some detail for they represent problems in design.

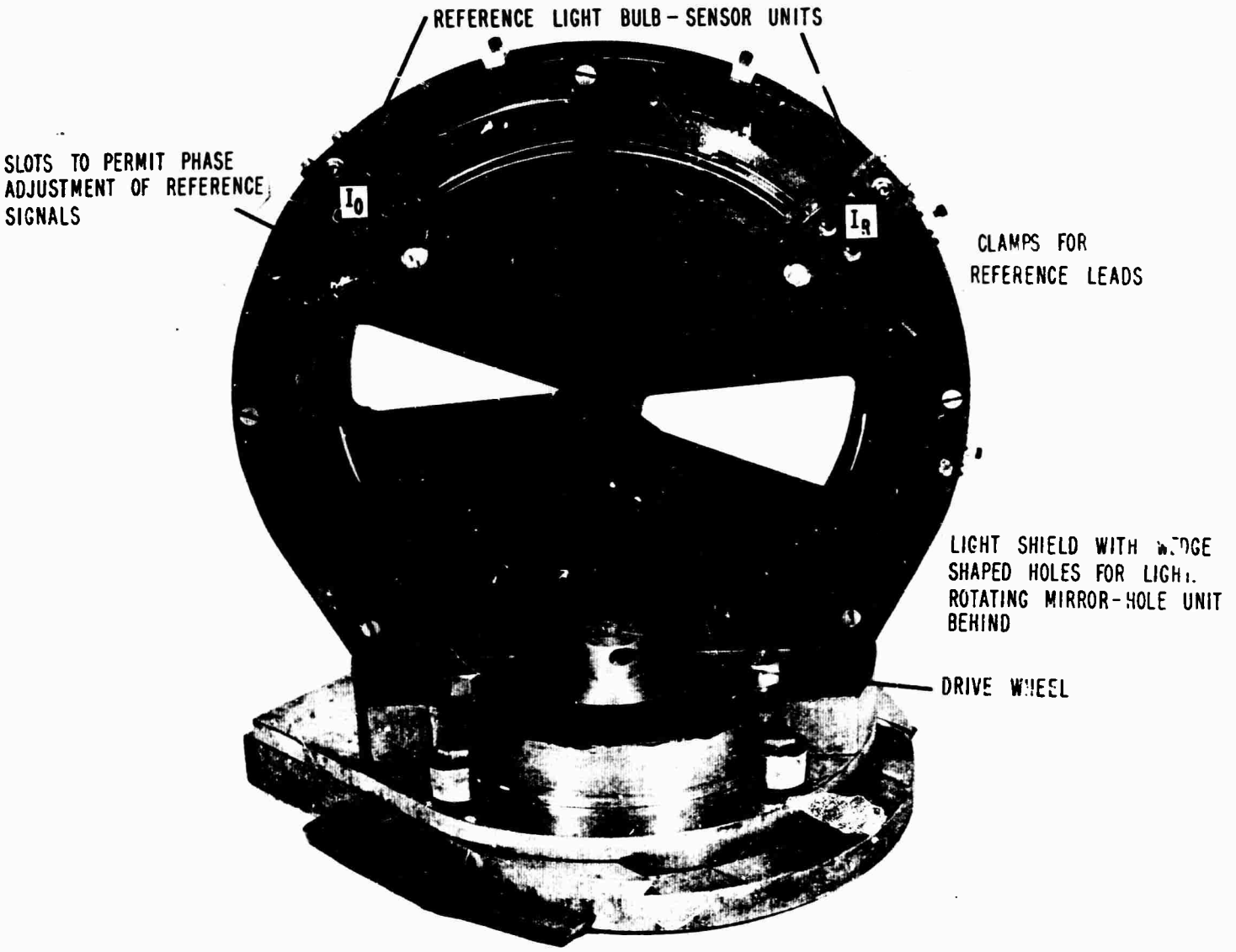

FIG. 2-10a BEAM SPLITTER: FRONT VIEW, ASSEMBLED

b. Rotating Mirror-Hole Unit. Note that each hole occupies 45° of arc as does each mirror. In between are 45° segments of non-reflecting surface. In conjunction with the 45° holes in the shield, this ensures that there is no overlap of the two channels.

The unit was manufactured from AISI 316 stainless steel. What was needed was a reasonably hard, noncorroding, nonmagnetic material. It was machined, ground, lapped and then polished to a flatness of 1 wavelength. Aluminum was evaporated onto its surface. Since it was likely to suffer a bit more wear and tear than the other mirrors, and because of the comparative expense of coating it, a protective layer of MgF_2 was evaporated on top of the aluminum. The protection is not as complete as a SiO_2 layer and hence the unit requires care in handling. The MgF_2 thickness was set at 380Å to maximize reflection in the ultraviolet.

Around its outer edge is a cam made up of two 78° segments. They alternately obscure and pass the light directed from the reference light bulbs to the sensors. The cam length was specifically chosen less than 90°, the maximum time, expressed in terms of arc length, that light would pass through the beam splitter for a given channel. With the shorter cam, the electronics, operated by the cam derived reference signals, would have no trouble in separating the two channels. As it turned out, the arc did not need to be as short as 78°; 86° would have been an appropriate choice, but the loss of signal is negligible.

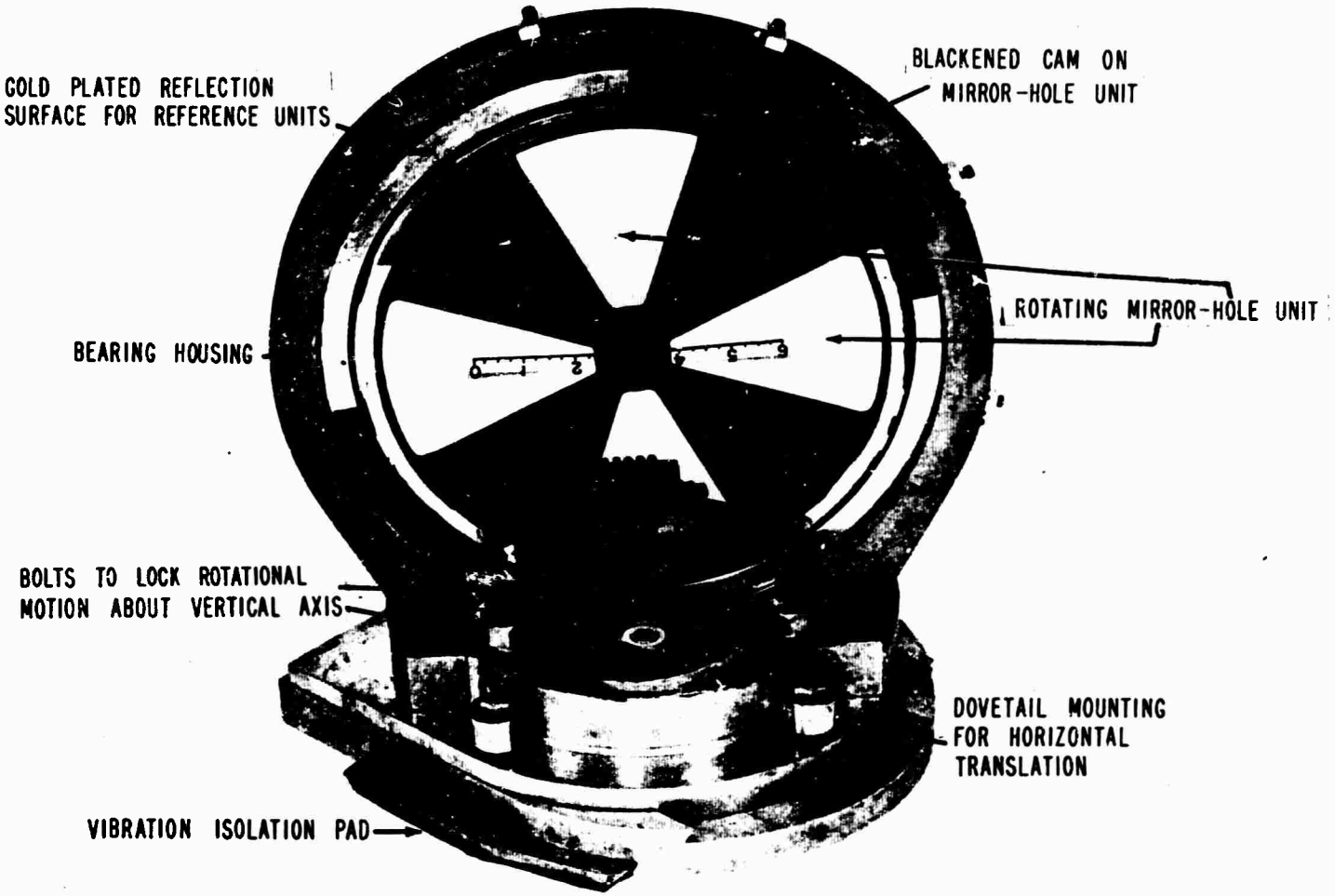

FIG. 2-10b BEAM SPLITTER: FRONT VIEW, DISASSEMBLED

The blackened portions of the unit are painted with a special optical flat black paint† designed to reflect poorly at all angles of incidence.

c. Light Shield. The light shield contains two wedge shaped holes: one for light entering the beam splitter and the other for light leaving it. The size and shape of the holes are related to the size and shape of the mirrors and holes behind, and take into account the 45° angle of incidence and the convergence of the light.

d. Mounting. The mirror-hole unit rotates in a very thin section stainless steel ball bearing.‡ This, in turn, is mounted in a cast-iron housing. The size of the balls and the amount of press fit of the bearing in its housing must be carefully balanced. If too tight, the drive wheel slips and the motor has inadequate power. If too loose, the mirror surfaces will jiggle under the axial thrust of the drive wheel. The balls are installed with no preload, in fact they have .001-.002 diametral clearance. Normal grease found in the bearing is removed since it imposes an excessive load. A light machine oil,†† designed to cling to moving surfaces, is used sparingly. Any excess is soon flung out.

The housing originally contained only a portion of the bearing, the lower third, since there was concern that a complete housing would block light. Unfortunately, the bearing was inadequately supported.

---

† Velvet Coating 9560 Series, Minnesota Mining and Manufacturing Corp., St. Paul, Minnesota.

‡ KC80XP5 4 pt. Contact Ball Radial Bearing with stamped bronze cage and #5 Precision, SST., Kaydon Engineering Corp., Muskegon, Michigan

†† Alemite Concentrated Oil #28, Alemite Division, Stewart Warner Corp., Chicago, Illinois.

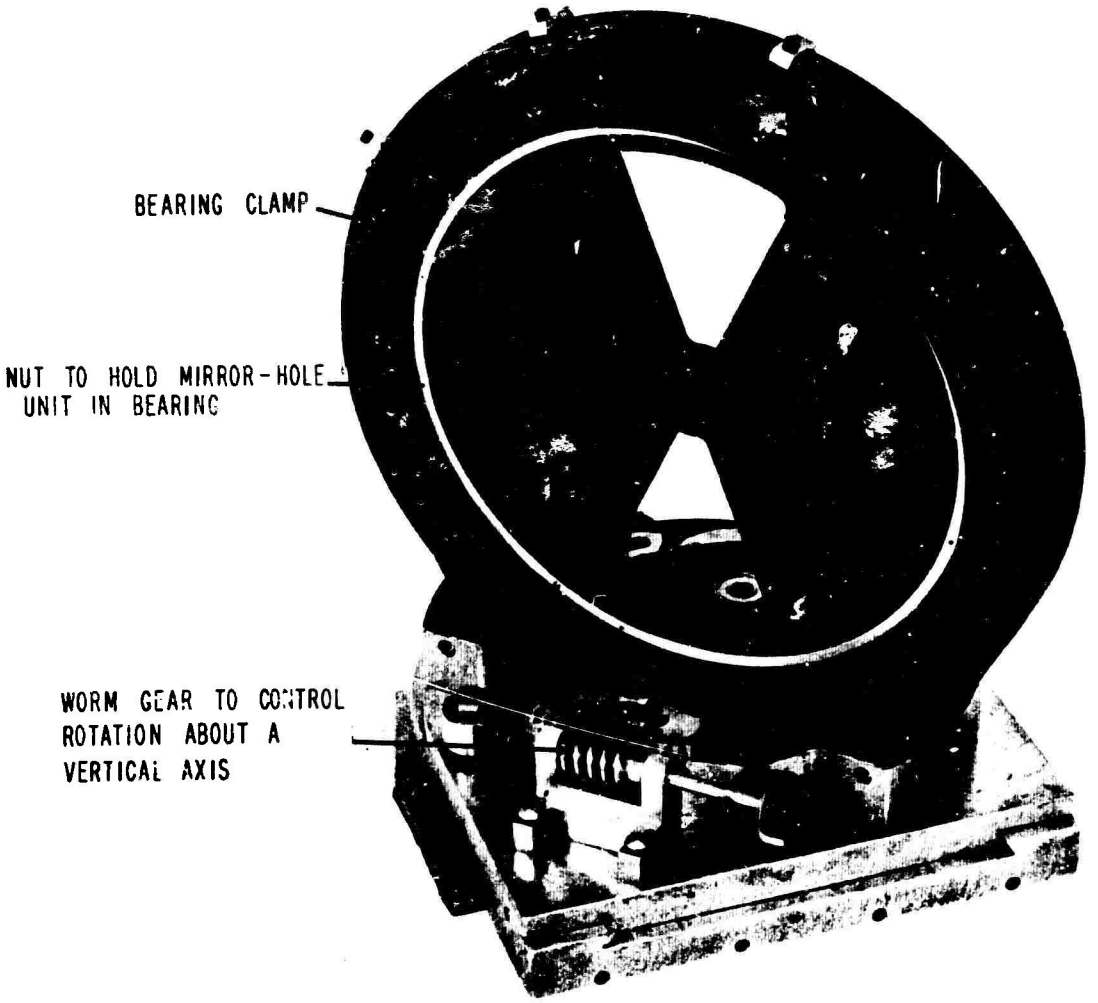

FIG 2-10c BEAM SPLITTER: REAR VIEW

It warped, resulting in excessive load. A slight readjustment in the optics permitted using a full housing. Even then, great care was necessary to ensure not only that the housing was accurately machined, but that it fitted smoothly into its base plate. Warpage imposes a drag, resulting in irregular speed.

The housing was made of cast-iron because of its superior vibration damping. The remainder of the mounting design was dictated by three concerns: beam splitter position adjustment, reference sensor mounting, and power drive.

e. Position Adjustments. Using dovetails, motion in two horizontal directions is possible. In addition, the mirror-hole unit can be rotated about a vertical axis running through the center of the unit. There is no height adjustment, for the heights of other optical components are adjusted relative to this.

To make any adjustments, the motor must be detached.

f. Reference Light Bulb-Sensor Units. Two light bulb-sensor units are clamped in slots on the shield. There is one unit for each of the sample and reference channels. Their angular positions can be changed by 65° of arc or 130° of a period, so that they have the proper relation to the experimental signals.

In the light chopper, light from a bulb was transmitted or obscured by the chopper blade and then passed to the detector. Here, the geometry demanded that reflection be used. Light from a bulb is reflected from a gold plated surface on the bearing housing unless it

is blocked by the blackened† cam. It returns to the detector only when the cam is absent.

There was some concern that light from the bulb might be scattered into the experimental optical path. This dictated the choice of gold as the reflecting surface rather than other materials brighter in the visible. If necessary, small filters could be installed in the units. These would pass only light beyond the range of the experimental signal detector. Fortunately, this did not prove necessary.

Light bulb intensity is kept as low as possible. The bulbs are DC powered because of a concern with intermodulation effects.

g. Splitting Speed--Choice and Fluctuations. In the initial design stages, a mechanical rather than an optical cam was considered. This suggested operating the beam splitter at 13 Hz, the speed used in Perkin-Elmer systems, so that we could use some of their components. Although the impractical aspects of a mechanical cam soon became evident, 13 Hz seemed a good figure to retain. The practical mechanical problems of a higher splitting speed seemed formidable. Anything lower was rejected because beam splitting should occur much faster than likely changes in source intensity. It has proved to be a good choice, since it is well separated from the light chopper frequency of 1080 Hz (see intermodulation effects, Sec. II-B-21).

Speed fluctuations are easily monitored by feeding the electronic signal derived from the reference signals into an electronic counter operating in the period mode. This signal can be selected at position

---

†Bearing oil spattered on the cam may result in partial reflection.

5 or 6 of the Upper Jack of the Channel Monitor. The DC level must be capacitively blocked. Under best conditions, the fluctuations are ± .1% in a 1 period measurement (Period .07548-.07562) and ± .013% in a 10 period measurement (Period .07553-.07555). This compares favorably with line frequency fluctuations.

In addition to fluctuations, drifts in speed can be noted. Before the housing was completely correct, and warpage imposed slight drag, the speed would build up to its maximum value slowly, increasing around ½%/hour.

h. Power Drive--Drive Wheel. The mirror-hole unit is coupled to the motor by a 2½" diameter brass drive wheel with a 2-3/16" ID rubber O-ring fitted to its outer edge. The O-ring is glued to a depression in the outer edge with Weldwood Contact cement.† After the cement is thoroughly dried (drying is encouraged by baking) the O-ring is ground, not machined, to a diameter of 2.600".

The drive wheel is attached to its shaft in a particular way. The concern is ensuring that there is no wobble in rotation, with a resultant radial oscillatory motion of the O-ring on the mirror-hole unit. This results in irregular speed, rapid wear, and increasing speed deviations. Good balance is also necessary. An earlier method used set screws to attach the wheel to the shaft and tipping resulted. Here the shaft is made first. A roughly made wheel has a hole accurately reamed. A cut is made through the hole and a piece removed to serve as a clamp. But most of the hole is left

†U.S. Plywood, New York, New York

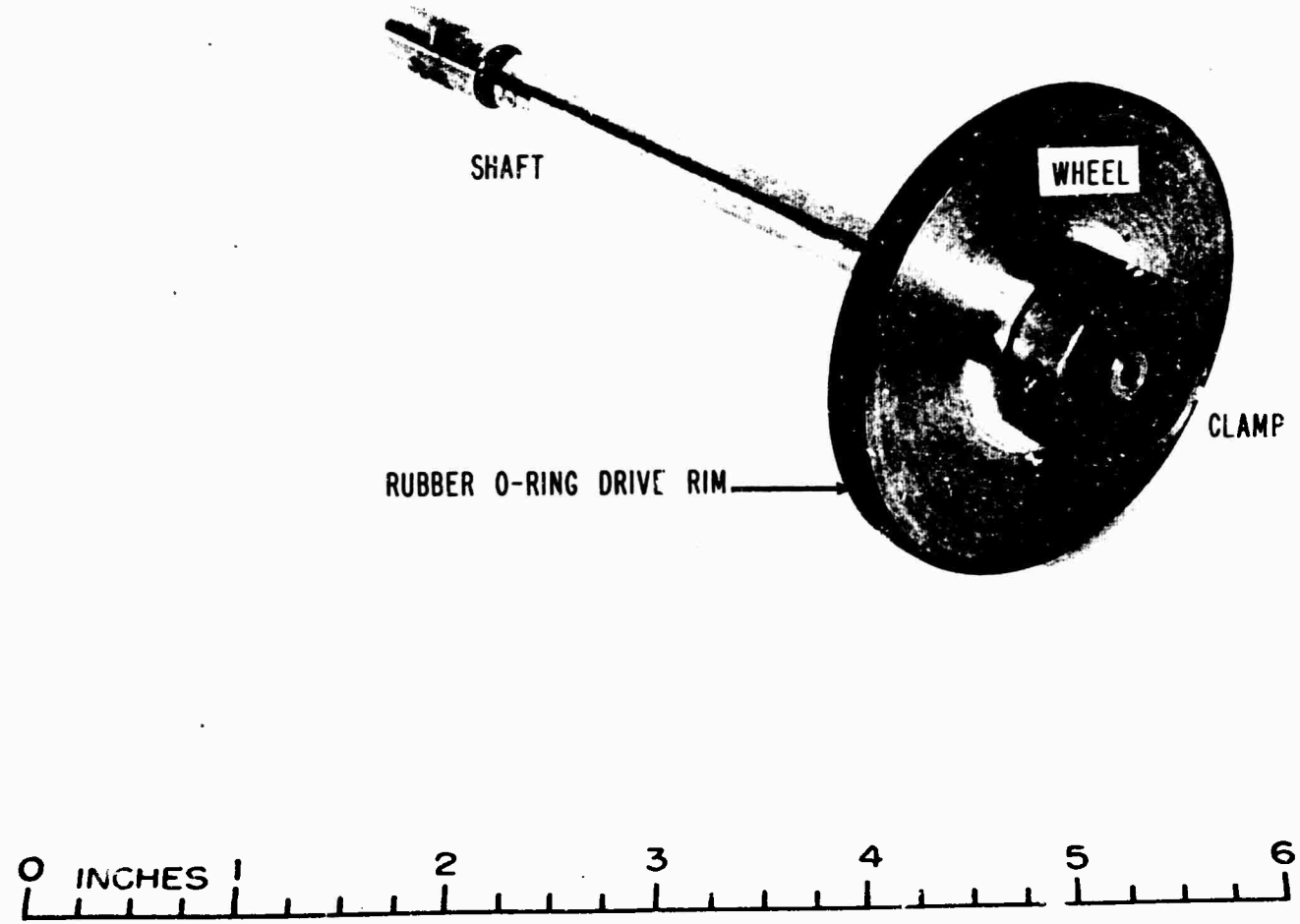

FIG. 2-10d BEAM SPLITTER: DRIVE WHEEL AND SHAFT

so that the position of shaft and wheel are well defined (Fig. 2-10d). With the wheel clamped on the shaft, it is machined. On reassembly the shaft and wheel retain their proper relative positions. This arrangement has worked well despite its very slight imbalance; one O-ring has over 300 hours of use without serious wear.

The rubber cement is a problem. It oozes out, eventually coating the drive wheel with lumps, increasing speed fluctuations tenfold. They are easily removed with trichlorethylene, but the lumps will recur for sometime. No better attachment has been found although others, including GE cement, were tried.††

i. Power Drive--Motor. A large, powerful motor is used. It is a 1/30 hp synchronous 1200 rpm Bodine B 7360.† The need for power and synchronous drive are the same as in the light chopper; speed fluctuations are intolerable. The motor is fed through a Variac with voltages up to 130 without overheating and will drive the mirror-hole unit at synchronous speed if components are properly mounted and lubricated.

The motor was formerly attached to a housing, suspended from the beam splitter itself. This was an unstable mount and the vibrations induced by the motor were transferred to the beam splitter. This method did have the advantage of easy beam splitter positioning.

The motor is now supported from the floor. A metal-rubber coupling‡ permits slight misalignment of the motor and drive wheel shafts. More importantly it isolates some motor vibration.

---

†Bodine Electric Company, Chicago, Illinois

‡J-1211-3-2 Lord Flexible Coupling, Lord Mfg. Co., Erie, Pennsylvania

††Eastman 910 cement (Eastman Kodak Company) has been suggested as a better bonding material. It is effective in joining rubber and metal.

7. Vibration Isolation. The motor-driven beam splitter vibrates. Part of this problem was solved by repositioning the motor. Coupling of vibration from the beam splitter to the table was reduced by placing the entire beam splitter assembly on a double pad of ½" polyurethane foam and felt. Mounting screws pass through clearance holes in the table top and through rubber stoppers. A nut presses the stopper against the table. There is no metallic contact

Table vibration was reduced 100 fold without increasing beam splitter vibration.

8. Reference Path Mirrors

The reference path mirrors provide a return path for reference channel light. This path is nearly of the same optical length as the sample channels. The two mirrors were made of stainless steel in the same way as the mirror-hole unit. All four were simultaneously coated with aluminum and MgF_2 in the hope that their reflectivities would be the same.

Their mount has many degrees of freedom so that their positions can be optimally chosen. These adjustments permit superposition of reference path and sample path light after leaving the beam splitter. There are two horizontal translation degrees of freedom for the unit as a whole. In addition, one mirror can be moved horizontally relative to the other. Both are adjustable in height and in rotation about horizontal and vertical axes (Fig. 2-11).

The attainment of perfect light image superposition following the beam splitter is frustrated by two factors.

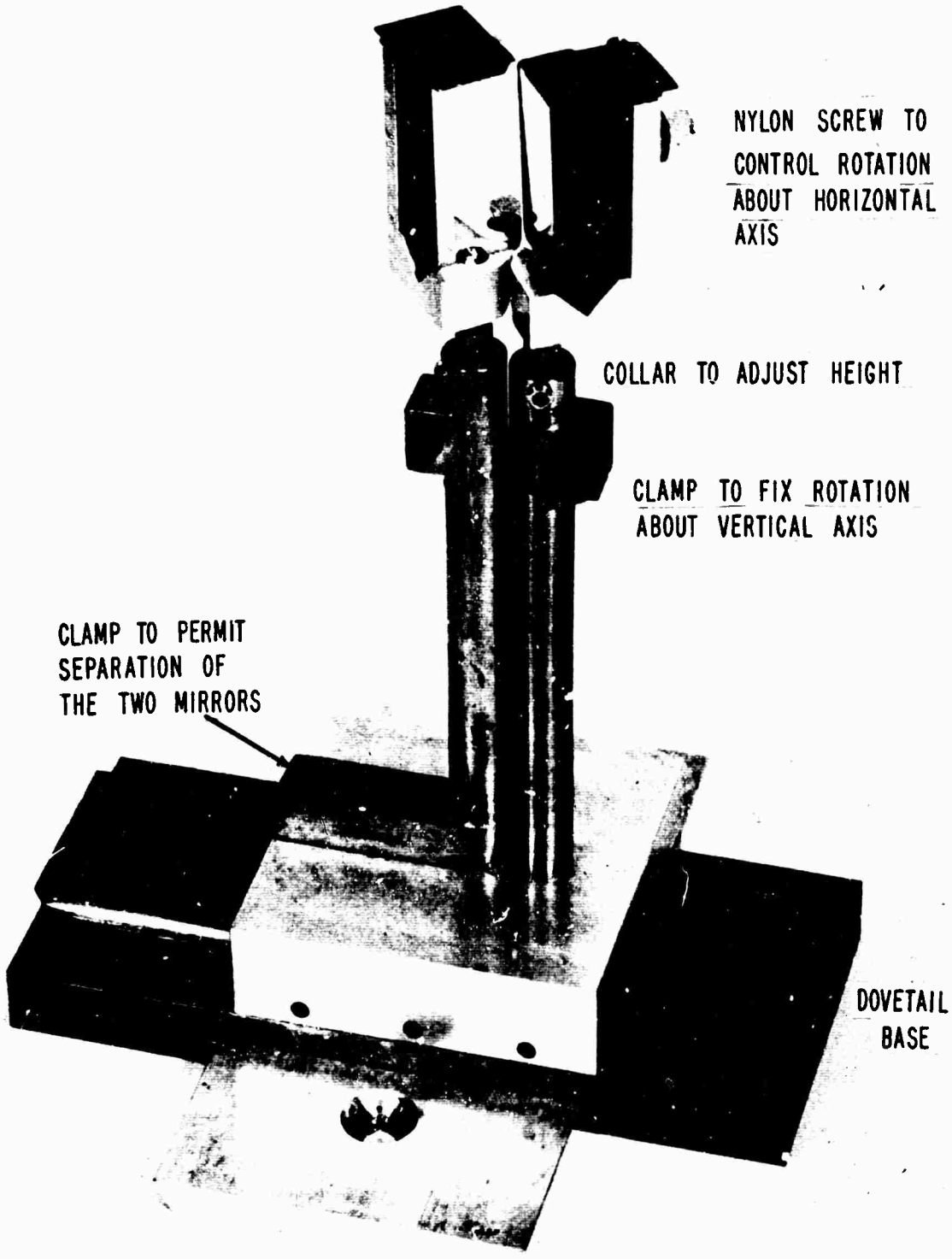

FIG. 2-11 REFERENCE PATH MIRRORS

(1) There are slight geometrical differences in the reference and sample paths caused by the need for two mirrors at the point of focus in the reference path.

The differences arise in the following way. Consider point A in Fig. 2-12a. Once the angle of the beam splitter is set and the sample positioned at focus, then point A is determined uniquely by a simple geometrical intersection. We should like to position our reference mirrors at point A to ensure perfect superposition for the I_O and I_R images at mirror 7 and beyond. Perfect superposition requires that the centers of the I_O and I_R images lie along the same line (be coaxial) and that path lengths for both beams be the same so that image sizes at any point along their common path be identical. This goal can be attained easily if a single mirror is placed at point A, but it is impossible to place the double mirror, 4 and 5, at that point (Fig. 2-12b), since light can leak through at their intersection. Further, only a slit of zero width could be incident on the intersection. When adjusting for slit widths up to 3 mm., the slit image must deviate slightly from the mirror intersection.

The solution of the problem is shown in Fig. 2-12c where 4 and 5 are moved back from point A. They could just as well be moved forward. Under this condition I_O and I_R light images are coaxial but of slightly different size. Therefore, as observed at the outset, superposition is imperfect.

(2) Light images passing through the holes or reflected from the mirrors become wedge shaped. Upon leaving the beam splitter,

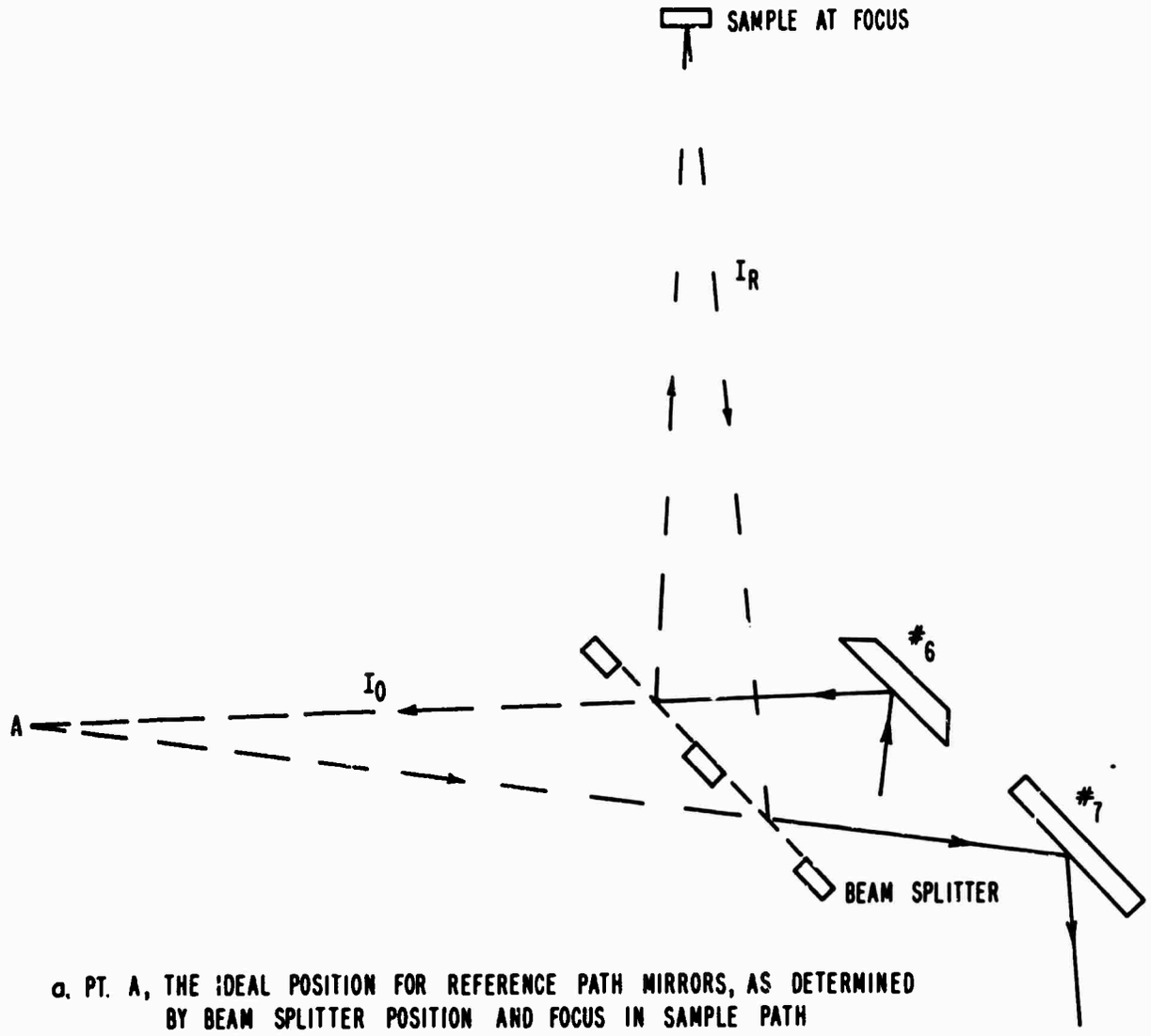

a. PT. A, THE IDEAL POSITION FOR REFERENCE PATH MIRRORS, AS DETERMINED BY BEAM SPLITTER POSITION AND FOCUS IN SAMPLE PATH

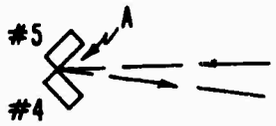

b. UNSUCCESSFUL ATTEMPT TO PLACE 2 REFERENCE MIRRORS AT POINT A. FINITE WIDTH BEAM CANNOT BE FOCUSSED ON THEIR LINE OF INTERSECTION

c. REFERENCE MIRRORS DISPLACED FROM POINT A

FIG. 2-12 GEOMETRICAL FACTORS PREVENTING LIGHT IMAGE SUPERPOSITION.

the two images are reversed relative to one another. This problem

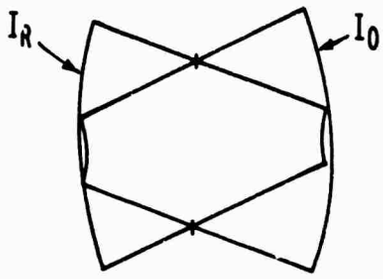

FIG. 2-13 IMPERFECT SUPERPOSITION OF I_O AND I_R LIGHT IMAGES FOLLOWING THE BEAM SPLITTER.

disappears when light constriction is used before the beam splitter (Sec. II-A-3-c). The light beam can be trimmed so that it is symmetrical on reflection from the sample and mirrors 4 and 5.

9. Photomultiplier Detectors

The detector requirements are good D* (low noise), a sufficiently large detector area to capture all the incident light, and appropriate frequency response at the light chopper frequency.

a. Tubes Used. For the present range of the system the requirements are satisfied by two photomultipliers. The EMI 6256B tube† has an S-13 response extending from 1650 to 6500Å (up to 7200Å in extreme cases). The RCA 7102‡ with its S-1 response is suitable from 4200 to 11,000Å.

b. Noise. There are two major sources of noise in photomultipliers. Shot noise arises from the quantum nature of light, the fact that a given photon has a probability less than 1 of releasing an

†EMI/US, Westbury, Long Island, New York

‡RCA, Electron Tube Division, Harrison, New Jersey

electrons and from the variation in the number of electrons released in later stages by each electron. Shot noise effects average out as the number of photons increases. S/N is proportional to $\sqrt{\text{Light Intensity}}$, so that brighter sources and wider slit widths are important.

The second source of noise is thermionic and is more serious in the S-1 response tube because of its larger area and its wavelength response: as a detector's sensitivity extends into the infrared, thermally excited dark current adds to the photon-derived current.

The choice of the particular S-13 response tube was dictated by the fact that thermionic emission may be reduced by keeping detector areas small. In the 6256B, thermionic noise is only one-tenth of the shot noise typically encountered. Cooling the tube to dry ice temperature has no noticeable effect on the thermionic noise.

In contrast, cooling is essential in the large area S-1 tube, where, without cooling, thermionic noise exceeds signal size. Dramatic improvement occurs on cooling to the temperature of dry ice: noise is cut by a factor of 20.

c. Housing. The tube housing serves a number of purposes. It geometrically positions the tube and protects the user from high voltages. By filling the housing's styrofoam well with dry ice, the tube can be sufficiently cooled. To prevent photocathode fogging, the tube housing is purged with dry N_2 gas and capped with a quartz window. The tube itself is surrounded by a mu-metal shield, for fields as low as two gauss can reduce anode current by a factor of

four [2-07]. The dynode resistor chain is inside the housing as are three capacitors in the last three stages of multiplication.†

d. Arrangement of Two Photodetectors. The two detectors are set up at right angles. Mirror #11 is removed when the S-13 is in use, but can be readily inserted to deflect light to the S-1.

e. Photocathode Saturation.‡ A convenient way to check total system linearity is to illuminate the monochromator slit with white light in a region where the spectrum is flat (or very slowly changing). Then, as the slit width is reduced, light intensities, as monitored on a chart recorder, should decrease at a rate proportional to slit width squared. A plot of $\sqrt{\text{Intensity}}$ vs. slit width should be a straight line. However, it proved to be two straight lines, meeting at a cusp, showing some sort of saturation.

Various tests proved that the position of this cusp depended only on the intensity of light on the photocathode (provided the image was in focus). Irregular action of slit width adjustment, any effect from changing photomultiplier voltage, and nonlinear electronic performance were all eliminated as causes. As source intensity decreased, the cusp moved to higher slit widths so that it always occurred at the same resultant intensity at the phototube. But defocussing the slit image would move the cusp to higher slit widths so that it could be entirely eliminated.

All these factors pointed to photocathode saturation. There is an easy cure: defocus the slit image so that it covers the entire photocathode area.

---

†For housing drawing refer to [2-08, Fig. 2-6].

‡A discussion of collector saturation and fatigue in the 6256B phototube can be found in ref. [2-09].

f. Circuitry. Circuitry for the photomultiplier is discussed in the Electronics section.

g. Additional Detectors. Detectors suitable for the infrared range are listed in Table 2-3.

TABLE 2-3 INFRARED DETECTORS

Detector	λ Range in μ	Time Constant in μSec.	Max. Freq. for Significant 1/f Noise, in Hz	D^*_{max} Under the Following Conditions:					Reference
				D^*_{max} in cm(Hz)/watt	λ in μ	Chop Freq. in Hz	Bandwidth in Hz	Temp. in °K	
PbS	1.0-4.0 at T=193°K	3500	more than 10^4	4×10^{11}	2.8	780	1	193	[2-10]
InAs	1.0-3.5	≤ 1	400	2.5×10^{11}	3.1	450	1	77	[2-11]
InSb	2.0-5.5	≤ 1	200	6×10^{10}	5.4	1000	1	77	[2-11]
Ge:Hg	2-14	< .1 when T < 20°K	300	2×10^{10}	11.3	1000	1	5	[2-11]
Ge:Cu	2-27	< .1 when T < 20°K	400	1.3×10^{10}	2.2	1000	1	5	[2-11]
Ge:Au	1-9	1	200	3×10^9	6.0	840	1	77	[2-10]

10. Optics Table and Shielding

The optical table is a sheet of ½" aluminum jig plate 78" × 48" mounted on a support base constructed of welded angle iron. The plate is maintained reasonably flat over its area and is covered with drilled and tapped holes to permit easy attachment of optical components. The surface is painted with a flat black optical paint.†

Over-all table height relative to the sample area may be adjusted by screw legs in each of the corners. Sitting on the table is a light shielding box, 15" high, which not only protects the optics from ambient room light but also isolates various sections of the optical system from one another. Various goals attained in the design were:

(1) Access to the optics by removal of a cover only.

(2) Capability to remove the box without modifying the optics significantly.

(3) Ease in removing the monochromator cover (for source alignment and grating interchange) and in removing the monochromator itself (for maintenance or adjustment).

(4) Easy access to the monochromator during an experimental run.

(5) Isolation of source optics from the rest of the system.

The sample area shielding encloses the entire sample area. When coupled to the optics table shielding, the total optical system is light tight enough to permit experimenting with room lights on.

---

†Velvet Coating 9560 Series cited in Section II-A-7-b.

11. System Improvements--Optical

Certain additions could expand system capabilities. None involves a fundamental change in design.

(1) A concave mirror behind the xenon arc source to double the amount of light incident on the monochromator. The transparency of the arc makes this possible.

(2) Globar for use in the infrared beyond the cutoff of quartz at 2.7μ.

(3) Gratings for use in the infrared. Jarrell Ash feels the wavelength limit of its 82-000 monochromator can be extended well into the infrared. The next logical grating choices are those blazed at 2.1μ (35-00-58-59) and 6μ (35-00-78-79A). Gratings blazed as high as 10μ have been sold for use in the instrument.

(4) Band pass filters for the edge of the UV range, 1900-2300Å, where scattered light is a problem.

(5) Repositioning of the hole used to constrict the light beam. Refer to Fig. 2-2, showing the optical layout.

(6) Design of a kinematic mount for mirror #11 so that light can be directed to either the S-1 or S-13 photomultiplier without extensive adjustment.

(7) Detectors for the infrared.

(8) Changes in the optics to permit absorption and differential measurements (Sec. II-C-6).

(9) Tests of the gray filters for the wavelength dependence of their transmission.

(10) Use of a high speed (>> 1080 Hz) light chopper in the I_0 channel as a truly gray filter. The chopper should have a variable opening so that transmission can be varied.

(11) An integrating sphere in front of the photomultiplier detector. The sphere, by diffusing the light for both I_R and I_0 channels, ensures that one's data are not distorted by variations in the photocathode sensitivity over its surface. The effect of slight shifts in sample position is also eliminated by the sphere.

Integrating spheres cannot be used in the infrared. Reference [1-12] shows a method for eliminating the effects of sample motion, which might be adapted to our system.

B. ELECTRONIC DESIGN FEATURES OF THE RATIO REFLECTOMETER IN ITS FINAL STATE AND RELEVANT PROBLEMS

1. Basic Concepts in Design

Electronic analogs of optical intensity data are amplified, separated into reference and sample channels, divided, and ultimately displayed as sample reflectivity on a chart recorder. Central concerns were noise reduction to maximize sensitivity and the optimization of linearity. Just as it is arranged that both optical signals are subject to the same reflections, so the electronic signals corresponding to I_R and I_0 are made to pass through the same active electronic elements. Once separated, they pass through passive elements only.

The block diagram, Fig. 2-1, outlines the logic of the electronic system and its multiple coupling to the optics. Figure 2-14 shows the relay rack arrangement of the components. The photomultiplier develops a voltage across its anode resistor proportional to the light intensity at a given wavelength. A preamplifier boosts the signal (by a factor of 10, 100, or 1000), which is then filtered by a variable band-pass unit. Further amplification, followed by phase sensitive detection, takes place in the phase sensitive detector. The detector receives its reference signal from the light chopper reference signal unit. Immediately following, the channel switch unit, activated by two signals from the beam splitter reference units, divides the signal into two channels, sample (called I_R) and reference (called I_0). Variable matched low-pass filters remove the ripple in the two channel signals, and a modified servo-type recorder performs the division of I_0 into I_R with pen position indicating reflectivity.

Arbitrary upper and lower limits on the reflectivity, I_R/I_C, can be selected, thus providing scale expansion. There are upper limits on the time constants used in the matched filter system. To permit longer integrations, a retransmitting slide wire followed by a circuit with adjustable time constants is coupled to the recorder. The output is displayed on a second recorder.

When signal changes are less than the noise-limited sensitivity of the system, the retransmitting slide wire output can be fed into a multichannel analyser. By making many sweeps through a spectrum,

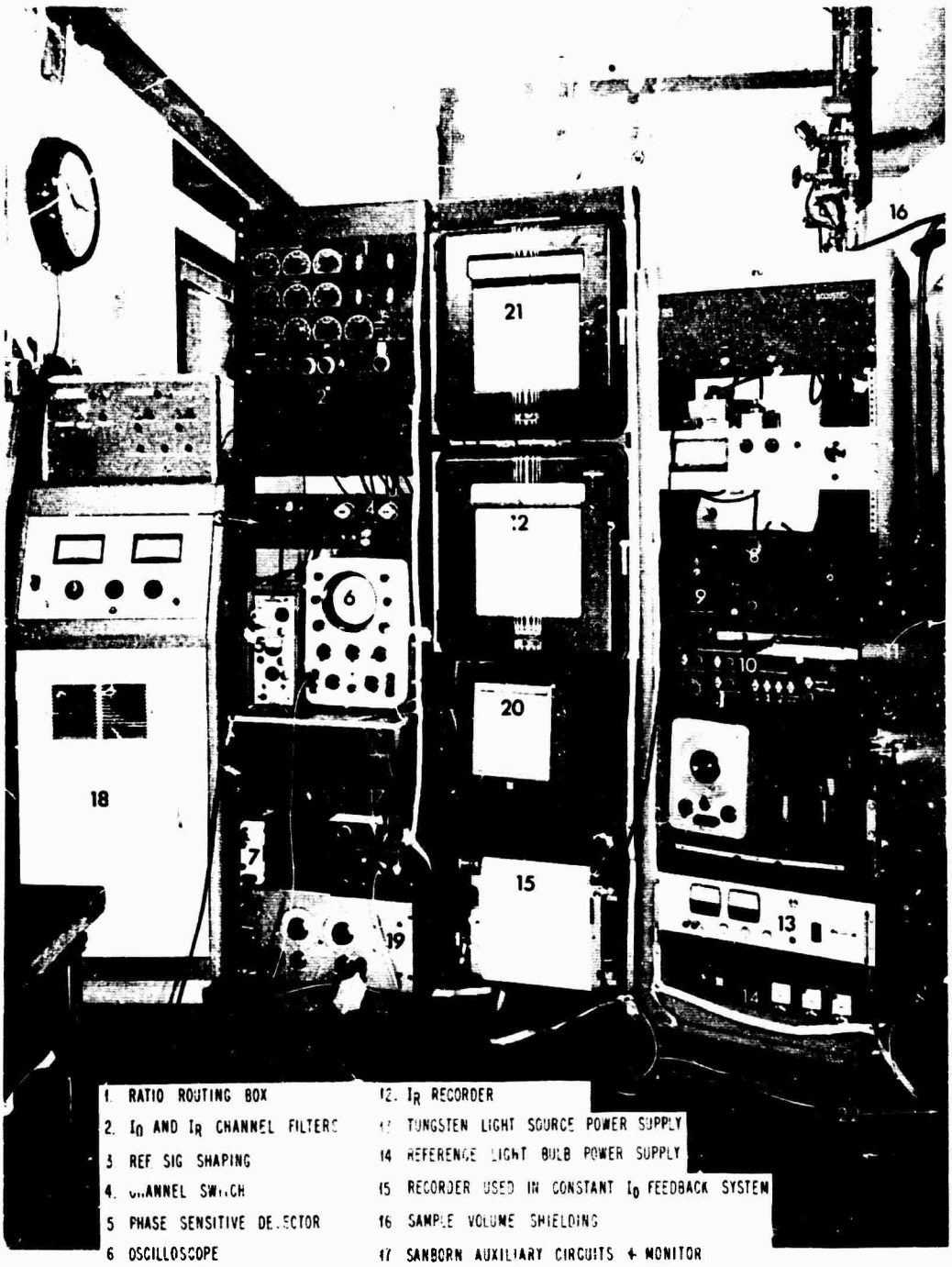

1. RATIO ROUTING BOX
2. I_0 AND I_R CHANNEL FILTERS
3. REF SIG SHAPING
4. CHANNEL SWITCH
5. PHASE SENSITIVE DETECTOR
6. OSCILLOSCOPE
7. PREAMPLIFIER
8. OFFSET + CALIBRATOR
9. 25 VOLT POWER SUPPLY
10. 50 VOLT PS WITH MISC CONTROLS
11. OPTICS TABLE SHIELDING
12. I_R RECORDER
13. TUNGSTEN LIGHT SOURCE POWER SUPPLY
14. REFERENCE LIGHT BULB POWER SUPPLY
15. RECORDER USED IN CONSTANT I_0 FEEDBACK SYSTEM
16. SAMPLE VOLUME SHIELDING
17. SANBORN AUXILIARY CIRCUITS + MONITOR
18. MAGNET POWER SUPPLY + AUXILIARY CONTROLS
19. VARIABLE BAND-PASS FILTER
20. I_0 RECORDER
21. RATIO RECORDER WITH RETRANSMITTING SLIDEWIRE
22. PHOTOMULTIPLIER POWER SUPPLY + CONTROL BOX

FIG 2-14 ELECTRONIC COMPONENTS

S/N can be improved by $\sqrt{\text{number of spectrum sweeps}}$. The analyser's output can be displayed on an x-y recorder.

Yet another mode of readout is a two-recorder display of I_0 and I_R.

A calibration and AC offset unit is driven by signals derived from the light chopper and beam splitter reference signals. Calibration and offset for both I_R and I_0 channels can be independently adjusted and ac coupled into the system through a resistor in series with the photomultiplier anode resistor.

There are several units to permit monitoring of the signal at various points throughout the electronic system, and there is a versatile oscilloscope for appropriate display.

In the sections that follow, the individual components will be described. The circuitry in some cases is quite simple but will be included so that there will be a complete record. Following these, problems associated with the attainment of constant I_0 and with system-wide intermodulation effects are discussed.

2. Photomultiplier Power Supply and Control Box

a. Power Supply. The photomultiplier power supply is a Beva HV 302B-5†, which is adjustable from 500 to 2600 volts, and from 0 to 5 milliamperes. The stability and regulation are 0.01% and there is only 10 mv. ripple. Polarity is reversible but is kept in the "ground polarity +" position.

---

† Beva Electronics Inc., 185 4th Street, Trenton. New Jersey

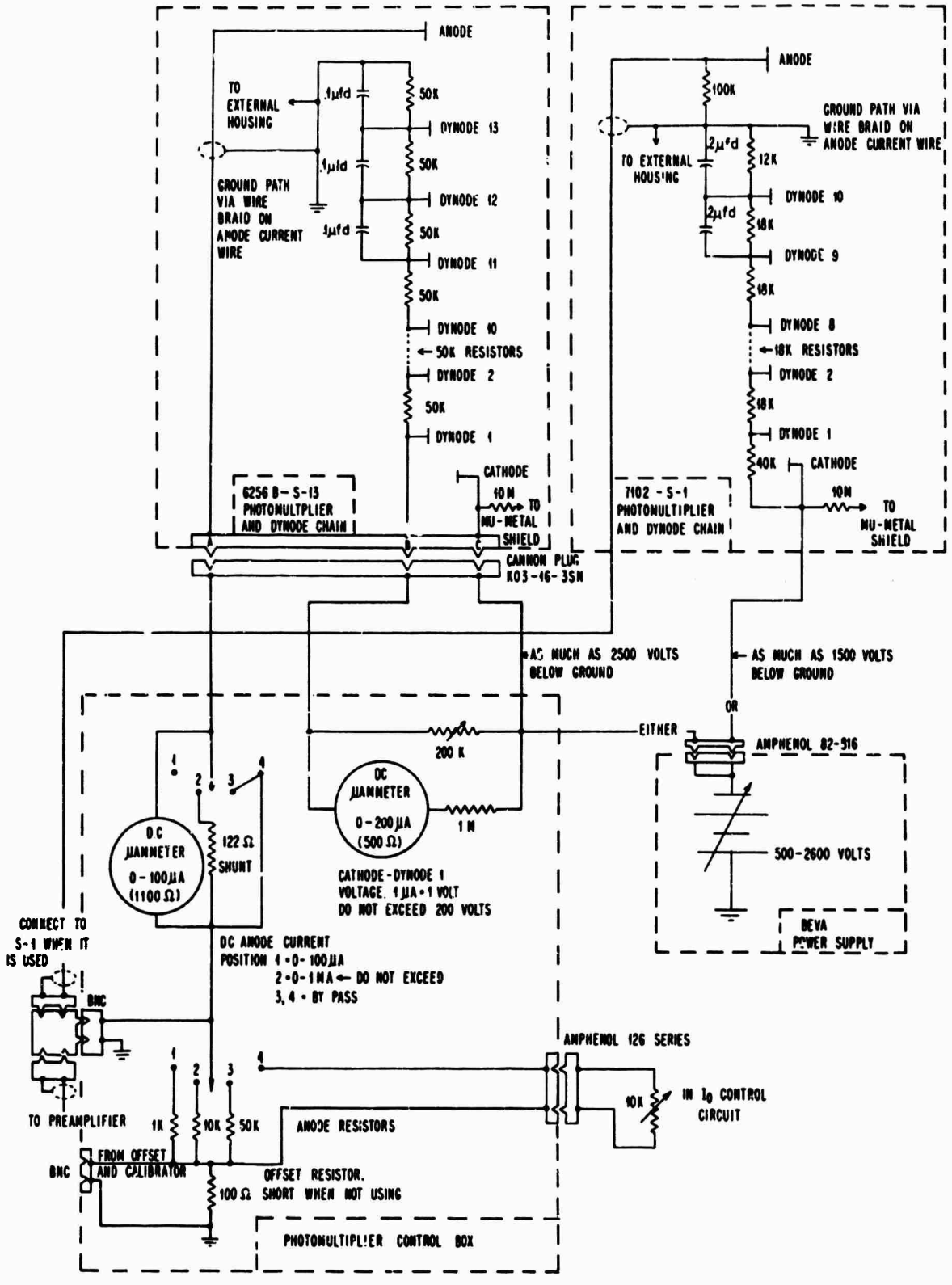

FIG 2-15 PHOTOMULTIPLIERS, POWER SUPPLY, AND CONTROL BOX: WIRING DIAGRAM

b. Control Box. The control box (Fig. 2-15) serves a number of functions for the 6256B photomultiplier, although not for the 7102.

(1) Control (through the 200 KΩ potentiometer) and monitoring (with the 200 μa. meter) of the voltage applied to the cathode-dynode 1 stage of the photomultiplier. A signal-to-noise study indicated an optimum setting of around 125 volts.

(2) Monitoring of the DC anode output to ensure it does not exceed the prescribed level. Switch positions are: 1) 100 μa. full scale; 2) 1 ma. full scale; 3) and 4) by-pass meter.

(3) Routing of power from the power supply to the 6256B tube.

(4) Routing of photomultiplier anode current to the control box when there is a choice of anode resistors with values of 1, 10, 50, and 100 KΩ as well as a variable 10 KΩ resistor. The 50 and 100 KΩ resistors introduced nonlinearities into the ratio measurement causing deviations of 2% and 5%, respectively, in an actual ratio of 42%. The 10 KΩ caused a negligible deviation of the ratio compared to the 1KΩ. Either is suitable, although the 1 KΩ is the more conservative choice. The variable resistor is mounted externally and is used for keeping I_R constant in $\Delta R/R$ measurements.

Anode resistor switching is accomplished with a shorting switch to ensure that current is bled off from the photomultiplier at all times.

(5) Addition of an AC offset voltage to the experimental signal, by means of a 100 Ω resistor in series with the anode resistor.

When this offset is not used, the 100 Ω resistor should be shorted to ground to eliminate noise from this resistor.

c. Resistor Chain. Davohm wire-wound 1% resistors were used in the photomultiplier resistor chain because of their low temperature coefficient, thereby ensuring a stable voltage distribution along the chain and hence minimum gain change as the unit heats up. The 1 watt size resistors proved a good choice because they do not overheat. Capacitors shunting the last three resistors before the anode reduce the modulation of the tube gain caused by the AC component of the experimental signal.

d. Exceptions in 7102 Control. The 7102 tube is not as carefully controlled as the 6256B. In its use the control box is bypassed except for the use of the anode resistors. A BNC connector from the 7102 attaches to the signal BNC on the control box.

e. Photomultiplier Settings. Settings for the 7102 and 6256B photomultipliers are given in Table 2-4.

3. Preamplifier

Because of limited gain in the phase sensitive detector, a preamplifier is necessary, particularly when small (1 KΩ) anode resistors are used to maximize photomultiplier linearity. Gain must be high enough so that no significant noise is added by the next stage -- the active filter. The system uses a transistorized, low noise, high source impedance preamplifier with a pass band of 5 Hz-1 MHz.† Its gain may be set at 10, 100, or 1000.

†Radiation Electronics Co., TA-5, now manufactured by Infra-Red Industries, Santa Barbara, California, and known as the model 617.

TABLE 2-4 SETTINGS FOR THE PHOTOMULTIPLIER TUBES

Tube Number	6256B	7102
Photocathode Characteristic	S-13	S-1
Maximum Cathode-Anode Voltage	2500 volts	1500 volts
Maximum Cathode-Dynode 1 Voltage	200 volts	400 volts[1]
Optimum Cathode-Dynode 1 Voltage	~ 125 volts	not measured
Maximum Dynode 10-Anode Voltage	not applicable	250 volts[1]
Maximum Anode Current	1 ma.	10 μa.
Optimum Anode Current for Gain Stability	10 μa.	not given

[1]Employing the resistor chain shown in Fig. 2-15, one will not exceed these limits so long as total voltage across the resistor chain is less than its limit, 1500 volts.

a. Noise. The preamplifier specifications indicate that the TA-5 is a low noise unit, adding only 2 db of noise above the Johnson noise of a 100 KΩ source resistor, when measured at 100 Hz with a 1 Hz bandwidth. 100 KΩ is the resistance of the preferred source. The added noise should become 5 db for a 1 KΩ source resistor. Actual noise measurements with a 100 KΩ resistor showed somewhat worse performance: 8 db instead of 2 db. However, in the usual R and $\Delta R/R$ measurements, the light intensity is high enough that photomultiplier shot noise is far in excess of any noise contributed by the preamplifier. Consequently, noise arising both from the failure of the preamplifier to meet specifications and the necessity to use a 1 KΩ source instead of the optimal 100 KΩ source is not important.

Preamplifier noise would become important only in experiments performed at light levels far lower than are used in the ratio system.

b. Linearity. The manufacturer claims that the maximum undistorted output is 3 volts peak to peak, but for linearity to lie within 1%, the output voltage should not exceed 2 volts. Under these conditions the linearity is within 0.1 db (1%) at a given frequency. Over the range 20 Hz to 60,000 Hz, it can deviate as much as 0.3 db.

When the instrument was first received the attenuator settings deviated by up to 1.7% from their prescribed values, but they can be adjusted to within 1% or less through use of resistors R215, R216, and R227.

c. Signal Distortion by the Preamplifier. The signal coming out of the photomultiplier has the shape shown in Fig. 2-OSC-5, which has the following Fourier components:

DC

$n \times 13$ Hz $\qquad n = 1,2,3,...$ (2.22a)

$m \times 1080 \pm n \times 13$ Hz $\qquad m = 1,3,5,...$ (2.22b)

The TA-5 is an AC amplifier with a 3 db down point at 5 Hz. There is a phase shift at 13 Hz, and more shift at 13 than at 26 Hz. This causes a distortion and an apparent partial merging of the I_0 and I_R signals (Fig. 2-OSC-6), which one might think would result in cross-talk between the channels. Actually, the distortion occurs only in the $n \times 13$ Hz components, which are rejected both by the band-pass filter and in phase sensitive detection.

4. Variable Band-Pass Filter

A band-pass filter can be introduced following the preamplifier to remove the n × 13 Hz components from the signal and to prevent noise saturation of the phase sensitive detector's amplifier. An active variable unit is used, the Krohn-Hite Model 310-AB(R),† which has adjustable low and high cutoff positions.

All signal information is to be found in the frequencies 1080 ± n × 13 Hz; i.e., in the fundamental of the light chop frequency and its modulation at 13 Hz by the reference and sample channel reflections. A low cutoff should be low enough to pass all important 1080 - n × 13 Hz components yet high enough to remove the n × 13 Hz components. The appropriate range is 350-450 Hz. The upper filter limit should permit the passage of all significant 1080 + n × 13 Hz components yet reject high frequency noise. This limit is 1800-2000 Hz.

The filter should be placed after the preamplifier, not before, since it adds noise to low amplitude signals (less than 100 mv.). There is a low frequency fluctuation in its output which can be blocked by a 1 μf capacitor in series with the 30 KΩ input impedance of the phase sensitive detector.

The phase of the 1080 Hz carrier is highly sensitive to the filter's low cutoff position. This could result in noise except for the good phase stability of the filter. However, the 1080 Hz reference phase must be reset mechanically at the light chopper whenever the filter pass band is changed.

---

†Krohn-Hite Corp., 580 Massachusetts Ave., Cambridge, Massachusetts

Use of a highly stable passive filter, preferably of adjustable pass band, would eliminate these sources of noise, although this had not been done at the time of writing.

5. Phase Sensitive Detector

The AC experimental signal must be converted to a DC level for display. In preference to the usual square-law detector, we select a phase sensitive detector which has superior noise characteristics. The improvement arises through elimination of the beating together of noise and experimental signals found in square-law detectors [2-12, pp. 249-267; 2-13, Chapters 12, 13].

A reference signal, which is locked in frequency and phase to the experimental signal, rectifies that signal in a bridge network. The component of the output near zero frequency is proportional to the experimental signal times the cosine of the phase angle between reference and experimental signals and is actually the envelope of the original experimental signal [2-12]. The output is filtered in a low-pass unit: the longer the time constant, the narrower the pass band around the original AC frequency.

Noise has a random phase relationship to the reference signal, and so causes excursions in the output about the proper signal level without any DC shift. Noise outside the pass band of the filter is removed.

a. Sanborn Performance. The system employs a Sanborn 350-1200 BT Phase Sensitive Demodulator with the associated Sanborn 350-500 AP

Preamplifier Power Supply.† Amplification with a gain of 200 is followed by phase sensitive demodulation in a four-diode bridge network. The bridge is switched by a square wave, which is an amplified version of the reference signal derived from the light chopper. Note that the reference and experimental signals have the same frequency and fixed phase because of the nature of the light chopper. The rectified signal passes through a three-stage R-C filter with three choices of cutoff frequency: 12, 80, and 200 Hz. The "Hi" filter setting is necessary when processing the dual beam signal,which has the components $1080 \pm n \times 13 \pm f$ Hz. (f is a very low frequency representing light intensity change with wavelength.) One must pass the $n \times 13$ components without distortion. If the "Medium" position filter is used in ratio measurements, the partial merging of the two signals will result in a slight change in R. The "Low" setting is appropriate for I_0 or I_R measurements alone where we detect $1080 \pm f$ Hz.

Following a DC zero-level adjustment of $\pm$ 3 volts, one has a choice of two outputs. Neither is at ground potential, so that all subsequent circuitry must be insulated from ground. The first output is from a vacuum tube which presents a source impedance of 1000 Ω. For system performance to be within specifications, the load must be 2200 Ω or more.

When smaller loads are desirable, the second output may be used. In this case a transistor unit serves as a buffer between the tube

---

†Sanborn Company, 175 Wyman St., Waltham, Massachusetts

and the load. The output impedance is 3 Ω and the preferred load, 50 Ω. In our system both outputs are utilized with appropriate loads.

The Sanborn unit's frequency range is 50-5000 Hz. The linearity is as shown in Table 2-5.

TABLE 2-5 SANBORN LINEARITY

Output	Load	Linearity in Volts is	When Peak Voltages do not Exceed	Linearity in % of Peak Values
Vacuum Tube	> 5000 Ω	.0125	5	1/4%
Vacuum Tube	2200 Ω	.045	6	3/4%
Transistor	50 Ω	.025	5	1/2%

Drift is specified at less than 2 mv./hour. This holds nicely after a one hour warmup and is bettered if the unit is left on continuously. The air conditioned, constant temperature room in which our system is located ensures that temperature induced drifts are minimized.

b. Sanborn Deficiencies. The Sanborn fails to live up to its specifications in certain respects. Following the output filters, ripple (at twice reference frequency) is about twice that specified. This is potentially undesirable because of noise arising from intermodulation effects (Sec. II-B-21).

For certain selected frequencies, there are adjustable resistors or capacitors in the reference signal amplifier to permit optimum phase adjustment of reference and experimental signals. These fail

to provide the specified range; using them alone, phase optimization is impossible. Fortunately, the mechanical phase adjustment on the light chopper eliminates this difficulty.

The rise time of the amplified reference signal is slow, 20 μsec., which is a sizable fraction of a period at 5000 Hz. This effectively prevents operation at frequencies higher than 5000 Hz. It appears to be no problem at the system frequency, 1080 Hz, since the diode bridge is switched at only a very small fraction of the reference signal's total voltage excursion.

The Sanborn has an overload light, but this will not indicate saturation of the experimental signal in the amplifier. It is designed to respond primarily to signals which are in quadrature with the experimental signal. When the quadrature signal is large enough to cause modification in the experimental signal due to amplifier saturation, the light will fire. Since this voltage is nearly twice that at which the experimental signal itself would saturate, signal saturation must be checked elsewhere, preferably by monitoring the Sanborn output wave shape on an oscilloscope.

A modification to let the overload light act at a lower voltage was tried and rejected since it both distorted the experimental signal and proved superfluous with oscilloscope monitoring of the output.

Sanborn disadvantages are noticeable in comparison with other units:

(1) Only slight internal phase adjustment and this in an awkward way.

(2) No preamplifier and amplification of only 200.

(3) No band-pass filter for experimental signal.

(4) Limited frequency range.

However, the first three objections are readily solved with additional components, and the fourth is not a limitation in the Sanborn's use in the ratio system. The lack of phase shift and limited frequency range are problems only in $\Delta R/R$ measurements. Yet, where it counts, in linearity and low drift, it performs superbly. Its superior performance to a far more expensive unit provided a dramatic vindication of its choice.

c. Comparison of Sanborn and PAR HR-8. The greater capabilities of the PAR HR-8,† together with its DC drift specification, which is comparable to the Sanborn, recommended it as a possible replacement for that unit.

Tests of both units were made under comparable conditions, contrived to reduce other possible noise sources. Light intensity was high and a high quality mirror of constant R over its surface was used as the sample. Table 2-6 shows the PAR results for reflectivity spans of 90-100% and 98-100% across the recorder. The effects of various time constants are included. Table 2-6 should be compared with Table 2-19 which gives similar data for the Sanborn.

Except for its slightly greater drift, the PAR, in its 500 μv. gain setting, is exactly equivalent to the Sanborn in reflectivity ratio noise on the 10% and 2% spans for various time constants. But

†Princeton Applied Research, P.O. Box 565, Princeton, New Jersey

TABLE 2-6 SYSTEM PERFORMANCE WHEN USING THE PAR HR-8

PAR Gain Setting	Ratio	Span	Time Constant in Seconds	Ratio Indeterminacy in Divisions of Chart Paper	Ratio Indeterminacy in Percent
500 μv.	99.5%	90-100%	τ_3 = 0.7	1.0	.1%
			τ_4 = 2.0	0.75	.075%
			τ_5 = 4.5	0.5 + drift	.05% + drift
			τ_6 = 9	0.5 or less + drift	.05% or less + drift
		98-100%	τ_3 = 0.7	5	.10%
			τ_4 = 2.0	2 + drift	.04% + drift
			τ_5 = 4.5	2 + drift	.04% + drift
			τ_6 = 9	2 + drift	.04% + drift
			τ_7 = 22	1 + drift	.02% + drift
1 mv.	95.0%	90-100%	τ_3 = 0.7	30	3%
			τ_4 = 2.0	20	2%
			τ_5 = 4.5	15	1.5%
			τ_6 = 9	10	1.0%
			τ_7 = 22	5	0.5%

in its 1 mv. gain position, the PAR is 10-30 times worse. The noise imparted by the PAR preamplifier depends on gain setting, and we would normally expect this to increase for higher gains since the noise of the first stage is amplified more and more. In fact, as one increases the gain from the 1 mv. to the 500 μv. setting in this particular preamplifier, the output noise actually decreases by a factor of 15-30. The reason is that at the change to the 1 mv.

setting, an attenuator is added to the PAR circuit, followed by another stage of amplification. Significant noise can then be added to the reduced input signal at the stage beyond the attenuator. (Despite this odd design feature, the PAR performs within its own specifications.)

Obviously, the PAR is unsatisfactory since one cannot always contrive to have his gain set at the 500 μv. position. In addition, the greater long term drift completes the case against the PAR.

6. Phase Sensitive Detector--Problems and Modifications

There are certain other inadequacies or limitations in the operation of the Sanborn. Some prove to be curable. Others require that special precautions be taken in using the instrument.

a. DC Drift and Noise Problem. The DC level at the Sanborn output is not completely stable. There is a long term drift of up to 2 mv./hour and the short term noise (period less than 1 second) can be as much as $\pm \frac{1}{2}$ mv. This affects the reflectivity ratio by adding a voltage $\Delta(t)$ to both V_{I_R} and V_{I_0}.† The effect of the $\Delta(t)$

---

†V_{I_0} = voltage corresponding to I_0 at Sanborn output.

voltage is analogous to that of the scattered light.† The measured reflectivity ratio is

$$R_m = \frac{V_{I_R} + \Delta(t)}{V_{I_0} + \Delta(t)} \qquad (2.23)$$

and is modified in three ways by $\Delta(t)$:

(1) Slow DC drift modifies the ratio slowly in time.

(2) A nonzero initial setting of $\Delta(t)$ modifies R_m.

(3) Noise in the DC level, $\Delta(t)$, causes short term ratio noise.

Manipulating R_m we get,

$$R_m = \frac{R_t + \frac{\Delta(t)}{V_{I_0}}}{1 + \frac{\Delta(t)}{V_{I_0}}}, \qquad R_t = \frac{V_{I_R}}{V_{I_0}}, \qquad t \Longrightarrow \text{true}. \qquad (2.24)$$

---

†It is instructive to outline this equivalence in detail. Optical and electronic analogs are: $I_R(\lambda)$ and $V_{I_R}(\lambda)$; $I_0(\lambda)$ and $V_{I_0}(\lambda)$; $I_0(\text{scatt})$ and $\Delta(t)$; R(scatt) and 1 (or equivalently 100%); $a(\lambda)$ and $\Delta(t)/V_{I_0}$; $R_m(\lambda)$ and $R_m(\lambda)$; and $R_t(\lambda)$ and $R_t(\lambda)$. Substituting directly in the optical equation, Eq. 2.13, we attain the electronic equivalent, Eq. 2.23. Alternate forms for the expressions for the error are:

$$R_m(\lambda) - R_t(\lambda) = [R(\text{scatt}) - R_m(\lambda)]a(\lambda) \qquad \text{Optical form}$$

$$R_m(\lambda) - R_t(\lambda) = [1 - R_m(\lambda)]\Delta(t)/V_{I_0} \qquad \text{Electronic form}$$

The optical form can be rewritten as:

$$R_m(\lambda) - R_t(\lambda) = (1 - [R_m(\lambda) + 1 - R(\text{scatt})])a(\lambda).$$

Figure 2-16, which is a plot of reflectivity errors created by $\Delta(t)$, can now be applied to finding the $R_m - R_t$ correction factor when there is scattered light. This is done simply by replacing $\Delta(t)/V_{I_0}$ by $a(\lambda)$ and $R_m(\lambda)$ by $R_m(\lambda) + 1 - R(\text{scatt})$ in the plots and reading off the correction factor.

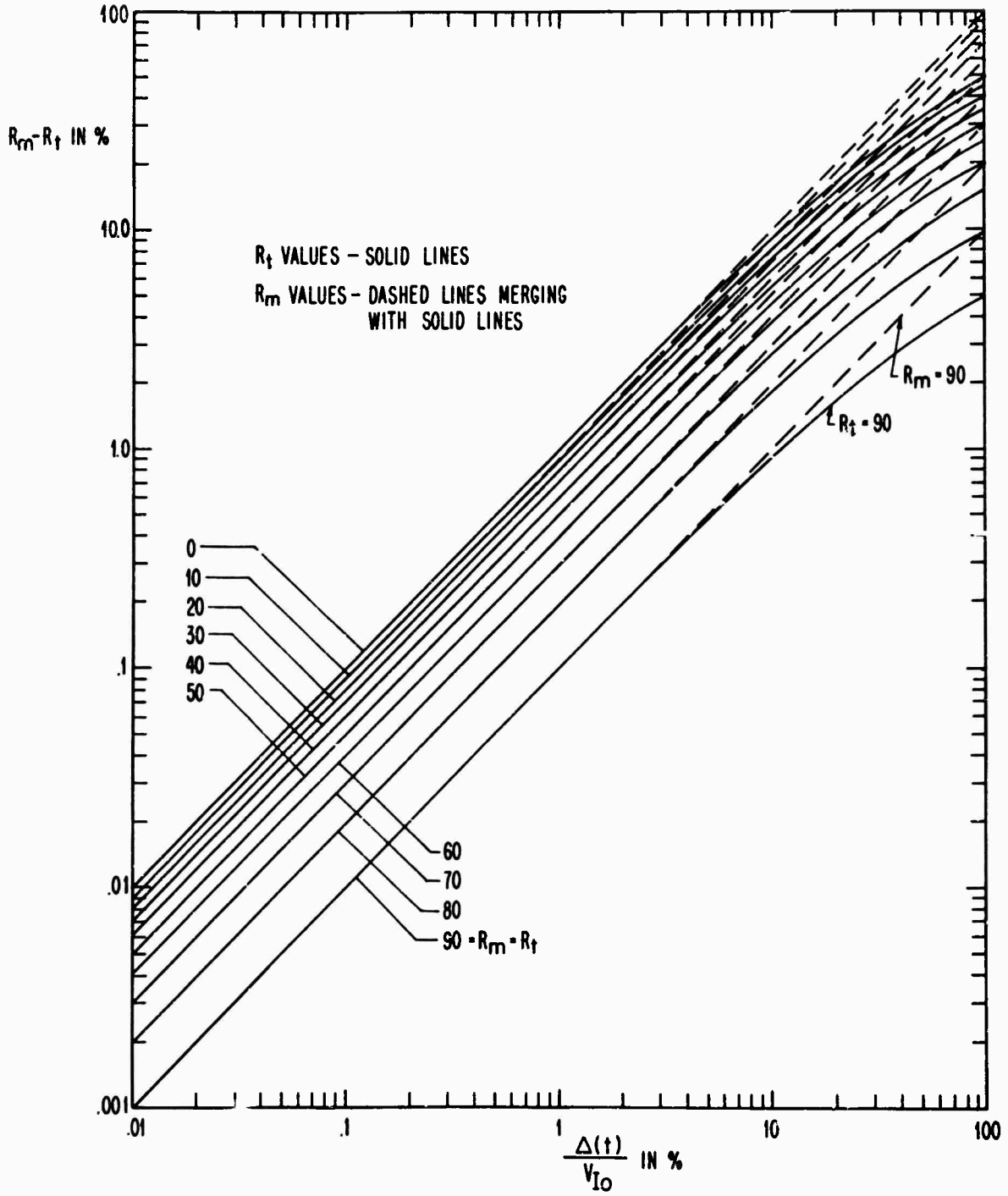

FIG. 2-16 REFLECTIVITY ERROR CREATED BY SANBORN DC LEVEL FOR VARIOUS R_m AND R_t VALUES.

The error is most serious for $R_t = 0$, and is zero for $R_t = 1$. Figure 2-16 is a plot of $R_m - R_t$ in % vs. $\frac{\Delta(t)}{V_{I_0}}$ in % for various R_t values. The magnitude and relevance of the problem is most forcefully demonstrated by an example. Suppose the maximum value of the I_0 triangle (Fig. 2-OSC-8) is $V_{I_0}^{max} = 2$ volts (chosen to ensure linearity) and $R_t = 40\%$. Then the average value of V_{I_0}, $\langle V_{I_0} \rangle$, is 500 mv. If $\Delta(t) = 0.5$ mv., $R_m - R_t = 0.06\%$ and % error is $\frac{0.06}{40} \times 100 = 0.15\%$. When $R_t = 10\%$, this becomes 0.09% and % error is $\frac{0.09}{10} \times 100 = 0.9\%$. Since these errors increase as V_{I_0} decreases, V_{I_0} should be kept as high as possible consistent with linearity.

The foregoing points up the desirability of increasing R_t which is easily accomplished by blocking part of the I_0 beam with a wavelength independent filter. If one then increases the Sanborn gain so that V_{I_0} is back to its former level, the effect of Δ on the ratio will be reduced.

For instance, let V_{I_0} become αV_{I_0}, $\alpha < 1$, where α is the filter transmission. Increase the gain by α^{-1}. Therefore, αV_{I_0} becomes V_{I_0}, V_{I_R} becomes $\frac{V_{I_R}}{\alpha}$

$$R_m = \frac{\frac{V_{I_R}}{\alpha} + \Delta(t)}{V_{I_0} + \Delta(t)} = \frac{1}{\alpha} \frac{R_t + \frac{\Delta(t)\alpha}{V_{I_0}}}{1 + \frac{\Delta(t)}{V_{I_0}}} = \frac{\frac{R_t}{\alpha} + \frac{\Delta(t)}{V_{I_0}}}{1 + \frac{\Delta(t)}{V_{I_0}}} . \qquad (2.25)$$

Now, for a given $\frac{\Delta}{V_{I_0}}$, R_m is less sensitive to Δ drift and noise. Of course, R_m must be corrected for α, but note an added boon: the peaks in one's experimental spectrum are accentuated by the factor $\frac{1}{\alpha}$.

The difficulty with this procedure lies in finding a suitable gray filter. Glass filters, which transmit a fraction of all the light incident, are never gray over much of a wavelength range. The metal plates with conical holes, cited in Sec. II-A-5-d, have a suitable wavelength range but transmit all the light incident on the holes and none incident on the other areas. In selecting certain portions of the beam, these metal filters can impart false structure to the reflectivity spectrum via the polarization dependent mechanism described in Chapter III. It is far better to use a high-speed light chopper in the I_0 beam as the gray filter; R_m will then be increased without a wavelength dependent error.

In addition to this over-all solution, the three $\Delta(t)$ effects can be attacked individually. The first effect, long term drift, is reduced by keeping the Sanborn turned on continuously; otherwise, for measurements on the 1% and 2% spans on the recorder, warmups of three to four hours are necessary. Frequent checks (every half hour) of DC level will keep drift to a minimum.

To reduce the second effect ($\Delta(t) \neq 0$ at $t = 0$) requires a foolproof way of setting the DC level at zero. The next section deals with this matter. Also necessary is sufficient resolution in the DC level control. The 100 KΩ carbon potentiometer, R1288, is a one-turn affair inadequate for the task. It was replaced by a 20 KΩ ten-turn wire-wound potentiometer† in series between two 40 KΩ resistors. The

†Helipot, 7210 Series, Beckman Instrument, Fullerton, California

6236 turns of the potentiometer give a resolution of 1/3 mv., less than the noise and drift of the DC level. Unfortunately, no 100 KΩ multiturn potentiometers of small size had a sufficient number of turns. The reduced adjustment range of the DC potentiometer is no problem since its range is still centered around zero.

The third effect, noisy behavior of $\Delta(t)$, must generally be tolerated. With care it need not be the limiting noise.

The $\Delta(t)$ noise is worsened by a poor cooling fan. At one time there was a 2 Hz, $\pm$ 1 mv. fluctuation in the DC level, correlated with a 2 Hz pulsation in the cooling fan. Disconnecting the fan stopped the fluctuation, which presumably was caused by variation in the cooling rate of the transistors. Shifting the fan blade on its shaft improved motor balance and eliminated the effect.

b. Three Types of DC Level Offset Error. By changing the operating conditions of the Sanborn, the operator gets a wide range of false zero levels. These arise in three distinct situations outlined in Table 2-7. Understanding these situations will provide rules for ensuring that the zero level is properly set.

(1) In the first type of situation, the Sanborn output level changes as the reference signal is turned on and off, provided the experimental signal input switch is in the "OFF" position. This level change is best observed with no experimental signal. The cause is a 120 Hz noise signal impressed on the external reference signal shaping circuit. Once introduced into the Sanborn, it is amplified sufficiently to cause switching of the bridge. That same

TABLE 2-7 THE CONDITIONS FOR DC LEVEL OFFSET ERROR IN THE SANBORN

Situation Number	Is There An Experimental Signal Out of Detector?	Position of Sanborn Experimental Signal Input Switch	Does Sanborn Receive a Reference Signal?	Source of Erroneous Voltage
1	Makes no difference. Observe with no signal, however.	OFF	No	120 Hz signal
2	Yes	OFF	Yes	Experimental signal
3	Makes no difference. Observe with no signal, however.	USE	Yes	Reference signal

120 Hz signal is picked up from the reference circuit by the experimental signal amplifier and rectified. This cross-talk results in a DC level change.

To corroborate this, we changed the 120 Hz level where it leaves the external reference signal shaping circuit (by turning its power supply on and off and the I_O, I_R, and 1080 Hz reference lights on and off). The DC offset was linearly proportional to this 120 Hz level. Further, the offset disappeared when the external shaping circuit and the Sanborn reference input were disconnected.

The offset is not a problem because it is presumably eliminated when the reference signal is turned on, the reference signal being 200-500 times larger than the 120 Hz signal. Even if it is not

eliminated, its residual shift should be constant and hence eliminated by DC level adjustment.

(2) The second effect involves a leakage of the experimental signal across the open circuit created when the input switch is in its "OFF" position; i.e., the signal leaks into the Sanborn. Provided there is a reference signal, this leakage is reflected in a change in DC output level proportional to the experimental signal. The change in DC level disappears when the experimental signal is disconnected from the Sanborn input.

This leakage should not be a problem during an actual run, since the direct connection of a signal to the Sanborn should almost completely shunt any paths occurring in the "OFF" position. At worst, the second path should increase the experimental signal in a linear way. An actual check corroborated this view: linearity is not affected.

The leakage obviously affects the setting of the zero level, a level which changes as experimental signal size changes. Thus, that level should be set with no experimental signal coming into the Sanborn, yet with the Sanborn fed from the same source impedance. This can be accomplished by replacing the anode resistor signal at the TA-5 input by a short. The "JSE-OFF" switch should be in the "USE" position to short out most of the effect.

(3) Pickup of the reference signal by the experimental signal channel accounts for the third type of error. This occurs whether

there is an experimental signal or not, though it is best observed with no signal. The input switch is in the "USE" position. The pickup takes place somewhere before the experimental signal amplifier's attenuator, because the setting of that attenuator directly determines the size of the offset. It is important for attenuator settings in the range 1-20.

Two experiments corroborate this analysis. Changing the phase of the reference signal external to the Sanborn (using the mechanical phase adjust) has no effect on the offset since this phase shift affects reference signal and its image in the experimental channel alike. But if one could change the phase of the two signals inside the Sanborn after the point where the reference is impressed on the experimental channel, offset should change. This indeed occurs when the phase shift variable capacitor (C-1224, C-1225) in the reference amplifier is adjusted.

To reduce the size of the effect, the capacitor can be varied, but there is still a residual offset which must be eliminated by zero adjust. One must follow certain precautions. Since the offset occurs when the Sanborn input switch is set to "USE", and this is the position of the switch during a run, adjustments must be made in this condition. The TA-5 input should be shorted so that one is not confused by noise or the experimental signal. One must <u>rezero</u> on changing gain when the attenuator setting is less than 20.

The serious modification of DC level with gain change was demonstrated by use of a gray filter of 47.6% transmission. Transmission was first measured at an attenuator setting of 50. When this was reduced to 1, transmission became 47.0%. This change was exactly matched by the zero offset change.

(4) Conclusions. A number of instinctively natural procedures are incorrect in setting the DC level. The proper guidelines can be summarized:

(a) Ensure that the reference signal is fed into the Sanborn and amplified to the proper level.

(b) Adjust with the Sanborn "USE-OFF" switch in its "USE" position, and the TA-5 input shorted.

(c) Rezero whenever the Sanborn gain is changed if the attenuator setting is less than 20.

(d) Adjust capacitors C-1224 and C-1225 to minimize crosstalk of the reference and experimental channels.

(e) For any gain setting zeroing can be checked by monitoring the output on a recorder with a short across the preamplifier (TA-5) input. This is the only way for high gain ($1 \leq$ attenuator setting < 20).

(f) For attenuator settings which are greater than or equal to 20, one can monitor the ratio, R, as the gain is varied. Since $R = \frac{V_{I_R} + \Delta}{V_{I_O} + \Delta}$, it will be constant as V_{I_R} and V_{I_O} ar changed only if $\Delta = 0$. This method is even more sensitive than (e) above.

c. External Monitor, Transfer and Service Circuits. An external monitor and transfer circuit, probing various interior points in the Sanborn, was constructed with the following purposes (Fig. 2-17):

(1) To monitor experimental and reference signals at various points in the Sanborn to ensure linear behavior.

(2) To monitor experimental and reference signals in order to adjust phase. The reference signal appears as sharp spikes on the experimental signal.

(3) To facilitate Sanborn adjustment and calibration.

(4) To transfer the following signals:

(a) Input of reference signal.

(b) Output signal from both Sanborn outputs.

Other circuits were tried and rejected since they failed in their original purpose or introduced spurious signals into the Sanborn. These included an input transformer bypass; a reference channel phase adjust via an external capacitor; an adjustment of the Sanborn amplifier overload set point and complementary alarm circuit; and a particular method of experimental signal monitoring.

At the monitor station there are two jacks, one to the left of the other. Their descriptions follow in Table 2-8.

d. Output Filter. The output filter is a variable three-stage R-C network. The "Hi" position filter passes nearly all the n × 13 Hz Fourier components necessary but its fall-off is slow enough that

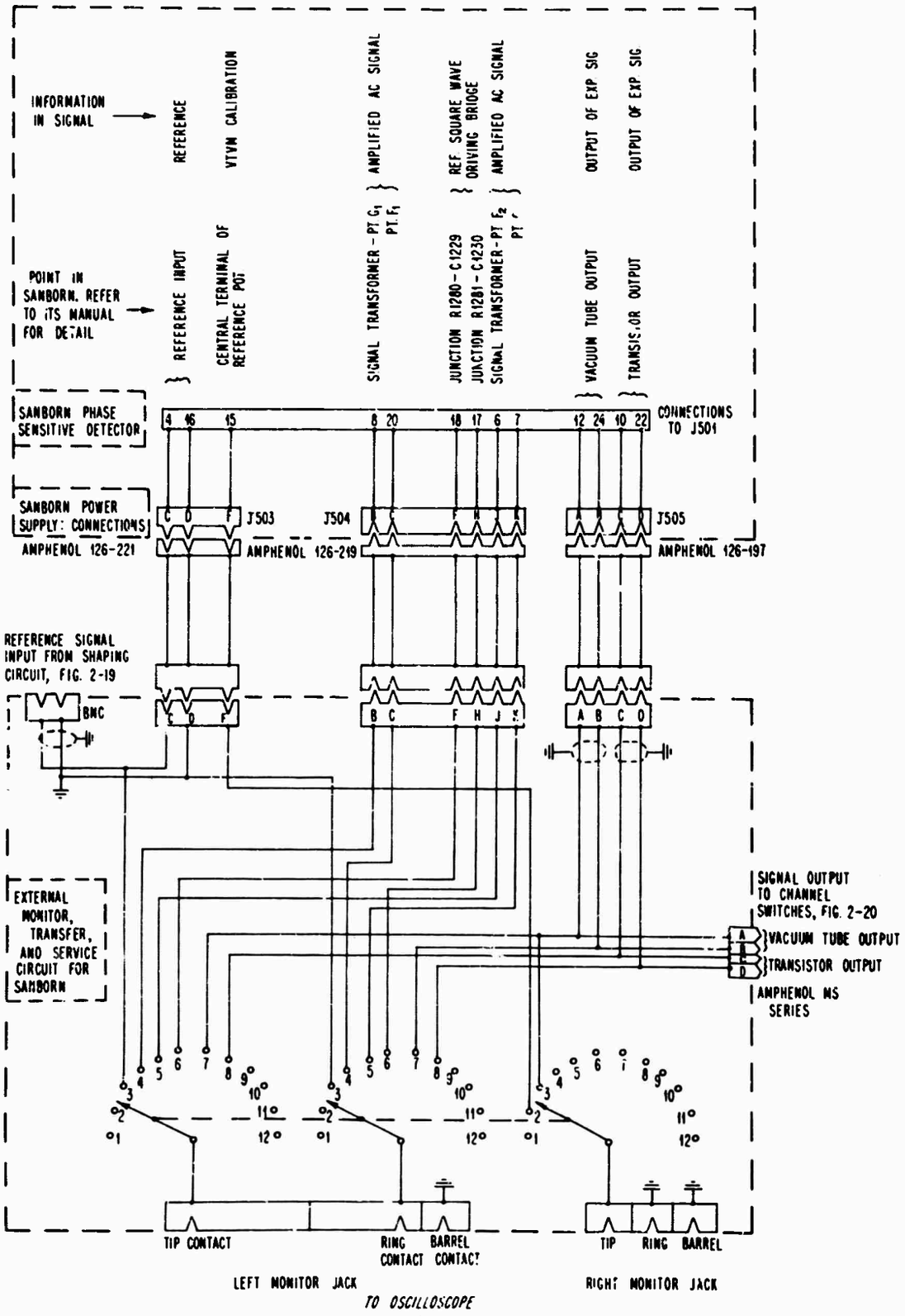

FIG. 2-17 SANBORN AUXILIARY CIRCUITS

TABLE 2-8 THE SANBORN MONITOR

Monitor Positions

Special Notes	Switch Position	Signal at Left Jack	Purpose	Figure Number
	1, 2	Unused.	Off.	
	3	Input reference signal.	Monitor the signal shape.	(sine wave)
CAUTION[1,2]	4	The experimental signal across the upper winding of the transformer preceding the bridge. Points G_1-F_1.	To ensure that amplified experimental signal is not saturated. Observe relative phase of experimental and reference signals.	2-OSC-18
CAUTION[1,2]	5	As in 4, except points G_2-F_2.	As in 4.	2-OSC-18
CAUTION[1,2]	6	Square wave reference signal at diode bridge.	Monitor size and shape of the switching square wave.	2-OSC-19
[2]	7	Output signal across vacuum tube output, V1208.	Monitor output signal size and shape. Useful in I_0 control.	
[2]	8	Output signal after transistor buffer.	As in 7.	2-OSC-8 through 13
	9-12	Unused.		

Adjustment Positions

	Switch Position	Signal at Right Jack	Purpose	
	1	Unused.	Off.	
	2	Center terminal of reference potentiometer and ground.	Sanborn VTVM Calibration. See p. 21 item 4c of Sanborn manual.	
	3	Output signal from vacuum tube V1208 to ground.	Sanborn AC ripple adjust. See p. 22, item 4g.	
	4-12	Unused.		

[1]CAUTION: Scope ground will be at a high potential relative to the Sanborn ground.

[2]In general the oscilloscope third wire should not be used since many monitor measurements are not made relative to system ground.

some residual 1080 Hz ripple passes through. This can be seen in Fig. 2-OSC-13. This ripple raises the spectre of intermodulation effects, discussed more fully in Section II-B-21. One possible way out was tried by replacing the three element R-C network with a five element L-C one which would have 12 db more attenuation/octave. The new unit filtered the 1080 Hz nicely but picked up an excessive amount of 120 Hz, making it useless.

The "Hi" filter position causes a very slight rounding in the triangular wave shape (compare Figs. 2-OSC-5 and 8). The problem is more strikingly demonstrated in the "Medium" filter position (Fig. 2-OSC-9). The curving of V_{I_R} is dependent on the magnitude of V_{I_O} as can be demonstrated by blocking the I_O light channel. V_{I_R} changes slightly. The reverse also holds. The changes are greater for the "Medium" than for the "Hi" filter position. By performing such an experiment for various R values, the correction to reflectivity can be determined. (R was changed by using gray filters.) For the "Hi" filter position the correction is less than $\pm$ 0.1% for $0 \leq R \leq 100\%$, while in the "Medium" position it is $\pm$ 0.5%. The change is small enough to be ignored, although it emphasizes the need to use the "Hi" position.

The magnitude of the correction could be adversely affected by distortion in the triangular wave shapes (Fig. 2-OSC-13). Distortion is eliminated if the light beam is vertically centered on the beam splitter mirrors.

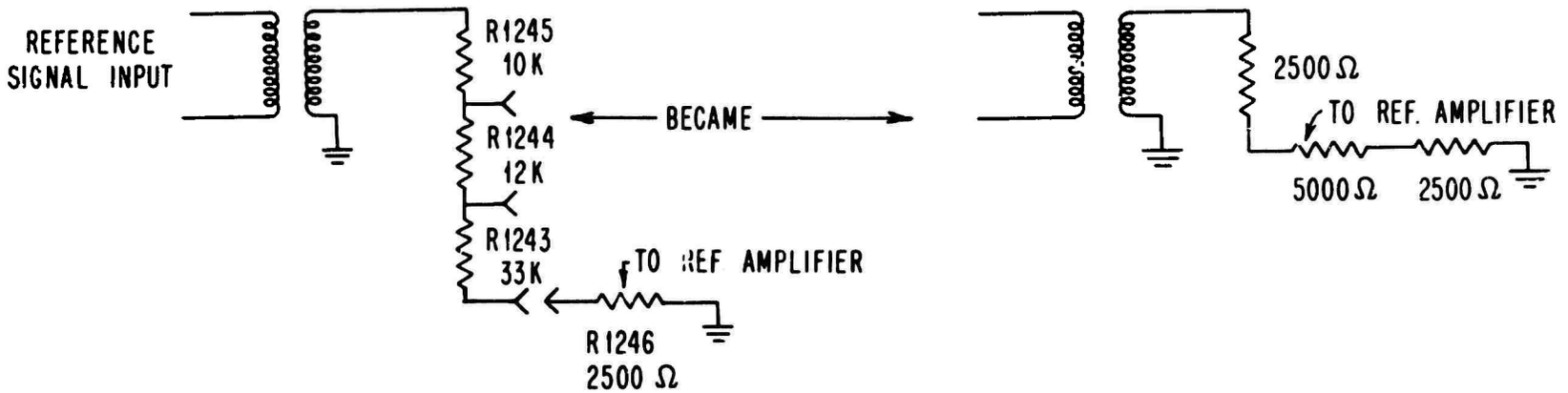

FIG. 2–18 CHANGES IN THE REFERENCE SIGNAL INPUT CIRCUIT IN SANBORN.

e. Reference Channel Resistor Changes. A small change in the reference signal input load resistors was made so that the load would be 10 KΩ, the appropriate match to the output impedance of the reference signal shaping circuit. Another change increased the sensitivity in the setting of the reference level (Fig. 2-18).

7. Beam Splitter Reference Signal Shaping Circuit

The beam splitter reference signals are small and somewhat ragged (0.1 volt) after leaving the light sensors (Fig. 2-OSC-24). They must be amplified and well squared before they can decisively actuate the electromechanical channel switches, thereby separating the two channels of information. A Schmitt trigger circuit (Fig. 2-19) gives the desired shaping. The light signal input from LS222 is first amplified by transistor 2N2219. Diode IN2071 ensures proper bias. The Schmitt trigger itself is a bistable unit having either full output, ~20 volts, or zero output. A relatively small signal, -2.2 volts, will switch it on; -0.54 volts will switch it off. Thus, an irregularly shaped input wave becomes a rectangular wave.

Uniformity of the output is good with low jitter. Risetime is sharp, 10 μsec., which is 0.013% of a period, and gives rapid switching.

There are two of these circuits, one for each of the beam splitter reference signals.

8. Light Chopper Reference Signal Shaping Circuit

This circuit is designed to amplify and shape the reference light signal so that it is suitable to drive the reference channel

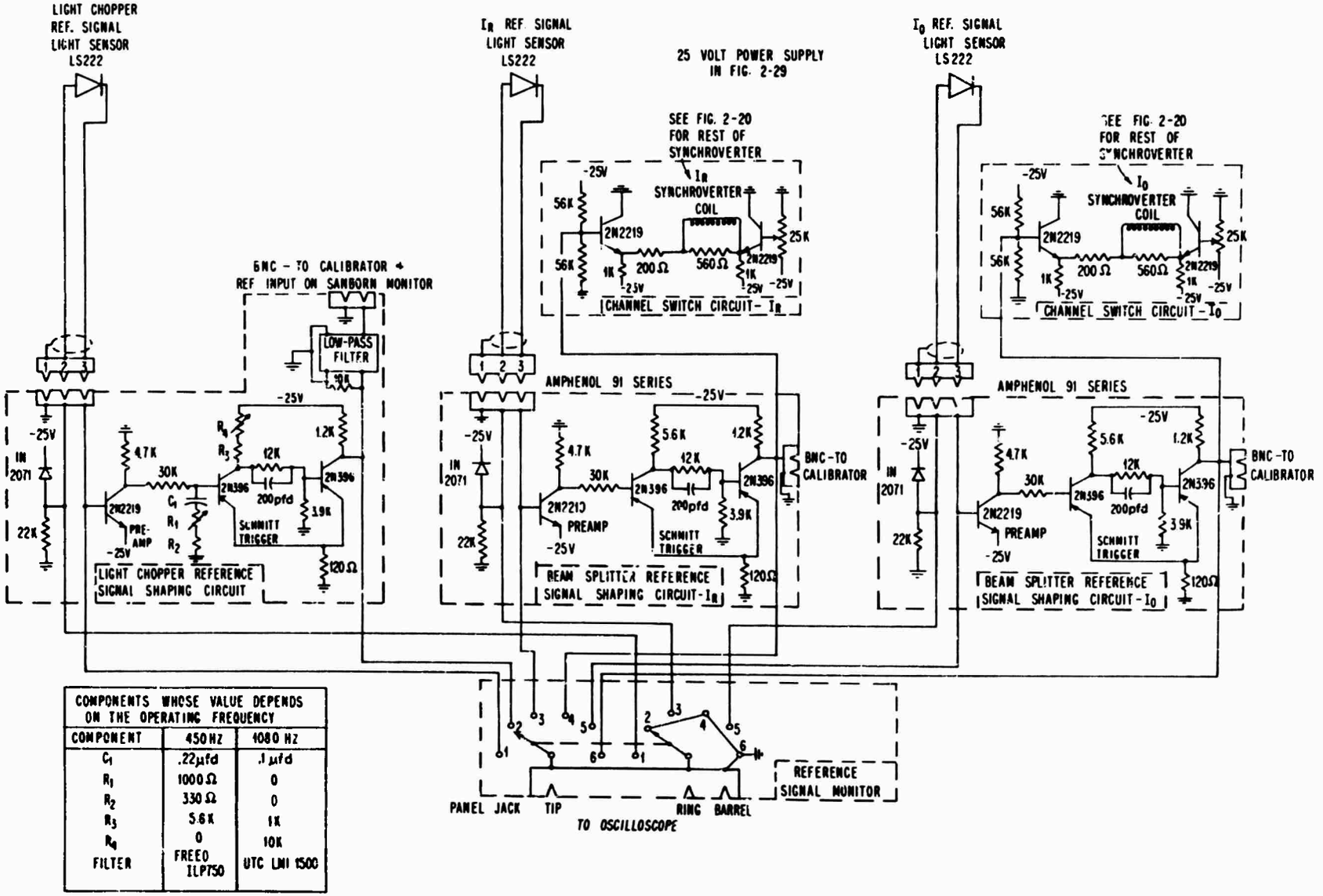

COMPONENTS WHOSE VALUE DEPENDS ON THE OPERATING FREQUENCY		
COMPONENT	450 HZ	1080 HZ
C_1	.22μfd	.1 μfd
R_1	1000Ω	0
R_2	330Ω	0
R_3	5.6K	1K
R_4	0	10K
FILTER	FREED ILP750	UTC LNI 1500

FIG. 2-19 REFERENCE SIGNAL SHAPING CIRCUITS WITH MONITOR AND CHANNEL SWITCH ACTUATING CIRCUITS

of the phase sensitive detector. In design, it is very similar to the two circuits which shape the beam splitter reference signals. However, there are some modifications dictated by factors discussed below. (Figure 2-19 shows the differences.)

The signal from the light sensor is irregular in shape (Fig. 2-OSC-22) and the resultant square wave is asymmetric. If the Sanborn is driven by an asymmetric reference signal, some strength is lost from the symmetric experimental signal. By adjusting the variable resistor, the voltage level at which the Schmitt trigger goes on and off is changed, and when the reference circuit output wave shape is monitored, symmetry within 3° is easily attained.

The low-pass filter at the circuit output is optional under usual operating conditions. It is necessary when the circuit's output is used to drive not only the Sanborn reference, but the AC calibrator and offset. By passing only the fundamental of the reference signal, the filter eliminates ringing in the offset caused by the higher harmonics in the square wave.

Figure 2-19 shows this circuit for both 450 Hz and 1080 Hz operation. The table found in the drawing gives a list of components which must be interchanged when changing frequency.

The shaping circuit operation is stable, although jitter can develop when transistor 2N2219 is overheated. Overheating or even loss of this component occurs when improper grounds are used while monitoring the reference light signal (Sec. II-B-9).

a. Speci l Demands on the Power Supply. The Schmitt trigger alternates suddenly between no load and full load. The power supply feeding all three signal shaping circuits must be highly stable under load changes to prevent mutual interference. This was indeed a problem in the original power supply design. The 1000 μf capacitor at the power supply output buffers the supply and the load (Fig. 2-29).

9. Reference Signal Monitor

The monitor's purpose is simple: to provide a means to check the operation of the reference signal shaping circuits (Fig. 2-19). Proper functioning can be checked quickly as can degradation of failure. The monitor positions are listed in Table 2-9.

TABLE 2-9 REFERENCE SIGNAL MONITOR POSITIONS

Special Notes	Switch Position	Purpose--To monitor	Figure Number
CAUTION[1]	1	The light chopper reference signal at detector.	2-OSC-22
	2	The shaped light chopper reference signal before filtering. This is applied to the low-pass filter and to the calibrator.	2-OSC-23
CAUTION[1]	3	The beam splitter reference signal at the detector-I_R channel.	2-OSC-24
	4	The shaped beam splitter reference signal-I_R channel.	2-OSC-25
CAUTION[1]	5	The beam splitter reference signal at the detector-I_0 channel.	2-OSC-24
	6	The shaped beam splitter reference signal-I_0 channel.	2-OSC-25

[1] Neither terminal of the light detector is at ground. An ungrounded oscilloscope must be used, otherwise transistor 2N2219 will be destroyed.

1C. Channel Switch, Sanborn Load, and Associated Monitor Circuits

The Sanborn output is made up of the I_R and I_O channel signals (Fig. 2-OSC-8). Up to this point both signals have been processed in the same electronic units. The channel switches separate this output into two physically distinct paths (Fig. 2-OSC-14). To optimize the separation, there is a monitor circuit. The phase sensitive detector resistive load is found in this unit.

a. Channel Switch. The channel switch is an electromechanical device, the Bristol Synchroverter, Model C-1414-8.† Current through a coil causes the single pole, double throw switch to close in one of its two positions, depending on the direction of current flow. Variation in switch closing time is minimized by driving it with the low frequency 13 Hz square wave; any residual variation is a source of noise. The effects of switch bounce on closing are reduced by capacitive integration.

Aging units may have pitted contacts and may close less decisively. They should be replaced.

b. Channel Switch Actuating Circuit. Each beam splitter reference signal shaping circuit drives a channel switch actuating circuit (Fig. 2-19). Each of these circuits reduces the signal from twenty volts to the six volts needed to drive the switch coil. Each circuit's variable potentiometer shifts the DC level so that it is centered at zero, thereby ensuring that there is sufficient

†Bristol Company, Waterbury, Connecticut

voltage to close the double throw Synchroverter in both directions.

We can now follow the experimental signal from the Sanborn through Fig. 2-20, which details the circuitry immediately following that component.

c. Sanborn Load. The choice of Sanborn load size is dictated by two considerations: the optimum resistive load of the Sanborn on the one hand, and the maximum permitted values of source impedance for the servo recorders on the other. Excess source impedances severely reduce recorder sensitivity. The filters between the Sanborn and the recorders pose some restrictions as well, since the resistors in question serve both as Sanborn load and filter source.

There are actually two sets of load resistors; one for the vacuum tube output and one for the transistor buffer output. The linearity of the vacuum tube output varies with the size of its load resistance, being optimized for resistances greater than 5 KΩ. Lower resistance values must be used to satisfy the other criterion cited above, and one must accept the reduced linearity when vacuum tube output is ultimately used to actuate the ratio recorder. This reduction need not occur when the transistor buffer is interposed and one loads the buffer. This is easily accomplished by unloading the vacuum tube output when the buffer is loaded.

A similar precaution does not need to be taken with the buffer; it is continuously loaded with its optimum 50 Ω load whether it or the vacuum tube drives the remaining system components.

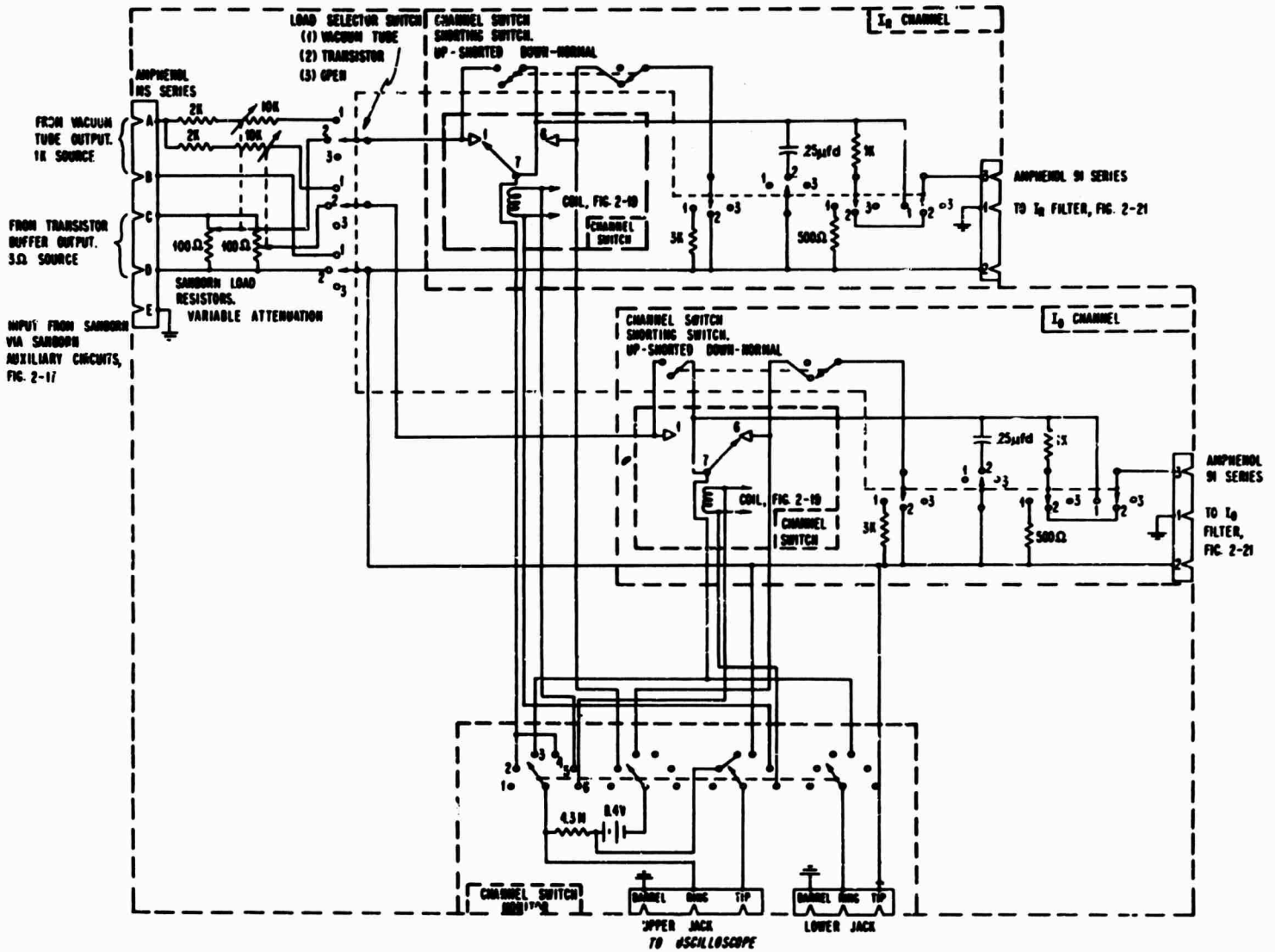

FIG. 2-20 CHANNEL SWITCH WITH MONITOR AND SANBORN LOAD

d. The Actual Load Potentiometers. There are four load potentiometers (upper left position of Fig. 2-20). Two 100 Ω units load the buffer, one to feed each channel switch. The magnitude of the signal selected from each can be scaled in direct proportion to its counter reading (0-1000) with a maximum deviation from linearity of 0.5%. The Sanborn loading is not significantly changed as one scales.

The second set of potentiometers are 10 KΩ units in series with 2 KΩ resistors and load the vacuum tube. Again, there is one potentiometer to feed each channel, but the scaling is not proportional to counter reading nor is the loading constant with scaling. Consequently, the transistor output is more convenient to use.

To simplify operation, the 100 Ω and 10 KΩ potentiometers for the I_R channel are ganged; so are those for the I_0 channel. They are ten-turn wire-wound Series A Helipots.† The inductance is low enough (1 mh. in a 100 Ω unit) that the n × 13 Hz signal components are not phase shifted relative to one another.

e. Experimental Signal Routing and Monitoring. Figure 2-20 shows the routing of the signal. A switch of twelve poles permits selecting the following:

(1) Routing of experimental signal from vacuum tube through two channel switches to two channel filters.

(2) Routing of experimental signal from transistor buffer through two channel switches to two channel filters.

---

†Helipot Division, Beckman Instruments, Fullerton, California

(3) No routing to channel filters.

The channel switches are in either of two positions: closed to permit routing of the signal from the Sanborn to the filters (contact 1), or touching the other position (contact 6). In the latter they present the filters with other resistances equivalent to the Sanborn load resistors. These maintain the filter time constant. The transition time from contact 1 to 6 is kept at a minimum by using a good square wave to drive the switch.

Near the output the 1 KΩ and 500 Ω resistors are part of a scheme to ensure that the filters have the same source impedance regardless of which Sanborn output is used. The 0.25 μf capacitor serves to eliminate noise due to bounce.

There are two switches to short out the Synchroverter for the two channels. They are necessary because the rest position of the channel switch is open circuit, and they are useful when the system is being used in something other than the ratio mode.

There are a number of purposes in monitoring:

(1) Check the separated I_R and I_0 signals to ensure continuity.

(2) Check the relative phases of the I_R (or I_0) channel signal and its switch to center the signal and maximize output. The signal is on for nearly 180° out of 360°, while the switch is closed for only 162°.

(3) See I_R and I_0 signals simultaneously on the double-beam oscilloscope. This is one way to check against overlap.

(4) Check for proper switch behavior.

(5) Check the voltage applied to the switch coils to ensure it is of good shape and is balanced relative to the zero level.

Table 2-10 indicates how these points can be checked at the various monitor positions.

TABLE 2-10 CHANNEL SWITCH MONITOR POSITIONS

Switch Position	Signal at Upper Jack	Signal at Lower Jack	Purpose	Figure Number
1	OFF	OFF		
2[1,2]	I_R channel switch position		4	2-OSC-20
3[1,2]	I_0 channel switch position		4	2-OSC-20
4[1]	I_R channel signal output	I_0 channel signal output	1,2,3	2-OSC-14 through 17
5	Voltage applied to coil of I_R switch		5	2-OSC-21
6	Voltage applied to coil of I_0 switch		5	2-OSC-21

[1] Use only an ungrounded oscilloscope.

[2] Check with load selector switch in third position.

11. Matched Channel Filters

The signal leaving each of the channel switches has both AC and DC components (Fig. 2-OSC-14). The AC signal is made up of 13 Hz and its harmonics. Since the recorders for I_R, I_O, and R respond to DC voltages, any low frequency AC results in rapid pen oscillation with a consequent loss in readout sensitivity. Low-pass filters are necessary to eliminate the 13 Hz signal. Since there is noise of all frequencies (up to the cutoff of the Sanborn filter) superposed on the signal, the filters are used to remove that as well.

a. Filter Requirements.

(1) Filters must be matched at all frequencies to prevent ratio wandering in response to transients.

(2) Cutoff should be steep so that 13 Hz is well filtered. The frequency region where any residual mismatch matters is that immediately above the cutoff. Here steep cutoff is important to reduce the width of this zone.

(3) Components should be stable in time and stable under voltage and temperature variations.

(4) A choice of filter cutoff frequencies is desirable as well as the ability to filter low frequency noise; the higher cutoff frequencies permit faster spectrum sweeps, and the lower remove more noise frequency components.

b. Filter Design. Our first filter, an R-C network, failed; the electrolytic capacitors employed to provide the high capacitance

needed could not be matched. In consequence the V_{I_C} and V_{I_R} signals came to equilibrium at different rates and their ratio drifted badly.

In contrast the L-C network shown in Fig. 2-21a required much lower capacitance values and fulfilled all four of the requirements. High Q, very stable mylar capacitors were used. The inductors were high Q, low frequency units.† By changing component arrangement the three separate filters shown in Fig. 2-21b were realized.‡ The filter characteristics are shown in Fig. 2-21c and are summarized in Table 2-11. The 6 Hz filter does not remove quite enough of the 13 Hz signal to prevent pen oscillation.

TABLE 2-11 CHANNEL FILTER DATA

Switch Position	Cutoff Frequency in Hz	db/ octave	Insertion loss: DC attenuation through filter
1	1	18	11.4 db
2	4	30	7.7
3	~6	18	6.6

Filter design has proceeded a long way from the original image impedance approach which presupposed physically impossible loads. Computer solutions of exact formulae for filters have yielded nomograms

†Type MQL-3, United Transformer Corp., 150 Varick St., New York, New York

‡In actuality there was a wiring error in the final assembly so that the central three capacitances in Fig. 2-21a are 11.4, 38.8, and 11.4 μf instead of 20.2, 21.2, and 20.2 μf. This error affects only the filter at switch position 3 shown in Fig. 2-21b, where capacitance values are 42.8 instead of 51.6 μf. Since this filter was rarely used, the error was not corrected.

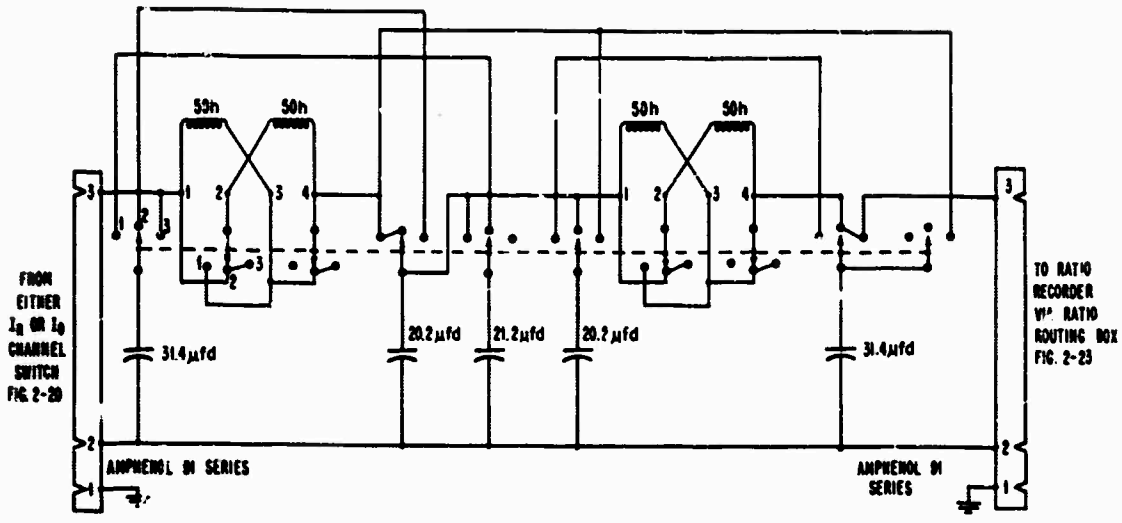

a. CHANNEL FILTER WIRING DIAGRAM

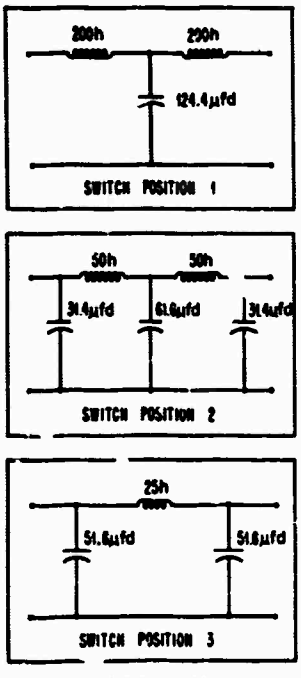

b. THE THREE FILTERS

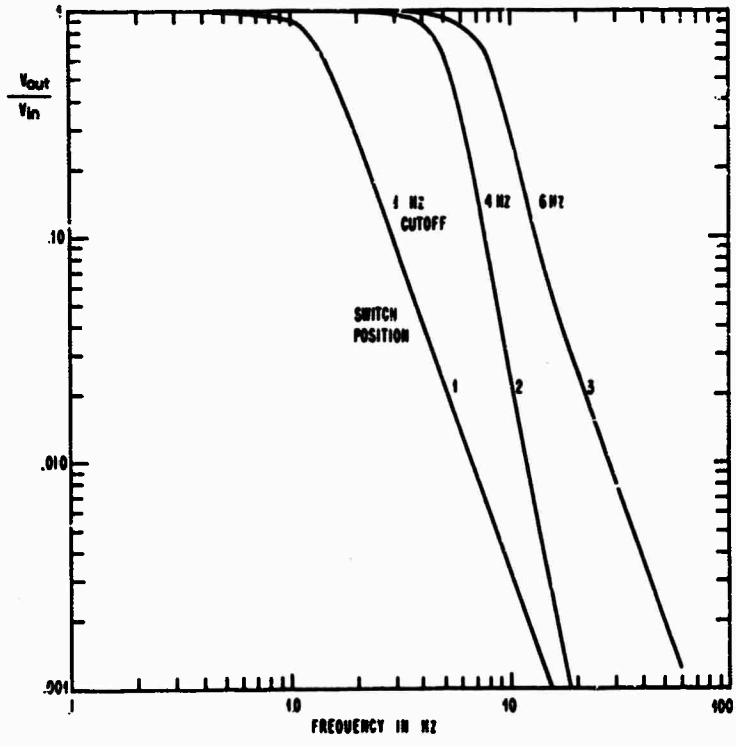

c. FILTER FREQUENCY CHARACTERISTICS

FIG 2-21 CHANNEL FILTER

where variables are source and load impedance, desired attenuation, component Q, frequency range, ripple in the pass band, and certain component values. An article by MacLean [2-14] was followed in computing filter component values. Actual filter performance matched the design criteria. Of the many possible designs the ones chosen were those which minimized the large capacitance needed, consistent with inductance values of coils commercially available. Curves for minimum band-pass ripple were used. Small resistors were added to certain sections of the inductors so that inductor Q's would be equal.

A symmetric filter design was chosen. The 1 KΩ load resistance ensured good recorder response. The symmetry implied a 1 KΩ source resistance. The arrangement of resistors in the channel switch unit provides a 1 KΩ source for both Sanborn output options, with a minimum insertion loss for the filter.

One criterion (4) was the ability to filter low frequency noise, but making additional matched filters with lower frequency cutoffs was not feasible. Inductor Q's are too low for sharp cutoff, and the necessary capacitors would cost far too much. The solution lies in the retransmitting slide wire (Sec. II-B-14) used with the ratio recorder, which permits filtering the ratio itself, not its two components.

There is a 60 Hz filter at the signal input to all Leeds and Northrup servo recorders. To ensure that the I_O and I_R filters are matched, this filter must be removed. However, the 60 Hz filter

is an integral part of the recorder damping circuit and prevents pen overshoot and hunting. Fortunately, our L-C filters damp almost as effectively. Various attempts to bring damping up to the original standard failed.

An alternative approach to filter design would be to isolate the filter from the channel switch with an operational amplifier. Then R and C values could be selected to give the same time constants with stable capacitors. This approach was rejected because it violated basic design philosophy, i.e., that the experimental signals be subject to active elements only when they are combined. For example, the DC drift in the operational amplifiers could have been troublesome. Further, the falloff with an R-C filter is one-half as steep as in an L-C unit.

12. Ratio Recorder†

The function of the ratio recorder is to divide the DC voltage corresponding to I_O (V_{I_O}) into that corresponding to I_R (V_{I_R}) and to display the result, R, as a pen trace on chart paper. The recorder receives the two voltages from the channel filters via the ratio routing box.

a. Normal Recorder Operation. A Leeds and Northrup Speedomax G Recorder‡ was employed. This is a DC recording, servo-operated, null balance unit, whose unmodified operation is summarized in

---

†While the ratio routing box precedes the ratio recorder in the circuit layout, it will be better understood following a discussion of the recorder.

‡Leeds and Northrup, Philadelphia, Pennsylvania

Fig. 2-22a. The battery current is controlled to give a fixed voltage drop across the slide wire, a resistor of many turns. The contact on the slide wire can move along its entire length, producing an output voltage proportional to the contact's instantaneous position. This voltage is compared with the experimental signal and their difference is first chopped and then amplified. Chopping the difference eliminates DC drift problems in the amplifier. After passing through a power stage, the error (difference) signal drives the motor, which is coupled to the slide wire contact. Provided polarities are properly selected, the system will come to balance with zero error signal and with the contact position proportional to the input signal. A pen, connected to the contact, indicates this voltage by a chart paper trace.

Certain other features are worth mentioning: 1) the input signal passes through a low-pass filter to remove the 60 Hz. It is this filter which must be removed if the matched channel filters are to function properly. 2) This filter is part of the damping circuit. Any recorder modifications must be made so that damping is not lost. This requires care in rewiring the recorder as well as in the use of the channel filters. 3) The amplifier has a gain control which must be varied as the voltage drop across the slide wire is changed, i.e., as one changes the recorder scale. Too low a setting causes sluggish response (deadband) and loss in sensitivity; too high a setting causes pen hunting. With proper gain, amplitude changes of 0.1% of full scale (pen trace width) are just discernible.

b. Recorder Modification. The Speedomax was modified in a conceptually simple way. The battery and the voltage control circuits actuating the slide wire were replaced by the output of the I_O channel filter (DC) (Fig. 2-22b). The I_R voltage serves as the experimental signal. Since the slide wire is linear, the balance position is $R = V_{I_R}/I_O$.

Increased sensitivity through scale expansion is a logical extension of this basic modification, but it must be done so that the load presented to the channel filters remains fixed at 1000 Ω; otherwise, filter matching is lost. In Fig. 2-22c we show how this was attained. The upper and lower limit resistor chains set the upper and lower percentage limits on reflectivity across the slide wire. The span resistance shunts the 400 Ω slide wire so that the percentage span is consistent with the upper and lower limits and the 1000 Ω requirement. Once the span is set, the range is changed by moving the upper and lower limit switches in synchronization. Table 2-12 shows the shunt values for various spans. General Radio Type 510 decade resistors† were used for the upper and lower limits and for the shunt. Their high linearity (0.05%) ensures accurate range changes. Per cent limits can be set in 0.1% increments and the span to within 0.05% of the actual desired value. These resistors are mounted in the ratio routing box, as is a selector switch for the span percentage described in Table 2-13.

†General Radio Company, 22 Baker Ave , West Concord, Massachusetts

TABLE 2-12 RATIO SLIDE WIRE SHUNT VALUES FOR VARIOUS SPANS

$R_{Slide\ Wire} = 403.7 \pm .2$, $1/R_{Slide\ Wire} + 1/R_{Shunt} = 1/(10 \times Span\ in\ \%)$	
Percent Span	R_{shunt} in Ohms
13.86	211.1 (maximum R_{shunt})
12.5	181.06 $\pm$ .04
10	132.93 $\pm$ .02
8	99.77 $\pm$ .02
5	57.068 $\pm$ .004
4	44.399 $\pm$ .003
3	32.408 $\pm$ .002
2	21.042 $\pm$ .001
1	10.254 $\pm$ .000
0.5	5.063 $\pm$ .000

TABLE 2-13 POSITIONS OF THE SELECTOR SWITCH FOR RATIO SPAN

Switch Position	Span and Comments
1	40% and 100%. Since the slide wire is only 400 Ω, some manipulation is necessary to get 100% span. The lower limit switch is set at zero, the upper at 40%. There is no shunt and the I_R attenuation potentiometer must be set at 0.400.
2	13.86%-8.01%. Continuous adjustment.
3	8.71%-0%. Continuous adjustment.

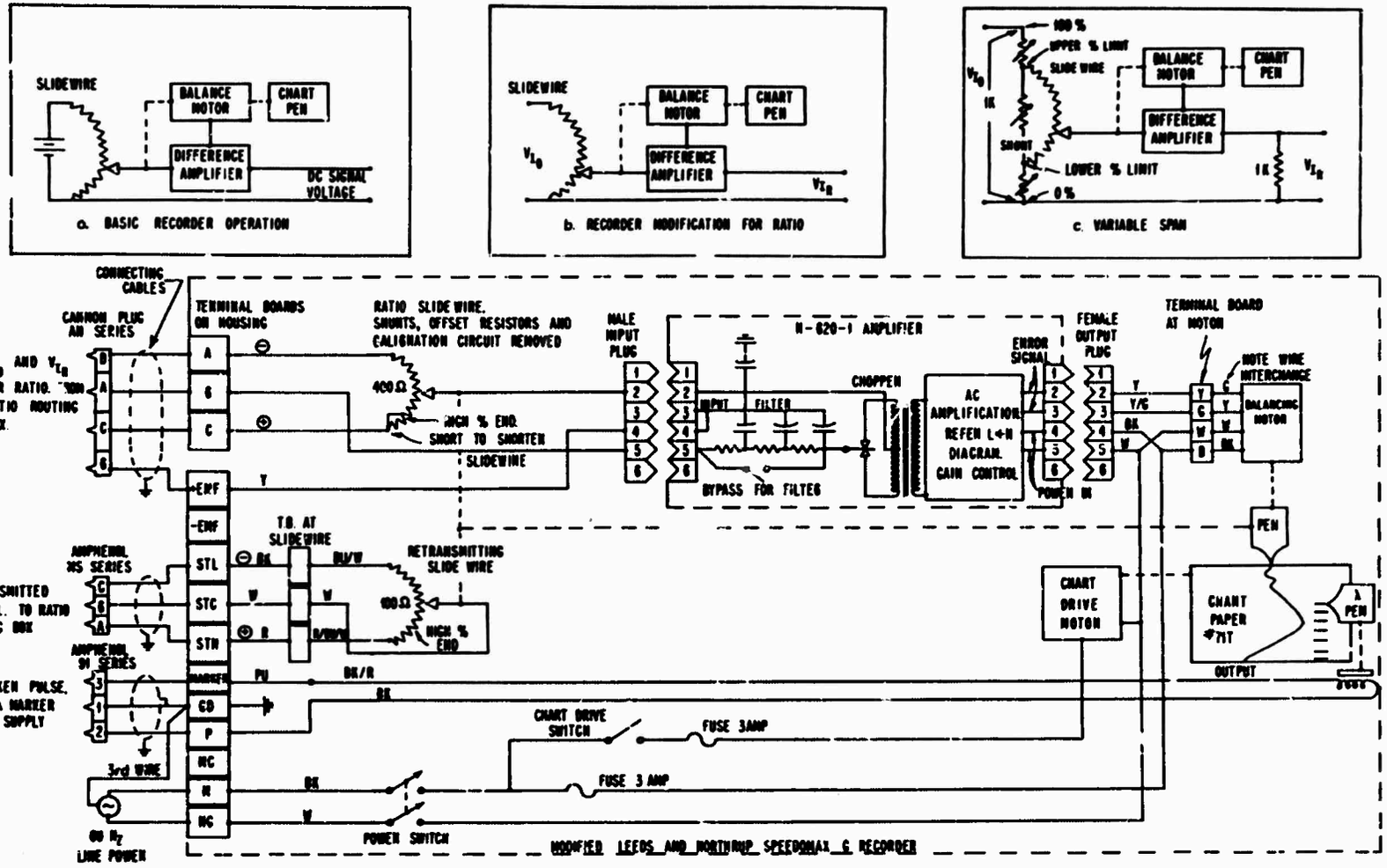

FIG. 2-22 THE RATIO RECORDER

Figure 2-22d is a wiring diagram of the modified recorder. The changes are relatively few but important, and are listed below.

(1) The battery, reference wet cell, and a second adjustable slide wire, designed to ensure that the prime slide wire voltage drop is calibrated, were removed.

(2) The voltage corresponding to I_0 was brought directly to the slide wire.

(3) The length of the slide wire is greater than the corresponding translational pen motion across the chart paper. When the pen is restricted to its permissible range, certain small ratio ranges lie in the inaccessible parts of the slide wire. To prevent loss of information, the unusable portions of the wire were shorted out with an adjustable press contact. Since there are about 1750 turns of wire this adjustment can be made within 0.05%.

(4) One could conceive of operating the recorder with certain variations in the input to the recorder amplifier at the male input plug. One such variation is the interchange of terminals 2 and 5; high amplitude hunting results. In fact, only one arrangement is satisfactory if deadband is to be reduced and damping to be proper. When this is done, signal polarities require interchanging the balancing motor polarities (yellow and green terminals).

(5) The 60 Hz filter in the recorder is utilized or bypassed through a simple switch.

(6) As the span is reduced, the voltage across the slide wire decreases in proportion. The error voltage corresponding to some

deviation of the recorder pen from its null position then decreases. Unless the amplifier gain is increased, the deadband increases. At maximum gain, the R-820-1 amplifier is limited to slide wire voltages of 10 mv., corresponding to spans of 7%. Amplifier improvements included substituting higher gain tubes. The 60 Hz filter removal, although necessitated by other considerations, provided a major improvement in sensitivity. A Leeds and Northrup 101122 high gain amplifier was tried and found worse than the modified R-820-1. The reason was unclear but was probably that enhanced 60 Hz pickup resulted in amplifier saturation. Various isolation procedures were unsuccessful.

Operationally, the modified amplifier works well down to 1% spans. Much lower spans are usually not useful because of:

(a) experimental signal noise causing excessive pen excursions.

(b) the change in ratio amplitude with wavelength, which results in the recorder pen's moving the full scale range after only a small wavelength change.

For a guide to system deadband with the R-820-1 consider the data in Table 2-14 on deadband. The DC level of the Sanborn was used as a suitably quiet signal and the 13 Hz switches were shorted out.

If amplifier deadband were the only consideration, performance would be adequate down to a span of 0.035%, where deadband would be 1 division out of 100.

TABLE 2-14 RATIO RECORDER DEADBAND IN DIVISIONS OF CHART PAPER AND IN VOLTAGE

Voltage Across Slide Wire in mv.	Corresponding Percent Span[1]	Deadband for Various L and N Amplifiers		
		R-820-1 With 60 Hz Filter	R-820-1 Without 60 Hz Filter	101122 With 60 Hz Filter
4	2.8	0.2 div. = 8 μv.	<.1 div. = 4 μv.	0.8 div. = 32 μv.
2	1.4	0.8 div. = 16 μv.	<.1 div. = 2 μv.	1.6 div. = 32 μv.
1	0.7	1.6 div. = 16 μv.	<.1 div. = 1 μv.	3.2 div. = 32 μv.
0.5	0.35		<.1 div. = 0.5 μv.	
0.25	0.175		.2 div. = 0.5 μv.	

[1]This column is computed as follows: I_0 = 2 volts, and the channel filter is set at position 1 (1 Hz cutoff). If span is then adjusted to give the slide wire voltage indicated in the prior column, span will be as indicated.

c. Wavelength Marker and Paper. A wavelength marker, placed at the edge of the chart paper, is an integral part of the recorder. It is actuated by the closing of contacts in the monochromator, permitting passage of a pulse from a 50 volt power supply. A more common approach is to add a voltage pulse to the signal, but the required circuitry was not compatible with certain ratio system criteria.

Since the marker's position shortens pen range, most chart papers are not suitable. Leeds and Northrup chart paper #717, with divisions running from -1 to 111, gives a usable range of 0 to 100. By rotating the slide wire, its lower limit can be set at the 0 position of the paper. The slide wire short can then be moved to the 100 position.

15. Ratio Routing Box

The box routes and processes the I_0, I_R, and R signals (Fig. 2-25). Two inputs are the I_R and I_0 signals from the channel filters. Their 1 KΩ loads are within the box. For I_0 it is the combination of resistors which permits selection of span and upper and lower percentage limits of the ratio. Note that the ratio recorder slide wire portion of the load is outside the box and is part of the Sanborn load in all modes of operation. A portion of the I_0 signal, selected by the lower limit resistors, can be routed to the I_0 recorder.

The I_R filter 1 KΩ load is a wire-wound potentiometer. The full voltage is fed to the ratio recorder during ratio operation, but a selected fraction can be sent to the I_R recorder. When routed to the I_R recorder, the I_R voltage can be filtered by a two-stage R-C network with time constants of 0, 1/6, 2/3, 2, 4.5, 9.5, 19, 38, and 90 seconds.

Monitor terminals permit checking the full I_R and I_0 voltages across their loads as well as the voltage across the shunted slide wire.

Another input is a voltage, proportional to R, received from the retransmitting slide wire. The voltage corresponding to full scale on the ratio recorder can be adjusted through the use of coarse and fine potentiometers in series with this second slide wire and a battery source. After filtering in the same R-C network used for the

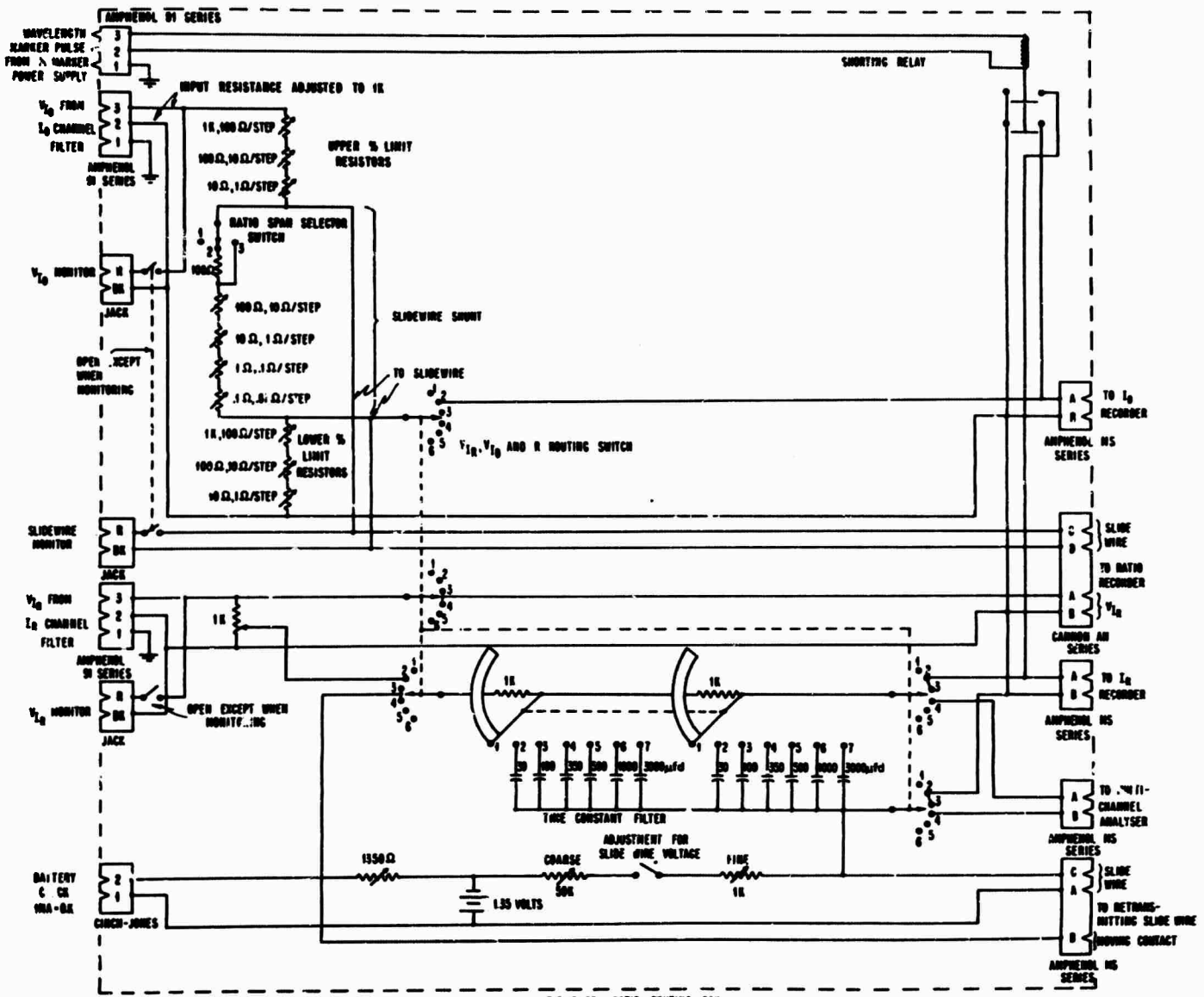

FIG. 2-23 RATIO ROUTING BOX

I_R signal, the R voltage can be transferred either to the I_R recorder or to the multichannel analyser system.

A selector switch permits choosing one of a number of routing modes, described in Table 2-15.

TABLE 2-15 V_{I_R}, V_{I_O}, AND R ROUTING SWITCH

Switch Position	Title	Effect
1	OFF	No signal to any of the three recorders.
2	I_R and I_O	A fraction of V_{I_R}, selected by the potentiometer setting, is routed to the I_R recorder via the R-C filter. A fraction of V_{I_O}, selected by the lower percent limit setting is routed to the I_O recorder.
3	R	V_{I_R} is routed to the ratio recorder, giving R. A voltage proportional to R is fed from the retransmitting slide wire through the R-C filter to to the I_R recorder.
4	R and MCA	Same as 3 except the filtered signal goes to the multichannel analyser instead of the I_R recorder.

A third input is a wavelength marker pulse which closes a relay. The closed contacts can be used to short the input to the I_O and I_R recorders, giving a negative marker pulse. This is not sppropriate

for use on the ratio recorder but serves nicely with the retransmitted ratio signal on the I_R recorder.

14. Retransmitting Slide Wire

We stated that the channel filter should serve a double purpose: elimination of the 13 Hz harmonics and noise reduction. Because of limitations imposed on matched filter construction, noise below 1 Hz cannot be removed even though such noise severely limits ratio sensitivity.

If one could filter the reflectivity ratio itself, rather than its two components, I_R and I_O, much longer time constants could be used. A retransmitting slide wire allows just this. It is mounted on the same shaft as the ratio recorder slide wire so that both slide wires have a fixed angular relationship. The two slide wire contacts effectively move in synchronization. Potentiometers, in series with a highly stable mercury battery, control the current through the slide wire to give the desired voltage drop. After filtering in the R-C network in the ratio routing box, this voltage can be displayed on the I_R recorder or stored in the multichannel analyser. As the retransmitting slide wire contact moves, the effective source resistance for the filter changes. However, the low resistance of the wire (100 Ω) ensures that the filter time constants are not significantly changed. Table 2-19 shows the typical improvement one can attain with the added filtering.

The angular position of the retransmitting wire must be adjusted so that its zero position corresponds to the zero position

on the ratio recorder wire. The procedure is complicated slightly by the fact that the sliding contact is lifted off the retransmitting slide wire before it reaches the zero resistance (and hence zero voltage) position. In lining up the zero positions of ratio, retransmitting, and I_R slide wires, the lowest division (out of 100) of retransmitted signal is lost.

The alignment of the 100 scale position of ratio signal and its analog on the I_R recorder is accomplished by adjusting the coarse and fine potentiometers. After alignment there is a maximum deviation of signal reproducibility of 0.2 divisions out of 100 over the full range.

If the signal is fed to the multichannel analyzer, voltage adjustments are made in accordance with the criteria discussed in Sec. II-B-16.

15. I_R and I_0 Recorders

The purpose of the I_R and I_0 recorders is to display I_R, I_0, and the retransmitted R.

The I_0 recorder is a Leeds and Northrup 10 mv. Speedomax H. It contains a control slide wire, potentially of use in a feedback system to set the I_0 level.

The I_R unit is a Leeds and Northrup 20 mv. Speedomax G.† The G has polarity opposite to the H. In standardizing polarity for the entire system, certain modifications were made to the G.

†There is no significance in the different ranges. These were merely the units readily available.

(1) Polarity change of the slide wire relative to its battery source.

(2) Interchange of the servo amplifier outlet leads to the servo motor (green and yellow wires) so that the motor will drive toward balance.

(3) Polarity change of the standard cell so that the calibrating system of the recorder would function. This ensures that the drop across the slide wire is 20 mv.

In the signal input channel of each recorder there is a capacitor between one side of the signal and ground. To prevent large deadband, the low side of the signal must be fed in here.

The I_R chart speed is varied by changing gears.

16. Multichannel Analyser

The basic purpose of a multichannel analyser is to improve the signal-to-noise ratio by summing a number of identical runs through a spectrum. The total signal is proportional to the number of runs summed. The noise increases only as the square root of the runs, since noise power rather than voltage is additive. Thus, the signal-to-noise voltage ratio improves with the square root of the number of scans. Any changes in experimental conditions invalidate this technique by modifying the signal itself. Such changes can occur in reflectivity work, particularly in measurements at low temperature.

One could ask why we do not quadruple the time constant rather than make four runs with a given constant. If the noise were like

Johnson noise, where $\sqrt{\langle V^2 \rangle} = \sqrt{4kTR\Delta f}$, the two techniques would be equivalent. System noise does not have the Johnson-noise-like characteristic. By filtering, the system noise can be reduced to 0.05% with time constants of 2 and 4.5 seconds. Longer values do not reduce the deviations further; the fluctuations merely occur over a longer period of time in proportion to the time constant used.

a. The RIDL Multichannel Analyser. The multichannel analyser used is the RIDL Model 34-12B Transistorized 400 Channel Analyser† used in conjunction with the RIDL Model 54-6 Time Base Generator, the RIDL Model 52-9 Time Mode System Controller, and the RIDL 52-39 Time Delay Generator units. The latter three permit time base operation rather than pulse height analysis.

The master unit, the RIDL Model 34-12B, has 400 channels, or storage bins, for information. The timing unit causes each channel to be open for a preselected period of time and then switches to the next. During that time only the open channel stores information, which is in the form of counts proportional to the average value of the signal. Thus, over the time a channel is open, noise is averaged. If one sweeps through a spectrum in time by running the monochromator wavelength drive, that spectrum can be separated into 400 segments by a suitable adjustment of wavelength sweep rate and time/channel. The spectrum is stored. If one then repeats the entire operation, the two spectra are added and stored. The limits on the number of

† Radiation Instrument Development Laboratory, Division of Nuclear-Chicago Corporation, 4501 West North Ave., Melrose Park, Illinois

spectra which may be added are storage capacity, spectrum stability, and patience.

b. The Voltage Converter. The Vidar Model 241 Voltage to Frequency converter† provides the pulses which the RIDL Model 34-12B counts and stores. The frequency of these pulses is directly proportional to the experimental input voltage and attains a maximum of 10^6 pulses/sec. for +2.0 volts. The Vidar is fed by the filtered voltage output of the retransmitting slide wire. This voltage is received from the ratio routing box.

There are upper and lower limits on the voltage across the slide wire.

(1) $\frac{\text{Voltage across the retransmitting slide wire}}{2 \text{ volts}} \times 10^6 \times$ channel width in seconds gives the maximum number of counts/channel/sweep ≡ C. There is an indeterminacy in C of one count depending on the relative time of channel opening and closing and pulse output (Fig. 2-24). C must be large enough to ensure that this indeterminacy adds insignificant noise. Since the resolution of the retransmitting slide wire is only 1000 units, C = 1000 is certainly adequate for a lower limit.

(2) Suppose one makes m runs. If $mC > 10^6$, overflow in each channel occurs and counting begins again from zero. A spectrum looking like Fig. 2-25a then looks like Fig. 2-25b. In such an instance interpretation is still easy, but more than one overflow causes some difficulty in unscrambling. Therefore, an upper limit on C must be $mC \leq 2 \times 10^6$.

---

†Vidar Corporation, 77 Ortega Ave., Mountain View, California

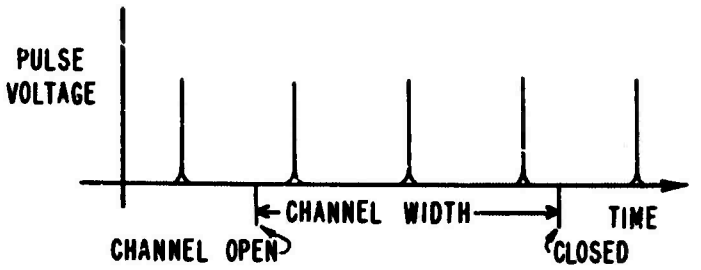

3 COUNTS IN THE TIME
OF ONE CHANNEL

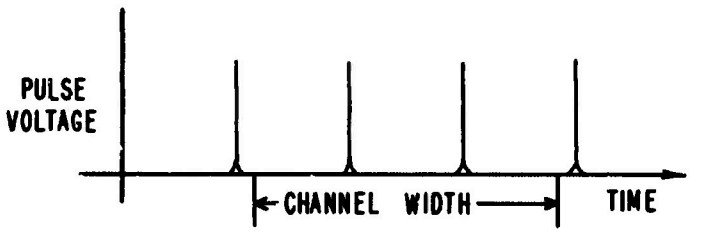

2 COUNTS IN THE TIME
OF ONE CHANNEL

FIG. 2-24 COUNTING INDETERMINACY IN MULTICHANNEL ANALYSER

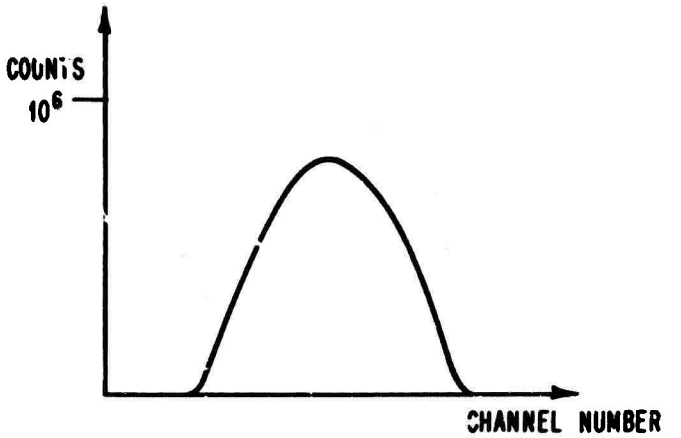

a. STORED SPECTRUM WITHOUT OVERFLOW

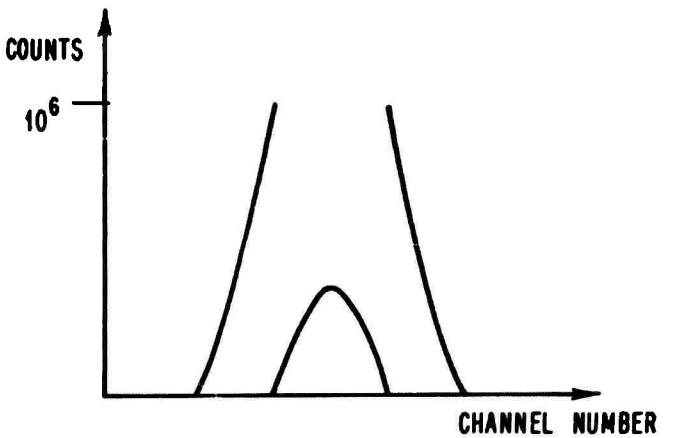

b. STORED SPECTRUM WITH OVERFLOW

FIG. 2-25 EFFECT OF OVERFLOW ON SPECTRUM SHAPE

c. Spectrum Initiation. For successive spectra to be stored properly, the start of the monochromator sweep must coincide with the start of the time sweep in the RIDL. The circuit described in the section on Miscellaneous Power Supplies and Controls (Sec. II-B-19) provides a pulse of the proper shape to initiate the RIDL time sweep. It, in turn, is actuated by the closure of contacts every 10Å in the monochromator.

By observing the time spacing of two pulses, the variation in firing time was measured. This variation was a maximum of .25Å at the 500Å/min. sweep rate and reduced to a minimum of .06Å for sweep rates of 50Å/min. or less. It is insignificant in terms of the typical structure variation with wavelength which is observed.

The operating procedure is simple. We start the monochromator wavelength drive about 5Å away from a marker pulse. As the drive passes through this first contact closure, the RIDL 54-6 time base generator will start its run. Further pulses, occurring every 10Å, are ignored by the RIDL Model 54-6, which switches the Model 34-12B through its 400 channels at a rate chosen by the operator. At the end of the sweep the RIDL rejects any further information until reset.

The time advance of the RIDL is very closely controlled by a crystal oscillator, but wavelength advance is determined by a less accurate synchronous motor. Nonetheless, the two remain in synchronization within 1/3Å over periods of 16 minutes.

d. Readout. During storage an oscilloscope, integral with the RIDL Model 34-12B, shows the individual channel counting. Following any spectrum sweep, the operator can display the total storage in all 400 (or any 100) channels. For a quick check there is the oscilloscope. For a more permanent record there is an x-y recorder output. The ordinate is a voltage proportional to counts in a channel and the abscissa is a voltage proportional to channel number. Using a versatile recorder† permits scale expansion and DC offset.

e. System Wiring and Use. Figure 2-26 shows the connections of the Vidar and RIDL units to the rest of the system as well as their internal connections for time base operation. In addition there is a summary of the functions performed by each unit and a listing of the various controls and their usual settings.

The operator must ensure that the following have the proper relationship:

(1) Wavelength sweep rate

(2) Retransmitting slide wire time constant

(3) Channel width

(4) Slide wire voltage.

We see no way to incorporate the RIDL 52-39, Time Delay Generator in the system. However, use of the RIDL 52-9 Time Mode System Controller would permit automatic control of multiple sweeps through a spectrum. On completion of a sweep through all 400 channels, the address overflow pulse, which is available at P2 on the RIDL 12-34B, could be used to reverse the direction of the monochromator wavelength

†Moseley Autograf Model 7000A x-y Recorder, F. L. Moseley Co., Pasadena, California

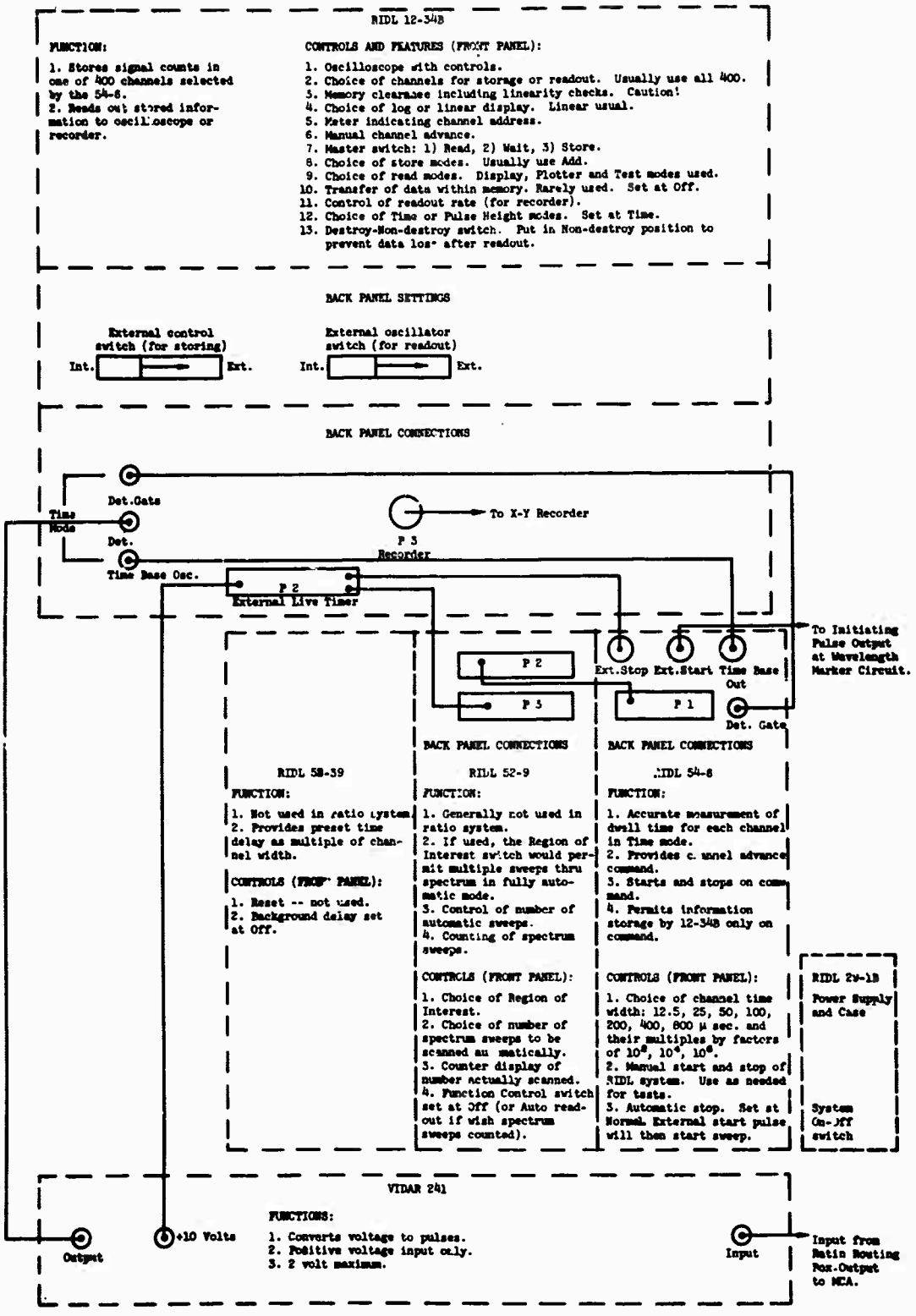

FIG. 2-26 WIRING CONNECTIONS, FUNCTIONS, AND CONTROLS OF THE MULTICHANNEL ANALYSER SYSTEM

scan. The Region of Interest switch, if set at position 2, would ensure that no data were stored during the time for return to the wavelength corresponding to channel 0. Using the address overflow pulse again, the wavelength drive could be reversed a second time, and the system would be ready to accept data from a second forward scan through the spectrum. Setting the Cycle Counter would determine the number of sweeps to be made prior to readout.

A possible improvement in the multichannel analyser system would be the addition of a magnetic tape unit to which the contents of the memory could be transferred. By transferring memory contents to tape before each spectrum scan, each new scan could be examined and rejected if unduly noisy. If suitable, the prior scans could then be added to the current scan by reading them back into the memory.

f. Signal Distortion by Vidar. The Vidar input impedance is 2 KΩ. One can consider its effect on the filter in comparison with the infinite impedance of the I_R recorder when the recorder is balanced. There results some change in time constants which is not serious. More important is signal distortion: the voltage across the 2 KΩ resistor is not exactly proportional to the position of the slide wire contact. Figure 2-27 shows the amount of this distortion for various settings of the resistor R_b. The calculation is found in Appendix II-*A*.

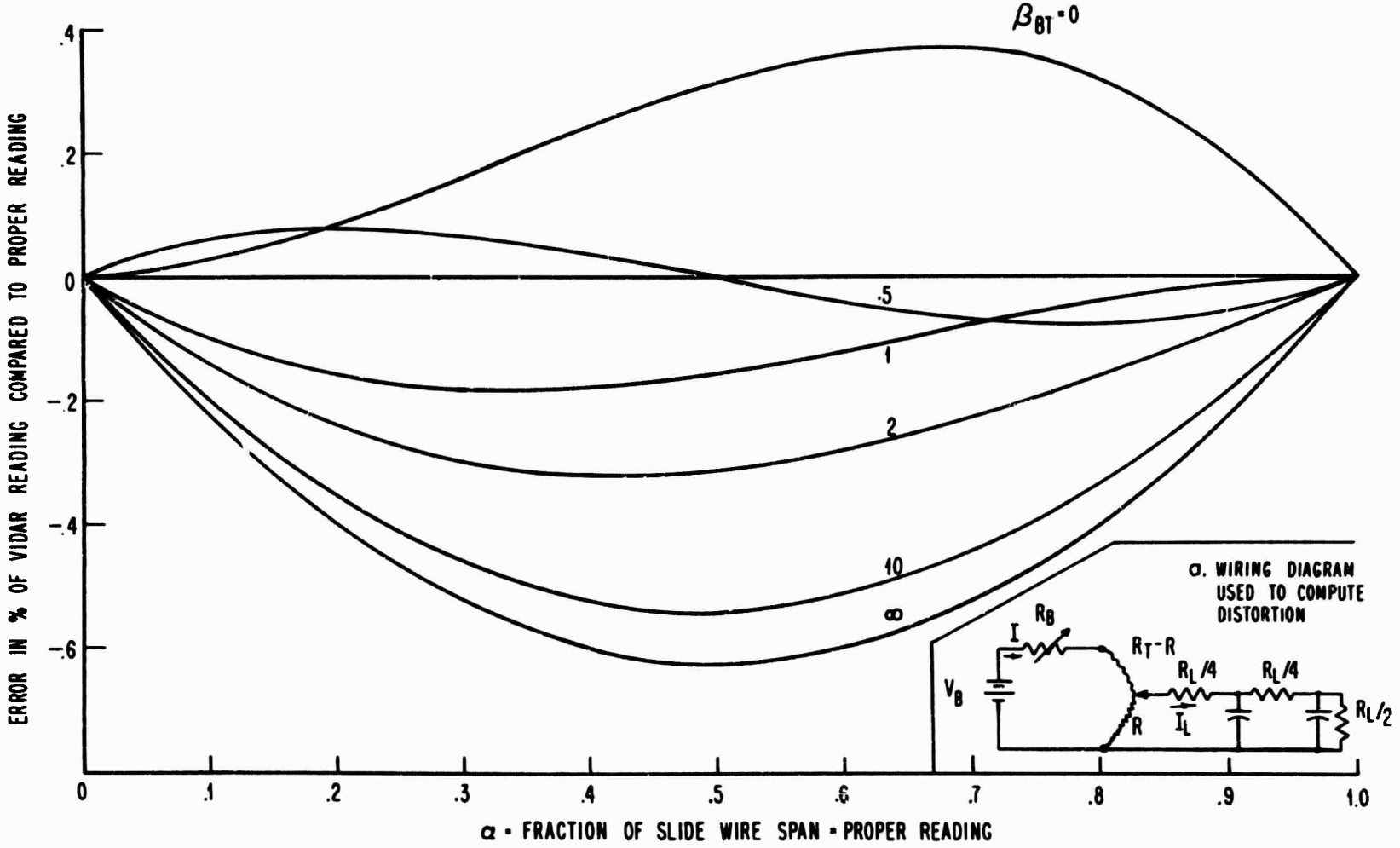

FIG. 2-27 DISTORTION OF THE RETRANSMITTING SLIDE WIRE READING BY THE VIDAR COMPONENT OF THE MULTICHANNEL ANALYSER PLOTTED FOR VARIOUS VALUES OF $\beta_{BT} = R_B/R_T$

Under the worst conditions the error does not exceed 0.65% of the full scale value. The importance of this distortion will depend on the percentage span corresponding to the full travel of the retransmitting slide wire and the size of the structure which is observed. In most instances where small percentage spans are studied, the error will not be significant. If it is, a correction could be made based on Eq. 2.41.

17. System Polarities

All electronic system voltage polarities were made consistent. They are:

(1) The Sanborn calibrator voltage which can have only positive sign.

(2) The Vidar input which must be positive.

(3) The experimental signal at the Sanborn output, where the sign is determined by the reference channel mechanical phase adjustment. 360° of variation is possible.

(4) The calibrator and offset voltage which can be set at either polarity with a switch.

(5) The I_O, I_R, and R recorders which have positive signal input polarity. This required a slide wire polarity change in the I_R recorder (and other changes) and a balancing motor polarity change in the R recorder.

(6) The retransmitting slide wire voltage, which is given positive polarity.

(7) The R-C filter for I_R and retransmitted R signals, in which electrolytic capacitors determine polarity.

18. Offset and Calibrator

The offset and calibrator allows the operator to add arbitrary amounts of voltage to both the I_R and I_O components of the experimental signal. Addition occurs at the 100 Ω resistor which is in series with the anode resistor.

The circuit is shown in Fig. 2-28. The first input is the 1080 Hz carrier from the reference signal shaping circuit output. The filtered fundamental of this signal must be used since the square wave causes ringing. It first encounters the 1 μf capacitor which blocks DC from the input transformers. After being divided into two paths, the carrier is switched on and off by the 2N2219 transistors. These are biased by the 13 Hz signals from the I_R and I_O beam splitter reference shaping circuits. The shaped carriers are brought back together at the common 100 Ω load. The result is shown in Fig. 2-OSC-26.

Switches permit selecting decade changes in the I_R and I_O offset values and two potentiometers provide continuous variation. Polarity switches allow one to add or subtract either voltage.

As a calibrator the unit has some usefulness since signals totally in phase with their reference can be traced through the entire electronic system.

Its potential utility as an offset lies in subtracting an AC level from the experimental signal, thereby permitting greater AC amplification

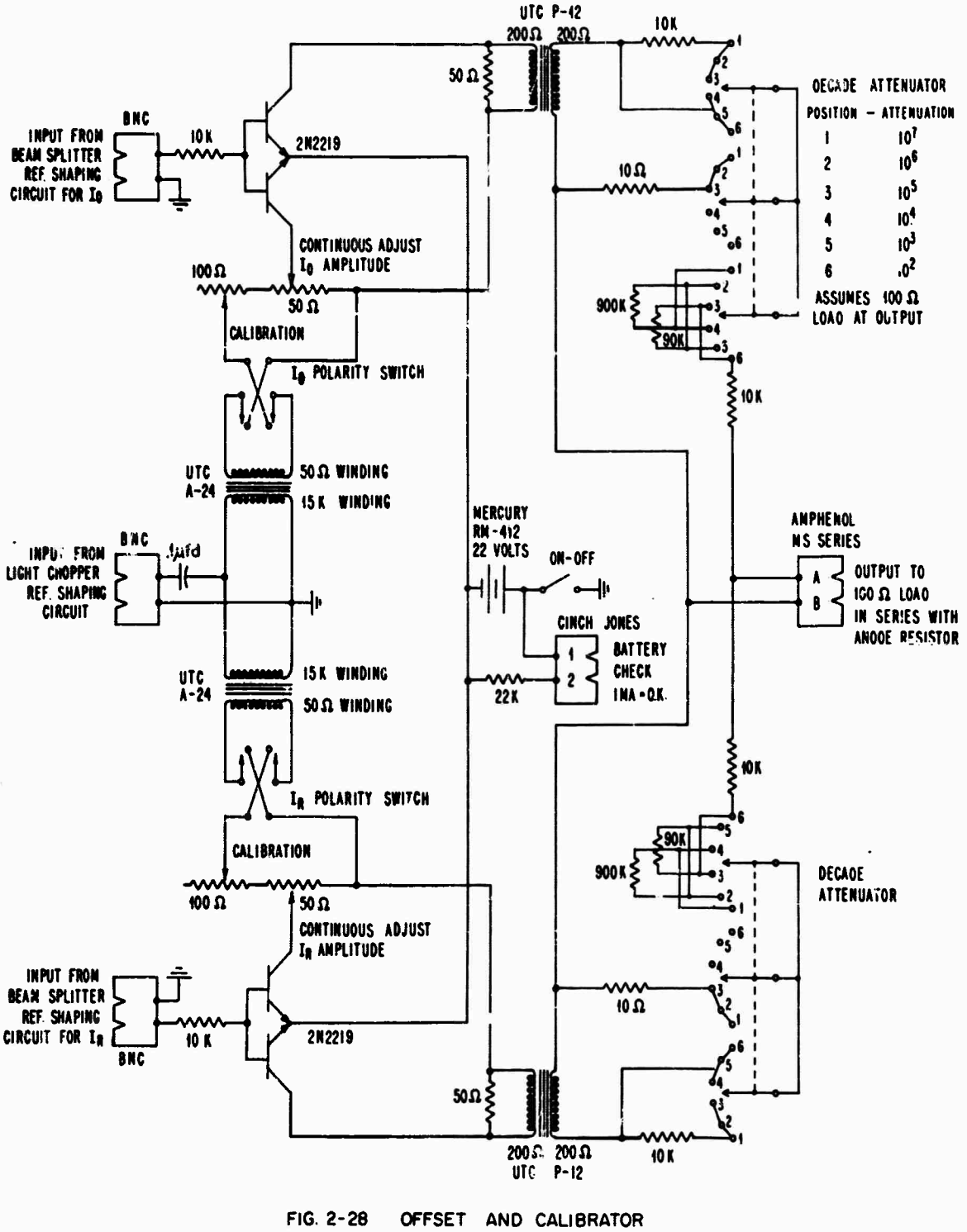

FIG. 2-28 OFFSET AND CALIBRATOR

before saturation in the Sanborn than would be possible if one were to use a DC offset alone. This cannot be realized, however, because of the different shape of the experimental and offset signals (Figs. 2-OSC-8 and 26). Figure 2-OSC-27 shows the difference between two such signals of nearly the same informational magnitude; i.e., their filtered sum is zero. Saturation would occur at nearly the same Sanborn gain as in the absence of the offset.

19. Miscellaneous Power Supplies and Controls

Three locally made power supplies are shown in Figs. 2-29, 2-30, and 2-31. The first is the 25 volt supply to power the reference signal shaping circuits and the channel switch actuating circuits. The second is the DC supply for the three reference light bulbs. This one includes an individual current meter and switch for each bulb.

Finally, there is the 50 volt DC supply to actuate the wavelength marker pulse solenoids in the I_R and R chart recorders. The supply can also be used to fire a relay in the ratio routing box to short the inputs to the I_O and I_R recorders. The Zener diode in the supply provides a bypass path to protect the wavelength marker contacts in the monochromator from pitting due to inductive decay of the solenoid coils.

The alternative circuit in the 50 volt supply, selected by a switch, provides a smaller pulse to initiate the time sweep of the multichannel analyser. Pulse requirements, imposed by the RIDL, are rise time < 0.15 μsec.; width > 10 μsec.; and height 5-10 volts. The capacitor is used to smooth out the very bouncy monochromator wavelength

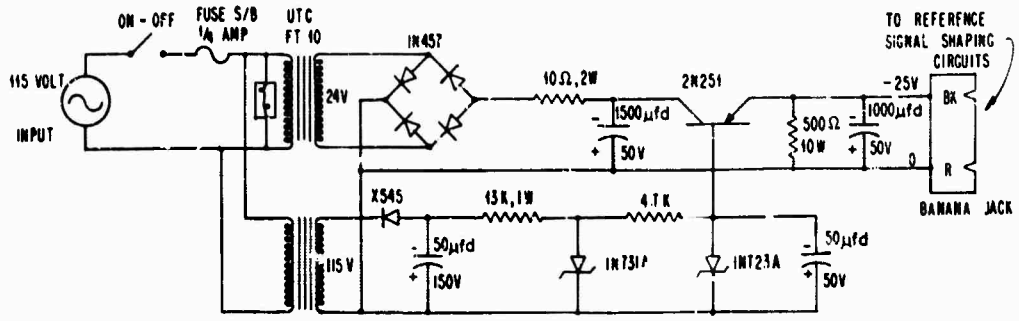

FIG 2-29 25 VOLT DC POWER SUPPLY FOR REFERENCE SIGNAL SHAPING CIRCUITS

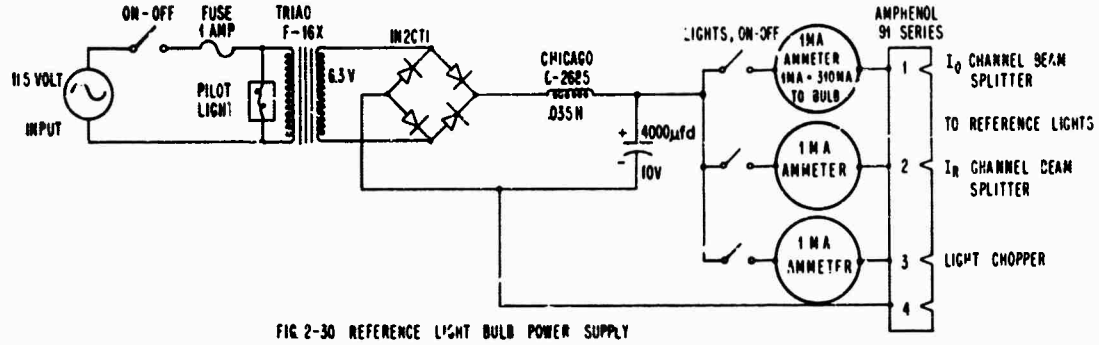

FIG 2-30 REFERENCE LIGHT BULB POWER SUPPLY

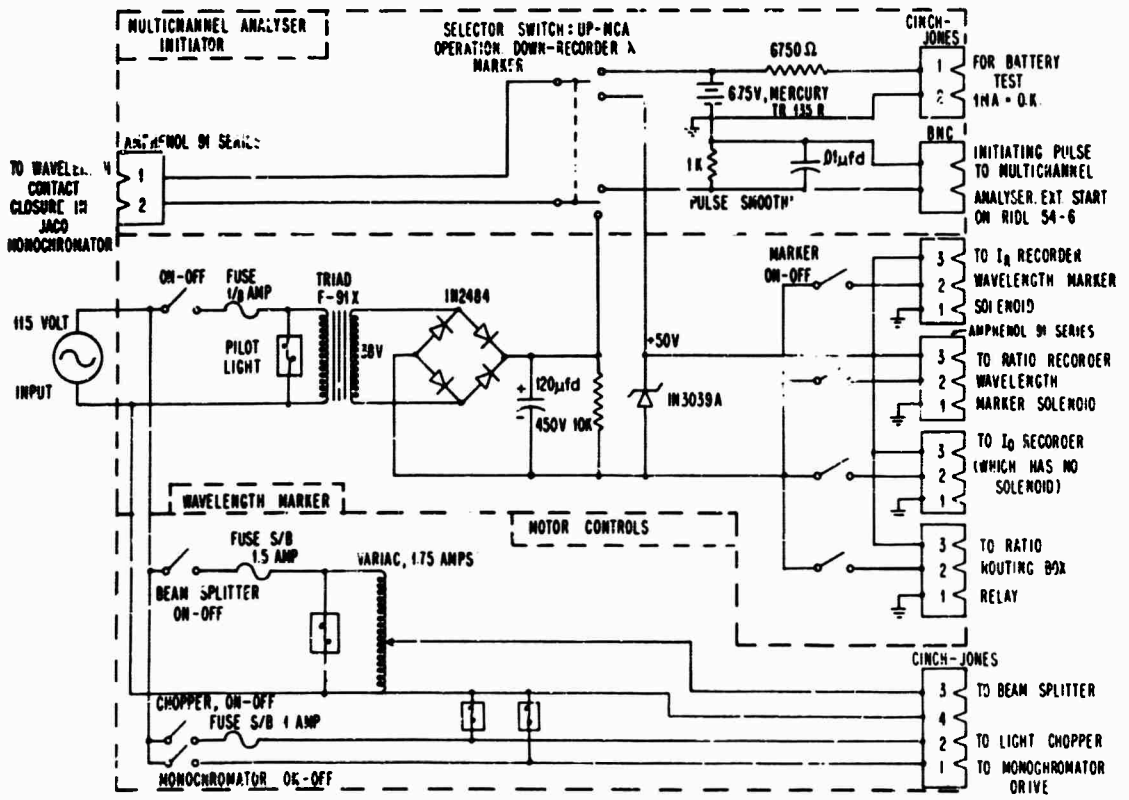

FIG 2-31 WAVELENGTH MARKER POWER SUPPLIES AND MOTOR CONTROLS

marker switch closure. Without it, final switch closure occurs some random time after initial switch actuation, resulting in increased irregularity in RIDL time sweep initiation. The capacitor must be kept small so that rise time requirements are fulfilled. The battery was chosen to be 6.75 volts. With the R and C chosen, voltage across the contacts does not exceed 10 volts and settles at 6.75 volts.

The wavelength marker pulse power supply also contains certain controls.

(1) The light chopper motor on-off switch.

(2) The beam splitter on-off switch and a Variac to vary voltage level up to 132 volts.

(3) The monochromator drive on-off switch.

20. Constant I_0 Feedback System

For each of the active electronic components, there is an optimum range of the I_0 signal size to maximize linearity and minimize noise. Also, as the I_0 level changes with wavelength, the voltage across the ratio recorder slide wire will vary in proportion, requiring a resetting of the servo amplifier gain whenever voltage across the slide wire changes by a factor of two. These problems suggested setting up a constant I_0 feedback system.

The possible approaches include optical and electronic techniques. In the optical, one varies slit width or obscures increasing amounts of the slit with a comb made up of wedge shaped teeth. There are at least two objections to this technique:

(1) By obscuring light one uses the minimum light intensity over the entire wavelength range of an experiment and must accept far lower S/N than is necessary at the brighter wavelengths.

(2) If sample reflectivity is not constant over its surface, changing slit illumination could introduce structure distortion. This effect can often be observed in the present system by noting change in R as the slit width is varied. Changes of 1 to 2% are common.

Another optical technique involves varying the angle of crossed polarizers. This was rejected since it imposes an additional limit on the wavelength range of the system.

Electronic variation avoids all these dilemmas The best place to control I_0 is in the photomultiplier, since this optimizes the operation of every active component, and both I_R and I_0 will be changed proportionately. The method employed at the time of this report is manual feedback. Hand variation of the photomultiplier dynode chain voltage while monitoring the V_{I_0} output of the Sanborn on an oscilloscope keeps V_{I_0} sufficiently constant.† An alternative method is hand adjustment

†There is one important precaution which must be noted. If the I_0 and I_R light images are not fully superposed at the photomultiplier, they may be subject to different photomultiplier gains. These gains could vary differently with photomultiplier voltage. This becomes reasonable if one thinks of an extreme case: one image in the center of the cathode and the other at its edge. There is a greater chance of loss of electrons freed from the edge of the cathode while passing to the next dynode than for those from the center. This loss is reduced as photomultiplier voltage is increased. Changes in R are indeed often noted as one changes photomultiplier voltage. They are eliminated by careful repositioning of the I_R and I_0 images.

In addition there is a significant qualification to hand control. Irregularities in hand control may obscure small structure. This point is discussed in Appendix II-A, Sec. 3.

of a variable anode resistor. This technique is actually used in $\Delta R/R$ measurements and is automated.

a. Automatic Control. We attempted to set up an automatic feedback system for R measurements by varying the gain potentiometer of the Sanborn phase sensitive demodulator. This is somewhat unsatisfactory since the active units before the Sanborn do not operate optimally; and for attenuation < 20, changing gain implies changing DC offset (see Sec. II-B-6-b-(3)).

The carbon gain potentiometer, R1218, was replaced by a low inductance wire-wound unit, the General Radio 975-4000, mounted external to the Sanborn. The "y-axis" portion of a Leeds and Northrup Speedomax G x-y recorder supplied the mounting for the potentiometer as well as the servo amplifier and balancing motor to drive it. The I_0 voltage level at the output of the I_0 channel filter was compared to a DC level set point derived from a battery driven potentiometer. This voltage difference was the error signal which drove the potentiometer to balance and kept I_0 constant (Fig. 2-32a). Unfortunately, the system hunted badly because of time delays. These were caused by the slow response of the potentiometer drive and the phase shifts introduced by the many stages of filtering between the Sanborn gain potentiometer and the I_0 channel filter output. In general only one stage of R-C filtering can be used if feedback is to be stable.

Reducing filtering to one stage in the Sanborn did not eliminate hunting, presumably because of the slow balancing motor response.

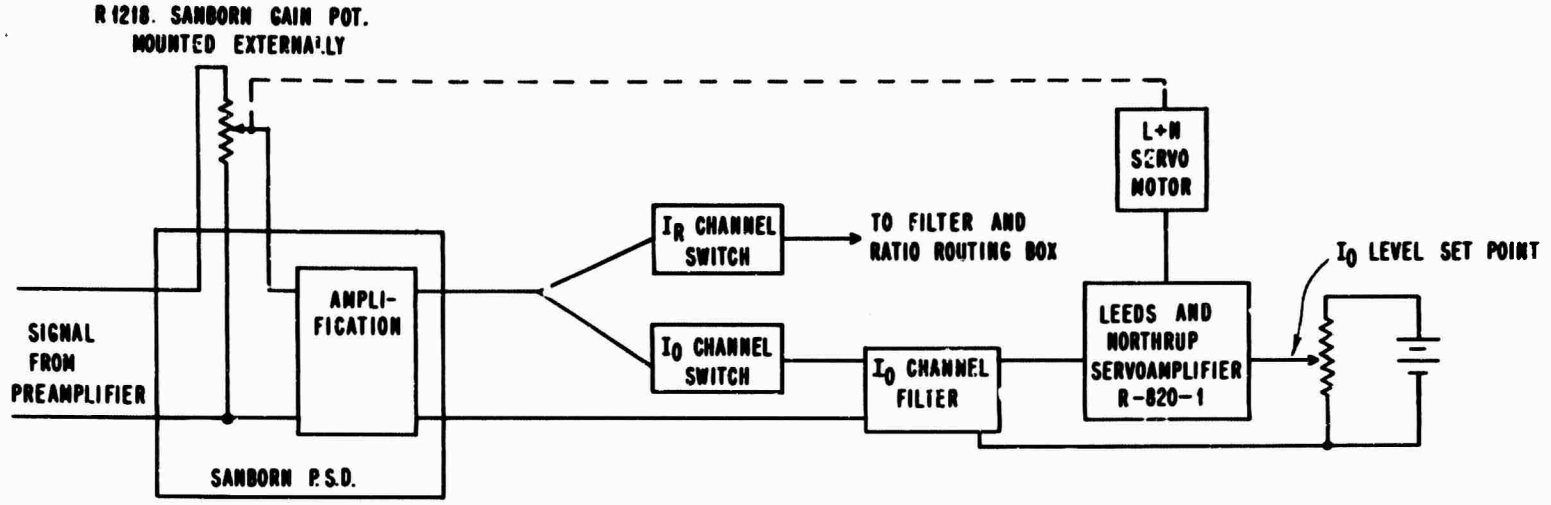

FIG. 2-32a AN I_0 LEVEL CONTROL SYSTEM: INADEQUATE DUE TO HUNTING

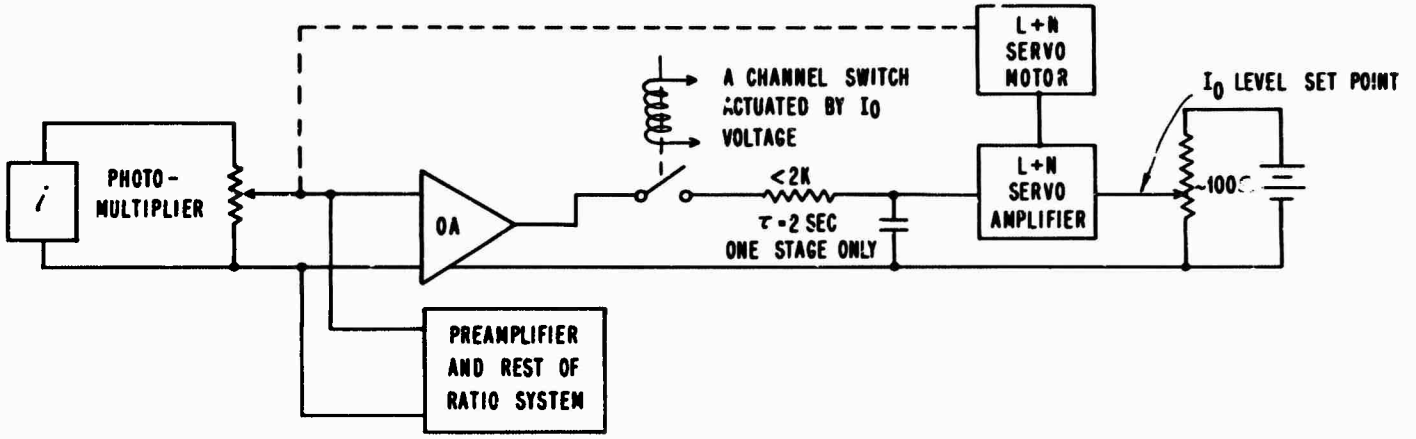

FIG. 2-32b A PROPOSED I_0 LEVEL CONTROL SYSTEM

Various other arrangements, including the use of the I_0 recorder control network, were unsuccessful. Pending solution of the hunting problem, manual feedback is satisfactory in most situations.

b. How to Make Automatic Control Work. The response time of the balancing motor should be reduced. When gearing changes speeded this up by a factor of 6 in the $\Delta R/R$ system, hunting was eliminated.

The photomultiplier anode resistor should be the variable unit rather than the Sanborn gain potentiometer. If the I_0 level is taken from the channel filter, hunting will surely ensue because of the excessive phase shifts from the potentiometer through the filter. It must probably be taken at the anode resistor itself. There, unfortunately, one must contend with the I_R signal in addition to the I_0.

The anode resistor should not be loaded by the control network. An operational amplifier of low drift could feed a channel switch selecting I_0 (Fig. 2-32b). One stage of R-C filtering would give a DC level proportional to V_{I_0}. Comparing this with a set point would give the error signal for the servo system. Any small drifts in the operational amplifier would not be anywhere near as serious as comparable drift in the Sanborn output, since we are only trying to keep I_0 within some linear range. Slight errors in I_0 due to drift would result in a different anode resistance value. This would not affect R, since I_R and I_0 are changed proportionately by the anode resistor variation.

21. The Intermodulation Problem

The intermodulation problem is a variation in a supposedly constant DC level as a result of two system frequencies beating against one another. To understand the problem and a number of possible solutions, consider the following signal (Fig. 2-33):

$$S = \underbrace{\left[\frac{1}{2} + \frac{2}{\pi}\sum_{m=0}^{\infty}\frac{1}{2m+1}\sin\left(\frac{2m+1}{2}\pi\right)\cos\left(\frac{2m+1}{2}(\omega_1 t - \pi)\right)\right]}_{\text{the square wave expansion}}[1+\alpha\cos(\omega_2 t - \varphi_2)] \tag{2.26}$$

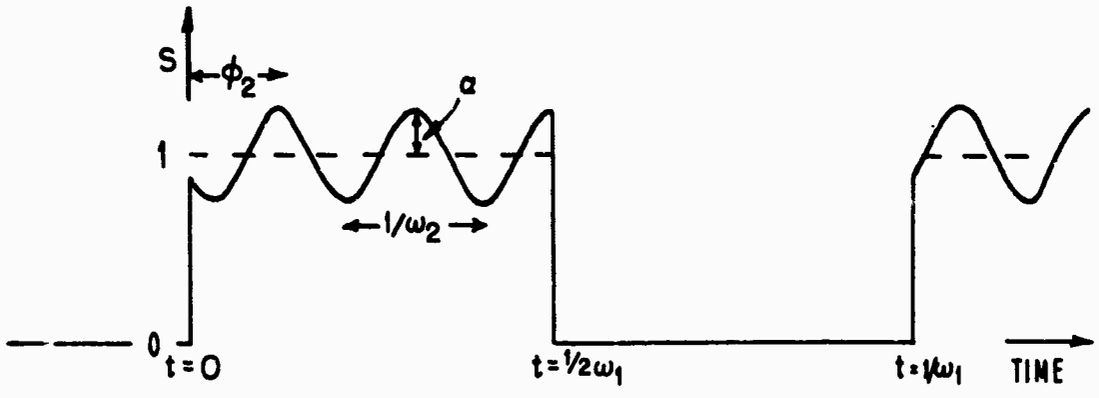

FIG. 2-33 THE INTERMODULATION PROBLEM

The average value of S over one period of the square wave, $2\pi/\omega_1$, is

$$\begin{aligned}\langle S\rangle &= \frac{1}{2\pi/\omega_1}\int_0^{\pi/\omega_1}[1+\alpha\cos(\omega_2 t - \varphi_2)]dt \\ &= \frac{1}{2} + \frac{\alpha}{\omega_2}\frac{\omega_1}{2\pi}\left[\sin\left(\frac{\omega_2}{\omega_1}\pi - \varphi_2\right) - \sin(-\varphi_2)\right] \\ &= \frac{1}{2} + \frac{\alpha}{\pi}\frac{\omega_1}{\omega_2}\sin\left(\frac{\pi}{2}\frac{\omega_2}{\omega_1}\right)\cos\left(\frac{\pi}{2}\frac{\omega_2}{\omega_1} - \varphi_2\right)\end{aligned} \tag{2.27}$$

The ω_1 signal is the information signal with an average value of $\frac{1}{2}$, whereas the ω_2 signal is extraneous. For instance ω_1 could be the 13 Hz I_0 signal and ω_2 a 120 Hz ripple imposed on the light intensity by an AC supply or poorly filtered DC power supply for the light sources. Alternatively, ω_2 could be the partially filtered light chopper frequency at the output of the Sanborn superposed on the information signal at ω_1 = 13 Hz.

In the general case φ_2 will vary from one period of ω_1 to the next giving a modulation in $\langle S \rangle$. If this occurs in an irregular way, the result is noise. The effects of the φ_2 change can be reduced or eliminated in three ways.

(1) Reduce α

(2) Decrease the ratio $\frac{\omega_1}{\omega_2}$

(3) Let $\frac{\pi}{2}\frac{\omega_2}{\omega_1} = n\pi$ so the sine = 0; i.e , $\omega_2 = 2n\omega_1$, (2.28)

making ω_2 a harmonic of ω_1.

a. Actual Solutions. The power supplies actuating the light sources and reference light bulbs are well filtered DC units (solution 1). The criterion for filtering was that noise from the 120 Hz source be much less than shot noise.

In attempting to eliminate the intermodulation of 13 Hz and light chopper frequencies, all three solutions were tried. We attempted to reduce α by substituting a sharper cutoff filter in the Sanborn to remove more of the high frequency ripple and pass the 13 Hz harmonics. Pickup of 120 Hz negated the attempt (see Sec. II-B-6-d).

The ratio ω_1/ω_2 was decreased by changing light chopper blades. Chop frequency was changed from 450 to 1080 Hz, reducing system noise.

Phase locking (solution 3) the 13 Hz and light chopper frequencies was tempting. Ordinarily, they were not harmonics, and slight slippages in the beam splitter rubber drive wheel could only add to noise by causing further φ_2 variations. Thus, the fact that both motors were synchronously driven by 60 Hz could not ensure phase lock. We took one of the 13 Hz reference signals, selected its fifth harmonic by filtering, power amplified the harmonic, and drove the light chopper motor (n = 45 in Eq. 2.28). Although the signals were then phase locked, there was some slight degradation in system noise, probably due to chopper blade inertia to small changes in the 65 Hz drive frequency. A further complication was that of coupling a power amplifier to the inductive motor load. Since there was no system improvement, the phase-lock method was discarded.

Most importantly, changing the chop frequency seemed to reduce noise from this source below that from others.

22. System Improvements--Electronic

We list a number of electronic improvements which would either expand the capabilities of the system or simplify its operation.

(1) Set up control and monitor components for the S-1 photomultiplier tube operation analogous to the S-13. Install a switch to permit powering either quickly.

(2) Acquire a proper preamplifier for infrared detectors. Many detectors have low impedances which match the TA-5 poorly. Use of a

high quality well-shielded transformer is an alternative: e.g., the Triad G4 Geoformer.

(3) Replace the active band-pass filter with an adjustable passive unit.

(4) Modify the shape of the offset voltage (Sec. II-B-18).

(5) Install battery check terminals in the Channel Switch Monitor.

(6) Correct the wiring error in the Channel Filters cited in Sec. II-B-11-b.

(7) Automate constant I_0 feedback control through use of a variable anode resistor (Sec. II-B-20-b). This has considerable importance in reducing distortion (Appendix II-B, Sec. 3).

(8) Modify monochromator drive, and design additional circuitry to take advantage of the automatic multiple sweep capabilities of the RIDL multichannel analyser (Sec. II-B-16-e).

(9) Improve the operation of the RIDL memory storage by installing a magnetic tape unit. This unit is discussed in Sec. II-B-16-e. Its purpose is to prevent the destruction of the contents of the multichannel analyser memory by a bad spectrum scan.

C. SAMPLE GEOMETRY--DESIGN FEATURES IN THE FINAL STATE AND RELEVANT PROBLEMS

In this section we consider the geometry of the sample volume, the methods of sample mounting, and the means of applying a variety of stimuli to samples.

1. Sample Volume

The sample volume is a large space (47" × 58" × 82" high) capable of enclosing a magnet or a vacuum system. It is defined by a rigid steel framework covered with blackened plywood and blackout cloth so that it is light-tight. There is a flat platform support from which sample holders and cryostats can be hung. They are held in an adjustable mounting bracket.

2. Cryostats

Cryostats suitable for use with the system include the Janis[†] demountable-tail, helium-temperature unit and a lab-built unit designed by Julius Feinleib. They are acceptable in the sense that their optical acceptance angles are wide enough so that they will not block light used for sample illumination.

3. Magnet

A large electromagnet capable of developing 31 kilogauss can be wheeled into or out of the sample volume. It is the Harvey Wells L-128.[‡] With the present tapered, standard-alloy pole tips, there is a cylindrical field area of 1.00" diameter and 0.685" length

---

[†] Janis Research Co., 21 Spencer St., Stoneham, Massachusetts

[‡] Magnion Inc./Harvey Wells, 144 Middlesex Turnpike, Burlington, Massachusetts

(separation of the pole tips). A specially designed cart and track were built, permitting the magnet to sit within 5-5/8" of the floor.

The power supply is a Harvey Wells Model HS1050, factory updated to conform to the specifications of their newer model HS1365. The modified unit has an increase of maximum current from 50 to 65 amperes. The increased power dissipation at full current limits operating time to an absolute maximum of four hours.

Certain local modifications were made to the power supply permitting:

(1) Current (hence field) reversal. An interlock prevents reversal when the current is nonzero.

(2) Cooling-water control including on-off switches for water and pump, and safety interlocks for inadequate flow, excess water pressure, and excess magnet temperature. This control can be shorted out during operation below 25 amperes, when cooling is unnecessary.

Because of inadequate water pressure a jet pump capable of delivering up to 90 psi was added. Heat transfer from the magnet to its cooling coils is inefficient enough that there is no need to use pressures above 50 psi. At higher pressures and water speeds the water runs through unheated.

The water to the magnet is filtered to remove vegetable matter and minerals in suspension. This was the only concession made to a concern about the deleterious effects of water, such as electrolytic action, oxide formation, algae growth or mineral deposition. A proper

solution to all these problems would have involved a highly expensive recirculation system with many types of filtering. It would be cheaper to replace the magnet cooling coils.

4. Uniaxial Stressor

A suitable design for uniaxial stressor is found in ref. [2-15]. The sample is held vertically and no window is necessary.

5. Electric Fields

High fields ($\sim 10^4$ volts/cm.) can be applied by any of the techniques described in refs. [4-30, 4-56, 4-55]. Generally, the field will be nonuniform, decreasing as it penetrates into the sample.

6. Sample Geometry--System Improvement

a. Absorption Measurements. The optical and electronic instrumentation and sample geometry have been discussed in terms of reflectivity measurements. Modifications are necessary in order to permit absorption measurements, specifically in cases of low αd. Certain changes in sample geometry optics are indispensable, but for $e^{-2\alpha d} \geq 0.1$ (i.e., low absorption, where d = sample thickness) no changes are necessary in the electronics.

Figure 2-34 shows three possible modifications to the optics. Transmission Configuration #1 is perhaps the easiest to set up. The sample is between mirrors 4 and 5 in what was formerly the I_0 beam and is now the I_T beam. The sample in the I_R beam is replaced by an aluminum mirror. This is now the I_0 path. Unfortunately, there are a number of disadvantages:

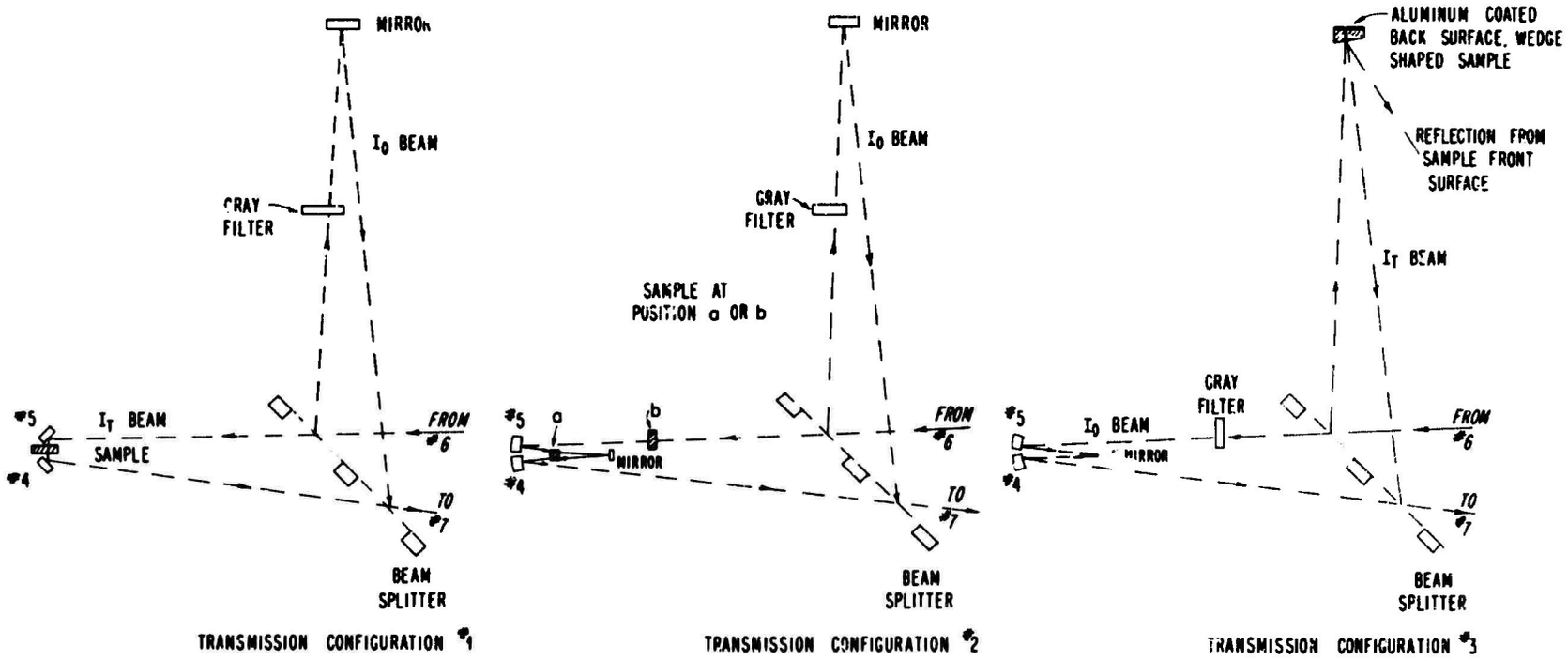

FIG. 2-34 THREE OPTICAL CONFIGURATIONS FOR TRANSMISSION MEASUREMENTS

(1) The I_0 path has one more reflection than the I_T path.

(2) After separating mirrors 4 and 5 to insert the sample, the I_T and I_0 beams are superposed less well on the mirrors following the beam splitter.

(3) There is little space in which to apply stimuli or cooling to the sample.

Transmission Configuration #2 solves objections 1 and 2 above, but one is still restricted in cooling and stimulus application, particularly if the sample is in position b. In position b there may be a problem with multiple reflections.

In Transmission Configuration #3 a wedge shaped sample is in the former I_R path. Its back surface is coated with aluminum by vacuum evaporation. Problems 2 and 3 are gone but there is an additional difficulty. The beam splitter could catch light from front surface reflection as well as that reflected from the back mirror. To minimize this distortion, the sample is wedge shaped. Note that the sample mirror, since it is not exposed to oxidation, will not completely match the new mirror in the I_0 path. Consequently, problem 1 is only partially solved.

We recall that I_0 and I_R (and hence I_T) should be of roughly the same magnitude to minimize distortion and noise arising from the Sanborn DC level. Further, if I_T and I_0 are widely separated in magnitude, an amplifier might add a significant fraction of noise to the smaller when the Sanborn's gain was set to pass the other without saturation.

An easy solution is to use gray filters or a high speed light chopper in the I_0 channel reducing I_0 to the I_T level. If these alternatives should be unsatisfactory for any reason, electronic changes are needed when $e^{-2\alpha d} \leq 0.1$. Such changes should permit treating each channel independently in a way to minimize noise and distortion.

b. Differential Measurements. Differential measurements, such as those suggested in Fig. 2-35, look productive at first glance. Two samples are matched in reflection or transmission over the wavelength range of interest, giving $I_R/I_0 = 1$ or $I_T/I_0 = 1$. Then a stimulus such as magnetic field or cooling is applied to one of the samples. When the spectrum is swept again, the deviations from 1 indicate the effect of the stimulus. AC offset (Sec. II-B-18) could magnify this as shown below:

Let $I_R(S) \equiv I_R$ when a stimulus is applied and $\Delta I_R(S) \equiv I_R(S) - I_R(0)$.

Let the AC offset be δ. Note that $I_0 = I_R(0)$. Then the recorded ratio is modified from $I_R(S)/I_0$ to

$$\frac{I_R(S) - \delta}{I_0 - \delta} = \frac{I_R(0) - \delta + \Delta I_R(S)}{I_R(0) - \delta} = 1 + \frac{\Delta I_R(S)}{I_R(0) - \delta} \quad . \tag{2.29}$$

This ratio increases as δ increases.

Unfortunately, there are certain difficulties with differential methods which could prevent their successful utilization in many cases.† For instance:

---

†An instrument where differential techniques were successfully applied is described by Sturge [2-16]. Differences smaller than .1% were noted.

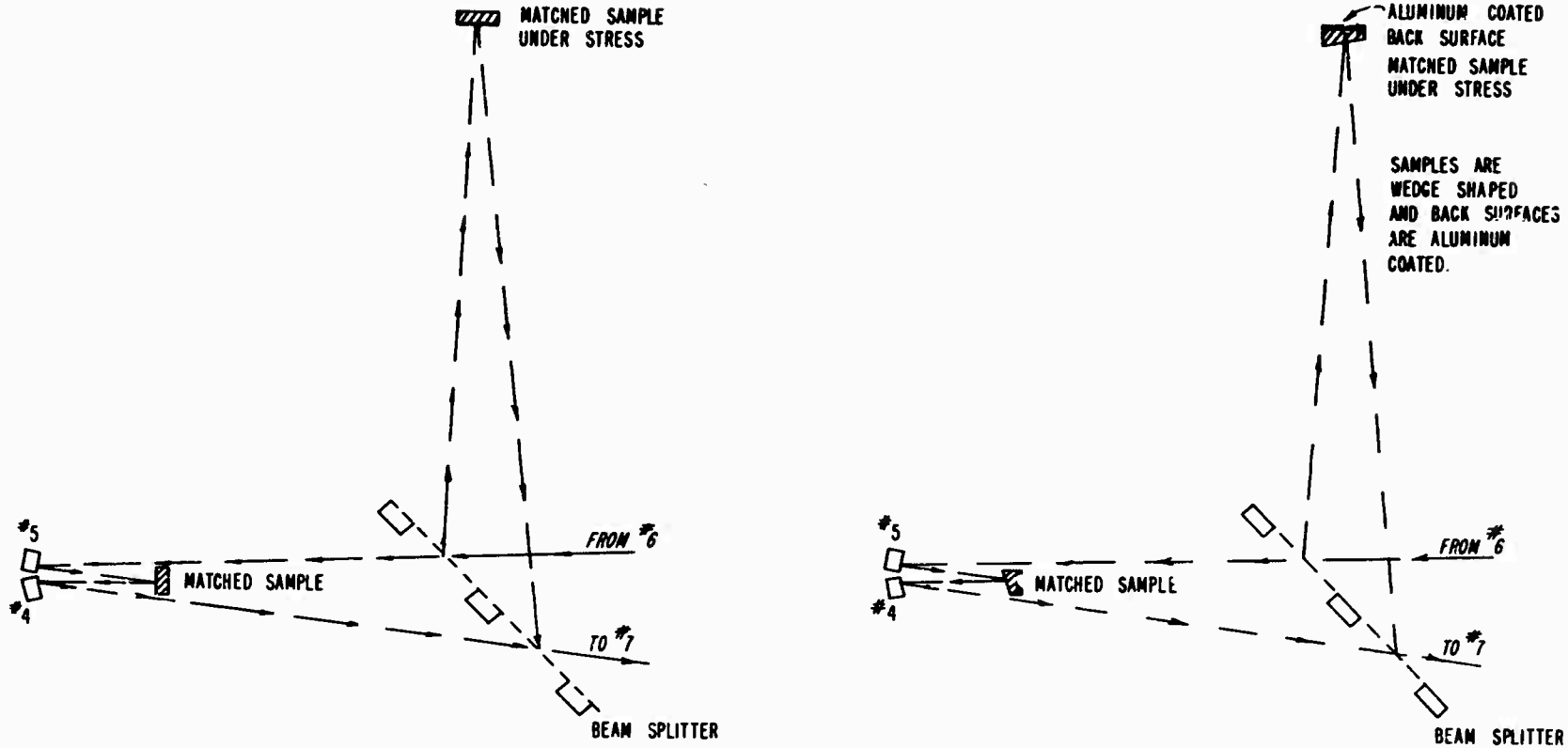

FIG. 2-35 OPTICAL CONFIGURATIONS FOR DIFFERENTIAL MEASUREMENTS.

(1) Because of differences in the shape of the offset and experimental signals, the offset does not permit the much higher AC amplifier gains which one might hope for (Sec. II-B-18).

(2) Matching two samples over a long wavelength range is a nearly impossible task. In transmission the samples would have to have the same thickness; the wedge-like shape used to eliminate reflections complicates this. Reflection measurements show that two portions of the surface of a single sample can vary. How then could one match two samples, particularly when reflectivity is dependent on the effective etching time and on oxidation in air?

Conversely, we can conceive of certain situations in which the differential technique could be used:

(1) Over short wavelength ranges matching might be good or at worst involve a monotonic change. The success of the differential technique in a given experiment presupposes that the change of interest occurs over a wavelength range which is small compared to the range of matching, or that the change is much sharper than the variation with wavelength due to improper matching. This favorable situation might occur in the case of the measurement of impurity absorption.

(2) Samples need not be matched if one performs his experiment at one wavelength. In magnetic field measurements one can as well sweep through magnetic field at fixed wavelength as sweep wavelength at fixed field. In this type of experiment the sample in the I_0 beam serves only to attenuate the I_0 beam to nearly the same level as

that in the I_R or I_T beam. Perfect matching is usually not critical. One can point up the limited utility of the differential approach even here, by noting that this I_0 attenuation could be accomplished through use of the offset voltage in the I_0 channel.

In many situations the differential technique is limited in its advantages over straight reflectivity measurements. When changes are smaller than can be seen with the reflectivity measurement, $\Delta R/R$ methods, discussed in Sec. I-E and Sec. IV-D-3, are a very productive avenue of approach, since they so often produce such large improvements in the signal-to-noise ratio and in resolution. But the differential technique must be employed when the difference between the two samples cannot be modulated, such as in impurity studies.

D. SYSTEM CAPABILITIES AND LIMITATIONS

1. Noise Sources

There are many sources of noise throughout the system. They arise in both the optics and the electronics. Table 2-16 lists these noise sources, notes whether they are primarily optical or electronic in nature, and indicates the relevant section of the text where they are discussed in more detail. These instances are selected both from the instrumental (Chapters II and III) and experimental (Chapter IV) portions of the text. To aid in troubleshooting, the noise sources are divided into four categories:

(1) Those noise problems which have been solved.

(2) Those noise problems requiring care in system adjustment or preparation.

(3) Those noise problems involving system degradation.

(4) Those noise problems which either cannot be or were not fully eliminated.

In the last category there are five noise sources which determine the system's noise limitations:

(1) Xenon arc instability.

(2) Beam splitter vibration.

(3) Photomultiplier shot noise.

(4) Zero level drift and noise in the Sanborn phase sensitive detector.

(5) Irregularities in the operation of the 13 Hz channel switches.

The relative importance of these sources will depend on certain circumstances which are discuss[illegible] remainder of this section.

For example, when a xenon source (1) is used instead of one of the quiet tungsten sources, it is the major noise source. In this case the indeterminacy in the reflectivity ratio is 0.1% and cannot be improved.

Photomultiplier shot noise (3) need not be the limiting factor, since its relative effect on the signal-to-noise ratio decreases with increasing light intensity. So long as necessary wavelength resolution is not lost, the monochromator slits may be opened until other noise

TABLE 2-16 SYSTEM NOISE SOURCES

OPTICAL NOISE SOURCES

Item #	A Description of the Noise Problem	Section where Discussed	Trouble-shooting Category
1	Tungsten light sources flicker at the end of their life. Iodine quartz sources are noisy if they are run too cool.	 II-A-2-a	(3) (2)
2	Xenon light sources show the following instabilities: Slight instabilities of a spike and step-like character are found in the best of them. Instabilities worsen in poor, old, or overheated lamps. A lamp without mu-metal shielding worsens in a magnetic field.	 II-A-2-b II-A-2-b II-A-2-b	 (4) (3) (1)
3	Ripple in the output of the light sources causes intermodulation effects.	II-A-2-f II-B-21	(1)
4	The monochromator grating vibrates when the mounting spring is weak. The vibration is increased by light chopper imbalance.	II-A-3-b	(1)
5	Vibration of the beam splitter results in a slight motion of the slit image on the sample and the photomultiplier. This motion becomes serious if: The reflectivity of the sample surface is irregular; The light image overlaps the sample, falling partially on the blackened area around the sample. The vibration then modulates R; The beam splitter drive wheel becomes worn or spotted with cement; The motor is not powerful enough to drive the beam splitter at the synchronous speed.	II-A-7-j II-A-3-b II-A-7-h II-A-7-d,g II-A-4-d	(4) (2) (2) (3) (1)
6	A nonsynchronous drive of the light chopper or the beam splitter results in intermodulation effects.	II-B-21	(1)
7	The photomultiplier shot noise is important and is light intensity dependent.	II-A-2,II-A-9-b	(4)
8	Stray light can enter the system from the room, but it becomes a problem only at low source intensities.	II-A-10	(1),(2)

ELECTRONIC NOISE SOURCES

9	The photomultiplier dark current is insignificant in the S-13 and in the cooled S-1.	II-A-9-b	(1),(2)
10	Failure to short the 100 Ω calibrator and offset resistor when it is not used can add noise.	II-B-2-b-5	(2)
11	Degradation of any of the active elements can cause noise. For instance: Preamplifier batteries as they start to weaken. Noise in the output phase of the band-pass filter.	 II-B-4	(3) (3) (3)
12	Operation of any of the active elements outside their optimum range is inadvisable: In the S-13 photomultiplier Cathode-dynode 1 voltages should be around 125; Low light intensities coupled with low dynode chain voltages are often noisier than with higher voltages; Anode currents in excess of 10μa. result in the loss of gain stability. The preamplifier's output should be high enough so that the band-pass filter adds no significant noise. The filter's noise level is 0.2 mv. p-p. The Sanborn output level should be high (around 2 volts) so that the effect of drift and noise on the DC zero level is minimal.	II-D-4 II-B-2-b-1 Tube specs II-B-3, 3a II-B-4 II-B-5-a II-B-6-a	(2) (2) (2) (2) (2) (2)

TABLE 2-16 CONTINUED

13	The preamplifier adds more noise than an optimally chosen unit. The noise is minor in R and ΔR/R measurements compared to other noise sources, except when the preamplifier is used in its full gain position. The excess noise is partially due to imperfect matching of the anode resistance, the operating frequency, and the preamplifier.	II-B-3-a	(1),(2)
14	When the warmup time is inadequate, the Sanborn output zero level will exhibit excess noise and drift. Some will remain even after warmup.	II-B-5-a	(2),(4)
15	An improper relative phase adjustment of the experimental and reference signals (as controlled at the light chopper) results not only in signal loss but also in the creation of an unfiltered signal of around 30 Hz at the Sanborn output. This can be a serious intermodulation noise source.	II-E-2-(6)	(2)
16	The use of a phase sensitive detector other than the Sanborn will often be more noisy.	II-B-5-c	(1),(2)
17	The three reference signal shaping circuits can interact through their common power supply.	II-B-8-a	(1)
18	Transistor 2N2219 in the reference signal shaping circuits can degrade.	II-B-8	(3)
19	There can be irregularities in the operation of the channel switches: The effects of channel switch bounce are partially removed by use of a capacitor. There is variable lag in the response of the channel switch to its driving voltage. When pitting occurs in the channel switch contacts, the switch should be replaced. Wear in the moving portions of the switch prevents contact closure. The switch should be replaced.	 II-B-10-a II-B-10-a II-B-10-a 	 (1) (4) (3) (3)
20	The gain of the ratio recorder servo amplifier can be too high or too low. If too high, the result is jitter; if too low, pen drift and excessive deadband result.	II-B-12-a-(3)	(2)
21	Recorder response can be noisy, sluggish, or erratic due to a dirty slide wire, a worn contact, or inadequate pressure of the contact on the slide wire.		(3)
22	The recorder trace may wander, or there may be a regular imposition of false structure if the electrolytic capacitors in the final R-C filter break down.	II-B-13	(3)
23	There is an indefiniteness by one count in the number of pulses stored in the multichannel analyser.	II-B-16-b	(2)
24	Ringing occurs in the signal delivered by the calibrator and offset unit when it is driven by a square wave at the carrier frequency instead of by the fundamental. The ringing is removed when the square wave is filtered.	II-B-18 II-B-8	(1)
25	The intermodulation problems are generally solved. See Items 3, 6, and 15.	II-B-5-b II-B-6-d,II-B-21	(1)
26	The relay rack steel does not provide a good common ground, as was dramatically demonstrated when the xenon power supply was turned on. The DC level at the photomultiplier anode jumped 100 mv. Noise from this source was removed by connecting all racks and units with a heavy copper braid.		(1)

sources predominate. If no filters or polarizers are used, a 100 μ slit width will provide adequate light at the wavelengths of maximum intensity. When filters and polarizers are added, slit widths of 300 to 400 μ will ensure sufficient light for nearly the entire wavelength range (the exception being the far UV limit of the system). The S-13 photomultiplier performs better in this regard than the S-1.

Nor is noise arising in the Sanborn zero level (4) paramount until the magnitude of the voltage corresponding to I_0 becomes less than 1.2 volts. Variations in I_0 in a large range above 1.2 volts show no change in ratio indeterminacy. We note that this guideline for I_0 level applies to both the tube and transistor outputs of the Sanborn.

Beam splitter vibration will be the main source of noise when the sample surfaces are rough, when the samples are poorly placed relative to the slit image, or when the sample and I_0 images are not superposed at the photomultiplier. When these difficulties are removed by choosing a large smooth mirror of large R as the sample, and when the effects of (1), (3), and (4) are minimized, then the noise is reduced to its absolute minimum. With a time constant of 22 seconds ratio indeterminacy was .02% (Sec. II-D-5). Nothing quite this good has been achieved with the typical small samples used in experimental measurements, their surfaces often roughened slightly by etching. Typical indeterminacy values are .05% after the system has been tuned to its best performance.

Thus, irregularity in the operation of the 13 Hz channel switches (5) appears as the present limit on system performance when perfect samples are used. This irregularity is the compounded effect of a number of factors:

(1) Variation in rotational speed of the beam splitter due to fluctuations in line frequency, residual roughnesses on the drive wheel surface, and variable friction in the thin section bearing.

(2) Very slight variations in the shape and magnitude of the 13 Hz light sensor signals as a result of variations in the reference light bulb intensity, arising from ripple in the bulb power supply.

(3) Variable lag in the response of the moving contact of the Synchroverter switch. This worsens with use due to wear, and closing can eventually become less definite requiring higher driving voltages. Contact bounce on closure also implies a certain indeterminacy in closing time.

The problems of lag, bounce and wear in the switch itself are probably more important than (1) and (2). Slight degradation in switch performance (increased bounce) which could be monitored on an oscilloscope (using the Channel Switch Monitor) were correlated with slight increases in ratio indeterminacy. Replacing the switch returned the system to its former peak.

However created, 13 Hz switching irregularities were shown to be a significant noise source in the following simple experiment: The Sanborn DC level was set at its maximum, providing a quiet source of voltage to drive the ratio recorder. A ratio was chosen by varying

TABLE 2-17 SYSTEM DISTORTION SOURCES

OPTICAL DISTORTION SOURCES

Item #	A Description of the Distortion Problem	Section where Discussed	Trouble-shooting Category
1	When sample reflectivity varies over its surface, separate measurements will show small inconsistencies when different portions of the sample are illuminated. This can occur when two separate sources, such as two iodine quartz lamps differently oriented, or a quartz and xenon source, are employed.	IV-C-5-c IV-D-3	(2),(4)
2	The xenon source moves under the influence of a magnetic field. The motion becomes important when the sample R varies over its surface or when I_O and I_R light paths are blocked in different amounts (Items 6 and 15). This problem is removed through the use of a mu-metal shield for the xenon source.	II-A-2-b	(1)
3	There are large spikes in the xenon spectrum in certain regions. The resultant large photomultiplier voltage changes, coupled with imperfect I_O and I_R superposition at the photomultiplier (Item 12) may give small spikes in R. These regions of the xenon spectrum should be avoided.	II-A-2-b	(1),(2)
4	Second order light from the monochromator can create false structure. The light is removed by a filter.	II-A-5-a-(3)	(1),(2)
5	Scattered light from the monochromator modifies magnitudes and may create false structure. Its effect is reduced by the use of filters.	II-A-3-b II-A-5-a-(1)& (2)	(1),(2) (4)
6	There is a polarization dependent variation of the light intensity along the monochromator exit slit. This variation is wavelength dependent and has an effect whenever the I_O and I_R beams are subject to different light blockage or reflectivity. The effect is removed by the use of light polarized parallel to the monochromator exit slit and by reduced beam size, provided additional precautions are taken, viz.:	III-B	(1),(2)
	The monochromator slit height should be reduced so that the slit image does not fall outside the sample.	II-A-3-b	(2)
	No light should extend beyond any mirrors.		(2)
	The beam splitter must not remove any light from the beam.		(2)
	Care must be taken in the use of gray filters in the I_O light path.	II-B-6-a	(2)
	Neither the I_O nor the I_R image should extend beyond the photomultiplier cathode.		(2)
	Both images should be superposed insofar as possible.		
7	Although the basic philosophy employed in system design was intended to eliminate any problems arising from imperfect mirror matching, different aging in the beam splitter mirrors as opposed to mirrors #4 and 5 could result in slight distortions in reflectivity spectra. (This problem is independent of Item 6.)		(4)
8	The geometrical effect of the light filters, which varies with filter thickness, is reduced but not eliminated by placing the filter at the photomultiplier instead of at the light chopper.	II-A-5-c	(1),(4)
9	Sample characteristics can change:		
	Some differences arise from variations in sample surface preparation.	IV-B-4-f	(2)
	Chemical etches can radically affect the condition of a sample surface.	IV-C-4	(2),(3)
	Surface oxidation will modify reflectivity structure.	IV-D-2	(2)
	When cooled, samples may pick up water and CO_2 films which modify R.	IV-D-2	(2)
	If a sample is moved and a different portion of the surface illuminated, the spectrum may change slightly if the surface is not uniform. An equivalent effect is the change in R as slit width is changed. Therefore, the use of slit width variation is a poor way to keep I_O constant.	IV-D-3	(2)
10	The plane of polarization of light is rotated by active elements. Also, mirror reflection varies with the plane of polarization at nonnormal incidence. Since these effects operating together can distort spectra, active elements should be eliminated except when they are needed by the experiment.	III-H	(2)

TABLE 2-17 CONTINUED

11	The photomultiplier sensitivity to light intensity changes varies with the position of the light image on the photocathode. E. Rossi of this laboratory noted that this effect was wavelength dependent. To minimize its distortion, measurements should be made at various angular positions of the photomultiplier and averaged. This is particularly important when trying to make measurements giving the accurate magnitude of R.	Ref. [2-17]	(2)
12	The photomultiplier sensitivity to the dynode chain voltage varies with the position of the light image on the photocathode. This results in changes in R as the voltage is changed. It is wavelength dependent in the S-1 phototube, imparting false structure, and is eliminated by ensuring good superposition of the I_O and I_R light images on the photocathode.		(2)
13	Saturation of the photomultiplier cathode results in a cusp in I_O and ultimately in R. The distortion is removed by defocussing the light images on the cathode.	II-A-9-e	(2)
14	The photomultiplier gain is modified by a magnetic field. If the light images are not perfectly superposed, there will be a change in R, which is more serious in the S-1 than in the S-13 phototube. The effect is reduced considerably by surrounding the phototube with a mu-metal shield.	IV-D-1	(1)
15	There is an indefiniteness in the real magnitude of R as determined by this system. Unless the light beam is suitably blocked as prescribed in Item 6, differing amounts of light will be lost in the I_O and the I_R light paths, making a determination of the magnitude of R impossible. When these paths are properly blocked, the R magnitude for the entire spectral sweep can be known to within $\pm 5\%$. This figure includes the effect of many of the factors cited above. Very slight changes in alignment where no light seems to be lost result in R changes of 1 to 2%, probably due to light scattering.	IV-C-5-c	(2)

ELECTRONIC DISTORTION SOURCES

16	Too high an anode resistor causes signal distortion.	II-B-2-b-4	(1)
17	Distortion results when operating the electronic components in nonlinear regions such as: The TA-5 with a peak-to-peak output voltage greater than 2 volts. The band-pass filter with a peak-to-peak output greater than 14 volts. The Sanborn vacuum tube output greater than 1.8 volts. The Sanborn transistor output greater than 3 volts.		(2)
18	An insufficient pass band in the band-pass filter will partially merge the I_O and I_R signals.	II-B-4	(2)
19	A nonzero DC level in the output of the Sanborn will modify the reflectivity.	II-B-6-a,b	(2),(4)
20	There is a very slight merging of the I_O and I_R signals by the Sanborn output filter in its "Hi" position. The "Medium" and "Low" positions should not be used during ratio operation since they cause even more merging.	II-B-6-d	(4) (2)
21	Signal distortion can be caused by degraded electrolytic filter capacitors.		(3)
22	There is a slight distortion caused by the time lag in the response of the channel filter output to changes in I_O. This could be cured by employing a constant I_O feedback.	Appendix II-A Sec. 3	(4)
23	There can be distortion due to the improper relative choice of time constant, monochromator wavelength sweep rate, and ratio recorder span.	Appendix II-A	(2)
24	The finite input impedance of the Vidar voltage-to-frequency converter causes a small distortion in the signal stored in the multichannel analyser.	Appendix II-A	(4)

the I_R attenuator, and the channel switches were shorted closed. The ratio was extremely quiet with an indeterminacy of less than .003%. However, when the shorting switches were opened, permitting the channel switches to function, ratio indeterminacy increased to .01 to .02%, when a time constant of 4.5 seconds was employed.

2. Distortion Sources

The various sources of signal distortion, both optical and electronic, are listed in Table 2-17. The table includes the sections of the text where these sources are discussed more fully and indicates the appropriate category for troubleshooting. These categories have the same meaning as in the preceding section (Sec. II-D-1), except that they apply to distortion instead of noise.

There is one general distinction between optical and electronic distortions. Optical distortions are a consequence of system inadequacies or limitations, whereas those of electronic character can also arise from nonlinearities in active elements occurring when they are operated in saturation regions.

3. System Linearity

In discussing system linearity we refer to the response of the active electronic elements, photomultiplier through the Sanborn phase sensitive detector, and to the effect of varying the monochromator slit width. When each component was tested, the optical and electronic distortions of other components in the system were minimized.

TABLE 2-18 LINEARITY CHECKS

Experiment	Effect on Linearity
I_0 vs. R anode	10 KΩ resistor is nonlinear, signal increasing by factor of 9.88 instead of 10, compared to 1 KΩ resistor.
R vs. R anode	1 KΩ and 10 KΩ resistors linear to better than .1%. 50 KΩ resistor causes a 2% increase in R; 100 KΩ, a 5% increase.
I_0 vs. photomultiplier voltage	Not checkable.
R vs. photomultiplier voltage	Provided I_0 and I_R light images are superposed and centered on the photocathode, R variation with photomultiplier voltage is less than 1%. This assumes that the peak to peak value of the signal out of the photomultiplier is within the following limits: Attenuator setting of TA-5 / Minimum voltage / Maximum voltage 40 / 3.2mv. / .2v. 20 / .32mv. / 20mv. 0 / .32mv. / 2mv.
I_0 vs. TA-5 amplifier settings	Linear within .1% (recorder pen width) up to 2 volts peak to peak at output.
R vs. TA-5 amplifier settings	It is not possible to observe the effects of a change in TA-5 settings on R, independent of changes in other gains, since the TA-5 gain increments are in factors of 10. It is reasonable to assume that it is within .1%.
I_0 vs. Sanborn gain setting	Linear within .1%.
R vs. Sanborn gain setting	Linear within .1% when the Sanborn tube output lies between .8 and 1.8 volts and when the transistor output lies between 1 and 3 volts. The lower limits are set by noise in the output DC level.
I_0 and R vs. slit width	Demonstrates the need for image defocussing on photocathode. When this is done, linearity within .1%.
Current corresponding to I_0 out of P.M. kept constant as slit width decreased, and photomultiplier voltage increased. Change in R noted.	For a change in light intensity by a factor of 25:1, an R value of 40% stayed within .5% of its value.

The linearity of both I_0 and R measurements was checked. When a difference was found, the greater deviations were in the I_0 measurements. The improvement in R measurements is not surprising, since the nonlinear portions of a signal occur over only the short time span corresponding to the apex of the signal triangle (Fig. 2-OSC-5,8), rather than the full time of the measurement (Fig. 2-OSC-1).

Table 2-18 outlines the results of various linearity checks. In an I_0 check the percentages represent deviation from linearity expressed as a percent of full scale value, where full scale is the maximum permissible signal to avoid saturation. In contrast R percentage deviations are expressed as percentages of the R value at which they were measured (in this case 40%).

Most components behave admirably, being linear within .1% over the voltage ranges in which they are used. In R measurements the primary nonlinearity is in the response of the photomultiplier to changing dynode chain voltage. It can be minimized by careful positioning of light images on the photocathode. This effect, when added to that created by other components, should result in R deviations of no more than 1%.

In I_0 measurements there must be the additional precaution of using no anode resistor higher than 1 KΩ. Then here as well, deviations from linearity will be limited to 1%.

4. Optimum Operating Conditions

Once the limits on the system which are imposed by linearity, distortion, and noise are understood, the optimum operating conditions can be delineated:

Photomultiplier anode resistor: 1 KΩ (10 KΩ is appropriate in many situations).

Current out of Photomultiplier: Assuming a 1 KΩ anode resistor, the anode current should be no less than .32μa. for the 0 and 20 db attenuator positions on the TA-5, and no less than 3.2μa. for the 40 db position. (Divide these minimum numbers by 10 for a 10 KΩ anode resistor.) This current should not exceed 10μa. for gain stability in the case of the S-13 response tube.

TA-5: Maximum voltage at output: 2 volts peak to peak

Minimum voltage at input at 40 db setting: 3.2mv.

20 db setting: .32mv.

0 db setting: .32mv.

The noise characteristics of the phototube are such that it is often slightly quieter at higher voltages. Consequently, the 20 db position is used with the 1 KΩ resistor and the 40 db position with the 10 KΩ.

Krohn-Hite Variable Band-Pass Filter: The level into the filter should be kept well above 100mv. p-p.

Sanborn output voltage range: Transistor output, 1 to 3 volts.

Tube output, .8 to 1.8 volts.

5. Best Performance Data

Using a large aluminum mirror as the reflecting element, we collected the best performance data. Table 2-19 indicates system settings and the final indeterminacy in the reflectivity value. In this particular experiment the measured reflectivity was higher than its true value since the light beam size was not restricted.

TABLE 2-19 BEST PERFORMANCE DATA

CONDITIONS: Sample -- Large flat aluminum mirror.
Source -- DXM iodine quartz lamp at 30 volts.
Monochromator -- 5000Å grating, set at intensity maximum, 5300Å, 100μ slit width, no filters or polarizers.
Detector -- 6256B S-13 photomultiplier at room temp. 625 volts across dynode chain and 130 volts across cathode-dynode 1. 10 KΩ anode resistor.
TA-5 -- in 40 db attenuation position.
Band-pass filter -- 425 Hz to 2000 Hz.
Sanborn -- long warmup resulting in no drift or noise on scale of I_0 chart paper. "Hi" filter on output filter. Transistor output. I_0 = 2 volts at output.
Channel filters -- Position #1.
Ratio recorder -- 10% and 2% spans.
I_R recorder -- time constants 3 to 7.

Ratio	Span	Time Constant in Seconds	Ratio Indeterminacy in Divisions of Chart Paper	Ratio Indeterminacy in Percent
99%	90-100%	τ_3 = 0.7	1.0	.1%
		τ_4 = 2.0	.75	.075%
		τ_5 = 4.5	.5	.05%
		τ_6 = 9	.5	.05%
	98-100%	τ_3 = 0.7	5.0	.1%
		τ_4 = 2.0	2.5	.05%
		τ_5 = 4.5	2.5	.05%
		τ_6 = 9	2.0	.04%
		τ_7 = 22	1.0 + slow drift	.02% + slow drift

There are circumstances when these conditions cannot be attained, due either to small sample size or to decreasing light as the wavelength extends into the ultraviolet. The oscilloscope pictures found in Figs. 2-OSC-2, 11, 12 show the effects of insufficient light on signal-to-noise. They should be compared with Figs. 2-OSC-1, 8 where shot noise is not the limiting noise. Yet even here, ratio indeterminacy is only 1.5% (Fig. 2-OSC-11) and 3% (Fig. 2-OSC-12).

E. SYSTEM ALIGNMENT AND USE

This discussion on system alignment and use is written as a recommended procedure for step by step adjustment by someone about to use the instrument.

1. Optical Alignment

(1) Preliminary Arrangement. The optical components should be positioned in accordance with Fig. 2-2. The center of each mirror should be set at six and a half inches above the table surface.

(2) Input Optics. After removing the cover of the monochromator, one observes its mirror illumination while adjusting the source and mirror 3 relative to one another. By observing the slit illumination from inside the monochromator, one can center the source in the slit.

Once the external optics have been aligned, the final adjustments to the input optics can be made by maximizing the signal output from the photomultiplier.

(3) General Comments on the External Optics. The goal is simple: one seeks a horizontal light beam which is centered on the various mirrors without overlap.† The beam should focus at the sample without overlap and be defocussed at the photomultiplier without overlap. Two tools are useful in carrying out these goals. The first is a simple grid sketched on cardboard and mounted on a vertical support; it is particularly useful in measuring the height of the light beam. The second is an adjustable mirror (Fig. 2-36) which is installed in the monochromator in front of the grating. Since the grating cannot be turned to the zero order (maximum intensity) position, this mirror reflects white light out at the exit slit, thereby providing sufficient light for external optics alignment.

(4) Large Mirror as Sample. In the first adjustments to the optics it is convenient to use a large mirror for the sample so that it need not be shifted each time a small change is made. It should be placed at about 60 cm. from the center of the beam splitter in a direction perpendicular to the side of the table.

(5) Mirrors 9 and 8. Mirror 9 should be adjusted first by centering the light beam on its surface and then rotating it about its two axes so that its image is horizontal and centered on mirror 8. A similar procedure is followed with mirror 8.

(6) Mirrors 1 and 6. Mirrors 1 and 6 are adjusted so that the image lies centered on the outermost beam splitter mirror with

---

†In this section we use the word "overlap" to describe the light beam's overspreading or extending beyond some surface such as a mirror or photocathode.

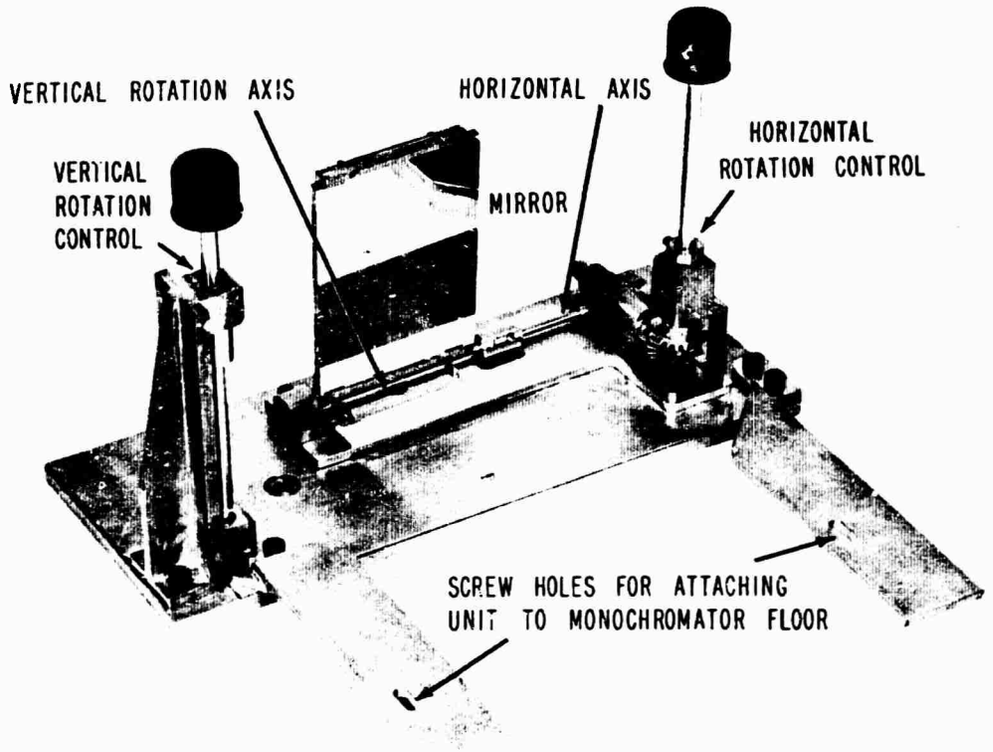

FIG. 2-36 ADJUSTABLE MIRROR FOR JACO MONOCHROMATOR TO FACILITATE EXTERNAL OPTICS ALIGNMENT

minimum overlap. Until light beam constriction is installed (14), there will always be some overlap. Then, by moving mirror 1 in and out on its horizontal axis, the slit image is focussed on the mirror located at the sample position. Mirror 6 will often have to be re-adjusted to reduce the overlap on the beam splitter.

(7) Mirror 4 and Beam Splitter. After the beam splitter is rotated 90°, so that the open holes replace the mirrors, light passing through the hole is focussed on mirror 4 by moving that mirror about on the horizontal plane.

(8) Mirrors 4 and 5. First moving the image close to the intersection of mirrors 4 and 5, we then rotate both mirrors about their horizontal and vertical axes so that the beam passes back through the second hole in the beam splitter onto mirror 7.

(9) Sample Mirror. The mirror is set at the sample position until the reflected light is incident on the second beam splitter mirror. Note the beam's position on mirror 7.

(10) Interdependence of Steps (6)--(9). These steps should be repeated until a minimum amount of light is lost at the beam splitter and so that the images for the I_0 and I_R paths overlap at mirror 7. This overlap will not be perfect nor can the I_0 and I_R paths be made completely equivalent for reasons touched upon in Sec. II-A-8. One can come quite close however. The beam splitter itself can be rotated about a vertical axis to aid in the general alignment procedure. It is useful to know that when the beam splitter

is rotated and the sample mirror counterrotated to bring the reflected image back onto the beam splitter, the I_R image on mirror 7 is not significantly moved.

(11) Mirrors 7, 2, and 10. Once mirror 7 is properly illuminated by the images of both the I_0 and I_R paths, it should be adjusted to illuminate mirror 2. The separation of 7 and 2 should be kept as high as possible so that the image at the photomultiplier will be reduced within the dimensions of the photocathode. Mirror 10 is adjusted in a routine way and its spacing to the S-13 photomultiplier set so that the images on the photocathode are defocussed.

(12) Mirror 11. Mirror 11 should be rotated to deflect the light to the S-1 photomultiplier. Unfortunately, it is very difficult to see if the photocathode is properly illuminated. It can be done, however, and once a good angle is determined, it should be marked in some way so that the mirror can be replaced in the same angular position each time that one switches from the S-13 to the S-1.

(13) Precaution in Adjustment of Concave Mirrors. The concave mirrors are used as close to an on-axis configuration as possible. Slight deviations (around 10°) from the on-axis position will increase image size at the sample or the photomultiplier by a factor of two. This increase in image size worsens as the configuration becomes more off-axis.

(14) Light Beam Constriction. To minimize the polarization dependent error, the light beam must be sufficiently constricted

before reaching the beam splitter so that no light is blocked at the splitter in either the I_0 or I_R paths. If an oversize hole is placed at the point marked in Fig. 2-2, it can be gradually reduced until no light is lost on the beam splitter.

Following this operation, some of the previous steps may have to be checked for slight changes.

(15) Normal Size Sample in Proper Position. The large mirror-sample should now be replaced with a sample of dimensions closer to those of the monochromator slit at its focus point, e.g., .1" wide by .8" long. This new sample should be mounted between the poles of the magnet after the magnet has been wheeled up to the optics table.

The sample will not coincide with the slit image. The two should be brought into coincidence by moving the entire optics table horizontally by pushing it and vertically by adjusting the screw feet at the four corners of the table. The sample will need to be rotated about vertical and horizontal axes so that the reflected image returns to the beam splitter mirror.

(16) Final Tune-up. Light should now be traced through the entire system to ensure proper alignment. The S-13 photomultiplier is best viewed from inside the box shielding the sample volume, by sighting past the sample into the optics table area.

(17) Procedure for New Samples once Optics are Aligned. New samples can usually be installed without modifying any of the optical alignment. One places the new sample in approximately the correct position and illuminates it with white light using the monochromator

mirror described in (3) above. The sample mount permits adjustment in enough degrees of freedom so that the sample can be placed at the slit focus and so that the reflected light can be returned to the beam splitter mirror. Very slight adjustments in the position of the sample can then be made by noting the relative position of the I_0 and I_R images on the S-13 photocathode. These adjustments are continued until the images are superposed. If adjustments in the sample will not accomplish the superposition, it can often be brought about by moving mirrors 4 and 5 in synchronization along their common dovetail in a direction perpendicular to the direction of the incident I_0 light.

Since the mirror which is installed in the monochromator is not a perfect replacement for the grating, there is sometimes a very slight shift between the white light image at the sample and the monochromatic light image. A similar shift can occur at the photomultiplier. Consequently, image positions should be checked with the monochromatic light of greatest intensity (found at 5300Å) at the slit width which will be used for measurements. For this check, the experimenter will need to acclimatize his eyes to the dark.

Slit height should be reduced sufficiently so that the light image of the slit lies entirely on the sample. Slit width is set by balancing shot noise and resolution requirements.

2. Electronic Alignment

(1) Preliminaries. The optics are assumed to be aligned, the light source is turned on, and a wavelength chosen for maximum light intensity. Monochromator slit width is set large enough so that shot noise is not a significant problem during alignment. (Compare the Figs. 2-OSC-2, 11, 12, showing the effects of insufficient light, with Figs. 2-OSC-1, 8.) The photomultiplier power supply, preamplifier (TA-5), band-pass filter, and phase sensitive detector (Sanborn) are assumed to be operating properly and to have had a warmup of at least one-half hour.

(2) Battery Checks. Mercury batteries each drive the calibrator-offset, the retransmitting slide wire, and the multichannel analyser initiator found in the wavelength marker unit. A Jones plug at each permits checking the batteries. A current of 1 ma. indicates the battery is healthy.

(3) Reference Signal. After turning on the light chopper, light chopper reference bulb, and the 25 volt power supply, one observes the light chopper signals at Reference Signal Monitor Positions 1 and 2 (Figs. 2-OSC-22, 23).

(4) Beam Splitter. Its position should be set by hand to pass the I_0 light. During the initial adjustments, the beam splitter is not operated.

(5) Photomultiplier, TA-5, and Filter. The photomultiplier power supply is set at minimum voltage (500 volts) and the high voltage turned on. Minimum voltage is used so that there is no

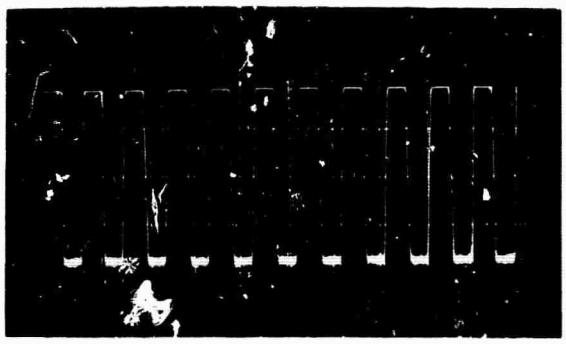

FIG. 2-OSC-1 LIGHT CHOPPED SIGNAL AT PHOTO-MULTIPLIER ANODE RESISTOR. H = 1, V = 10

FIG. 2-OSC-2 AS IN 1, EXCEPT LIGHT INTENSITY REDUCED BY FACTOR OF 250. H = 1, V = 10

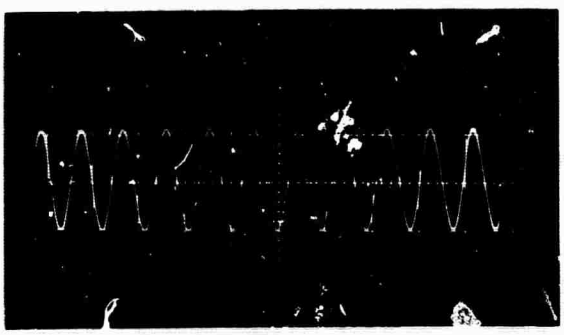

FIG. 2-OSC 3 SAME SIGNAL AS IN 1, AT BAND-PASS FILTER OUTPUT. H = 1, V = 500

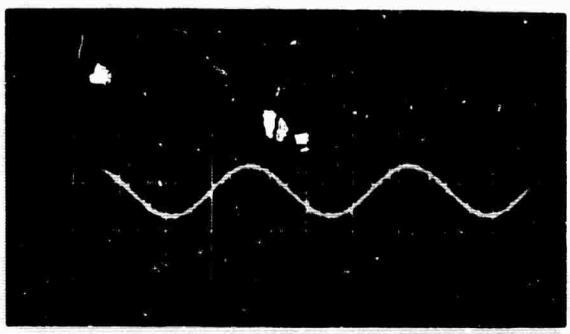

FIG. 2-OSC-4 AC COMPONENT OF SIGNAL IN 1 AT SANBORN OUTPUT (LOW FILTER). POOR PHASE ADJUST-MENT. H = 10, V = 5

OSCILLOSCOPE PHOTOGRAPHS OF THE EXPERIMENTAL SIGNAL AT VARIOUS POINTS IN THE SYSTEM WHEN THE BEAM SPLITTER IS NOT ROTATING. SEE ALSO FIG. 2-OSC-18.
H = HORIZONTAL SCALE IN MSEC/CM. V = VERTICAL SCALE IN MV/CM.

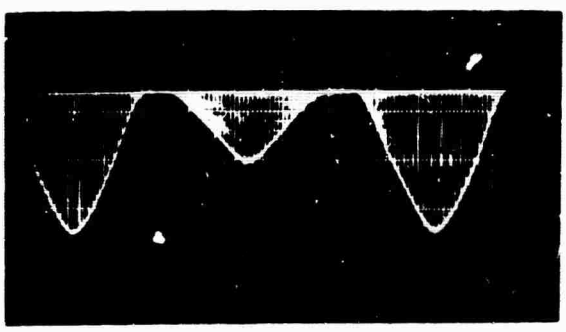

FIG. 2-OSC-5 SIGNAL AT PHOTOMULTIPLIER ANODE RESISTOR. SHOT NOISE NOT THE MAJOR NOISE.
H = 10, V = 25

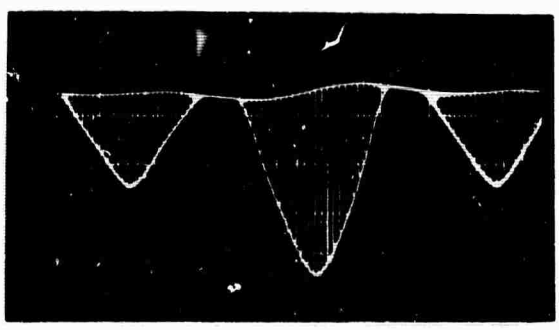

FIG. 2-OSC-6 SIGNAL IN 5 FOLLOWING PREAMPLIFIER.
H = 10, V = 200

OSCILLOSCOPE PHOTOGRAPHS OF THE EXPERIMENTAL SIGNAL AT VARIOUS POINTS IN THE SYSTEM WHEN THE BEAM SPLITTER IS ROTATING. H = HORIZONTAL SCALE IN MSEC/CM.
V = VERTICAL SCALE IN MV/CM.

danger of an excessive anode current flowing. The photomultiplier voltage is increased until the anode current lies within the limits set in Sec. II-D-4. The waveform can be compared to Fig. 2-OSC-1. After setting the TA-5 at 40 db attenuation for a 10 KΩ anode resistor, or 20 db for a 1 KΩ, and setting the band-pass filter at a low cutoff of 425 Hz and a high cutoff of 1950 Hz, one compares the waveform to Fig. 2-OSC-3.

(6) Sanborn. The transistor buffered output is selected, the Sanborn attenuator set at 20 and the zero level adjusted in accordance with Sec. II-B-6-b-(4). In the "Hi" filter position the Sanborn output, as observed at Sanborn Monitor Position 8, will have the ripple shown in Fig. 2-OSC-13. This ripple is about 20 mv. high and is quite normal. It is not evident in the "Low" filter position.

Now the relative phase of the reference and experimental signals can be adjusted. The TA-5 input short suggested in Sec. II-B-6-b-(4)-(b) is removed and the Sanborn filter set to its "Low" position. By mechanical adjustment of the reference signal unit found on the light chopper, the DC level of the Sanborn output can be maximized. It is best observed on an oscilloscope using the scope's DC offset to maximize sensitivity. Under proper adjustment the trace will look flat except for noise of 1 to 2 mv., yet a deviation of only 10° of phase from the maximum results in the large low frequency ripple seen in Fig. 2-OSC-4. This ripple poses an intermodulation hazard.

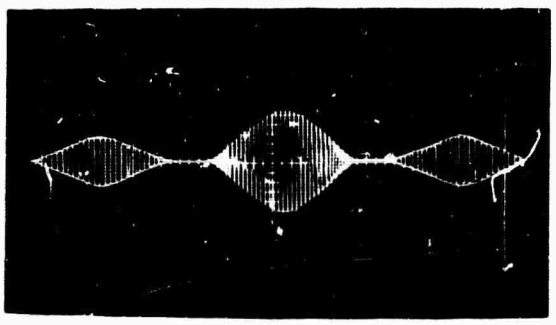

FIG. 2-OSC-7 SIGNAL IN 6 FOLLOWING BAND-PASS FILTER. H = 10, V = 500

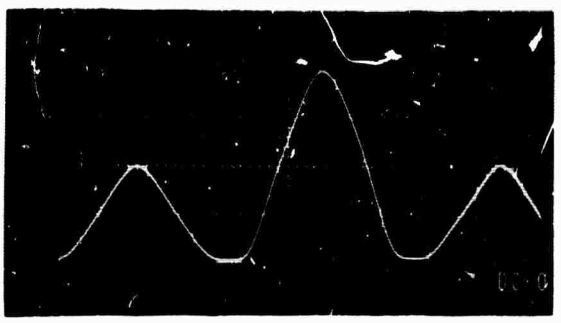

FIG. 2-OSC-8 SIGNAL IN 7 AT SANBORN OUTPUT, HI FILTER. OBSERVE AT SANBORN MONITOR -- POSITION 8. H = 10, V = 500

FIG. 2-OSC-9 AS IN 8, EXCEPT MED FILTER. H = 10, V = 500

FIG. 2-OSC-10 AS IN 8, EXCEPT LOW FILTER. H = 10, V = 500

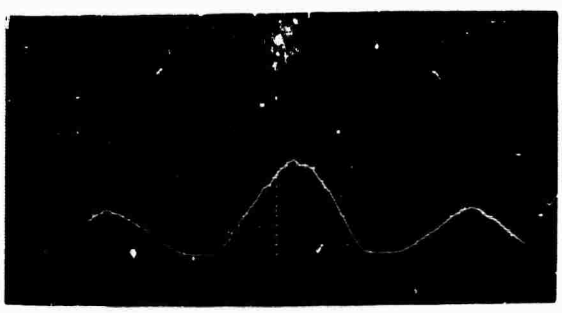

FIG. 2-OSC-11 AS IN 8, EXCEPT LIGHT INTENSITY REDUCED BY FACTOR OF 250 (AS IN 2 [illegible]) NOISE = 1.5%. H = 10, V = 1000

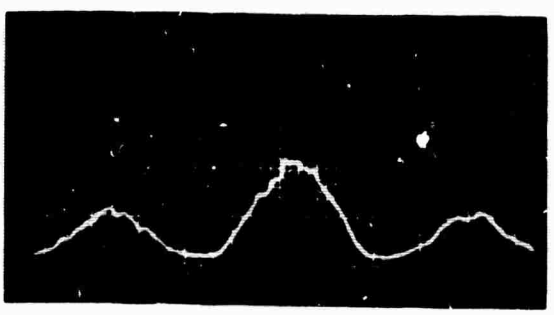

FIG. 2-OSC-12 AS IN 11, EXCEPT LIGHT INTENSITY REDUCED FURTHER. RATIO NOISE = 3%. H = 10, V = 1000

OSCILLOSCOPE PHOTOGRAPHS OF THE EXPERIMENTAL SIGNAL AT VARIOUS POINTS IN THE SYSTEM WHEN THE BEAM SPLITTER IS ROTATING, CONTINUED. H = HORIZONTAL SCALE IN MSEC/CM. V = VERTICAL SCALE IN MV/CM.

An alternative, although less sensitive, method of phase adjustment is suggested in Fig. 2-OSC-18. This is the signal seen at Sanborn Monitor Position 4 and 5, Left Jack; the sinusoidal curve is the experimental signal and the spikes occur at the zero crossings of the reference signal. These two signals move relative to one another as the light chopper reference signal unit is adjusted, and are in phase when the spikes coincide with the experimental signal zero crossings.

The Sanborn signals at various interior points can be observed to ensure proper Sanborn operation (Sec. II-B-6-c).

(7) Photomultiplier Voltage. After the Sanborn adjustments are complete, the photomultiplier voltage should be shifted to give an output of two volts. Then the electronic elements will operate in their optimum range.

(8) Channel Filters. The filter is set at position 1 and the 13 Hz switches shorted out.

(9) Recorders. All recorders are turned on.

(10) I_0 Noise Check. The selector switch on the Ratio Routing Box is set to Position 2 and R-C filter to Position 1 (no additional filtering). The I_R 1 KΩ load is adjusted so that the signal on the I_R recorder is full scale. Under these conditions there should be no evidence of noise in the recorder trace.

(11) First Ratio Noise Check. This check does not employ the beam splitter, and the 13 Hz switches remain shorted. One turns off the experimental signal through use of the Sanborn "USE-OFF" switch and in its place sets the Sanborn DC level at its maximum value.

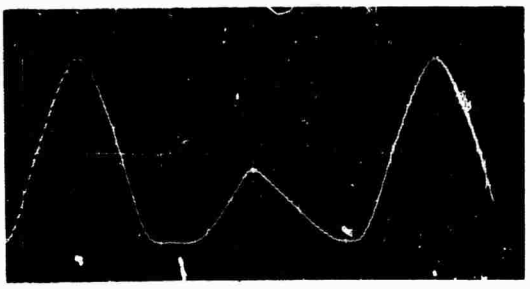

FIG. 2-OSC-13 AS IN 8, EXCEPT I_R SIGNAL IS DISTORTED DUE TO POOR LIGHT IMAGE POSITIONING. H = 10, V = 500

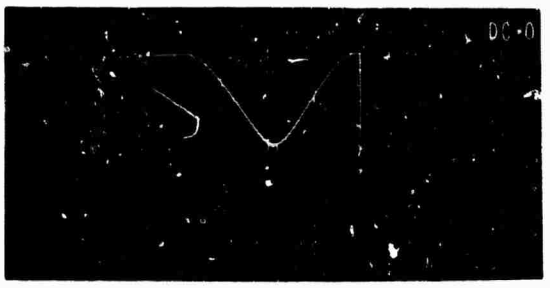

FIG. 2-OSC-14 SIGNAL IN 8 AFTER PASSING THROUGH I_R CHANNEL SWITCH. HI FILTER IN SANBORN. OBSERVE AT CHANNEL MONITOR -- POSITION 4. H =10, V = 500

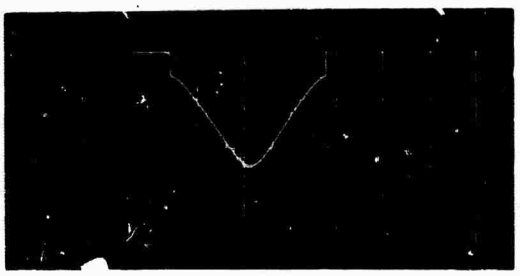

FIG. 2-OSC-15 AS IN 14, EXCEPT SANBORN DC LEVEL 0. H = 10, V = 500

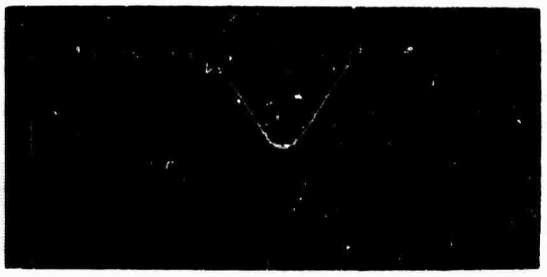

FIG. 2-OSC-16 AS IN 14, EXCEPT MED FILTER IN SANBORN. H = 10, V = 500

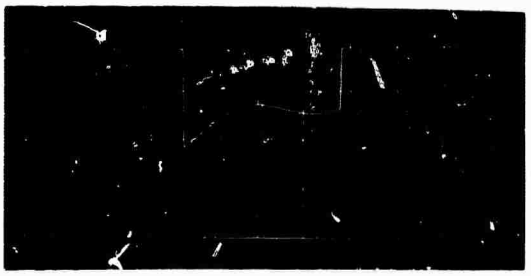

FIG. 2-OSC-17 AS in 14, EXCEPT LOW FILTER IN SANBORN. H = 10, V = 500

OSCILLOSCOPE PHOTOGRAPHS OF THE EXPERIMENTAL SIGNAL AT VARIOUS POINTS IN THE SYSTEM WHEN THE BEAM SPLITTER IS ROTATING, CONTINUED. H = HORIZONTAL SCALE IN MSEC/CM. V = VERTICAL SCALE IN MV/CM.

The ratio displayed is then determined by the setting of the I_R attenuator which serves as part of the Sanborn load. If the ratio is displayed on the .5 or 1% spans, noise should be less than ratio recorder deadband which is less than .003% under these circumstances.

(12) Second Ratio Noise Check. This shows the small effect of photomultiplier shot noise. When the Sanborn DC level is reset to zero and its switch returned to the "USE" position, ratio indeterminacy should again be less than the deadband of .003%.

(13) Beam Splitter. We are now ready to start actual ratio operation. After opening the shorting switches, one turns on the beam splitter and the two beam splitter reference light bulbs, and compares the beam splitter reference signals found at Reference Signal Monitor Positions 3, 4, 5, and 6 with Figs. 2-OSC-24, 25. The modified beam splitter signals used to drive the channel switches can be observed at Channel Monitor Positions 2, 3, 5, and 6, and compared with Figs. 2-OSC-20, 21.

(14) Signal Shapes. In analogy with (5) and (6) one observes the ratio wave shapes and compares them with the relevant figures to ensure proper operation. The signal at the photomultiplier anode is seen in Fig. 2-OSC-5, while that at the preamplifier output is given in Fig. 2-OSC-6. The band-pass filter output is found in Fig. 2-OSC-7, and Figs. 2-OSC-8, 9, 10 give the "Hi", "Med", and "Low" filter outputs of the Sanborn.

Nonsymmetric wave shapes are shown in Fig. 2-OSC-13 and should be eliminated by repositioning the light images symmetrically on the

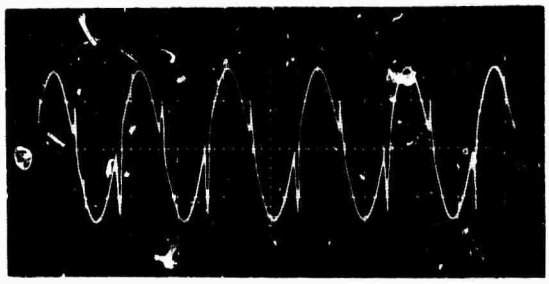

FIG. 2-OSC-18 LEFT JACK, POSITIONS 4 AND 5: AMPLIFIED EXPERIMENTAL SIGNAL PRECEDING DIODE BRIDGE. BEAM SPLITTER NOT ROTATING. H = .5 V = 10,000

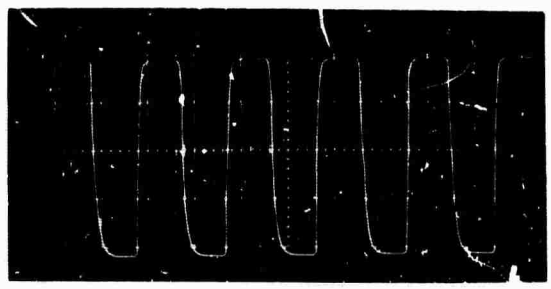

FIG. 2-OSC-19 LEFT JACK, POSITION 6: SQUARE WAVE REFERENCE SIGNAL AT DIODE BRIDGE. H = .5, V = 40,000

OSCILLOSCOPE PHOTOGRAPHS OF THE SIGNALS AT THE SANBORN MONITOR POSITIONS. OTHER MONITOR POSITIONS AT LEFT JACK, POSITION 8: SEE FIGS. 8-13. H = HORIZONTAL SCALE IN MSEC/CM. V = VERTICAL SCALE IN MV/CM.

FIG. 2 OSC-20 UPPER JACK, POSITIONS 2 AND 3: CHANNEL SWITCH POSITION FOR BOTH I_R AND I_O. H = 10, V = 5000

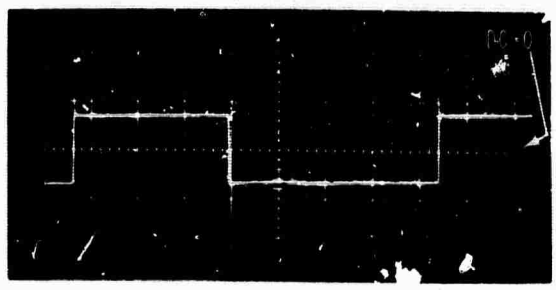

FIG. 2-OSC-21 UPPER JACK, POSITIONS 5 AND 6: VOLTAGE APPLIED TO COIL OF CHANNEL SWITCH, I_R AND I_O. H = 10, V = 1000

OSCILLOSCOPE PHOTOGRAPHS OF THE SIGNALS AT THE CHANNEL SWITCH MONITOR POSITIONS. OTHER MONITOR POSITIONS: UPPER AND LOWER JACK, POSITION 4, SEE FIGS. 14-17. H = HORIZONTAL SCALE IN MSEC/CM. V = VERTICAL SCALE IN MV/CM.

beam splitter openings and mirrors. Nonsymmetry often indicates that light is blocked by the beam splitter and hence lost. It can result in a more serious merging of the I_0 and I_R signals than usually occurs.

(15) Beam Splitter Light Sensors. The I_R light sensor unit is moved mechanically so that the I_R signal is symmetrically placed with respect to the period of channel switch closure. This operation can be monitored at Channel Switch Monitor Position 4, Upper Jack, and is repeated for the I_0 signal at Position 4, Lower Jack. These adjustments will ensure that there is minimal channel overlap (less than .1%) and that signals are maximized, but success presupposes that the I_0 and I_R wave shapes are symmetric (see (14)).

(16) Ratio Display. We leave the channel filters in Position 1 and select ratio operation with Position 3 of the selector switch on the Ratio Routing Box. The retransmitting slide wire battery is actuated and the two-second time constant chosen. One selects the slide wire span by adjusting the shunt resistor and selects upper and lower percentage limits appropriate to the sample being examined. The recorder's servo amplifier gain is adjusted.

(17) Third Ratio Noise Test. Under the conditions cited above, with 10% span, ratio noise should be checked. With typical smooth surface samples, indeterminacy should not exceed .05% and with large mirrors may go as low as .02% (Sec. II-D-5).

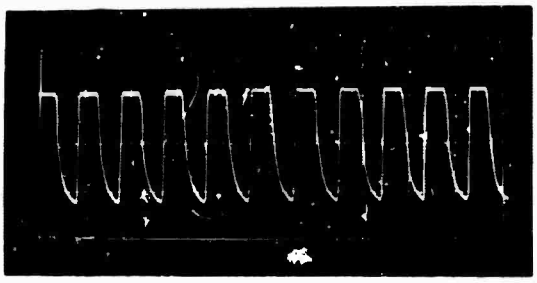

FIG. 2-OSC-22 POSITION 1: LIGHT CHOPPER REFERENCE SIGNAL AT DETECTOR. H = 1, V = 50

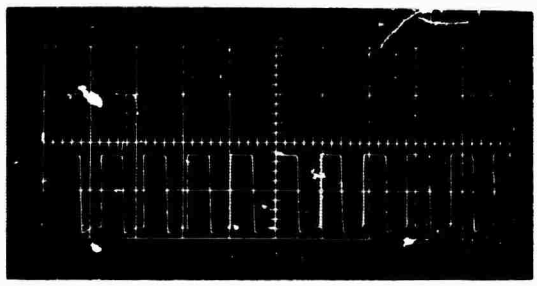

FIG. 2-OSC-23 POSITION 2: SHAPED LIGHT CHOPPER REFERENCE SIGNAL BEFORE FILTERING. H = 1, V = 10,000

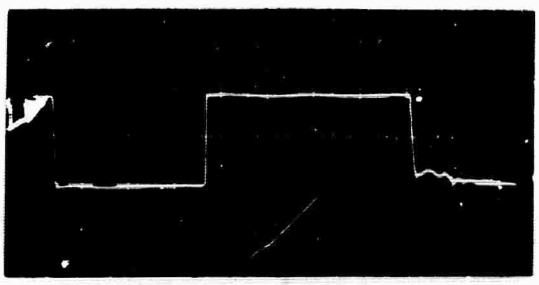

FIG. 2-OSC-24 POSITIONS 3 and 5: BEAM SPLITTER REFERENCE SIGNAL AT DETECTOR, I_R AND I_O CHANNELS. H = 10, V = 50

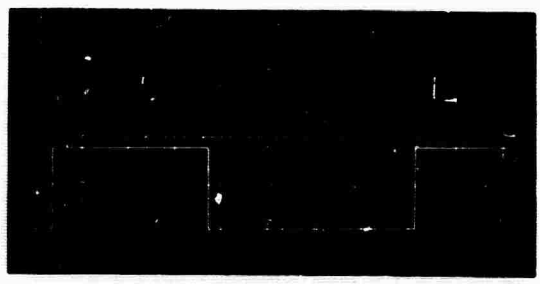

FIG. 2-OSC-25 POSITIONS 4 AND 6: SHAPED BEAM SPLITTER REFERENCE SIGNAL, I_R AND I_O CHANNELS. H = 10, V = 10,000

OSCILLOSCOPE PHOTOGRAPHS OF THE SIGNALS AT THE REFERENCE SIGNAL MONITOR POSITIONS.
H = HORIZONTAL SCALE IN MSEC/CM. V = VERTICAL SCALE IN MV/CM.

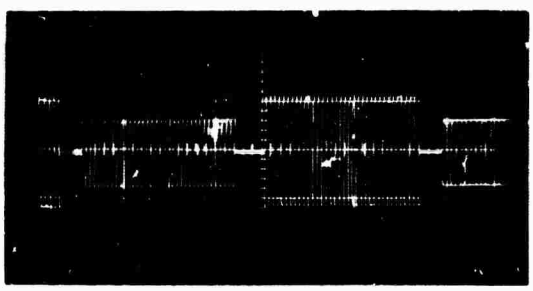

FIG. 2-OSC-26 THE AC OFFSET AND CALIBRATOR VOLTAGE. OBSERVED AT ANODE RESISTOR. H = 10, V = 50

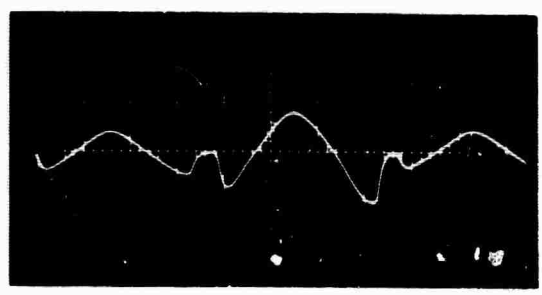

FIG. 2-OSC-27 AC OFFSET SUBTRACTED FROM EXPERIMENTAL SIGNAL OF FIG. 8. BOTH HAVE SAME INFORMATIONAL MAGNITUDE. OBSERVED AT SANBORN MONITOR. - 8. H = 10, V = 10,000

OSCILLOSCOPE PHOTOGRAPHS OF THE CALIBRATOR-OFFSET AND ITS EFFECT.
H = HORIZONTAL SCALE IN MSEC/CM. V = VERTICAL SCALE IN MV/CM.

(18) Fourth Ratio Noise Check. To see the effect of the rotating beam splitter on noise, one sets the Sanborn "USE-OFF" switch at "OFF" and employs the Sanborn DC level as the experimental signal. After a suitable warmup of the beam splitter of around one-half hour, ratio indeterminacy should not exceed .01 to .02% with a time constant of 4.5 seconds.

(19) Calibrator and Offset Alternative. On occasion one might want to check out the electronics with a signal completely independent of the optics. This requirement can be partially fulfilled with the Calibrator and Offset. No light is necessary nor is the photomultiplier used. However, the signals are derived from the light chopper and beam splitter references, which are optical components.

(20) Fifth Ratio Noise Test. Using the Calibrator and Offset, ratio indeterminacy should not exceed .04% when employing time constants of one second or longer.

3. Spectrum Scan

(1) Preliminaries. The adjustments discussed in Secs. II-E-1 and 2 are assumed to have been made. One actuates the wavelength marker power supply and selects which recorders will record wavelength. The wavelength marker mode for solenoid action is selected as opposed to multichannel analyser initiation.

(2) Optical Selections. One chooses a light source, monochromator grating, light filter, light polarizer, and detector appropriate for the wavelength range of interest as given in Table 2-20. The drive should always run toward decreasing wavelength to reduce the effect of wavelength drive backlash.

TABLE 2-20 OPTICAL COMPONENTS
FOR VARIOUS WAVELENGTH RANGES

Wavelength Range	Source	Grating	Filter[3]	Polarizer	Detector
1.32μ-7700Å	Sylvania DXM Iodine Quartz Tungsten	1.1μ Blaze	Corning 7-57	Polaroid HR	RCA 7102, S-1 Response
9000-7500Å		7500Å Blaze (or 5000Å blaze when using other JACO monochromator)	Corning 3-70		
8000-5000Å				Polacoat	
7000-5000Å				For-mula 150 UV	EMI 6256B, S-13 Response
5500-3500Å			None		
4500-2200Å[1]	Osram Xenon Arc				
4000-2300Å			Corning 7-54		
3100-2200Å[2]			None	None	

[1] Over the full range this option is less satisfactory than some others, due to scattered light.

[2] No evidence of the polarization dependent phenomena was found in this range so that a polarizer is not necessary.

[3] Other possible filter combinations, suitable over restricted ranges, are suggested by Figs. 2-5a through d.

(3) I_0 Control. By using human feedback, one can keep I_0 equal to about 2 volts. While varying the photomultiplier dynode chain voltage, one can see the effect on I_0 by observing the Sanborn output on the oscilloscope. Thereby, one ensures that the system operates in the optimal regions for linearity and noise, and one need not make adjustments in the servo amplifier gain.

(4) First Scan. The experimenter should use a 40% recorder span, fast wavelength sweep of 500Å/min. or 250Å/min., and a low time constant of 1 or 2 seconds to get a preliminary idea of the spectrum.

(5) More Detailed Scans. These can be made on the basis of structure noted in the first scan or in regions where structure is predicted. One has control over four quantities: recorder span, wavelength scan speed, time constant, and recorder chart speed. These should not be set independently.

Time constant is set first on the basis of system noise and the size of structure. That same structure size will determine span; and span and time constant together will give sweep rate. Scan rate is then a function of the preceding three and is usually chosen so that the slope of the recorder trace is 45°. Appendix II-B discusses the rationale behind this sequence and develops criteria for choosing values for each of the four parameters.

In practice it is often easiest to decrease sweep rate until structure shape is unmodified rather than to apply the criteria. However, when effects are small and integration times long, application of the criteria is more efficient.

(6) Span. In adjusting span, refer to Table 2-12 for values of the shunt resistance.

(7) Multichannel Analyser. If the signal is masked by noise, the multichannel analyser should be coupled into the system. Figure 2-26 shows appropriate connections, and Sec. II-B-16 discusses the analyser's use. In the wavelength marker pulse power supply the multichannel analyser Initiate mode is selected.

(8) I_0 and I_F Operation. This is quite simple. Once the optics are aligned, one follows the procedures found under electronic alignment, Sec. II-E-2, (1)--(10), and of this section in (1), (2). Conditions analogous to those discussed in (5) apply to the choice of time constant, sweep rate, and chart speed. Use of the AC offset has an effect similar to span choice in ratio measurements.

APPENDIX II-*A*

THE ERROR IN THE RETRANSMITTING SLIDE WIRE READING WHEN USED WITH THE MULTICHANNEL ANALYSER

The slide wire circuit is found in Fig. 2-27a, where the various symbols have the following meanings:

V_B = battery source. (2.30a)

R_B = adjustable resistance 0 to 51 K. (2.30b)

R_T = retransmitting slide wire = 100 Ω. (2.30c)

R = portion of retransmitting slide wire feeding the Vidar input. (2.30d)

$R_L/4$ = 1000 Ω (2 resistors in filter). (2.30e)

$R_L/2$ = 2000 Ω = input impedance of Vidar. (2.30f)

I_L = fraction of total current, I, through the Vidar source impedance. (2.30g)

The correct ratio reading is that corresponding to the retransmitting slide wire contact position on the slide wire. Expressed as a fraction, it is

$$\frac{R}{R_T} \equiv \alpha \ . \tag{2.31}$$

The voltage reading at the Vidar input which corresponds to this position is incorrect because R_L loads the slide wire. To determine the significance of this error, we compute

$V(\alpha)$ = voltage across the Vidar when the slide wire contact position is such that $R/R_T = \alpha$. (2.32)

$$I = \frac{V_B}{R_B + R_T - R + \frac{R\,R_L}{R+R_L}} \tag{2.33}$$

$$I_L = \frac{IR}{R + R_L} \tag{2.34}$$

$$V(\alpha) = \frac{R_L I_L}{2} = \frac{R_L}{2} \frac{V_B}{R_B + R_T - R + \frac{R\,R_L}{R+R_L}} \frac{R}{R+R_L}$$

$$= \frac{\alpha\beta_{LT}}{\alpha\beta_{BT} + \beta_{LT}\beta_{BT} + \beta_{LT} + \alpha - \alpha^2} \quad \text{where} \tag{2.35}$$

$$\beta_{LT} = R_L/R_T \,, \quad \beta_{BT} = R_B/R_T \tag{2.36a,b}$$

$V(0)$ = 0 which is a correct reading. (2.37)

$V(1)$ = the voltage we arbitrarily select to correspond to full scale on the ratio recorder. Hence, it is correct by definition. (2.38)

$\frac{V(\alpha)}{V(1)}$ = the measured voltage normalized to the full scale value

$$= \frac{\alpha(\beta_{BT} + \beta_{LT}\beta_{BT} + \beta_{LT})}{(\alpha\beta_{BT} + \beta_{LT}\beta_{BT} + \beta_{LT} + \alpha - \alpha^2)} \tag{2.39}$$

The error is simply $= \alpha - \frac{V(\alpha)}{V(1)}$

$$= \frac{\alpha(1-\alpha)(\alpha - \beta_{BT})}{[(\alpha+\beta_{LT})(\beta_{BT}+1) - \alpha^2]} \tag{2.40}$$

Since $\beta_{LT} = 40$ and $\alpha \leq 1$, we can closely approximate the error by dropping α relative to β_{LT}.

$$\text{Error} \approx \frac{\alpha(1-\alpha)(\alpha-\beta_{BT})}{\beta_{LT}(\beta_{BT}+1)} \qquad (2.41)$$

Error vs. α is plotted in Fig. 2-27 for various values of β_{BT} ranging from 0 to ∞.

APPENDIX II-8

CHOICE OF SPAN, SCAN RATE, TIME CONSTANT, AND CHART SPEED

1. Purpose

We wish to develop consistent criteria for the choice of ratio recorder percentage span, monochromator wavelength scan rate, system time constants, and recorder chart speed. If the system is to operate without spectrum distortion, and if it is to make small spectrum features stand out, these four parameters must be selected with attention to their interdependence.

2. A Simple Model Showing the Effect of Time Constant

Consider the R-C filter shown in Fig. 2-37a when subject to the input voltage, V_{in}, shown in Fig. 2-37b. The solution to its differential equation is

$$V_{out} - V_{in} = (dV_{in}/dt)\tau(e^{-(t-t_o)/\tau} - 1) , \qquad (2.42)$$

which is pictured in Fig. 2-37c. For time long compared to the time constant, τ, the separation of V_{out} and V_{in} is $(dV_{in}/dt)\tau$. Our goal is equality of V_{out} and V_{in}.

3. Application of Model to the Voltage Outputs of the Channel Filters

V_{in} refers to the input voltages to the channel filters and V_{out} to their outputs. Were it not for the use of feedback to keep V_{I_0} nearly constant, V_{in} would vary widely with wavelength because of source and detector variations. Feedback reduces these variations and hence reduces dV_{in}/dt for the I_0 channel. Automatic feedback

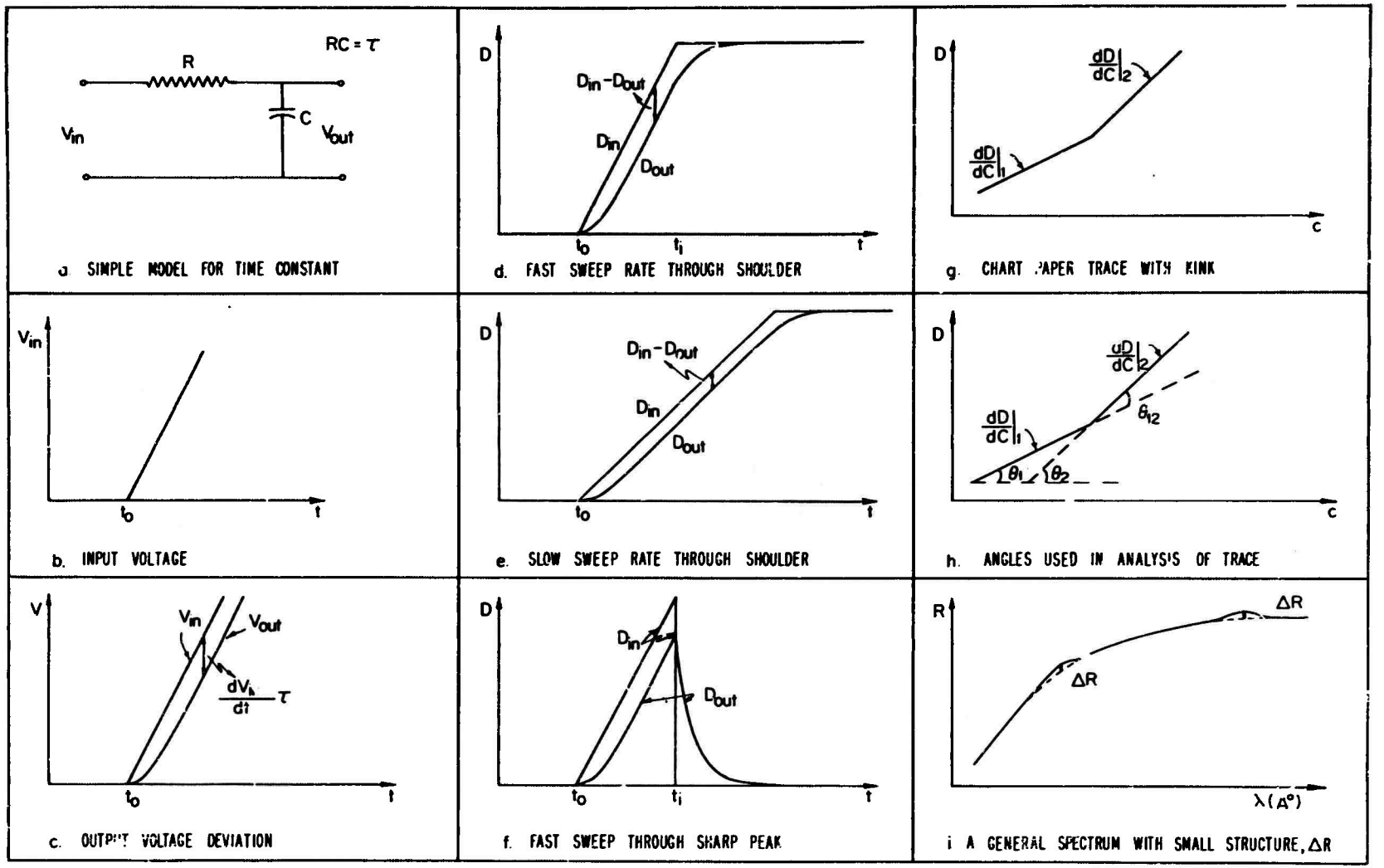

FIG. 2-37 DIAGRAMS USED IN ANALYSIS DETERMINING SPAN, SCAN RATE, TIME CONSTANT, AND CHART SPEED

could reduce dV_{in}/dt effectively to zero and V_{out} would equal V_{in}. Unfortunately, human feedback is less finely controlled so that dV_{in}/dt is still nonzero, and irregularities in control can result in added noise.

Due to the limitations on human feedback, one must at times abjure its use when looking for very small changes in amplitude in small recorder spans. Then one must worry about the full effects of source and detector variations on dV_{in}/dt. To consider this in more detail, let Å = wavelength in Ångstroms, $\langle V_{in} \rangle$ = average value of V_{in} over a small range, ΔV_{in} = the variation in V_{in} over that same range. Note that $d\text{Å}/dt$ = wavelength scan rate and $dV_{in}/d\text{Å}$ = rate of change of voltage with wavelength, and hence with source and detector variations. $dV_{in}/d\text{Å} \cong \Delta V_{in}/\Delta\text{Å}$. Equation 2.42 then becomes

$$\frac{V_{out} - V_{in}}{\langle V_{in} \rangle} = \frac{1}{\langle V_{in} \rangle} \frac{\Delta V_{in}}{\Delta \text{Å}} (d\text{Å}/dt)\tau = \frac{\Delta \ell n V_{in}}{\Delta \text{Å}} (d\text{Å}/dt)\tau \ . \qquad (2.43)$$

The left side of this equation is the fractional indeterminacy in our measurement of the voltage, and it would be desirable that this be no larger than the indeterminacy in the ratio, .0005. Setting the left side equal to .0005, and noting that the usual value of the channel filter time constant is 1 second, we get

$$\frac{\Delta \ell n V_{in}}{\Delta \text{Å}} = \frac{.0005}{(d\text{Å}/dt)\tau} = \frac{.03}{(d\text{Å}/dt)} \qquad (2.44)$$

where the scan rate is in Å/minute. Equation 2.44 provides one criterion for the choice of scan rate, as determined by the rate of

change of voltage with wavelength. For example, if we choose a scan rate of 50Å/min., the fractional change of V_{in} over a 100Å range should not exceed .03.

The preceding discussion has considered V_{I_O} as V_{in}. If we consider V_{I_R}, two distinct situations can be described. If V_{I_O} is kept constant by feedback, then V_{I_R} is just the ratio, and the material in the next section is relevant. On the other hand, if V_{I_O} is not constant, then Eq. 2.44 is equally applicable to the I_R information.

4. Application of Model to the Ratio Output of the Ratio Filter

In applying Eq. 2.42 to the ratio filter, we shall assume that V_{I_O} = constant, so that the problems discussed in Sec. 3 above need not be an issue.

Let R = the reflectivity ratio in percent, S = ratio recorder span in percent, L = the lower percentage limit on the ratio recorder, and D = the actual experimental reflectivity ratio reading on the ratio recorder, expressed in divisions out of 100. The following simple relation applies:

$$R = L + DS/100 \tag{2.45}$$

R_{in} is the experimental ratio and D_{in} is its reading in divisions of chart paper on the ratio recorder. The retransmitting slide wire picks off a voltage, V_{in}, exactly proportional to D_{in}, without time lag. V_{in} is the input to the ratio filter, and V_{out} is the filter's output. V_{out} determines D_{out} which is displayed on the I_R recorder. This proportionality is expressed as

$$V_{in} = \alpha D_{in} , \qquad D_{out} = V_{out}/\alpha . \qquad (2.46a,b)$$

Equation 2.45 applies for both in and out signals:

$$R_{in} = L_{in} + D_{in}S/100 , \quad R_{out} = L_{out} + D_{out}S/100 . \qquad (2.47a,b)$$

Equations 2.42 and 2.46 combine to give, for times long compared to the time constant,

$$D_{out} - D_{in} = (dD_{in}/dt)\tau . \qquad (2.48)$$

The derivative of Eq. 2.47a is $dR_{in}/dt = S/100\ (dD_{in}/dt)$, and $dR_{in}/dt = (dR_{in}/d\text{Å})\ d\text{Å}/dt$. With Eq. 2.48 they give

$$D_{out} - D_{in} = (100/S)(dR_{in}/d\text{Å})(d\text{Å}/dt)\tau \qquad (2.49)$$

Equation 2.49 supplies a criterion for choosing the relative sizes of span, scan rate, and time constant. It states that the indeterminacy in a chart recorder reading of ratio is directly proportional to scan rate, time constant, and rate of change of ratio with wavelength, and is inversely proportional to span. This indeterminacy is expressed in terms of chart paper divisions, not in terms of ratio percentage. This criterion's utilization will be deferred until Sec. 7 where all the criteria will be synthesized.

Figures 2-37d and e display the effect of decreasing the sweep rate on the indeterminacy in D. Comparing Figs. 2-37d and f shows that the maximum value of D_{out} may differ from that of D_{in} by an amount varying from zero (Fig. 2-37d) to the amount given in Eq. 2.49 (Fig. 2-37f). Thus, Eq. 2.49 is a good measure of amplitude error.

b. Wavelength Error

Figures 2-37d and f also indicate that there can be an error in the wavelength at which a maximum seems to occur. In Fig. 2-37f there is no error while in Fig. 2-37d it is a number of time constants. If this number could be determined, we should have an upper limit on the wavelength indeterminacy.

For time after t_1 in Fig. 2-37d, using Eq. 2.49,

$$D_{in} - D_{out} = \Delta D(t = t_1)e^{-(t-t_1)/\tau} = (100/S)(dR_{in}/d\mathring{A})(d\mathring{A}/dt)\tau\, e^{-(t-t_1)/\tau} .$$

We wish to know the time at which D_{out} appears to reach its maximum. This will occur approximately when D_{out} comes within the noise level of D_{in}, where the noise level is expressed in divisions of chart paper. Call this level N.

$D_{in} - D_{out} = N$. Solve for $(t-t_1)/\tau =$ number of time constants.

$$(t - t_1)/\tau = \ell n_e[(100/NS)\tau\,(dR_{in}/d\mathring{A})(d\mathring{A}/dt)] \qquad (2.50)$$

We can now compute the wavelength indeterminacy.

$$\delta\mathring{A} = \text{Wavelength indeterminacy} = (d\mathring{A}/dt)\tau\,(t - t_1)/\tau$$

$$= (d\mathring{A}/dt)\tau\,\ell n_e[(100/NS)\tau\,(dR_{in}/d\mathring{A})(d\mathring{A}/dt)] \qquad (2.51)$$

When the system is operating optimally, ratio indeterminacy is .05%, and NS/100 = .05. Equation 2.51 is then written as

$$\delta\mathring{A} = (d\mathring{A}/dt)\tau\,\ell n_e[(\tau/.05)(dR_{in}/d\mathring{A})(d\mathring{A}/dt)] . \qquad (2.52)$$

Equation 2.51, or equivalently, Eq. 2.52, provides additional criteria for the choice of time constant and sweep rate. It indicates the maximum indeterminacy in wavelength, as dictated by the

time necessary for the measured ratio to approach within the noise level of its proper value.

6. Model to Determine Chart Speed

The following is a derivation of the best slope for a trace on chart paper in order that small changes in slope be most readily picked out. This slope is 45° and can be used to determine chart speed.

D has the same definition as in Sec. 4, while C = distance along the chart paper in the direction of advancing time, where the unit distance is the single division used for D. dC/dt is chart speed. Note that dD/dC = the actual slope of the curve on chart paper for some arbitrary chart speed. dD/dÅ is the slope when C has been converted to wavelength, Å. Let the constant of proportionality be

$$\beta = \text{Å}/C = (d\text{Å}/dt)/(dC/dt) \ . \tag{2.53}$$

Figure 2-37g shows a trace on chart paper in which two straight lines are joined in a small cusp. By adjusting chart speed, we shrink or stretch the horizontal axis. That adjustment is equivalently expressed as a variation in β, and is to be carried out so that the cusp is most noticeable. Reference to Fig. 2-37h shows that we wish to maximize θ_{12}. We do so by varying β.

$$\theta_{12} = \theta_2 - \theta_1 = \text{arc tan } (dD/dC)_2 - \text{arc tan } (dD/dC)_1 \tag{2.54}$$

From Eq. 2.53

$$\theta_{12} = \text{arc tan } \beta\,(dD/d\text{Å})_2 - \text{arc tan } \beta\,(dD/d\text{Å})_1 \ . \tag{2.55}$$

$$\frac{d\theta_{12}}{d\beta} = \frac{(dD/d\text{Å})_2}{1+\beta^2(dD/d\text{Å})_2^2} - \frac{(dD/d\text{Å})_1}{1+\beta^2(dD/d\text{Å})_1^2} = 0 \tag{2.56}$$

$$(dD/d\mathring{A})_2 - (dD/d\mathring{A})_1 = \beta^2 (dD/d\mathring{A})_1 (dD/d\mathring{A})_2 [(dD/d\mathring{A})_2 - (dD/d\mathring{A})_1] \qquad (2.57)$$

$$\beta = [(dD/d\mathring{A})_1 (dD/d\mathring{A})_2]^{-\frac{1}{2}} \qquad (2.58)$$

If we assume that there is only a small change in slope so that

$(dD/d\mathring{A})_2 = (dD/d\mathring{A})_1 + \Delta$, then

$$\theta_2 = \arctan [(dD/d\mathring{A})_2/(dD/d\mathring{A})_1]^{\frac{1}{2}} = \arctan (1 + \Delta/(dD/d\mathring{A})_1)$$
$$\cong 45^\circ , \qquad (2.59)$$

and

$$\beta \cong (dD/d\mathring{A})_1^{-1} \cong (dD/d\mathring{A})^{-1} . \qquad (2.60)$$

Since $(S/100)(dD/d\mathring{A}) = dR/d\mathring{A}$ (from Eq. 2.45), chart speed is given by the following equation provided we use Eqs. 2.53 and 2.60:

$$dC/dt = \text{chart speed} = (d\mathring{A}/dt)/\beta = (d\mathring{A}/dt)(100/S)(dR/d\mathring{A}) \text{ div./min.} \qquad (2.61)$$

These are divisions in the horizontal, ratio amplitude, scale.

Equation 2.59 shows that the optimum slope for structure determination on chart paper is at 45°, while Eq. 2.61 indicates the appropriate chart speed to attain that slope, once scan rate, span, and the reflectivity change with wavelength are given. Multiplying Eq. 2.61 by the factor 5.27 gives the chart speed in inches per hour when using Leeds and Northrup #717 paper.

7. Criteria Summarized

Suppose we have a small change in structure, ΔR, such as is found in Fig. 2-37i, over a wavelength range $\Delta\mathring{A}$, which we wish to detect. How do we choose τ, S, $d\mathring{A}/dt$, and dC/dt, using the criteria?

First determine the percentage noise (= SN) for various τ in the wavelength range in question. Table 2-19 in Sec. II-D-5 provides an estimate of SN under optimum conditions. An actual measurement of noise can also be quickly made. Then one chooses the lowest τ such that $\Delta R \geq 2SN/100$, i.e., so that ΔR can be seen above the noise.

Secondly one chooses the span, S, so that the change in chart reading, ΔD, corresponding to ΔR will be no less than one division and preferably around 10. This choice ensures adequate display of the effect. Since $S\Delta D/100 = \Delta R$, S is given by

$$S = (10 \text{ to } 100) \times \Delta R \ .$$

The criteria are summarized here:

$$\frac{\Delta \ell n V_{in}}{\Delta \mathring{A}} = \frac{.03}{d\mathring{A}/dt} \ (\text{Angstroms})^{-1} \tag{2.44}$$

$$D_{out} - D_{in} = (100/S)(dR_{in}/d\mathring{A})(d\mathring{A}/dt)\tau \text{ divisions} \tag{2.49}$$

$$\delta\mathring{A} = (d\mathring{A}/dt)\tau \, \ell n_e[(100/NS)\tau \, (dR_{in}/d\mathring{A})(d\mathring{A}/dt)] \ \mathring{A}\text{ngstroms} \tag{2.51}$$

$$dC/dt = (d\mathring{A}/dt)(100/S)(dR/d\mathring{A}) \text{ divisions/minute} \tag{2.61}$$

Equation 2.49 shows that there must be a lower limit on span. For, as we decrease span, the indeterminacy in D increases unless we decrease sweep rate. The choice of span becomes a compromise between the need for adequate display of the change in R and the need for a tolerable sweep rate.

Sweep rate is determined next from Eqs. 2.44, 2.49, and 2.51. Some comments can be made on these equations when using them for

calculations: $dR_{in}/d\mathring{A}$ is $\cong 2\Delta R/\Delta\mathring{A}$; the log term in Eq. 2.51 can usually be replaced by a number in the range 2 to 3; $D_{out} - D_{in}$, the indeterminacy in D, cannot be less than the noise, SN, and could be set equal to the noise to determine maximum sweep rate.

In those measurements requiring only wavelength values, only Eqs. 2.44 and 2.51 need apply. $\delta\mathring{A}$ should be no more than the indeterminacy due to the combined effect of residual noise and peak broadness.

Finally, chart speed, dC/dt, is determined using Eq. 2.61.

The logical progression in the choice of system parameters begins with the anticipated signal change and noise which determine time constant. These lead to chart recorder span and then sweep rate. Chart speed is the final determination. The rules apply to the general situation where one wishes to display effects with maximum clarity, and when experimental conditions are constant in time. They will obviously be set aside in specific instances when it is better to get distorted data than none at all.

CHAPTER III

THE POLARIZATION DEPENDENCE OF FALSE REFLECTIVITY STRUCTURE

False structure occurs in the measurement of reflectivity or transmission with the JACO monochromator when one uses light polarized perpendicular to the exit slit. This structure in the ratio is correlated with abnormal structure found when measuring $I_0(\lambda)$under the same polarization conditions. Conversely, when the light is polarized parallel to the slit, the false structure disappears as does the anomalous $I_0(\lambda)$ structure. The discovery is disturbing since it suggests a breakdown in the execution of the basic postulates used to construct the system: that the I_0 and I_R optical and electronic paths be made alike to eliminate all such false effects.

In this chapter we consider the experimental and theoretical aspects of this peculiar effect in detail. In A and B we discuss the experimental evidence from transmission and reflection studies made as a function of polarization. In addition we observe that unequal amounts of light are lost in the I_0 and I_R light paths at the beam splitter, and that the false structure is considerably reduced if the beam is constricted before the beam splitter so that the two paths become more truly equivalent.

The theoretical analysis found in the remainder of the chapter shows how the light intensity at any point along the monochromator exit slit, when measured relative to its center, changes with wavelength. Then when the I_0 and I_R light paths pass different portions

of the light along the exit slit (as happens at the beam splitter with an unconstricted beam), the changing light distribution along the slit results in false structure in reflectivity (the ratio of the I_0 and I_R signals) as we change wavelength.

The variation in relative intensity along the exit slit with wavelength is the result of two interrelated factors:

(1) The striking variation of $I_0(\lambda)$ with wavelength for polarization perpendicular to the slit is postulated to be the result of the change in the angle of incidence of light on the monochromator grating. Evidence in support of this hypothesis is summarized in D. In reflection from a plane there are marked differences for the two polarizations. We call this the Brewster angle effect, discuss it in C, and describe in D its relevance to the hypothesis.

(2) At a given monochromator setting (which is calibrated in terms of wavelength) light is incident on the grating with a small range of angles of incidence -- not just one angle -- and that range changes with wavelength setting. This span arises from the succession of source points along the entrance slit and from the resultant deviations from perfect collimation of light incident on the grating. Tracing through each source point from the entrance to exit slit shows that to each point on the exit slit corresponds a slightly different angle of incidence on the grating. By our hypothesis in (1) this means a slightly different intensity at each point on the exit slit. Further, the relative intensity varies with wavelength. We discuss these geometrical factors in E.

With this background we derive in F an expression for the false structure, evaluate it for certain functional forms of $I_0(\lambda)$, and plot the result.

In G we show that the variation in angle of incidence on the grating for rays from different parts of the entrance slit does not lead to a loss of resolution.

Finally, in H we discuss how false structure can arise from another mechanism -- different optical activity in the I_0 and I_R light paths.

A. TRANSMISSION EVIDENCE

The first observation of peculiar behavior with a JACO monochromator was made by T. Shankland of this laboratory [3-01]. He measured the transmission of light through a hole in a copper plate. The plate was placed at the focus of the monochromator exit slit and partially obscured the slit image.

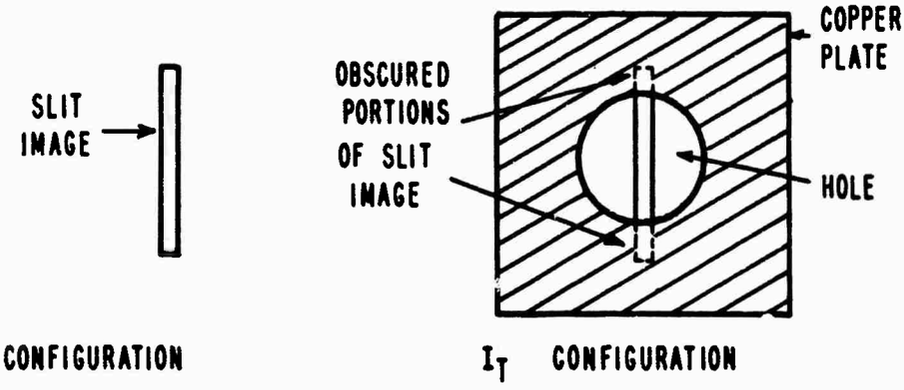

FIG. 3-1a LIGHT TRANSMISSION THROUGH A HOLE.

The transmission, I_T/I_0, was measured versus wavelength and, instead of being constant, showed a substantial dip.

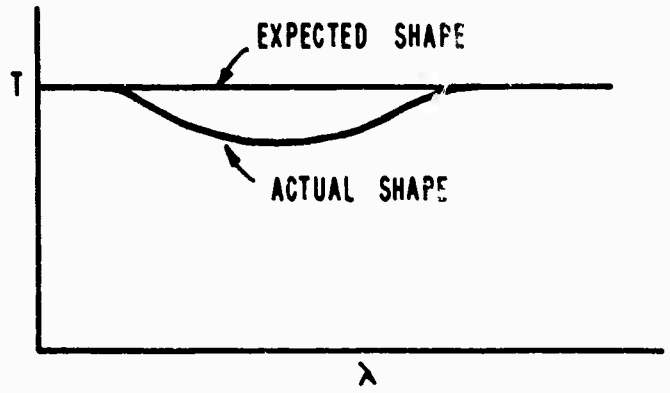

FIG. 3-1b THE TRANSMISSION CURVE

Heuristically, Shankland argued that the light distribution along the slit changed with wavelength, at times favoring the center of the slit, at others favoring the extremes (as at the dip), so that the apparent structure in the transmission was due to the variation with wavelength of the fraction of the light blocked by the metal plate.

B. REFLECTION EVIDENCE

If the light distribution does change along the slit with wavelength, the ratio reflectometer measurements will be affected since the beam splitter removes a small amount of light from the I_0 and I_R light paths. The amount removed differs for the two paths.

$I_0(\lambda)$ and $R(\lambda)$ measurements were made under five sets of conditions to see if there were an effect in reflectivity comparable

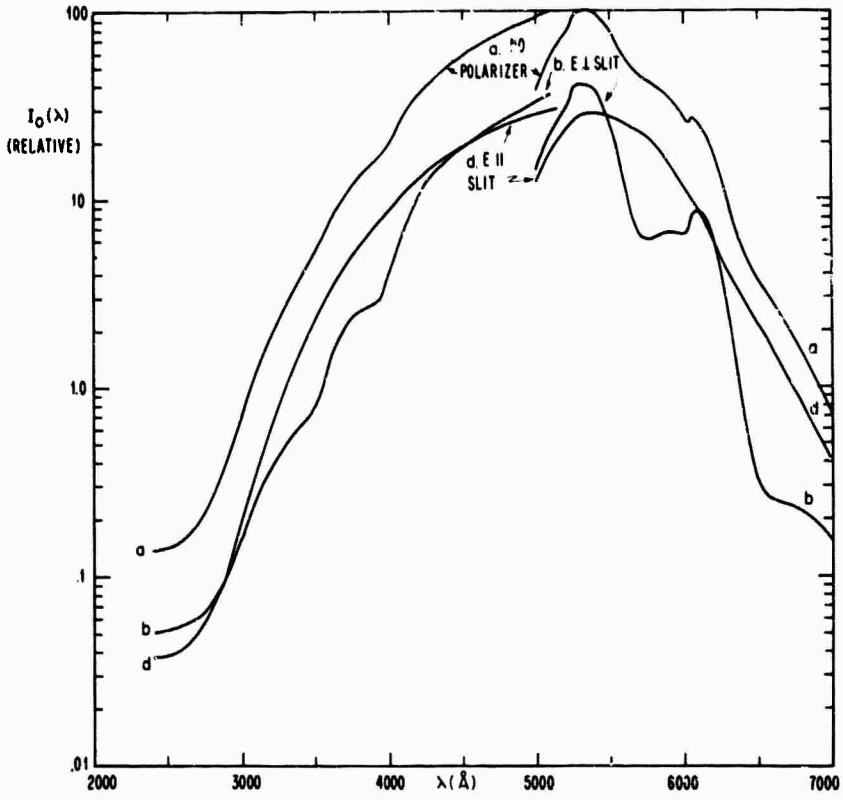

FIG 3-2 $I_o(\lambda)$ FOR THREE POLARIZATION CONDITIONS. System Components: GE Iodine Quartz Tungsten Source, 7500Å Blaze Grating, S-13 Photomultiplier, Polacoat 105 Polarizer, and 100μ Slit Width. Corning Filter 3-70 used in the range 5000-7000Å; no filter used in the range 2400-5150 Å.

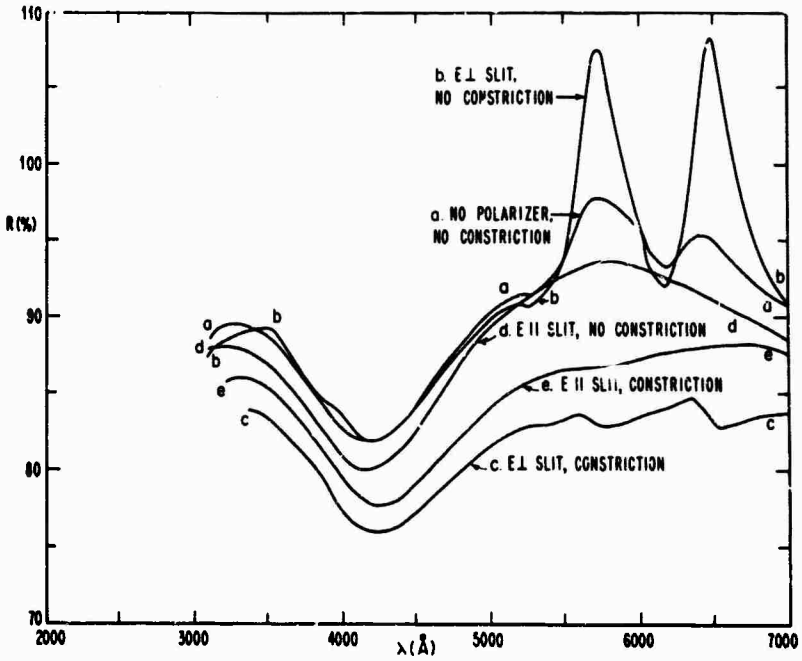

FIG. 3-3 R(λ) OF AN ALUMINUM MIRROR FOR FIVE POLARIZATION AND BEAM CONSTRICTION CONDITIONS. System Components: GE Iodine Quartz Tungsten Source, 7500Å Blaze Grating, S-13 Photomultiplier, and Polacoat 105 Polarizer.

the distortion found in transmission. In some measurements the beam was constricted prior to the beam splitter so that no light was lost at the beam splitter itself, and the two light paths again became equivalent. The five conditions were:

a. No polarizer, no beam constriction

b. Light polarized perpendicular to slit, no beam constriction

c. Light polarized perpendicular to slit, beam constriction

d. Light polarized parallel to slit, no beam constriction

e. Light polarized parallel to slit, beam constriction

The results are shown in Figs. 3-2, 3-3, and 3-4 for reflection from an aluminum mirror. There is indeed distortion. Certain features can be noted.

(1) $I_0(\lambda)$ and $R(\lambda)$ structural features are correlated in general position and in magnitude. Thus the case where $I_0(\lambda)$ structure is greatest, b, is also the condition where $R(\lambda)$ structure is largest.

(2) Reflectivity structure is minimized by using beam constriction and light polarized parallel to the slit. The maxima in $R(\lambda)$ at 3500Å, 3950Å, 5725Å, and 6475Å (plot b in Fig. 3-3) are correlated with minima in $I_0(\lambda)$ (Figs. 3-2 and 3-4). In the same diagrams regions of nearly vertical slope in $I_0(\lambda)$ at 5230Å and at 6050Å are correlated with abrupt changes in $R(\lambda)$.

(3) Beam constriction alone cannot remove the structure (condition c) if I_0 structure is pronounced (see (4)). Thus no measurements should be made with light polarized perpendicular to the slit.

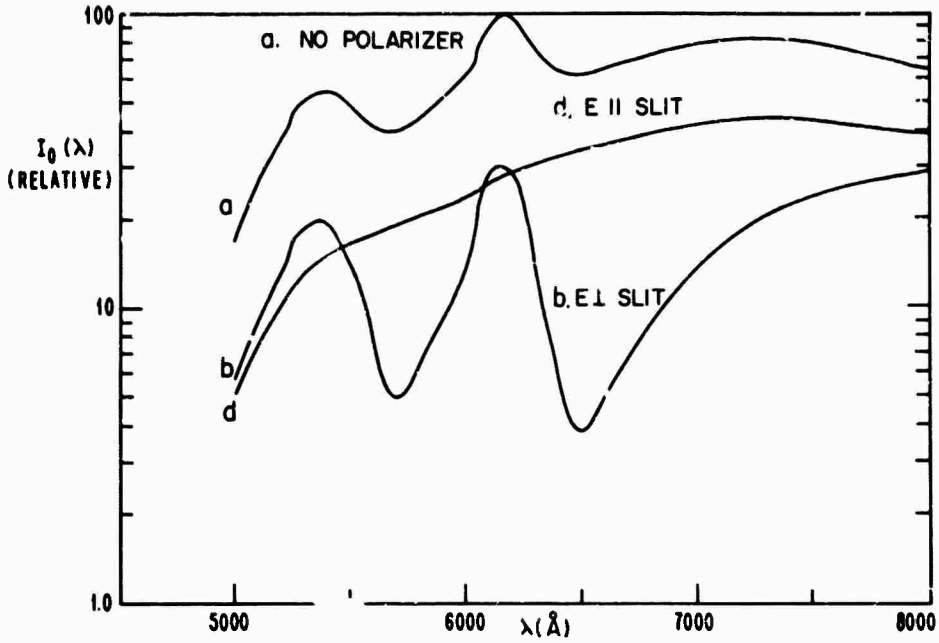

FIG. 3-4 $I_0(\lambda)$ FOR THREE POLARIZATION CONDITIONS. System Components: GE Iodine Quartz Tungsten Source, 7500Å Blaze Grating, S-1 Photomultiplier, Corning Filter 3-70, Polacoat 105 Polarizer, and 100μ Slit Width.

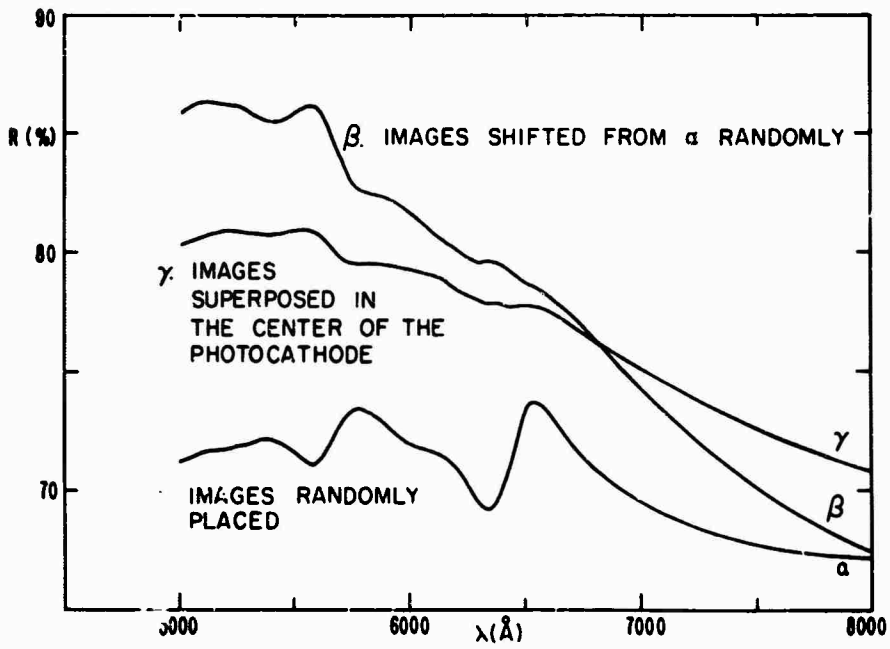

FIG. 3-5 THE DEPENDENCE OF THE REFLECTIVITY OF AN ALUMINUM MIRROR ON THE RELATIVE POSITIONING OF THE I_R AND I_0 IMAGES ON THE S-1 PHOTOCATHODE. The light is polarized perpendicular to the slit, and the beam is constricted. System Components: GE Iodine Quartz Tungsten Source, 7500Å Blaze Grating, S-1 Photomultiplier, Corning Filter 3-70, and Polacoat 105 Polarizer.

If data are needed showing the variation of R with polarization direction, the sample should be rotated.

(4) The structure in R worsens when the S-1 phototube is used instead of the S-13 (Fig. 3-5). This effect arises from the greater variation in sensitivity across the S-1 photocathode -- a variation which is wavelength dependent. The structure found with the S-1 varies widely as one changes the relative positions of the I_0 and I_R images (Fig. 3-5α and β) and is minimized when they are superposed (Fig. 3-5γ).

To a much lesser degree, varying sensitivity in the S-13 will have a similar effect. This variation presumably accounts for the structure still found under condition c in Fig. 3-3.

C. THE BREWSTER ANGLE CONCEPT

Figures 3-2 and 3-4 show a striking distinction between those $I_0(\lambda)$ curves for polarization perpendicular to the slit and those for polarization parallel to the slit. As a first step in trying to account for this difference, we consider a related problem -- the strong dependence on polarization direction of reflectivity from a plane surface. We find that a greater variation with angle of incidence is predicted for light polarized perpendicular to the slit than for that polarized parallel.

When light is reflected from a dielectric plane, the reflectivity not only varies with the angle of incidence, θ_i', but is different for light polarized in the plane of incidence, $E_{\parallel}$, and light

polarized perpendicular to that plane, $E_\perp$. The variation is more pronounced for the $E_\parallel$ light, the reflectivity going to zero at some θ_i' known as the Brewster angle. The Brewster angle occurs when reflected and transmitted rays are separated by 90°. Then the dipoles, excited by the transmitted ray, will not radiate in the direction of the reflected ray.

Analogous results are found when studying reflection from a metallic surface, which is relevant in our problem since the monochromator grating is coated with aluminum. Using formulae in Born and Wolf [3-02, Sec. 13.2] we have derived expressions for $r_\parallel$ and $r_\perp$, the ratios of the reflected to the incident fields for polarization parallel and perpendicular to the plane of incidence, respectively. Summarizing the results, we have

$$R_\perp = |r_\perp|^2 , \qquad R_\parallel = |r_\parallel|^2 \tag{3.1a,b}$$

where $R_\perp$ and $R_\parallel$ are the measured reflectivity intensities.

$$r_\perp \approx - \frac{n(1+\kappa^2) - \cos\theta_i' + i\kappa\cos\theta_i'}{n(1+\kappa^2) + \cos\theta_i' - i\kappa\cos\theta_i'} \tag{3.2}$$

$$|r_\parallel| = \frac{|r_\perp|}{\tan\psi} \tag{3.3}$$

$$\tan\psi = \tan\left[\tfrac{1}{2} \arccos\left(\frac{-2na}{n^2 + n^2\kappa^2 + a^2}\right)\right] \tag{3.4}$$

$$a = \sin\theta_i' \tan\theta_i' \tag{3.5}$$

Using n and κ values from Ehrenreich et al. [3-03], we have evaluated $R_\perp$ and $R_\parallel$ versus θ_i' at 4000Å, 5500Å, and 6500Å for aluminum

and plotted the results in Fig. 3-6. Although $R_{\parallel}$ does not go to zero as in a dielectric, it does have a minimum at some θ_i' known as the quasi-polarizing or pseudo-Brewster angle. We note the marked difference between $R_{\parallel}$ and $R_{\perp}$.

1. The Experimental and Theoretical Conventions on Light Polarization Direction

The definitions of perpendicular and parallel polarization directions are interchanged in our experimental and theoretical discussions. In experimental work it is natural and conventional to define the polarization direction in relation to the monochromator slits: this is the procedure we have followed in Sec. III-B. In theoretical analyses it is conventional to define the direction of polarization relative to the plane of incidence of the light, as we have done in the discussion immediately above. If we refer to Fig. 3-9, we can understand the distinction between the two sets of definitions in the particular case of light incident on a grating from a slit: the plane of incidence is defined by a grating groove and the direction of the incoming ray. Within the theoretical convention $E_{\perp}$ is perpendicular to this plane, but it is also parallel to the groove lines, which are in turn parallel to the slit. Within the experimental framework this is just the condition of E being polarized parallel to the slit.

To minimize confusion arising from this point, we shall indicate which convention is followed at the relevant places in the text.

The theoretical curves in Fig. 3-6 show that we should expect a greater variation of $R_{\parallel}$ with θ_i' than of $R_{\perp}$. This corresponds to our

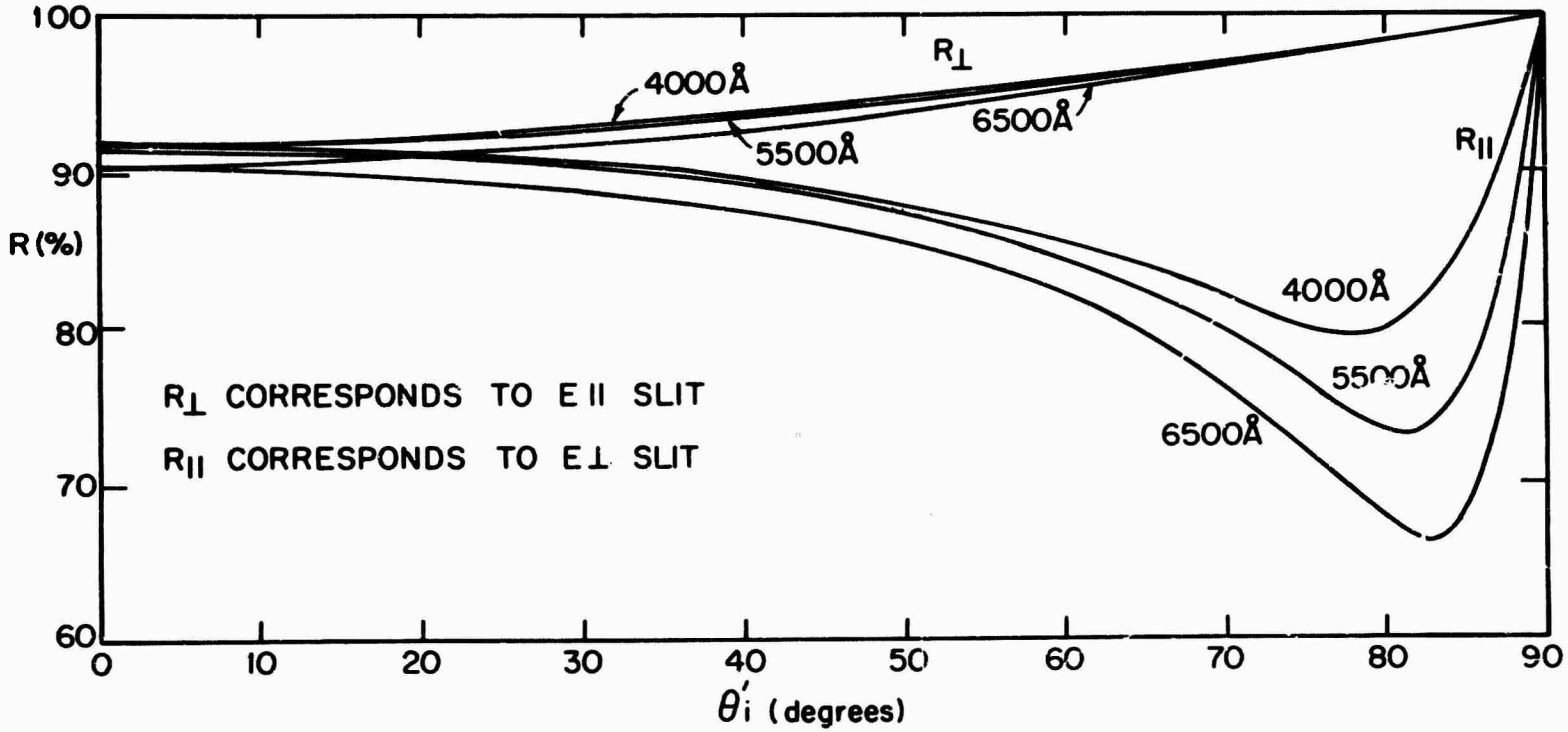

FIG. 3-6 ALUMINUM REFLECTIVITY, $R_\perp$ AND R_{II}, VERSUS ANGLE OF INCIDENCE ON AN INFINITE PLANE FOR TWO POLARIZATIONS AND THREE WAVE LENGTHS.

experimental observation that light polarized perpendicular to the slit shows the greater variation with wavelength and hence (via the grating sine law, Appendix III-A) with angle of incidence.

D. THE POLARIZATION DEPENDENCE OF DIFFRACTION BY A GRATING

The angular dependence of reflection from a plane, which differs for the two polarizations and which was discussed in the preceding section, should affect diffraction by a metallic reflection grating, for, as wavelength is changed, the grating is rotated thereby changing the angle of incidence. We feel that this mechanism accounts for the difference in $I_0(\lambda)$ for the two polarizations, although our attempts at a calculation, outlined here in 1., were largely unsuccessful. In 2. we discuss the evidence for this assertion.

1. Attempts at a Calculation

Exact solutions of the problem of diffraction by lossy surfaces are very complex [3-02, Chapter 11] even for simple geometries. One common simplification is the assumption of infinite conductivity, but since reflection from such a surface is total, this assumption is not productive in distinguishing between polarizations. Going to the other extreme, we tried computing diffraction from a lossless dielectric grating using an integral equation formulation of Maxwell's equations [3-02, Sec. 2.4]: the complicated geometry of the steplike diffracting surface prevented our realizing a solution in closed form.

Kirchhoff-Fraunhofer diffraction theory [3-02, Secs. 8.3 and 8.6.7] is an approximation which yields theoretical results in agreement with experiment provided the grating groove spacing (= d) is much greater than the wavelength. It would not be expected to give an accurate prediction of the behavior of our grating where d is comparable with λ. Nonetheless, we did apply the theory, suitably modified for reflection. The calculation exhibited no striking structure such as that observed experimentally, and gave no insight not already attained by our consideration of reflection from a plane.

2. Relevant Factors Bearing on the Hypothesis that the Change in the Angle of Incidence of Light on the Grating Determines the Abnormal $I_0(\lambda)$ Structure

Despite the failure of our calculations we feel that it is proper to hypothesize that the large variations observed experimentally in $I_0(\lambda)$ for light polarized perpendicular to the slit are due to changes in the angle of incidence of light on the grating and not just due to wavelength changes. The pertinent considerations are as follows:

(1) The Brewster angle effect discussed in Sec. III-C shows that there is a difference in the amount of light reflected from a plane for the two polarizations and that light polarized in the plane of incidence (which is also perpendicular to the slit if we view the grating groove as a plane) shows the more striking variation with angle of incidence.

(2) The failure of our attempts to compute the diffracted intensity as a function of the angle of incidence and of polarization

did not arise from an error in our hypothesis. Rather, it arose either from computational difficulties or from assumptions known to be inappropriate.

(3) The wavelength and the angle of incidence on the grating are functionally related in the monochromator via the grating sine law (Appendix III-A). Since a change in wavelength then involves a change in angle, we cannot say that all changes in $I_0(\lambda)$ are due solely to wavelength variation.

(4) Strong support for this hypothesis is illustrated in Figs. 3-7a and b, showing $I_0(\lambda)$ and $R(\lambda)$ curves for aluminum for polarization perpendicular to the slit and without beam constriction (to maximize abnormalities). In the overlapping wavelength range of 7600 to 9000Å there are curves for the 7500Å and 1.1μ blaze gratings. The R curve for the 1.1μ grating shows a small bump at 8200Å not found in the other. This bump is matched in the I_0 curves by a sharper depression at 8200Å in the 1.1μ grating than is found in the 7500Å one. In addition, the 1.1μ blaze shows the start of a bump at 8900Å not seen in the 7500Å blaze. The lack of structural similarity implies that the effects at 8200Å and 8900Å are not a consequence of wavelength changes. It is then reasonable to suppose that they are the consequence of changes in the angle of incidence since this is the other variable.

(5) The curve for $I_0(\lambda)$ for light polarized perpendicular to the slit changes wildly in regions where the n and k changes for

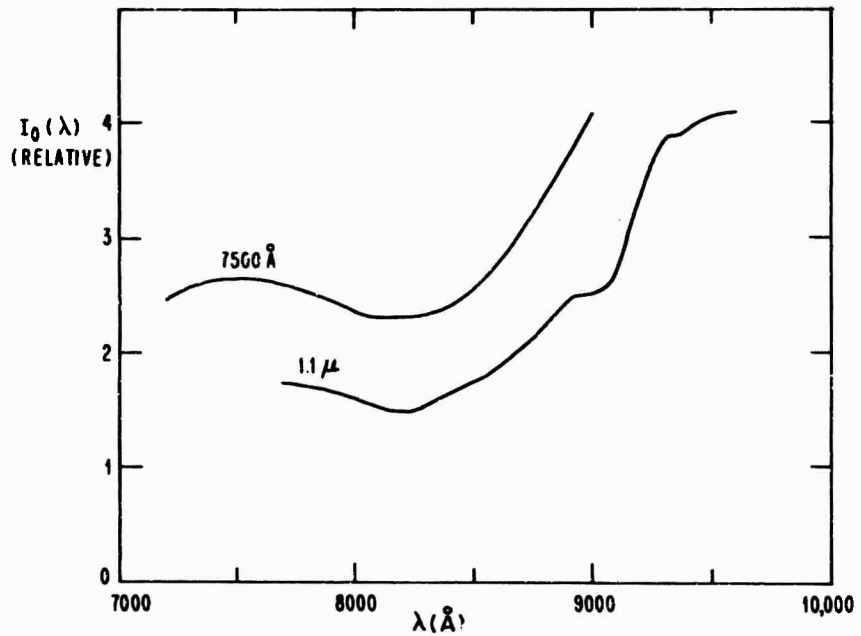

FIG. 3-7a A COMPARISON OF THE $I_0(\lambda)$ STRUCTURE FOR THE 7500Å AND 1.1μ BLAZE GRATINGS IN THE REGION OF THEIR OVERLAP. Light is polarized perpendicular to the slit.

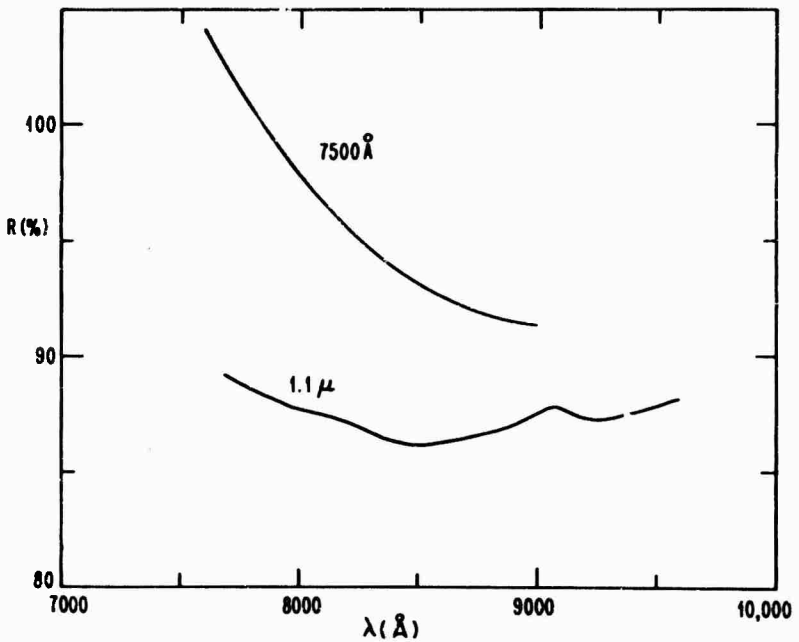

FIG. 3-7b A COMPARISON OF THE $R(\lambda)$ STRUCTURE OF AN ALUMINUM MIRROR FOR THE 7500Å AND 1.1μ BLAZE GRATINGS IN THE REGION OF THEIR OVERLAP. Light is polarized perpendicular to the slit and there is no beam constriction.

aluminum (due to wavelength changes) are monotonic. Hence some mechanism other than wavelength change must be operating.

(6) The effect of varying the angle of incidence onto a grating groove[†] on the relative intensities of diffracted light polarized in the two perpendicular directions has been isolated in an experimental study by R. Schmitt [3-04]. He has varied the blaze angle in a series of gratings while leaving the spacing unchanged, and finds that grating efficiency[‡] for the two polarizations is equal at the blaze wavelength. Below the blaze light polarized perpendicular to the plane of incidence has the greater efficiency, while the reverse holds above the blaze. Thus we can conclude that the angle of incidence on a grating groove is a significant parameter in determining the relative intensities of light of the two polarizations. We emphasize "relative" since it is already well-known from the scalar Kirchhoff-Fraunhofer theory (which ignores polarization) that over-all intensity at a given wavelength is determined by the blaze.

(7) The rest of our computation in Secs. III-E and F follows consistently from this hypothesis and exhibits false structure in reflectivity correlated with anomalous $I_0(\lambda)$ structure.

[†]This is known as θ_i' in our notation of Secs. III-C and E.

[‡]Efficiency at a given wavelength and order m is defined as the percentage of light at that wavelength diffracted into order m.

E. GEOMETRICAL FACTORS

We now discuss those geometrical features of the JACO monochromator which are necessary for an understanding of how the hypothesized variation with angle of incidence of $I_0(\lambda)$ can modify $R(\lambda)$. Figure 3-8 shows the over-all geometrical relationship of the entrance and exit slits, the grating, and the mirrors. Light from the entrance slit is collimated by mirror 1 and is directed to the grating. Diffracted light is collected at mirror 2 and focussed at the exit slit.

In 1. we show that light from the entrance slit is not perfectly collimated by mirror 1: in fact the deviation from collimation of a source point on the slit is proportional to its height relative to the center of the slit.† This deviation is employed in 2. to compute the range in the angle of incidence of light on a grating groove ($\delta\theta_i'$) for a given wavelength. The functional expression for this $\delta\theta_i'$ is given as well as the condition under which it is valid. Light loss is a second consequence of imperfect collimation. The computation of the magnitude of that loss is found in 3.

Before discussing each of these points in detail, we describe the coordinate systems. The x_s, y_s, z_s and x_m, y_m, z_m systems are located midway between the slits and mirrors respectively (Fig. 3-8).

---

†The deviation from collimation we are considering is that arising from the vertical extent of the entrance slit and not the much smaller deviation caused by the finite slit width. The latter results in the usual small spread in wavelength at the exit slit.

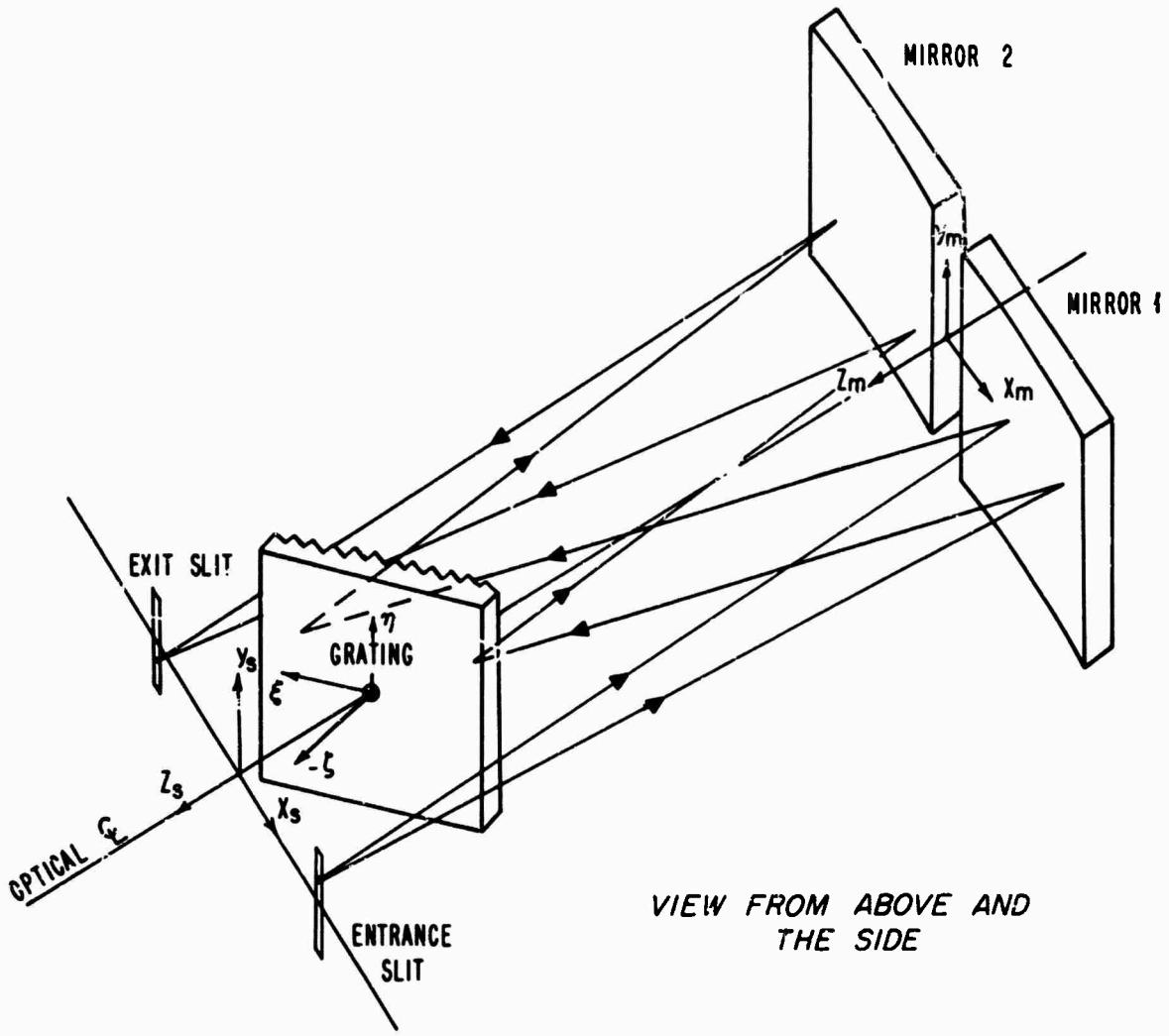

FIG. 3-8 A DRAWING OF THE SLITS, MIRRORS, AND GRATING IN THE JACO MONOCHROMATOR.

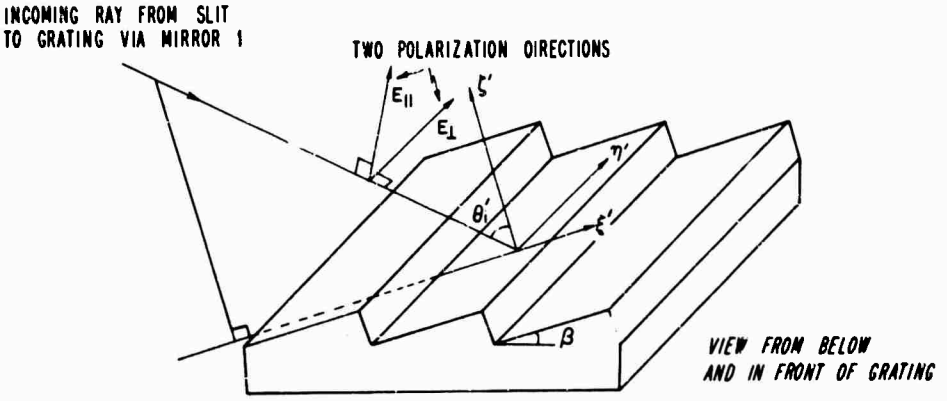

FIG. 3-9 LIGHT INCIDENT ON A GRATING GROOVE SURFACE SHOWING THE ξ', η', ζ' COORDINATE SYSTEM AND THE TWO POLARIZATION VECTORS.

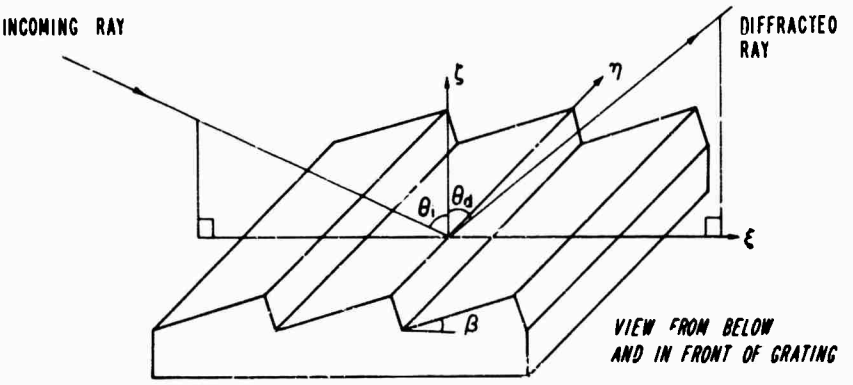

FIG. 3-10 LIGHT INCIDENT ON AND DIFFRACTED FROM THE GRATING SURFACE SHOWING THE ξ, η, ζ COORDINATE SYSTEM.

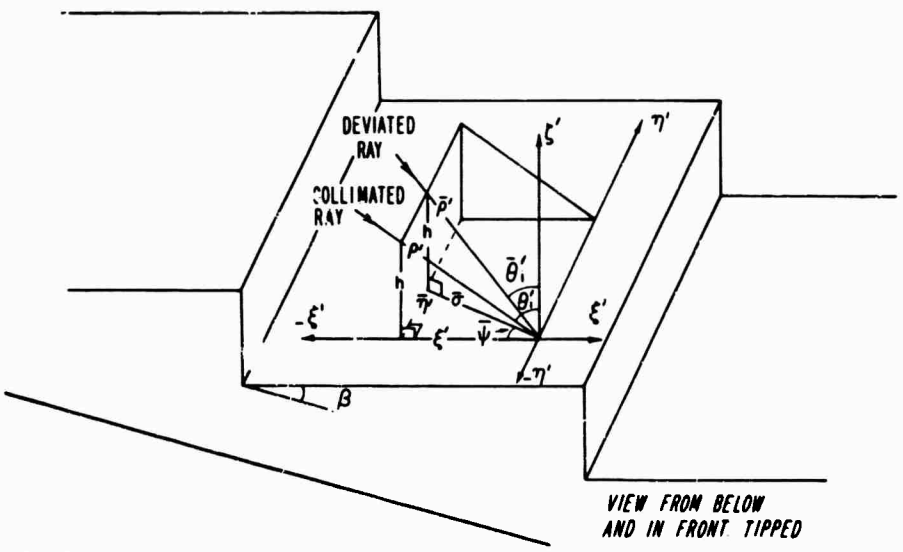

FIG. 3-11 GEOMETRY OF THE COLLIMATED AND DEVIATED RAYS INCIDENT ON A GRATING GROOVE TO PERMIT COMPUTATION OF $\delta\theta$

The unprimed coordinates, ξ, η, ζ, describe the grating as a whole. ζ is perpendicular to the grating surface, and ξ, η lie in the grating plane with η parallel to the grooves and pointing upward (Figs. 3-8 and 3-10). η is also parallel to the slits. The primed coordinates involve a rotation of β, the blaze angle, about η so that ξ' and η' lie in the plane of a groove and ζ' is perpendicular to a groove (Fig. 3-9). The actual value of β for our grating is computed in Appendix III-B since it is needed in the calculations.

1. Direction Cosines of the Collimated Light Beam

The collimated beam is the light reflected from mirror 1, and its cosines will be measured relative to the optical centerline. They are most simply computed by viewing the projection in the x_m, z_m plane. This is valid for the small angles involved. Referring to Fig. 3-12 we see that the direction cosines of interest are $\cos\mu$ and $-\sin\mu$. For small angles, $\cos\mu = 1$ and $\sin\mu = \mu$. Noting certain angular relations, we have

$$\mu = \frac{x_m^{(i)} - x_s^{(r)}}{R/2} \tag{3.6}$$

$$\tau = \frac{x_m^{(i)}/2}{R/2} \tag{3.7}$$

$$\tau + \nu = \frac{\ell}{R/2} \tag{3.8}$$

$$2\nu = \frac{\ell - x_s^{(r)}}{R/2} \; . \tag{3.9}$$

Combining these gives

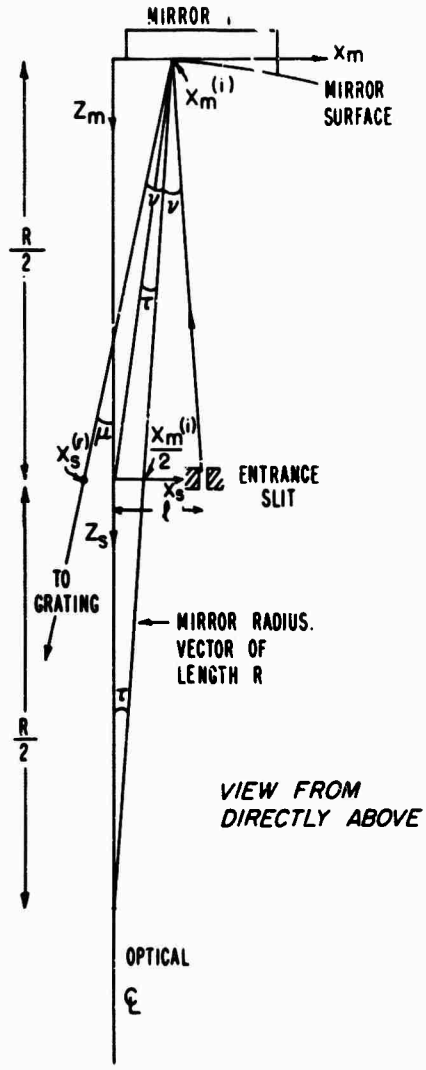

FIG. 3-12 GEOMETRY FOR COMPUTATION OF DIRECTION COSINES

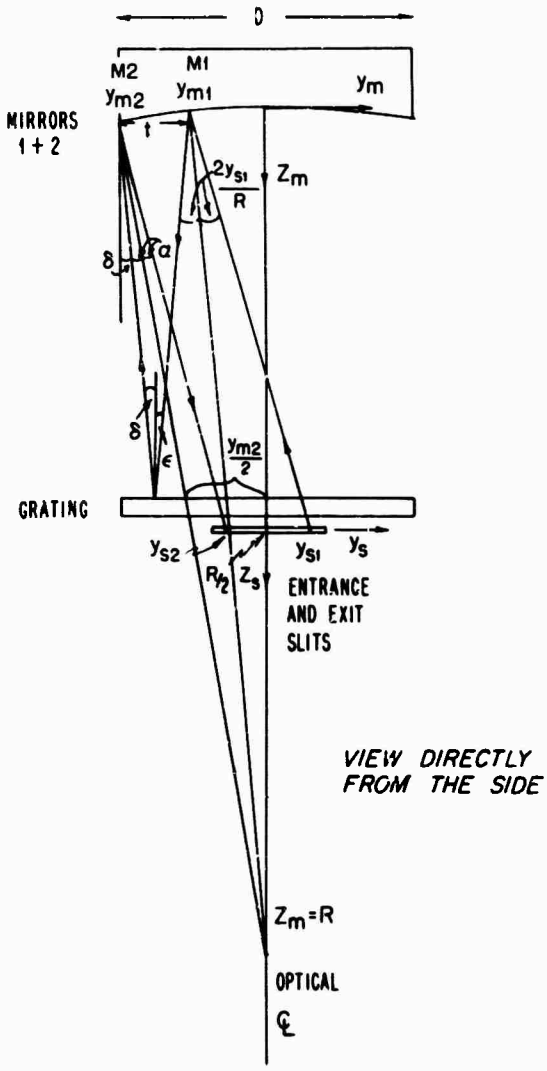

FIG. 3-13 GEOMETRY FOR COMPUTATION OF LIGHT LOSS AT MIRROR 2

$$\mu = \frac{2\ell}{R} \quad . \tag{3.10}$$

Thus in the x_m, z_m plane the direction cosines are

$$(-2\ell/R, 1) \quad . \tag{3.11}$$

Reflected light is collimated and is directed at an angle so that it will encounter the grating. Deviations from collimation in the x_m, z_m plane due to the finite slit width (usually of the order of 100μ) will be insignificant.

A similar calculation in the y_m, z_m plane would show that the three direction cosines are

$$(-2\ell/R, -2y_{s1}/R, 1) \tag{3.12}$$

where y_{s1} is distance along the entrance slit measured from its center.

$$0 \leq |y_{s1}| \leq s_m/2 \qquad \text{where } s_m = \text{maximum slit height.} \tag{3.13}$$

In conclusion, the beam reflected from mirror 1 and made up of all source points on the entrance slit is collimated in the horizontal (x, z) plane but not in the vertical (y, z) plane. The deviation from parallelism is determined by the position on the entrance slit, $|y_{s1}|$, of the source point.

2. Variation in Angle of Incidence on the Grating Groove

In Fig. 3-11 we have a view of light incident on a grating groove. The collimated ray is that from the center of the entrance slit and represents the family of rays we could expect if the beam were perfectly collimated by mirror 1. It is described by the "unbarred" system of coordinates. The deviated ray is a typical ray

from some point on the entrance slit, $y_{s1} > 0$. It is described by the "barred" coordinate system. Here we compute the difference between $\bar{\theta}'_i$ and θ'_i. The analysis is made relative to the grating groove surface (primed coordinates), rather than the over-all grating surface (unprimed coordinates), since it is the former surface from which light is actually diffracted.

Geometrically, Fig. 3-11 shows that

$$\bar{\sigma} = h \tan \bar{\theta}'_i \tag{3.14}$$

$$\xi' = \bar{\sigma} \cos \bar{\psi} \tag{3.15}$$

$$\xi' = h \tan \theta'_i \ . \tag{3.16}$$

Combining these gives

$$\tan \theta'_i = \tan \bar{\theta}'_i \cos \bar{\psi} \ . \tag{3.17}$$

The direction cosine, $-2y_{s1}/R$, is easily related to $\bar{\psi}$. $-2y_{s1}/R$ is measured relative to the optical centerline of the monochromator. When measured relative to the line $(-2\ell/R, 0, 1)$, which is the direction of the collimated ray in Fig. 3-11, the direction cosine is still $-2y_{s1}/R$ to first order in the angle since the angular change in direction between the centerline and the collimated beam is small. Analytically, this direction cosine is the projection of the deviated ray on the η' axis.

$$\left(\frac{2y_{s1}}{R}\right) = \frac{\bar{\eta}'}{\bar{\rho}'} \tag{3.18}$$

Geometrically

$$\frac{\bar{\eta}'}{\bar{\sigma}} = \sin \bar{\psi} \tag{3.19}$$

$$\frac{\bar{\sigma}}{\bar{\rho}'} = \sin \bar{\theta}'_i \ , \tag{3.20}$$

and combining these three

$$\left(\frac{2y_{s1}}{R}\right) = \sin\bar{\psi}\,\sin\bar{\theta}'_i \quad . \tag{3.21}$$

Squaring Eq. 3.17 permits eliminating $\bar{\psi}$.

$$\frac{\tan^2\theta'_i}{\tan^2\bar{\theta}'_i} = 1 - \sin^2\bar{\psi} = 1 - \left(\frac{2y_{s1}}{R}\right)^2 \frac{1}{\sin^2\bar{\theta}'_i} \tag{3.22}$$

$$\tan^2\theta'_i = \tan^2\bar{\theta}'_i - \left(\frac{2y_{s1}}{R}\right)^2 \frac{1}{\cos^2\bar{\theta}'_i} \tag{3.23}$$

$$(\tan\bar{\theta}'_i + \tan\theta'_i)(\tan\bar{\theta}'_i - \tan\theta'_i) = \left(\frac{2y_{s1}}{R}\right)^2 \frac{1}{\cos^2\bar{\theta}'_i} \tag{3.24}$$

Let $\delta\theta'_i = \bar{\theta}'_i - \theta'_i$. (3.25)

If θ'_i is large, Eq. 3.22 can be simplified, since $\bar{\theta}'_i \approx \theta'_i$:

$$2\tan\theta'_i(\tan\bar{\theta}'_i - \tan\theta'_i) = \left(\frac{2y_{s1}}{R}\right)^2 \frac{1}{\cos^2\theta'_i} \quad . \tag{3.26}$$

From Dwight Tables [3-05, 405.06]

$$\tan\bar{\theta}'_i - \tan\theta'_i = \frac{\sin(\bar{\theta}'_i - \theta'_i)}{\cos\bar{\theta}'_i\,\cos\theta'_i} \approx \frac{\delta\theta'_i}{\cos^2\theta'_i} \quad . \tag{3.27}$$

Then

$$2\tan\theta'_i\,\delta\theta'_i = \left(\frac{2y_{s1}}{R}\right)^2 \quad \text{or}$$

$$\delta\theta'_i = \frac{1}{2}\left(\frac{2y_{s1}}{R}\right)^2 \cot\theta'_i \quad . \tag{3.28}$$

This is the formula describing the deviation of the angle of incidence of light on a grating groove as the position of the source point on the entrance slit changes. It will be employed in calculations in the next section.

One important question is how small θ_i' can get before Eq. 3.28 for $\delta\theta_i'$ becomes invalid. For small θ_i', $\delta\theta_i'$ becomes

$$\delta\theta_i' = \frac{1}{2}\left(\frac{2y_{s1}}{R}\right)^2 \frac{1}{\theta_i'} \quad , \tag{3.29}$$

whereas the exact expression, Eq. 3.23, can be approximated by

$$(\tilde{\theta}_i')^2 - (\theta_i')^2 = \left(\frac{2y_{s1}}{R}\right)^2 \tag{3.30}$$

and solving for $\delta\theta_i'$ gives

$$\delta\theta_i' = -\theta_i' + \sqrt{\left(\frac{2y_{s1}}{R}\right)^2 + (\theta_i')^2} = -\theta_i' + \theta_i'\sqrt{1 + \left(\frac{2y_{s1}}{R}\right)^2 \Big/ (\theta_i')^2} \quad . \tag{3.31}$$

Expanding to second order gives

$$\begin{aligned}\delta\theta_i' &= -\theta_i' + \theta_i'\left[1 + \left(\frac{2y_{s1}}{R}\right)^2 \frac{1}{2(\theta_i')^2} - \left(\frac{2y_{s1}}{R}\right)^4 \frac{1}{8(\theta_i')^4} + \cdots\right] \\ &= \frac{1}{2}\left(\frac{2y_{s1}}{R}\right)^2 \frac{1}{\theta_i'} - \left(\frac{2y_{s1}}{R}\right)^4 \frac{1}{8(\theta_i')^3} + \cdots\end{aligned} \tag{3.32}$$

The first term is just the approximate expression for $\delta\theta_i'$ found in Eq. 3.29 so the second is a measure of the error we can expect in using Eq. 3.28. The fractional error is

$$\left(\frac{2y_{s1}}{R}\right)^2 \frac{1}{4(\theta_i')^2} \quad . \tag{3.33}$$

When we consider the maximum value of y_{s1}, (= 1 cm.), the direction cosine is $2 \times 1/100 = .02$ radians, so that if $\theta_i' = .06$ radians, the fractional error is only 3.2%.

3. Light Loss at the Second Mirror

We have seen one consequence of imperfect collimation: that the angle of incidence on the grating is variable. A second consequence is loss of light, which can be seen if the beam is traced from y_{s1} on the entrance slit through to the exit slit.

If y_{s1} is greater than zero, some light reflected from mirror 1 will fall off the lower edge of the grating, and some of the diffracted light will fall off the lower edge of mirror 2. It is the loss at mirror 2 which determines over-all loss. In Fig. 3-13 we project the light rays onto the y_m, z_m plane and note the following relationships, holding for small angles:

$$\alpha = \frac{\frac{y_{m2}}{2} - |y_{s2}|}{R/2} = \frac{\frac{y_{m2}}{2} + y_{s2}}{R/2} \tag{3.34}$$

$$\delta + \alpha = \frac{y_{m2} - y_{m2}/2}{R/2} \tag{3.35}$$

$$\delta + \epsilon = \frac{t}{R/2} \tag{3.36}$$

$$\delta + \frac{2y_{s1}}{R} = \frac{t}{R/2} \quad . \tag{3.37}$$

There is no simple reason to assume that δ and ϵ are equal. ϵ expresses the fact that the incoming beam is not incident in the ξ, ζ plane. The diffraction now becomes more complicated, but other geometrical factors cancel out its effect. The consequence is that

$$\delta = \epsilon \ . \tag{3.38}$$

The steps in the calculation are rather long and since the result is so simple, the calculation is not included here.

Combining $\delta = \epsilon$ with the prior four equations, we get

$$\epsilon = \frac{2y_{s1}}{R} \tag{3.39}$$

$$t = R\epsilon \tag{3.40}$$

$$y_{s1} = -y_{s2} \, . \tag{3.41}$$

The last expresses the simple fact that the image of a point on the entrance slit is oppositely placed relative to the center of the slit, compared to the source point.

t is a measure of the light lost. In fact

$$t/D = \text{the fraction of light lost.} \tag{3.42}$$

If $I(y_{s1})$ = the intensity of light at the entrance slit at y_{s1} and (3.43)

$I(y_{s2})$ = the intensity at the exit slit, then (3.44)

$$\frac{I(y_{s2})}{I(y_{s1})} = 1 - \frac{|t|}{D} = 1 - \frac{2|y_{s1}|}{D} \, . \tag{3.45}$$

Figure 3-14 is a plot of this relationship.

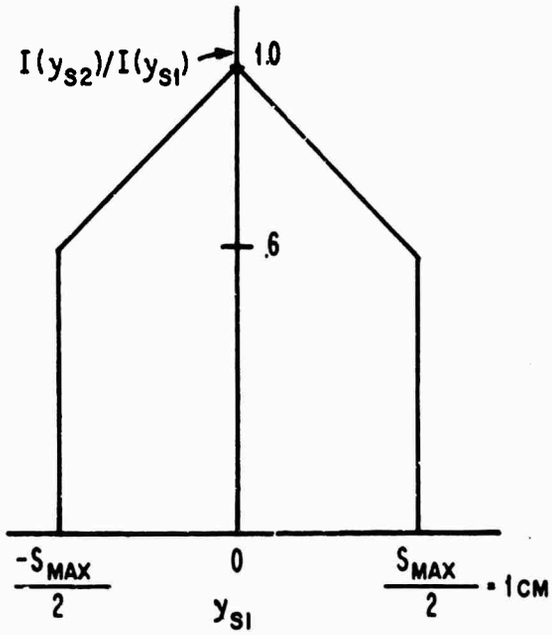

Fig. 3-14 LIGHT LOSS AT THE EXIT SLIT COMPARED TO THE ENTRANCE SLIT VERSUS POSITION ON THE ENTRANCE SLIT OF A SOURCE POINT.

F. A CALCULATION OF FALSE REFLECTIVITY STRUCTURE

In this section we compute a factor, $J(s_R, \lambda_m)/J(s_0, \lambda_m)$, which multiplies the true reflectivity of a sample, thereby representing false structure. Three factors are important in the calculation:

(1) The light intensity curve is hypothesized to vary only with the angle of incidence on the grating groove, θ_i'.

(2) We make use of the $\delta\theta_i'$ variation discussed in III-E.

(3) We add a new geometrical feature -- that different amounts of light are removed from the beams in the I_0 and I_R light paths. This can indeed occur at the beam splitter in our system. When this loss occurs, a false wavelength-dependent variation is imposed on any measurement.

The hypotheses which are necessary for the calculation are discussed in 1. In 2. we give the derivation of $J(s_R, \lambda_m)/J(s_0, \lambda_m)$ for light intensity of an arbitrary functional form, $f(\lambda)$, and in 3. we employ specific functions for $f(\lambda)$, permitting a graphic display of the false structure (Fig. 3-15). We discuss conclusions affecting system operation in 4.

1. Definitions and Hypotheses

Our starting point is a function, $f(\lambda)$, which we define as the total light intensity at a given polarization measured at the detector. By total light intensity we mean the integrated effect of the light leaving the entire exit slit. $f(\lambda)$ is distinguished from $I_0(\lambda)$ in two ways, where $I_0(\lambda)$ is the <u>experimentally</u> measured total light intensity at the detector:

(1) $f(\lambda)$ is a function used in our theoretical analysis. In 3. it is supposed to have certain simple functional forms which approximate but do not exactly reproduce $I_0(\lambda)$.

(2) We assume that any variation of $f(\lambda)$ with λ is due solely to changes in the angle of incidence on a grating groove, θ_i'. Then the seeming variation of $f(\lambda)$ with λ occurs only because of the functional relationship between λ and θ_i described by the grating sine law (Appendix III-A). That law is

$$\lambda = \lambda(\theta_i) = 2d \sin(\theta_i - \gamma) \cos\gamma \ , \tag{3.65}$$

and, since

$$\theta_i = \theta_i' + \beta \ , \tag{3.46}$$

$$\lambda = 2d \sin(\theta_i' + \beta - \gamma) \cos\gamma = \lambda(\theta_i') \ . \tag{3.47}$$

This assumption may seem extreme since $I_0(\lambda)$ changes do occur because of source, grating, mirror, and detector changes with λ; we make it to simplify the analysis and to discover how θ_i' variation alone can create false structure in $R(\lambda)$.

In Sec. III-D we discussed experimental and theoretical information which supported the hypothesis that some $I_0(\lambda)$ variation with λ was due to θ_i' variation. In this section we carry that hypothesis to the extreme and assume that the $f(\lambda)$ change is due entirely to θ_i' change.

$f(\lambda)$ is similar to $I_0(\lambda)$ in that it describes the integrated intensity at the detector of all the points along the exit slit. It is thus an operationally valid definition. The first part of

our calculation (in 2.) computes the variation of intensity along the exit slit for a given monochromator setting (wavelength) using $f(\lambda)$, the average intensity, as a starting point. (Since by hypothesis we ignore any changes in $f(\lambda)$ due to mirrors or the detector, $f(\lambda)$ at the exit slit is the same as $f(\lambda)$ at the detector.)

To do this we make use of the geometrical factors discussed in Sec. III-E -- $\delta\theta_i'$ (the range in the angle of incidence on a grating groove at a given monochromator setting) and the loss of light factor. We assume that the range in intensity values along the exit slit at a given monochromator setting and arising from $\delta\theta_i'$ is given by the same $f(\lambda(\theta_i'))$ we use to describe the change in intensity with changing monochromator setting. That is, we take some setting $\lambda = \lambda_m$, which implies $\theta_i' = \theta_{im}'$ in Eq. 3.65, the grating sine law. This law is valid for the "central" ray -- a ray that starts at the center of the entrance slit, strikes the center of the two mirrors and the grating, and leaves at the center of the exit slit. For deviated rays starting from a point away from the entrance slit center, θ_i' is increased by $\delta\theta_i'$, and we assume that the intensity of light at the exit slit is proportional to $f(\lambda(\theta_{im}' + \delta\theta_i'))$. f at point y_{s2} on the exit slit will be reduced by the loss of light factor, $I(y_{s2})$, in Eq. 3.45. Since $\delta\theta_i' = \delta\theta_i'(y_{s2})$ (from Eqs. 3.28 and 3.41), the intensity of light at point y_{s2} and at monochromator setting λ_m will be given by

$$j(y_{s2}, \lambda_m) = cI(y_{s2}) f\left(\lambda(\theta_{im}' + \delta\theta_i'(y_{s2}))\right) , \qquad (3.48)$$

where c is a constant of proportionality. Thus the $f(\lambda)$ curve, giving the variation in average intensity with monochromator setting, is used to derive the intensity as a function of position on the exit slit at a given monochromator setting. We note that since $f(\lambda(\theta'_{im}+\delta\theta'_i))$ is a function not only of θ'_{im} but also of position on the slit (through $\delta\theta'_i$), the relative intensity at a given exit slit position will vary with monochromator setting.

Finally, we define $J(s, \lambda_m)$ as the integral of $j(y_{s2}, \lambda_m)$ over the exit slit. s represents the unblocked limit for the slit height and will be different for the two light paths.

$$J(s, \lambda_m) = 2\int_0^{s/2} j(y_{s2}, \lambda_m)\, dy_{s2} \tag{3.49}$$

The maximum slit height is s_m (= 2 cm.). In a completely self-consistent approach $J(s_m, \lambda_m)$ should be identically equal to $f(\lambda_m)$. In our development they are only approximately equal because the intensity of the "central" ray at $\lambda = \lambda_m$ is not the average intensity since $\delta\theta'_i$ is not symmetric about θ'_{im}. Since our interest in this calculation is to demonstrate a probable source of false structure in $R(\lambda)$ and not to reproduce that structure in its every detail, we feel that this slight inconsistency is not important.

2. The General Calculation

Utilizing the material in 1. above, we can quickly compute the false structure factor, $J(s_R, \lambda_m)/J(s_0, \lambda_m)$, for an arbitrary $f(\lambda)$. Combining Eqs. 3.45, 3.48, 3.49, and 3.28, we have

$$J(s,\lambda_m) = 2c \int_0^{s/2} I(y_{s1}) \left(1 - \frac{2|y_{s2}|}{D}\right) f\left(\lambda\left(\theta'_{im} + \frac{2y_{s2}^2}{R^2} \cot\theta'_{im}\right)\right) dy_{s2} \quad . \quad (3.50)$$

Computing the integral $J(s, \lambda_m)$ for both reference and sample channels, we can get the measured reflectivity, R_m:

$$R_m = R_t \frac{J(s_R, \lambda_m)}{J(s_0, \lambda_m)} \quad . \quad (3.51)$$

R_t is the true reflectivity and $J(s_R, \lambda_m)/J(s_0, \lambda_m)$ represents the structural distortion. Note that if the light beam is blocked before reaching the beam splitter so that $s_R = s_0$, there is no distortion from this source, and

$$R_m = R_t \quad . \quad (3.52)$$

This analysis presupposes that the detector is completely uniform over its surface.

3. Specific Functional Forms

In the computations the structure plotted in Fig. 3-15 is hypothesized for $f(\lambda)$. It has the following functional forms:

$$f_I = C_{II} = \text{constant} \qquad \lambda \leq 2700\text{Å} \quad (3.53a)$$

$$f_{II} = C_{II} + B_{II} + B_{II} \cos\left(\frac{(\lambda - \lambda_{II})\pi}{\Delta\lambda_{II}}\right) \qquad 2700 \leq \lambda \leq 3500\text{Å} \quad (3.53b)$$

$$\lambda_{II} = 3100\text{Å}$$

$$\Delta\lambda_{II} = 400\text{Å}$$

$$B_{II} = 2C_{II}$$

$$f_{III} = C_{III} + \frac{\lambda - \lambda_{III}}{\Delta\lambda_{III}} A_{III} \qquad 3500 \leq \lambda \leq 4500\text{Å} \quad (3.53c)$$

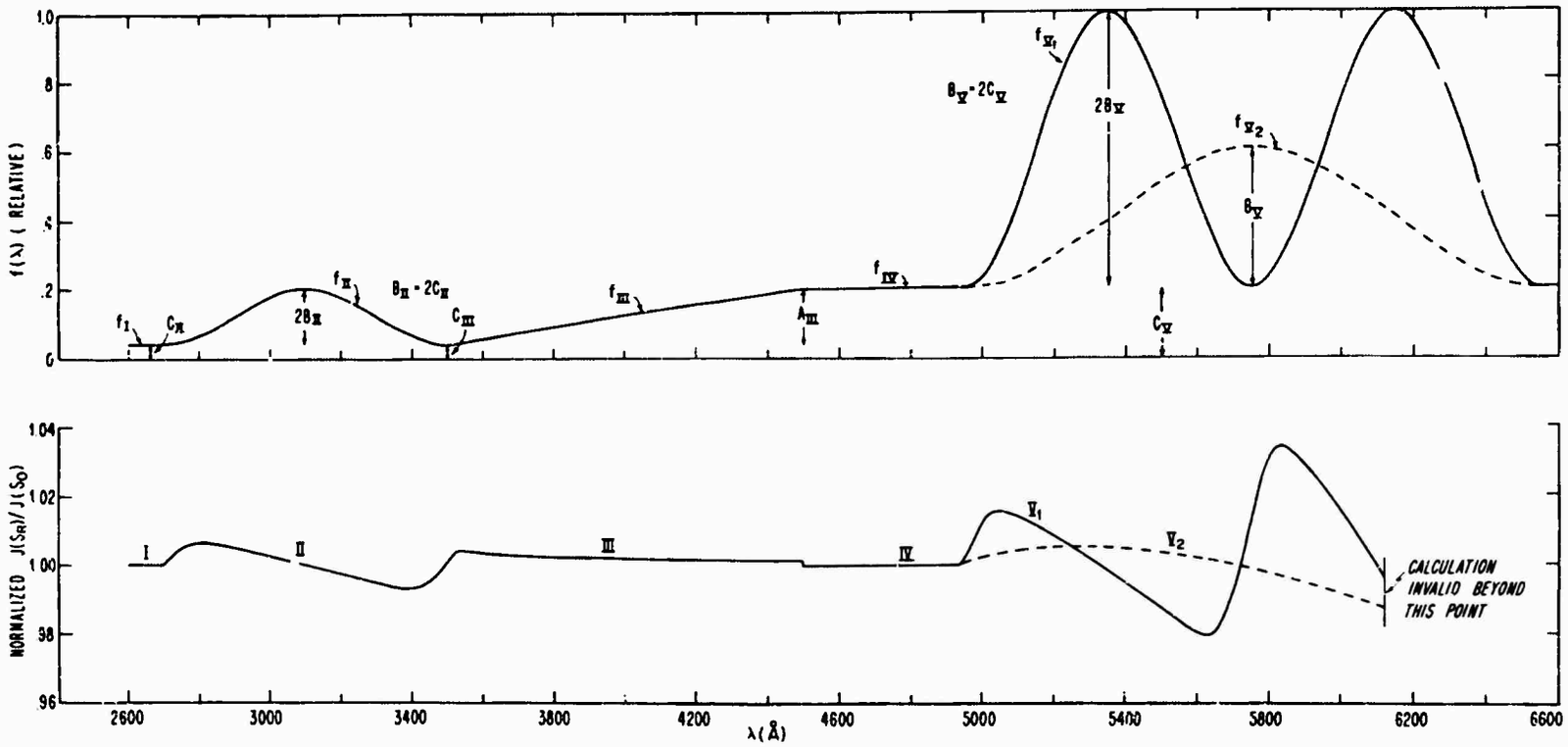

FIG 3-15 THE EFFECT OF STRUCTURE IN $I_O(\lambda)$(OR $f(\lambda)$) IN CREATING FALSE STRUCTURE IN THE REFLECTIVITY. This plot is a result of a calculation. $J(S_R)/J(S_O)$ is a factor multiplying the true sample reflectivity, thereby giving false structure when it deviates from 1.

$$\lambda_{III} = 3500\text{Å}$$

$$\Delta\lambda_{III} = 1000\text{Å}$$

$$A_{III} = 4C_{III}\ , \quad C_{III} = C_{II}$$

$$f_{IV} = A_{III} = \text{constant} \qquad 4500 \leq \lambda \leq 4950\text{Å} \qquad (3.53d)$$

$$f_{V_1} = C_V + B_V + B_V \cos\left(\frac{(\lambda - \lambda_V)}{\Delta\lambda_V}\pi\right) \qquad 4950 \leq \lambda \leq 6550\text{Å} \qquad (3.53e)$$

$$\lambda_V = 5350\text{Å}$$

$$\Delta\lambda_V = 400\text{Å}$$

$$B_V = 2C_V = A_{III}$$

$$f_{V_2} = C_V + \frac{B_V}{2} + \frac{B_V}{2} \cos\left(\frac{(\lambda - (\lambda_V + \Delta\lambda_V))\pi}{2\Delta\lambda_V}\right) \quad 4950 \leq \lambda \leq 6550\text{Å} \qquad (3.53f)$$

f_{V_1}, the double sine wave, approximates the structure seen in Fig. 3-4 made with the S-1 phototube for polarization perpendicular to the slit. Although not all the structure is due to angular dependence, since there is a known fall-off starting around 5300Å, most of it is so dependent.

f_{V_2} is a shallower and broader structure than f_{V_1} so that the importance of sharpness in f structure can be seen.

f_{IV} is flat as is f_I.

f_{III} is a constant slope.

f_{II} has the same relative size and same wavelength spread as f_{V_1}, but it is much farther from the blaze angle. (Refer to Eqs. 3.28 and 3.46 which show that $\delta\theta_i'$ depends on $\cot(\theta_i - \beta)$). The effect of f_{II} on ratio is to be compared with f_{V_1}.

The values for s_R and s_0, the effective slit heights for the I_R and I_0 light paths, were set at 2 cm. and 1.75 cm. respectively. These values were computed from the experimental deviation in R for aluminum from the expected value of 90% at 6500Å when the light was polarized parallel to the slit. The choice for s_R and s_0 is somewhat arbitrary since the beam splitter is located well away from the slit focus. Consequently, the beam splitter blocks light somewhat differently than it would were it at the focus.

$J(s, \lambda_m)$ is computed in the Appendix III-C for each of the f functions listed above. $I(y_{s1})$, the illumination of the entrance slit, is assumed to be a constant to simplify the calculation. The results are as follows:

$$J(s, \lambda_m)_I = cI(y_{s1})C_{II}\left[s - \frac{s^2}{2D}\right] \tag{3.74}$$

$$J(s, \lambda_m)_{IV} = cI(y_{s1})C_{II}\left[s - \frac{s^2}{2D}\right] \tag{3.75}$$

$$J(s, \lambda_m)_{III} = 2cI(y_{s1}) \times$$

$$\left[E(\theta_{im})\frac{s}{2} + \frac{A_{III}h(\theta_{im})}{\Delta\lambda_{III}}\frac{s^3}{24} - \frac{E(\theta_{im})}{D}\frac{s^2}{4} - \frac{A_{III}}{\Delta\lambda_{III}}\frac{h(\theta_{im})}{D}\frac{s^4}{32}\right] \tag{3.77}$$

where

$$E(\theta_{im}) = C_{III} + \frac{\lambda_m - \lambda_{III}}{\Delta\lambda_{III}}A_{III}$$

$$h(\theta_{im}) = \frac{4d\cos\gamma}{R^2}\cos(\theta_{im} - \gamma)\cot(\theta_{im} - \beta)$$

$$J(s, \lambda_m)_{V_1} = 2cI(y_{s1})B_V \times$$

$$\left[\left(1 + \frac{C_V}{B_V}\right)\frac{s}{2} + \sqrt{\frac{\Delta\lambda_V}{2h(\theta_{im})}}\left\{\cos\left(\frac{\pi(\lambda_m - \lambda_V)}{\Delta\lambda_V}\right)C\left[\sqrt{\frac{h(\theta_{im})}{2\Delta\lambda_V}}\,s\right] - \sin\left(\frac{\pi(\lambda_m - \lambda_V)}{\Delta\lambda_V}\right)S\left[\sqrt{\frac{h(\theta_{im})}{2\Delta\lambda_V}}\,s\right]\right\}\right.$$

$$\left. - \left(1 + \frac{C_V}{B_V}\right)\frac{s^2}{4D} - \frac{\Delta\lambda_V}{\pi D h(\theta_{im})}\left\{\sin\left(\pi\frac{(\lambda_m - \lambda_V) + h(\theta_{im})\frac{s^2}{4}}{\Delta\lambda_V}\right) - \sin\left(\frac{\pi(\lambda_m - \lambda_V)}{\Delta\lambda_V}\right)\right\}\right] \tag{3.84}$$

where C and S are the Fresnel cosine and sine functions. $J(s, \lambda_m)_{V_2}$ and $J(s, \lambda_m)_{II}$ are the same except for some simple substitutions outlined in Appendix III-C.

The false structure was then determined by using these functions to compute $J(s_R, \lambda_m)/J(s_O, \lambda_m)$. When this ratio is computed for f_I and f_{IV}, the constants, the result is a constant number less than one. The values of $J(s_R, \lambda_m)/J(s_O, \lambda_m)$ have been normalized by dividing by this number and are plotted in Fig. 3-15. Any deviation of the plotted value from 1 represents false structure.

4. Conclusions Based on the Calculation and on the Experimental Measurements

The calculation, in providing a mechanism for the creation of false reflectivity structure, corroborates and extends the conclusions drawn from the system measurements alone.

The strong structure in f_{V_1} is matched by the structure in the ratio, the ratio structure worsening as one nears the wavelength corresponding to β, the blaze angle. Note in Fig. 3-3 that the strongest experimentally observed structure is at the high wavelength end (5500-6700Å) near the blaze. It is interesting to note that the computed structure is asymmetrical, being compressed at the lower wavelength and elongated at the higher. The experimental curves in Fig. 3-3 show the same asymmetry.

It is instructive to compare the ratio structure due to f_{V_1} with that due to both f_{V_2} and f_{II}. The first shows that more slowly changing structure in I_O (e.g., for light polarized parallel to the slit)

has less effect on the ratio while the second shows the diminished effect at wavelengths further from the blaze accounting for the comparatively weak ratio structure seen in Fig. 3-3 at 3500Å and 3900Å.

When I_0 is flat as in f_I and f_{IV}, there is no ratio structure. When I_0 has a constant slope as in f_{III}, the ratio is changed by a nearly constant amount from the proper value. This is less serious than continual change in the ratio. A sharp transition in I_0, such as that between f_{IV} and f_{III}, results in a quick change in R. There is an experimental equivalent. The regions of vertical slope in the I_0 curve at 5230 and 6050Å (Fig. 3-2) result in discontinuous changes in the ratio (Fig. 3-3).

In consequence, I_0 curves should be chosen so they are flat or slowly changing. If they do change quickly, one should feel sure that the change is due to wavelength changes (e.g., source or detector sensitivity) and not θ_i changes. An example of this last is the I_0 behavior in the region below 3000Å.

These arguments, as well as experimental evidence, all point to using light polarized parallel to the monochromator exit slit. Further, the beam should be carefully constricted so no light is lost at the beam splitter. Then $s_R = s_0$ and $J(s_R, \lambda_m)/J(s_0, \lambda_m) \equiv 1$, implying that there will be no false structure.

This last statement presupposes that the photomultiplier photocathode sensitivity is constant over its surface, for the calculation has not taken account of such variation. Thus I_0 and I_R images must be carefully superposed as pointed out in Sec. III-B. Please refer to that section for other precautions.

G. WAVELENGTH RESOLUTION DISCREPANCIES

Our discussion in Sec. III-F-1 implicitly suggests that one could expect a variation in wavelength along the exit slit. To see this, consider the following:

If we substitute $\theta'_{im} + \delta\theta'_i$ for θ'_i in Eq. 3.65, we get

$$\lambda = 2d \sin(\theta'_{im} + \delta\theta'_i + \beta - \gamma) \cos\gamma$$

$$= 2d \cos\gamma[\sin(\theta'_{im} + \beta - \gamma) \cos\delta\theta'_i + \cos(\theta'_{im} + \beta - \gamma)\sin\delta\theta'_i] \quad . \qquad (3.54)$$

Since $\delta\theta'_i$ is small,

$$\lambda = 2d \cos\gamma[\sin(\theta'_{im} + \beta - \gamma) + \cos(\theta'_{im} + \beta - \gamma)\delta\theta'_i]$$

$$\equiv \lambda_m + \delta\lambda \quad . \qquad (3.55)$$

Thus there is a $\delta\lambda$ which is determined by $\delta\theta'_i$. The functional relationship of $\delta\theta'_i$ and y_{s2} then seems to imply a range of wavelengths along the exit slit. Ebert design monochromators, such as the JACO 82-000, do exhibit such a variation when one uses straight entrance and exit slits [3-06] as we do. The variation arises from two factors, astigmatism and the skew incidence on the grating, and is generally less than 1Å for typical Ebert design monochromators used in the UV-visible range [3-06]. We face a serious difficulty in that the $\delta\lambda$ we compute from Eq. 3.55 is in the range of 10 to 100Å, depending on θ'_i. This $\delta\lambda$ implies a significant loss in resolution which is not in fact observed. We resolve the discrepancy in this section.

In computing the factor J(s), we determine the range in θ'_i values which can occur as we move along the entrance slit. The $\delta\lambda$ which is functionally determined by this $\delta\theta'_i$ just tells us how much of the

$f(\lambda(\theta_i'))$ curve we sample as our source point moves along the entrance slit, for we recall our hypothesis that the $f(\lambda)$ variation is due entirely to θ_i' and not to λ changes.

In contrast, if we wish to compute $\delta\lambda$ to determine wavelength resolution loss, we must compute two $\delta\lambda$ terms for deviated rays. One is due to changes in θ_i[†], and the other is due to changes in θ_d, the angle of diffracted light. It turns out that the effect of θ_d nearly cancels that due to θ_i. An abbreviated calculation follows:

From Appendix III-*A*, Eqs. 3.60 and 3.62 give for the case m = -1

$$\lambda = d(\sin\theta_d + \sin\theta_i) ,$$

and, taking its derivative, we get

$$\delta\lambda = d(\cos\theta_d\delta\theta_d + \cos\theta_i\delta\theta_i) . \tag{3.56}$$

$\delta\theta_i$ is computed in the unprimed coordinate system in a fashion exactly analogous to the way we computed $\delta\theta_i'$ in the primed system. From Eq. 3.28 we get

$$\delta\theta_i = \frac{2y_{s1}^2}{R^2}\cot\theta_i . \tag{3.57}$$

Similarly,

$$\delta\theta_d = -\frac{2y_{s2}^2}{R^2}\cot\theta_d ^{\ddagger}. \tag{3.58}$$

[†]We use θ_i (the angle of incidence relative to the grating surface) rather than θ_i' in computing the direction in which light is diffracted. The blaze angle, β ($\theta_i' = \theta_i - \beta$), of a groove determines intensity at a given wavelength, but not direction.

[‡]The grating sine law, Eq. 3.65, has been computed using the particular geometry of Fig. 3-16. With that geometry an increase in the angle of diffraction corresponds to a decrease in θ_d. Therefore, we have a minus sign for $\delta\theta_d$ in Eq. 3.58.

One characteristic of the grating diffraction is that $y_{s1} = -y_{s2}$ (Eq. 3.41) so that

$$\delta\lambda = \frac{4y_{s1}^2}{R^2}\left[\frac{\cos^2\theta_i}{\sin\theta_i} - \frac{\cos^2\theta_d}{\sin\theta_d}\right] . \qquad (3.59)$$

Note that the two terms subtract. Over much of the θ_i range of our monochromator the computed $\delta\lambda$ is 1 to 2Å except at low θ_i where the approximations used to compute $\delta\theta_i$ and $\delta\theta_d$ break down.

Thus the $\delta\lambda$ given in this resolution study is much less than the $\delta\lambda$ used in the structure calculation, yet both arise out of the same analysis. The fact that the $\delta\lambda$ we just calculated is still greater than that implied by system resolution is probably due to our numerous first order approximations. A more detailed calculation with higher order terms might remove the discrepancy.

A more involved calculation might also disclose that other wavelength dependent variations in path direction affect the light distribution at the exit slit. For instance, Fastie [3-06] discusses a loss in resolution arising from the S-shaped wave front created in the Ebert system and incident on the grating.

Since there is wavelength range along the straight slits in an Ebert monochromator, one might wonder if the observed false structure in reflectivity is due solely to that (in conjunction with sharp changes in $I_0(\lambda)$ with λ) and not to the θ_i' variation we have hypothesized. We feel that false structure could arise from this source, but it would be far smaller than that observed. After all, our calculation involved far larger $\delta\lambda$ changes and still did not reproduce structure as large as that observed.

H. FALSE EFFECTS CREATED BY OPTICALLY ACTIVE ELEMENTS

We describe now another form of reflectivity structure distortion which arises when the I_0 and I_R beams pass through elements of different optical activity. To understand how this occurs, let us suppose that the I_R path has an optically active component while the I_0 path has none. The light is assumed to be polarized parallel to the slit. The active element rotates the polarization in a wavelength dependent manner. The light is then incident on aluminum mirrors at about 45° incidence (mirrors 7, 10, 11, and the beam splitter). Referring to Fig. 3-6, we see that the light reflection of the I_0 channel is governed by the $R_\perp$ curves, whereas the light reflection of the I_R channel will be determined by a linear combination of $R_\perp$ and $R_\parallel$, dependent on the amount of polarization rotation.† As we change wavelength, the net R from all the mirrors varies due to changes both in the aluminum reflectivity and in the optical rotation. Thus, in Eq. 2.7, which functionally describes system design philosophy, R_7, R_{10}, R_{11}, and $R_{B.S.}$ will be unequal in numerator and denominator, and consequently their quotient will be wavelength dependent. Distortion or even false structure can ensue.

A dramatic example was provided by a crystal quartz window in a cryostat. The quartz is a very strong rotator. The grey tin peak at 3380Å was shifted by as much as 50Å and its magnitude changed by 11%

†$R = R_\parallel \cos^2\alpha_i + R_\perp \sin^2\alpha_i$ where α_i is the angle the E vector makes with the plane of incidence [3-02, Sec. 1.5, Eq. 32].

as the window was rotated. The effect disappeared when a fused quartz window was used.

If one's experimental sample is active, our optical system cannot be used for reflectivity measurements without corrections or unless compensation can be made.

APPENDIX III-A

THE GRATING SINE LAW

The following equation is the well-known expression of the condition for maxima in a diffraction pattern and describes the angular spreading of wavelengths of various orders (= m) by a grating of spacing d.

$$m\lambda = pd \tag{3.60}$$

It can be rendered in a form which describes the angular dependence of wavelength for the JACO monochromator. Figure 3-16 describes the geometry for a "central" ray, where 2γ is the angle between the centers of the mirrors 1 and 2 in the monochromator. These are the mirrors intermediate between the grating and the entrance and exit slits.

$p = \ell - \ell_o$ and is measured relative to the ξ axis. (3.61)

$$p = -\sin\theta_d - \sin\theta_i \ . \tag{3.62}$$

$\theta_i = \theta_c + 2\gamma$, from Fig. 3-16. (3.63)

Using Dwight Tables [3-05, 401.08]

$$p = -2 \sin(\theta_i - \gamma) \cos\gamma \ . \tag{3.64}$$

With the geometry shown in Fig. 3-16 m = -1 rather than 1 for the first order light. The grating equation becomes

$\lambda = 2d \sin(\theta_i - \gamma) \cos\gamma$ for first order light, and (3.65)

$\lambda = \frac{2d}{-m} \sin(\theta_i - \gamma) \cos\gamma$ for higher orders. (3.66)

This is the so-called sine law for gratings.

In our geometry $\gamma = .06$. (3.67)

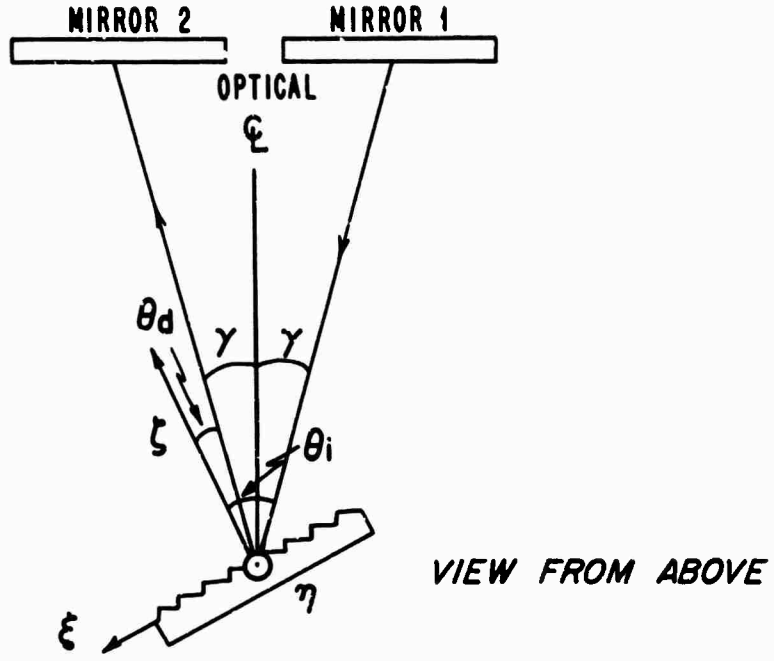

FIG. 3-16 GEOMETRY FOR COMPUTING GRATING SINE LAW.

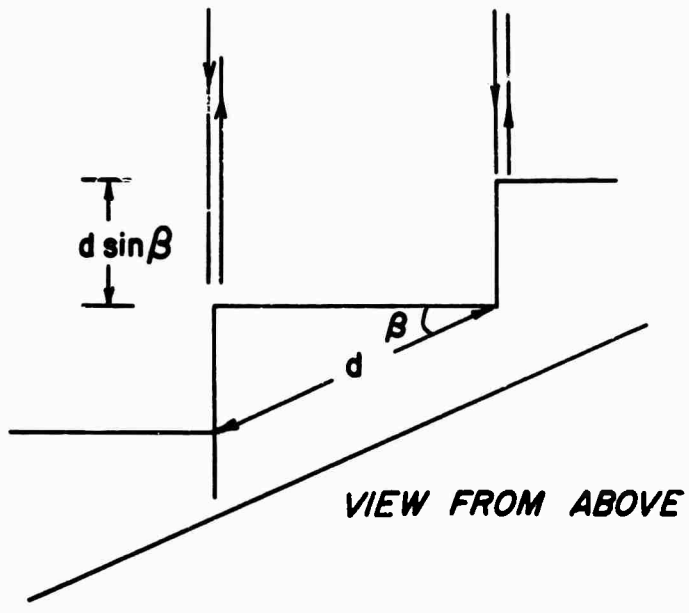

FIG. 3-17 GEOMETRY FOR COMPUTING GRATING BLAZE ANGLE, β.

APPENDIX III-B

THE GRATING BLAZE ANGLE

The grating regularly employed in the monochromator for the visible and UV range is described as blazed for 7500Å by the manufacturer, Jarrell Ash.† The grating is operated at its blaze wavelength when the diffracted pattern from the grating is in the direction of reflection from the groove face. The reflected direction changes as one changes the angle of incidence on the groove; the blaze wavelength will vary as well. To describe the blaze in a unique way, the light is considered to be normally incident on the groove face. Using the geometry in Fig. 3-17, we can then determine the blaze angle, β.

$$2d \sin\beta = \text{the blaze wavelength} = 7500\text{Å} \tag{3.68}$$

$$d = 8470\text{Å} \tag{3.69}$$

$$\sin\beta = .4425, \qquad \beta = .4586 \tag{3.70a,b}$$

β is nearly .46. This simpler value will be used in the computations. In the monochromator, $\lambda_{Blaze} = 7500\text{Å}$ corresponds to an angle of incidence $\theta_i = .52$ radians.

---

†This value has changed as the accuracy with which the blaze is measured has improved.

APPENDIX III-C

THE CALCULATIONS OF $J(s, \lambda_m)$ FOR VARIOUS f FUNCTIONS

The quantities which are computed in this appendix are defined and discussed in Secs. III-F-1, 2, and 3. Equation 3.50 gives the general expression for $J(s, \lambda_m)$.

$$J(s,\lambda_m) = 2c\ I(y_{s1}) \int_0^{s/2} \left(1 - \frac{2y_{s2}}{D}\right) f\left(\lambda\left(\theta'_{im} + \frac{2y_{s2}^2}{R^2}\cot\theta'_{im}\right)\right) dy_{s2} \tag{3.50}$$

From Eq. 3.55 we see that f can be written as $f(\lambda_m + \delta\lambda)$ where

$$\delta\lambda = 2d\cos\gamma\cos(\theta'_{im} + \beta - \gamma)\frac{2y_{s2}^2}{R^2}\cot\theta'_{im} \tag{3.71}$$

$$= 2d\cos\gamma\cos(\theta_{im} - \gamma)\frac{2y_{s2}^2}{R^2}\cot(\theta_{im} - \beta) \tag{3.72}$$

$$\equiv h(\theta_{im})y_{s2}^2 . \tag{3.73}$$

We can now turn to the evaluation of $J(\ ,\ \lambda_m)$ for the different functional forms of $f(\lambda)$ listed in (1) through (3) below:

(1) f_I and f_{IV}, constants

$$f_I(\lambda) = C_{II} = \text{constant} \tag{3.53a}$$

$$J(s,\lambda_m)_I = 2c\ I(y_{s1})C_{II}\int_0^{s/2}\left(1 - \frac{2y_{s2}}{D}\right)dy_{s2} = 2C\ I(y_{s1})C_{II}\left[\frac{s}{2} - \frac{s^2}{4D}\right]$$

$$= c\ I(y_{s1})\ C_{II}\left[s - \frac{s^2}{2D}\right] \tag{3.74}$$

$$J(s,\lambda_m)_{IV} = c\ \ I(y_{s1})A_{III}\left[s - \frac{s^2}{2D}\right] \tag{3.75}$$

(2) f_{III}, the ramp

$$\lambda \equiv \lambda_m + \delta\lambda \tag{3.55}$$

where λ_m is the nominal measured wavelength.

$$f_{III} = C_{III} + \frac{\lambda - \lambda_{III}}{\Delta\lambda_{III}} A_{III} = C_{III} + \frac{\lambda_m - \lambda_{III}}{\Delta\lambda_{III}} A_{III} + \frac{A_{III}\,\delta\lambda}{\Delta\lambda_{III}} \tag{3.53c}$$

$$\equiv E(\theta_{im}) + \frac{A_{III}}{\Delta\lambda_{III}} h(\theta_{im}) y_{s2}^2$$

$$E(\theta_{im}) = C_{III} + \frac{\lambda_m - \lambda_{III}}{\Delta\lambda_{III}} A_{III} \tag{3.76}$$

$$J(s,\lambda_m)_{III} = 2c\, I(y_{s1}) \int_0^{s/2} \left(1 - \frac{2y_{s2}}{D}\right)\left(E(\theta_{im}) + \frac{A_{III}}{\Delta\lambda_{III}} h(\theta_{im}) y_{s2}^2\right) dy_{s2}$$

$$= 2c\, I(y_{s1})\left[E(\theta_{im})\frac{s}{2} + \frac{A_{III} h(\theta_{im})}{\Delta\lambda_{III}} \frac{s^3}{24} - \frac{E(\theta_{im})}{D}\frac{s^2}{4} - \frac{A_{III}}{\Delta\lambda_{III}} \frac{h(\theta_{im})}{D} \frac{s^4}{32}\right] \tag{3.77}$$

(3) f_{II}, f_{V1}, f_{V2}, the sine waves.

$$f_{V_1} = C_V + B_V + B_V \cos\left(\frac{(\lambda - \lambda_V)}{\Delta\lambda_V}\,\pi\right) = C_V + B_V + B_V \cos\left(\pi \frac{(\lambda_m - \lambda_V) + \delta\lambda}{\Delta\lambda_V}\right) \tag{3.53e}$$

$$= (C_V + B_V) + B_V \cos\left(\pi \frac{(\lambda_m - \lambda_V) + h(\theta_{im}) y_{s2}^2}{\Delta\lambda_V}\right)$$

$$J(s)_{V_1} = 2c\, I(y_{s1}) \int_0^{s/2} \left[(C_V + B_V) + B_V \cos\left(\pi \frac{(\lambda_m - \lambda_V) + h(\theta_{im}) y_{s2}^2}{\Delta\lambda_V}\right)\right] dy_{s2}$$

$$+ 2c\, I(y_{s1}) \int_0^{s/2} -\frac{2y_{s2}}{D}(C_V + B_V) - \frac{2y_{s2}}{D} B_V \cos\left(\pi \frac{(\lambda_m - \lambda_V) + h(\theta_{im}) y_{s2}^2}{\Delta\lambda_V}\right) dy_{s2} \tag{3.78}$$

$$= 2c\, I(y_{s1})[I_1 + I_2 + I_3 + I_4] \tag{3.79}$$

I_1 and I_3 are very straightforward.

$$I_4 = -\frac{B_V}{D} \frac{\Delta\lambda_V}{\pi h(\theta_{im})} \sin\left(\pi \frac{(\lambda_m - \lambda_V) + h(\theta_{im}) y_{s2}^2}{\Delta\lambda_V}\right)\Bigg|_0^{s/2}$$

$$= -\frac{B_V}{D} \frac{\lambda_V}{\pi h(\theta_{im})} \left[\sin\left(\pi \frac{(\lambda_m - \lambda_V) + h(\theta_{im})\frac{s^2}{4}}{\Delta\lambda_V}\right) - \sin\left(\pi \frac{(\lambda_m - \lambda_V)}{\Delta\lambda_V}\right)\right] \tag{3.80}$$

I_2 is a form of the Fresnel integral. Abramowitz et al. [3-07, 7.4.38] provide a formula for expressing the integral in terms of the Fresnel sine and cosine integrals which are tabulated.

$$I_2 = B_V\sqrt{\frac{\Delta\lambda_V}{2h(\theta_{im})}}\left\{\cos\left(\pi\frac{(\lambda_m-\lambda_V)}{\Delta\lambda_V}\right)C\left[\sqrt{\frac{h(\theta_{im})}{2\Delta\lambda_V}}\,s\right]\right.$$

$$\left. - \sin\left(\pi\frac{(\lambda_m-\lambda_V)}{\Delta\lambda_V}\right)S\left[\sqrt{\frac{h(\theta_{im})}{2\Delta\lambda_V}}\,s\right]\right\} \qquad (3.81)$$

$$S(z) = \text{Fresnel sine integral} = \int_0^z \sin\frac{\pi}{2}t^2\,dt \qquad (3.82)$$

$$C(z) = \text{Fresnel cosine integral} = \int_0^z \cos\frac{\pi}{2}t^2\,dt \qquad (3.83)$$

$$J(s,\lambda_m)_{V_1} = 2cI(y_{s_1})B_V \times$$

$$\left[\left(1+\frac{C_V}{B_V}\right)\frac{s}{2} + \sqrt{\frac{\Delta\lambda_V}{2h(\theta_{im})}}\left\{\cos\left(\frac{\pi(\lambda_m-\lambda_V)}{\Delta\lambda_V}\right)C\left[\sqrt{\frac{h(\theta_{im})}{2\Delta\lambda_V}}\,s\right] - \sin\left(\frac{\pi(\lambda_m-\lambda_V)}{\Delta\lambda_V}\right)S\left[\sqrt{\frac{h(\theta_{im})}{2\Delta\lambda_V}}\,s\right]\right\}\right.$$

$$\left. - \left(1+\frac{C_V}{B_V}\right)\frac{s^2}{4D} - \frac{\Delta\lambda_V}{\pi Dh(\theta_{im})}\int\sin\left(\pi\frac{(\lambda_m-\lambda_V)+h(\theta_{im})\frac{s^2}{4}}{\Delta\lambda_V}\right) - \sin\left(\frac{\pi(\lambda_m-\lambda_V)}{\Delta\lambda_V}\right)\right\}\Bigg] \qquad (3.84)$$

$J(s)_{II}$ is of the same general form as $J(s)_{VI}$, except that B_{II}, C_{II}, λ_{II}, and $\Delta\lambda_{II}$ replace B_V, C_V, λ_V, and $\Delta\lambda_V$, respectively.

$J(s)_{V_2}$ differs from $J(s)_{V_1}$ in that $B_V/2$, $\lambda_V+\Delta\lambda_V$, and $2\Delta\lambda_V$ replace B_V, λ_V, and $\Delta\lambda_V$, respectively.

REFERENCES

NUMBER

CHAPTER I

1-01 D. Brust, "Electronic Spectra of Crystalline Germanium and Silicon", Physical Review 134, A 1337 (1964).

1-02 F. Herman, R. Kortum, C. Kuglin, R. Short, "New Studies of the Band Structure of Silicon, Germanium, and Grey Tin", Quantum Theory of Atoms, Molecules, and the Solid State: A Tribute to J.C. Slater, editor P. Löwdin (Academic Press, New York, 1966).

1-03 E. Kane, "Band Structure of Silicon from an Adjusted Heine-Abarenkov Calculation", Physical Review 146, 558 (1966).

1-04 P. Grant, Optical Properties of Thin Germanium Films, Technical Report HP-14 (Gordon McKay Laboratory, Harvard, Cambridge, Mass., 1965), pp. xiii, 5-7.

1-05 H. Philipp, E. Taft, "Optical Constants of Germanium in the Region 1 to 10 eV", Physical Review 113, 1002 (1959).

1-06 J. Tauc, E. Antončík, "Optical Observation of Spin-Orbit Interaction in Germanium", Physical Review Letters 5, 253 (1960).

1-07 L. Gerhardt, "Polarization Dependence of the Piezoreflectance in and Ge", Physical Review Letters 15, 401 (1965).

1-08 K.S. Viswanathan, J. Calloway, "Dielectric Constant of a Semiconductor in an External Electric Field", Physical Review 143, 564 (1966).

1-09 M.S. Dresselhaus, J. G. Mavroides, "Magneto-reflection Experiments in Graphite", Carbon 1, 263 (1964). Diagrams in B. Lax, "Progress in Magneto-Optical Effects", Proceedings of the International Conference on the Physics of Semiconductors, Paris, 1964 (Dunod, Paris, 1964), p. 256.

1-10 C.B. Duke, "Optical Absorption by Excitons in a Strong Electric Field", Physical Review Letters 15, 625 (1965).

1-11 W.E. Krag, H. J. Zeiger, "Infrared Absorption Spectrum of Sulfur-Doped Silicon", Physical Review Letters 8, 485 (1962).

1-12 H.E. Bennett, W. F. Koehler, "Precision Measurement of Absolute Specular Reflectance with Minimal Systematic Errors", Journal of the Optical Society of America 50, 1 (1960).

1-13 B.O. Seraphin "The Effect of an Electric Field on the Reflectivity of Germanium", Proceedings of the International Conference on the Physics of Semiconductors, Paris, 1964 (Dunod, Paris, 1964), p. 165.

1-14 B. Seraphin, R. Hess, "Franz-Keldysh Effect Above the Fundamental Edge in Germanium", Physical Review Letters 14, 138 (1965).

1-15 W.E. Engeler, H. Fritzsche, M. Garfinkel, J.J. Tiemann, "High Sensitivity Piezoreflectivity", Physical Review Letters 14, 1069 (1965).

1-16 I. Balslev, "Influence of Uniaxial Stress on the Indirect Absorption Edge in Silicon and Germanium", Physical Review 143, 636 (1966).

1-17 A. Frova, P. Handler, "Franz-Keldysh Effect in the Space-Charge Region of a Germanium p-n Junction", Physical Review 137, A1857 (1965).

1-18 K.S. Viswanathan, J. Calloway, "Dielectric Constant of a Semiconductor in an External Electric Field", Physical Review 143, 564 (1966).

1-19 D. Aspnes, "Electric Field Effects on Optical Absorption near Thresholds in Solids", Physical Review 147, 554 (1966).

1-20 R. Williams, "Electric Field Induced Light Absorption in CdS", Physical Review 117, 1487 (1960).

1-21 M. Cardona, K.L. Shaklee, F.H. Pollak, "Electroreflectance at a Semiconductor-Electrolyte Interface", Physical Review 154, 696 (1967).

1-22 M. Cardona, F. McElroy, F.H. Pollak, K.L. Shaklee, "Electroreflectance and Band Structure of Gray Tin", Solid State Communications 4, 319 (1966).

CHAPTER II

2-01 L. Holland, Vacuum Deposition of Thin Films (John Wiley and Sons, Inc., New York, 1960), p. 322.

2-02 S. Zwerdling, J.P. Theriault, "Calibration of Prism Spectrometers in the UV, Visible, and Near-IR Regions", Spectrochimica Acta 17, 819 (1961).

2-03 R. Schwantes et al., "Flicker Noise in Secondary Emission Tubes and Multiplier Phototubes", Journal of Applied Physics 27, 573 (1956).

2-04 D.A. Bell, Electrical Noise (D. Van Nostrand Co., London, 1960), p. 272.

2-05 H. Levinstein, "Impurity Photoconductivity in Germanium", Proceedings of I.R.E. 47, 1478 (1959).

2-06 B. Kosicki, private communication, 1966, on the basis of tests in the near infrared only.

2-07 RCA 7102 Multiplier Phototube Data Sheet, (RCA, Electron Tube Division, Harrison, New Jersey, Dec. 1957).

2-08 R. Zallen, The Effect of Pressure on Optical Properties of Semiconductors, Technical Report HP-12 (Gordon McKay Laboratory, Harvard, Cambridge, 1964).

2-09 J. P. Keene, "Fatigue and Saturation in Photomultipliers", Review of Scientific Instruments 34, 1220 (1963).

2-10 Santa Barbara Research Center, Catalog on Infrared Detectors, Brochure No. 66 CM (SBRC, Goleta, California).

2-11 Infrared Devices (Texas Instruments Inc., Semiconductor Components Division, Dallas, Texas, SC-8385-366).

2-12 J.J. Freeman, Principles of Noise (John Wiley and Sons, Inc., New York, 1958), pp. 249-267.

2-13 W.B. Davenport, W.L. Root, An Introduction to the Theory of Random Signals and Noise (McGraw-Hill Book Co., New York, 1958), Chapters 12 and 13, "Non-Linear Devices".

2-14 D.J.H. MacLean, "Design Curves for Simple Filters", Electronic Engineering 30, 654 (1958).

2-15 D.G. Thomas, "Excitons and Band Splitting Produced by Uniaxial Stress in CdTe", Journal of Applied Physics, Supp. to Vol. 32, 2298 (1961).

2-16 M.D. Sturge, "A Differential Absorption Spectrometer for the Infrared", Journal of Scientific Instruments 38, 96 (1961).

2-17 E. Rossi, private communication, 1965.

CHAPTER III

3-01 T. Shankland, private communication, 1966.

3-02 M. Born, E. Wolf, Principles of Optics (Pergamon Press, 3rd edition, New York, 1965).

3-03 Ehrenreich, Philipp, and Segall, "Optical Properties of Aluminum", Physical Review 132, 1918 (1963).

3-04 R. Schmitt of Jarrel Ash, private communication, 1967.

3-05 H.B. Dwight, Tables of Integrals (Macmillan Company, New York, 3rd edition, 1957).

3-06 W.G. Fastie, "Image Forming Properties of the Ebert Monochromator", Journal of the Optical Society of America 42, 647 (1952).

3-07 M. Abramowitz, I. Stegun, editors, Handbook of Mathematical Functions (National Bureau of Standards, Government Printing Office, Washington, D.C., 1964).

ACKNOWLEDGMENTS

I offer thanks to Professor William Paul for his assistance at various stages of this work. It was he who originally suggested reflectivity studies to me. He played a significant role in conceiving the ratio reflectometer and lent a sympathetic ear to the numerous design problems as they arose. He has carefully read this manuscript, and I both appreciate and have used his comments.

Dr. Jan Tauc was another major contributor to the conception of the reflectometer and assisted in the first stages of its construction. Mr. Stephan Prevot assisted both in the system conception and in the original construction of a number of electronic components.

Our two machinists, Mr. James Inglis and Mr. Albert Manning, provided me with superb support. Mr. Manning made the beam splitter, while Mr. Inglis carefully constructed numerous system components.

My wife, Linda, edited every line of this work, looking for internal consistency. My father was a frequent source of useful technical perspective.

Unclassified
Security Classification

DOCUMENT CONTROL DATA - R & D

Security classification of title, body of abstract and indexing annotation must be entered when the overall report is classified)

1. ORIGINATING ACTIVITY (Corporate author)
Division of Engineering and Applied Physics
Harvard University
Cambridge, Massachusetts

2a. REPORT SECURITY CLASSIFICATION
Unclassified

2b. GROUP

3. REPORT TITLE
THE CONSTRUCTION AND ANALYSIS OF A RATIO REFLECTOMETER

4. DESCRIPTIVE NOTES (Type of report and inclusive dates)
Interim technical report

5. AUTHOR(S) (First name, middle initial, last name)
Paul T. McElroy

6. REPORT DATE	7a. TOTAL NO. OF PAGES	7b. NO. OF REFS
May 1968	283	46

8a. CONTRACT OR GRANT NO.
N00014-67-A-0298-0012 & ARPA SD-88

b. PROJECT NO.

c.

d.

9a. ORIGINATOR'S REPORT NUMBER(S)
Technical Report No. HP-20
Technical Report No. ARPA-33

9b. OTHER REPORT NO(S) (Any other numbers that may be assigned this report)

10. DISTRIBUTION STATEMENT
Reproduction in whole or in part is permitted by the U. S. Government. Distribution of this document is unlimited.

11. SUPPLEMENTARY NOTES

12. SPONSORING MILITARY ACTIVITY
Office of Naval Research

13. ABSTRACT

In our work we have conducted four related investigations: (1) the design and construction of a ratio reflectometer for optical measurements; (2) the description and analysis of a polarization dependent false structure in the reflectivity, which arises in the system monochromator; (3) the application of the ratio reflectometer to the accurate measurement of reflectivity structure in germanium and gray tin, which are then interpreted in terms of energy band models, and (4) the development of an improved method for theoretically computing ϵ_2 through the study of the dependence of the diamond double group selection rules on light polarization direction, and a suggested modification to the double group labels at L, with particular reference to gray tin.

In this technical report we discuss (1) and (2) while (3) and (4) are considered in Technical Report HP-21 (ARPA-34), entitled "The Application of the Ratio Reflectometer to Energy Band Studies in Germanium and Gray Tin".

(1) We have designed and built an optical-electronic system for reflectivity studies which has the following characteristics. Amplitude changes as small as .05% can be detected, permitting the experimenter to measure fine structure and the effects of perturbations. The readout of reflectivity data is direct and rapid, and the sample volume is very large, enabling one to modify the sample crystal environment with a variety of stimuli.

Our discussion of the ratio reflectometer contains a full description of the design problems and the final form of the optical, mechanical, and electronic components. We deal with the various sources of noise and their reduction, the factors affecting linearity and its optimization, and scattered light and electronic drift as sources of false reflectivity structure. Normal operating conditions are described and a guide for locating system malfunctions is included.

(2) False reflectivity structure of small magnitude, arising from the polarizing characteristics of our monochromator grating, was exactly correlated with peaks in the I_0 curve occurring under the same polarization conditions. Our analysis shows the effect is not unique to our system; it may account for fine structure occasionally noted in the work of other investigators.

We have studied the false structure in detail, dividing our effort into two parts. First, we examine the evidence supporting the hypothesis that some of the structure in $I_0(\lambda)$ arises from changes in the angle of incidence of light on the grating, rather than wavelength changes. Second, we assume that all the $I_0(\lambda)$ variation is due to angle of incidence variation in order to determine the importance of this in creating false structure. We derive an expression for the reflectivity which indeed shows false structure correlated with the I_0 structure. In carrying out this analysis, we make use of two geometrical facts: the light incident on the grating is not perfectly collimated; and our optical system obscures varying amounts of light from the incident light and reflected light optical paths.

The false structure has been eliminated from our system by using light polarized parallel to the monochromator slit and by ensuring that the incident and reflected light paths do not obscure differing amounts of light.

DD FORM 1 NOV 65 1473 (PAGE 1)
S/N 0101-807-6811

Unclassified
Security Classification

A-31409

14 KEY WORDS	LINK A		LINK B		LINK C	
	ROLE	WT	ROLE	WT	ROLE	WT
Optical Reflectivity Measurements Ratio Reflectometer Construction Ratio Reflectometer Analysis Excellent Amplitude Resolution False Reflectivity Structure Polarization Effects						